U.S. Department
of Transportation

**Federal Railroad
Administration**

PASSENGER RAIL VEHICLE SAFETY ASSESSMENT METHODOLOGY

Volume II: Detailed Analyses and Simulation Results

Office of Research
and Development
Washington, DC 20590

G. Samavedam
J. Gomes
F. Blader

Foster-Miller, Inc.
350 Second Avenue
Waltham, MA 02451-1196

DOT/FRA/ORD-00/03

Final Report
April 2000

NOTICE

This document is disseminated under the sponsorship of the Department of Transportation in the interest of information exchange. The United Sates Government assumes no liability for its contents or use thereof.

NOTICE

The United States Government does not endorse products or manufacturers. Trade or manufacturers' names appear herein solely because they are considered essential to the objective of this report.

REPORT DOCUMENTATION PAGE

Form Approved
OMB No. 0704-0188

1. AGENCY USE ONLY *(Leave blank)*	2. REPORT DATE	3. REPORT TYPE AND DATES COVERED
	April 2000	Final Report, July 1995 - January 1997

4. TITLE AND SUBTITLE

Passenger Rail Vehicle Safety Assessment Methodology
Volume II: Detailed Analyses and Simulation Results

5. FUNDING NUMBERS

6. AUTHOR(S)

G. Samavedam , J. Gomes, F. Blader**

7. PERFORMING ORGANIZATION NAME(S) AND ADDRESS(ES)

Foster-Miller, Inc.
350 Second Avenue
Waltham, MA 02451-1196

8. PERFORMING ORGANIZATION REPORT NUMBER

9. SPONSORING/MONITORING AGENCY NAME(S) AND ADDRESS(ES)

U.S. Department of Transportation
Federal Railroad Administration
Office of Research and Development
Washington, DC 20593

10. SPONSORING/MONITORING AGENCY REPORT NUMBER

DOT/FRA/ORD-00/03 Vol II

11. SUPPLEMENTARY NOTES

**Consultant

12a. DISTRIBUTION/AVAILABILITY STATEMENT

This document is available to the public through the National Technical Information Service, Springfield, VA 22161

12b. DISTRIBUTION CODE

N/A

13. ABSTRACT *(Maximum 200 words)*

This report presents detailed analytic tools and results on dynamic response which are used to develop the safe dynamic performance limits of commuter passenger vehicles. The methodology consists of determining the critical parameters and characteristic properties of both the vehicle and the track, establishing the failure modes, and then using a computer model to determine under what conditions the failure occurs. The computer tool predicts the dynamics of the vehicles at varying speeds. Safety limits and margins are based on when the predicted behavior approaches a derailment.

This report also presents numerical examples of this methodology, derived from the software tool OMNISIM to predict the response of single and bi-level vehicles as they negotiate both tangent tracks and tracks with curves up to 20 deg. To determine conditions of unsafe vehicle behavior, simulations included truck and body hunting, steady-state curving, dynamic curving, transient response to vertical and lateral track perturbations and transient response at switches.

14. SUBJECT TERMS

Passenger rail vehicles, equalized and non-equalized trucks, OMNISIM, safety limits

15. NUMBER OF PAGES

232

16. PRICE CODE

17. SECURITY CLASSIFICATION OF REPORT	18. SECURITY CLASSIFICATION OF THIS PAGE	19. SECURITY CLASSIFICATION OF ABSTRACT	20. LIMITATION OF ABSTRACT
Unclassified	Unclassified	Unclassified	

NSN 7540-01-280-5500

Standard Form 298 (Rev. 2-89)
Prescribed by ANSI Std. 239-18

PREFACE

The work reported here has been performed under the contract DTFR53-95-C-00049 from the Federal Railroad Administration (FRA). Dr. Thomas Tsai of the FRA is the Technical Monitor.

Special thanks are due to Dr. David Wormley for his valuable technical inputs throughout the program. Thanks are also due to Mr. Brian Marquis of the Volpe Center for his comments on an earlier version of this report.

CONTENTS

Section **Page**

ILLUSTRATIONS

Figure **Page**

Figure **Page**

Figure **Page**

Figure **Page**

TABLES

Table **Page**

LIST OF ACRONYMS

FRA	Federal Railroad Administration
GSI	General Steel Industries
AAR	Association of American Railroads
AREMA	American Railway Engineering and Maintenance-of-Way Association

1. INTRODUCTION

The 1994 amendment of the Federal Railroad Safety Authorization Act required that the Federal Railroad Administration (FRA) establish regulations for minimum safety standards of conventional railroad passenger vehicles including commuter or intercity passenger cars operating at speeds of 110 mph or less. Passenger rail vehicles may have to be operated over a variety of track geometries: tangent, curved, and spirals connecting tangents to constant radius curves.

The maximum levels of vertical and lateral misalignment that can be safely negotiated, as well as the maximum amount of crosslevel variation, are important results of safety evaluations. The limiting track conditions and the associated issues for safe vehicle operation can be determined through the detailed simulations and evaluations of the vehicle dynamic response. A number of potentially unsafe situations need to be investigated, including truck and body hunting, steady-state curving, dynamic curving, and transient response to vertical and lateral perturbations in track alignment.

The overall objective of this work sponsored by the FRA was to develop a methodology for assessment of safety of existing commuter rail vehicles as well as new and emerging vehicle designs.

In the companion report, Volume I, a framework of the methodology has been described. The methodology consists of the following steps.

1. Identify generic types of commuter cars in revenue service with sufficient variations in their design for use as candidates in the simulation studies and testing.

2. Assemble car and truck parameters, which will be used in the analysis. Supplement the experimental parameter characterization with the manufacturer's data.

3. Identify the critical track parameters that significantly affect the performance of the vehicle. The parameters act as the input conditions to the vehicle dynamic system.

4. Measure the values of the critical track parameters that are expected in service and in any acceptance/qualification testing that may take place.

5. Define conditions and criteria for safe operations.
   - High speed operations on tangent track to assure stability against possible truck hunting.

- Steady-state curve negotiation.
- Dynamic curving under single cusp crosslevel variations.
- Dynamic curving under multiple "down and out" cusp crosslevel and misalignment variations.
- Negotiation of gage narrowing variations.
- Negotiations through switches.

6. Select investigation tools, which are capable of providing the analysis required to determine the vehicle's performance under the conditions and failure modes identified.

7. Using the assembled vehicle and track data, analyze the vehicle's dynamic response under the critical scenarios.

8. Develop performance limits for safe vehicle operations on the basis of analysis and safety criteria in the form of limiting speeds, crosslevels, misalignments, and lateral to vertical force ratios generated in the vehicle operations.

9. Perform validation tests.
   - Validate the simulation model by measuring vehicle parameters and dynamic response under the scenarios listed in item 5.
   - Verify safe performance limits generated through selective tests on candidate car designs.

10. On the basis of the foregoing tasks, develop and formalize a practical safety assessment methodology for new car equipment.

The scope of this report is mainly to address the items 1 through 7. The experimental work required to supplement the track and track parameter data will be presented in a forthcoming report.

The focus of this report is to determine use and applicability of analytic and simulation tools to predict the vehicle dynamic response and evaluate the limits of safe behavior under a variety of track scenarios encountered on revenue lines. Wheel climb and wheel lift are specifically addressed here and appropriate criteria for these failure modes are used. Descriptions of analysis tools are given in Appendix A.

Based on extensive numerical studies carried out here, a set of safe performance limits are formalized for the two types of trucks (equalized and non-equalized) and have been presented in the companion report, Volume I. This fulfills step 8 of the methodology referred to above. The rationale and analytic background for these limits is provided in this report (Volume II).

Section 2 presents a description of typical commuter equipment and required parameters for the analysis. Section 3 evaluates the truck dynamic instability and critical speeds for hunting using a simplified model and OMNISIM. Section 4 describes the vehicle dynamic response to crosslevel variations in curves.

Vehicle response to single rail alignment variations including gage narrowing is studied in Section 5, whereas Section 6 gives the vehicle response under combined variations in alignment and crosslevel. The vehicle behavior as it negotiates switches is presented in Section 7.

Conclusions of practical interest in regard to vehicle safety under all the track scenarios studied are presented in Section 8.

2. PARAMETERS OF COMMUTER CAR EQUIPMENT AND TRACKS

In this section a brief description of typical modern commuter carbody and truck designs and their relevant structural (and other) parameters for analysis are described. In addition, important track parameters are also identified.

2.1 Equipment

The design and implementation of the suspension system has the strongest influence on vehicle dynamic behavior and performance. Examples of suspension design alternatives are found in trucks with and without bolsters, with and without wheel load equalization, and inboard versus outboard axle bearings. Reference (1) contains compilation data on the design features and parameter values for the commuter passenger railroad cars and trucks in current U.S. service. Based on the data contained therein, Tables 2-1 and 2-2 present a summary of the unpowered commuter passenger car truck population (placed into service since 1950) for both single-level and bi-level cars, respectively.

For single level cars, the General Steel Industries (GSI) "General 70," which is an equalized truck design, accounts for 44 percent of all trucks in service; 87 percent of these trucks have been placed into service since 1970.

Table 2-1. Commuter passenger car truck population (single-level)

Car Type	Truck Manufacturer/ Model	Truck Type	No. Cars in Service	Percent	Year Put into Service
Single Level	GSI/Traditional	Equalizer beam primary, outboard bearings, swinghanger secondary	254	34	1955-1963
	GSI/General 70	Equalizer beam primary, inboard bearings, yaw pivot below secondary suspension	750	44	1971-1991
	Nippon Sharyo/NT319	Journal spring primary, outboard bearings, yaw pivot below secondary suspension	75	7	1958-1993
	Tokyu Car	Journal spring primary, outboard bearings, yaw pivot below secondary suspension	38	3	1992
Total			1117		

Table 2-2. Commuter passenger car truck population (bi-level)

Car Type	Truck Manufacturer/ Model	Truck Type	No. Cars in Service	Percent	Year Put into Service
Bi-Level	GSI/Traditional	Equalizer beam primary, outboard bearings, swinghanger secondary	464 73	40 6	1950-1970 1985-1987
	GSI/General 70	Equalizer beam primary, outboard bearings, yaw pivot below secondary suspension	243	21	1973-1993
	Dofasco (Atchison)	Journal spring primary, inboard bearings, yaw pivot below secondary suspension	300	26	1992-1994
	Kawasaki	Journal spring primary, outboard bearings, yaw pivot below secondary suspension	75	6	1993-1994
	Comeng	Journal spring primary outboard bearings, bolsterless secondary suspension	10	1	1990
Total			1165		

For bi-level cars, the GSI "Traditional," which is also an equalized truck design, represents 46 percent of trucks in service. However, the majority of these were placed into service prior to 1970. For those trucks placed into service after 1970, the GSI "General 70" (equalized) and the Dofasco/Atchison (non-equalized) designs constitute the majority of the population.

Within each class of car (that is, single-level and bi-level), differences in body design were generally found to be of lesser importance. Two "generic" cars were selected as the basis around which variations such as single-level and bi-level vehicle bodies and different loading conditions could be built. This allowed key design features and parameter variations to be systematically modeled and studied. The conclusion reached from this data is that the study should evaluate both equalized and non-equalized truck designs. Accordingly, the following significant design features are considered for the truck designs:

1. Rigid truck frame.
2. With and without equalizer beam primary suspension.
3. Axle bearings located outboard of the wheels.
4. Yaw pivot located beneath the secondary suspension.

Exploded views of trucks incorporating these design features are presented, for the equalized truck in Figure 2-1, and for the non-equalized truck in Figure 2-2.

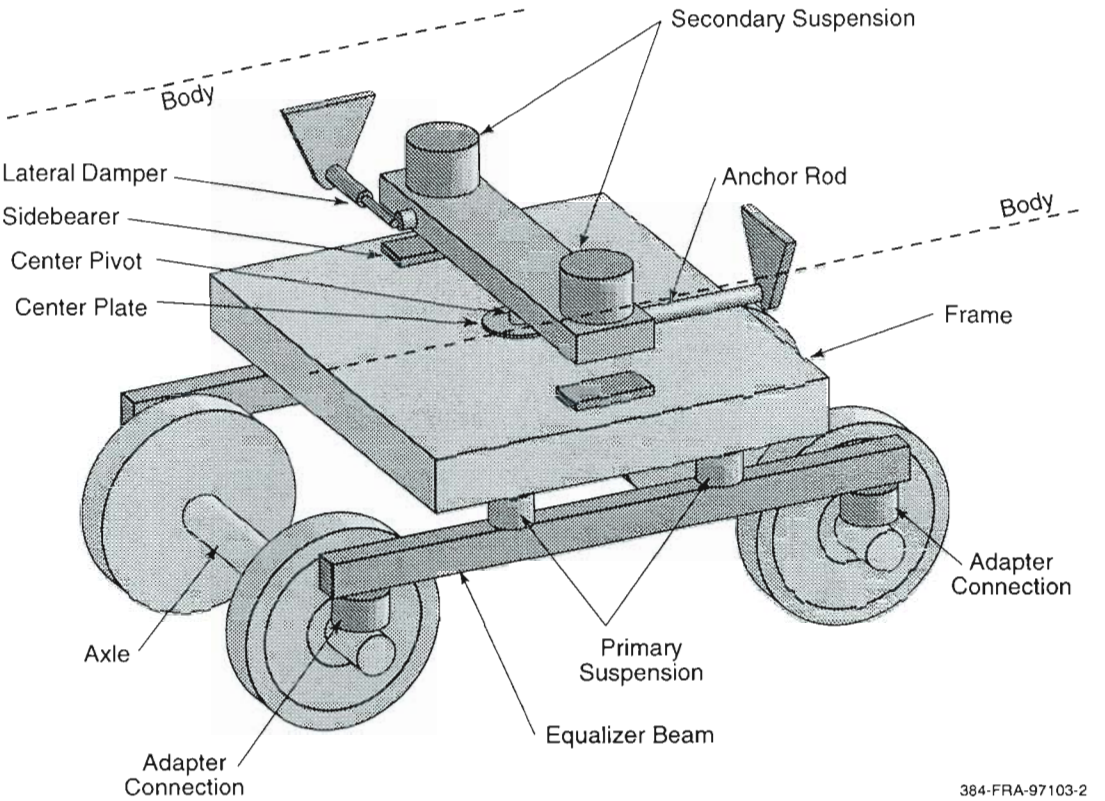

Figure 2-1. Exploded view of the equalized truck

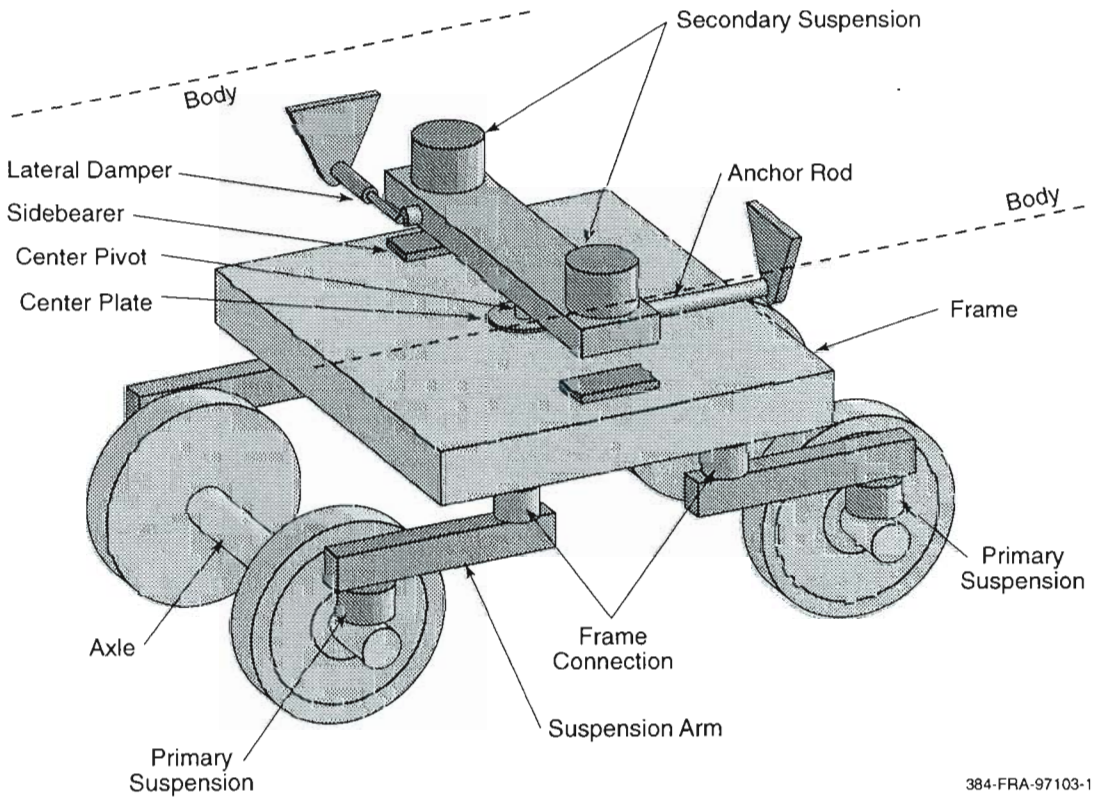

Figure 2-2. Exploded view of the non-equalized truck

2.2 Car Parameters

The parameters governing the behavior of the carbody dynamics can be broadly classified as:

- Mass and inertias.
- Primary suspension stiffness.
- Secondary suspension stiffness and damping.
- Geometry and c.g. location.
- Wheel profiles.

The damping in the primary suspension is considered to be negligible. The stiffnesses can degrade in revenue service operations. It is necessary to evaluate them through testing and not depend on the manufacturer's data.

Typical parameters (used in the numerical study presented in this report) are presented in Tables 2-3 through 2-5. Data for cars with equalized and non-equalized trucks are presented in these tables for both fully loaded and empty conditions. The wheel profiles are not shown in these tables. The assumed wheel profiles correspond to new Association of American Railroads (AAR) 1B, Amtrak AAR1B, and worn AAR1B wheels.

These parameters are required for detailed simulation programs such as OMNISIM used here. For simplified analytic methods, some of the parameters are not required.

2.3 Track Parameters

In addition to the variations in car design and loading, certain track features, important to safety from derailment, are required when using the OMNISIM simulation program. These are labeled "hard" and "soft." The "hard" track uses stiffnesses at the rail, tie and ballast connections typical of the simple models used in previous studies. However, the "soft" track allows for slippage against friction laterally at all connections. The model is shown in Figure 2-3. The stiffness and friction values are shown in Table 2-6. It should be emphasized that the "soft" track is not necessarily representative of a particular soft track but rather has values chosen to exercise the rail motions and demonstrate that such a track might see movements affecting the vehicle behavior.

Table 2-3. Data for the bi-level car with equalized trucks

Parameter Description	Empty	Loaded	Units
Truck frame mass	14.5	14.5	lb-sec^2/in.
Car body mass	250	350	lb-sec^2/in.
Wheelset mass	8.8	8.8	lb-sec^2/in.
Truck frame yaw moment of inertia	10000	10000	lb-in.-sec^2
Car body yaw moment of inertia	2.30E+07	3.00E+07	lb-in.-sec^2
Wheelset yaw moment of inertia	6060	6060	lb-in.-sec^2
Truck frame roll moment of inertia	7499	7499	lb-in.-sec^2
Car body roll moment of inertia	1.00E+06	1.40E+06	lb-in.-sec^2
Longitudinal primary stiffness (per wheel)	3500	3500	lb/in.
Lateral primary stiffness (per wheel)	3500	3500	lb/in.
Vertical primary stiffness (per wheel)	6064	6064	lb/in.
Inter-axle yaw stiffness (per truck)	1.56E+08	1.56E+08	lb/in.
Inter-axle shear stiffness (per truck)	0	0	lb/in.
Lateral secondary stiffness (per truck)	2100	2100	lb/in.
Yaw secondary stiffness (per truck)	0	0	in.-lb/rad
Roll secondary stiffness (per truck)	1.57E+07	1.57E+07	in.-lb/rad
Lateral secondary damping (per truck)	560	560	lb-sec/in.
Yaw secondary damping (per truck)	285	285	in.-lb-sec/in.
Roll secondary damping (per truck)	1.63E+06	1.63E+06	in.-lb-sec/in.
Half of truck wheelbase	51	51	in.
Half lateral distance between primary suspension	39.5	39.5	in.
Half distance between truck centers	357	357	in.
Half distance between primary springs	29	29	in.
Vertical distance, truck c.g. to secondary suspension	16.3	16.3	in.
Vertical distance, carbody c.g. to secondary suspension	46.2	51.2	in.

Table 2-4. Data for the bi-level car with non-equalized trucks

Parameter Description	Empty	Loaded	Units
Truck frame mass	14.2	14.2	lb-sec^2/in.
Car body mass	250	350	lb-sec^2/in.
Wheelset mass	11	11	lb-sec^2/in.
Truck frame yaw moment of inertia	19400	19400	lb-in.-sec^2
Car body yaw moment of inertia	2.30E+07	3.00E+07	lb-in.-sec^2
Wheelset yaw moment of inertia	7200	7200	lb-in.-sec^2
Truck frame roll moment of inertia	14755	14755	lb-in.-sec^2
Car body roll moment of inertia	1.00E+06	1.40E+06	lb-in.-sec^2
Longitudinal primary stiffness (per wheel)	2.25E+05	2.25E+05	lb/in.
Lateral primary stiffness (per wheel)	60200	60200	lb/in.
Vertical primary stiffness (per wheel)	12100	12100	lb/in.
Inter-axle yaw stiffness (per truck)	0	0	lb/in.
Inter-axle shear stiffness (per truck)	0	0	lb/in.
Lateral secondary stiffness (per truck)	3220	3220	lb/in.
Yaw secondary stiffness (per truck)	0	0	in.-lb/rad
Roll secondary stiffness (per truck)	1.32E+07	1.32E+07	in.-lb/rad
Lateral secondary damping (per truck)	520	520	lb-sec/in.
Yaw secondary damping (per truck)	260	260	in.-lb-sec/in.
Roll secondary damping (per truck)	1.41E+06	1.41E+06	in.-lb-sec/in.
Half of truck wheelbase	51	51	in.
Half lateral distance between primary suspension	39.5	39.5	in.
Half distance between truck centers	357	357	in.
Half distance between primary springs	51	51	in.
Vertical distance, truck c.g. to secondary suspension	15.8	15.8	in.
Vertical distance, carbody c.g. to secondary suspension	46.2	51.2	in.

Table 2-5. Data for the empty single-level cars

Parameter Description	Equalized	Non-equalized	Units
Truck frame mass	14.5	14.2	lb-sec^2/in.
Car body mass	170	170	lb-sec^2/in.
Wheelset mass	8.8	11	lb-sec^2/in.
Truck frame yaw moment of inertia	10000	19400	lb-in.-sec^2
Car body yaw moment of inertia	1.50E+07	1.50E+07	lb-in.-sec^2
Wheelset yaw moment of inertia	6060	7200	lb-in.-sec^2
Truck frame roll moment of inertia	7499	14755	lb-in.-sec^2
Car body roll moment of inertia	6.60E+05	6.60E+05	lb-in.-sec^2
Longitudinal primary stiffness (per wheel)	3500	2.25E+05	lb/in.
Lateral primary stiffness (per wheel)	3500	60200	lb/in.
Vertical primary stiffness (per wheel)	6064	12100	lb/in.
Inter-axle yaw stiffness (per truck)	1.56E+08	0	lb/in.
Inter-axle shear stiffness (per truck)	0	0	lb/in.
Lateral secondary stiffness (per truck)	2100	3220	lb/in.
Yaw secondary stiffness (per truck)	0	0	in.-lb/rad
Roll secondary stiffness (per truck)	1.57E+07	1.32E+07	in.-lb/rad
Lateral secondary damping (per truck)	560	520	lb-sec/in.
Yaw secondary damping (per truck)	285	260	in.-lb-sec/in.
Roll secondary damping (per truck)	1.63E+06	1.41E+06	in.-lb-sec/in.
Half of truck wheelbase	51	51	in.
Half lateral distance between primary suspension	39.5	39.5	in.
Half distance between truck centers	357	357	in.
Half distance between primary springs	29	51	in.
Vertical distance, truck c.g. to secondary suspension	16.3	15.8	in.
Vertical distance, carbody c.g. to secondary suspension	27.2	27.2	in.

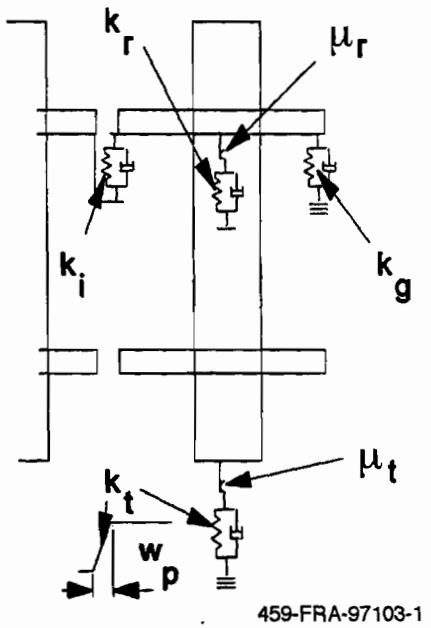

Figure 2-3. Track model for use in OMNISIM

Table 2-6. Track lateral stiffness

Parameter	Soft Track	Hard Track
k_i (lb/in.)	2.50E+03	1.00E+05
k_r (lb/in.)	2.00E+04	1.00E+05
k_g (lb/in.)	1.00E+04	1.00E+05
k_t (lb/in.)	NA	1.00E+05
w_p (in.)	0.05	NA
μ_r	0.4	No slip
μ_t	0.5	No slip

3. ANALYSIS OF DYNAMIC STABILITY - HUNTING

Hunting refers to the self-excited lateral response of rail vehicle body and trucks. This behavior is due to energy transferred from forward to lateral motions under adverse conditions through the interaction of the wheels with the rails. This self-excited lateral response occurs on tangent tracks. The predominant mode of behavior is often the lateral displacement and yaw of the truck, although independent axle and car body hunting have also been recorded. A particular indication of the proximity of the vehicle to a hunting condition is the amount of damping in the lowest damped mode. As the speed increases, this generally decreases. In linear models, the unstable behavior commences at a speed called the critical speed. In reality, the advent of flange contact at the extremes of the lateral oscillation of the wheel on the rail is preceded by a period of beating oscillations and may even remain at amplitudes below flange contact in "limit cycles."

3.1 Linear Hunting Analysis - NEWHUNT

The hunting critical speeds and modes for single-level and bi-level commuter passenger cars under varying wheel/rail conditions on tangent track were evaluated using the computer program NEWHUNT. As discussed in Appendix A, NEWHUNT, a revised version of CARHNT, determines the eigenvalues of the linearized equations-of-motion. The results presented below for the equalized truck are from the corrected equations of motion in NEWHUNT. The original results from CARHNT did not compare well with the OMNISIM results and are not included.

The results given here are based on nominal body and suspension parameter values that were established in Section 2. The wheel/rail effective conicity was varied from 0.025 to 0.2, and vehicle forward speeds ranged from 10 mph to the hunting speed. While the commuter cars investigated are typically operated at speeds of 80 mph or less, the analysis included the higher speed range so as to identify the threshold of hunting. This establishes the safety margin inherent in a particular vehicle configuration. The Amtrak wheel profile has a 1:40 cone angle on the tread and is the only profile used having this low conicity. The AAR profile has a 1:20 tread section. Worn wheels with effective conicities increasing to 1:5 used the 1:20 tread as a base value.

The base case results for the empty bi-level cars are first presented in the form of plots of the damping ratio and hunting frequency versus speed. The critical speed is the speed at which the damping goes negative. This speed is plotted against effective conicity. The dominant mode for all of the hunting oscillations discovered, included a dominant lateral wheelset and truck frame activity with yaw. Figures 3-1 through 3-3 present the results for a bi-level car with equalized trucks. The results for the bi-level car with non-equalized trucks are shown in Figures 3-4 through 3-6. Their results are quite different both in magnitude and variation with speed.

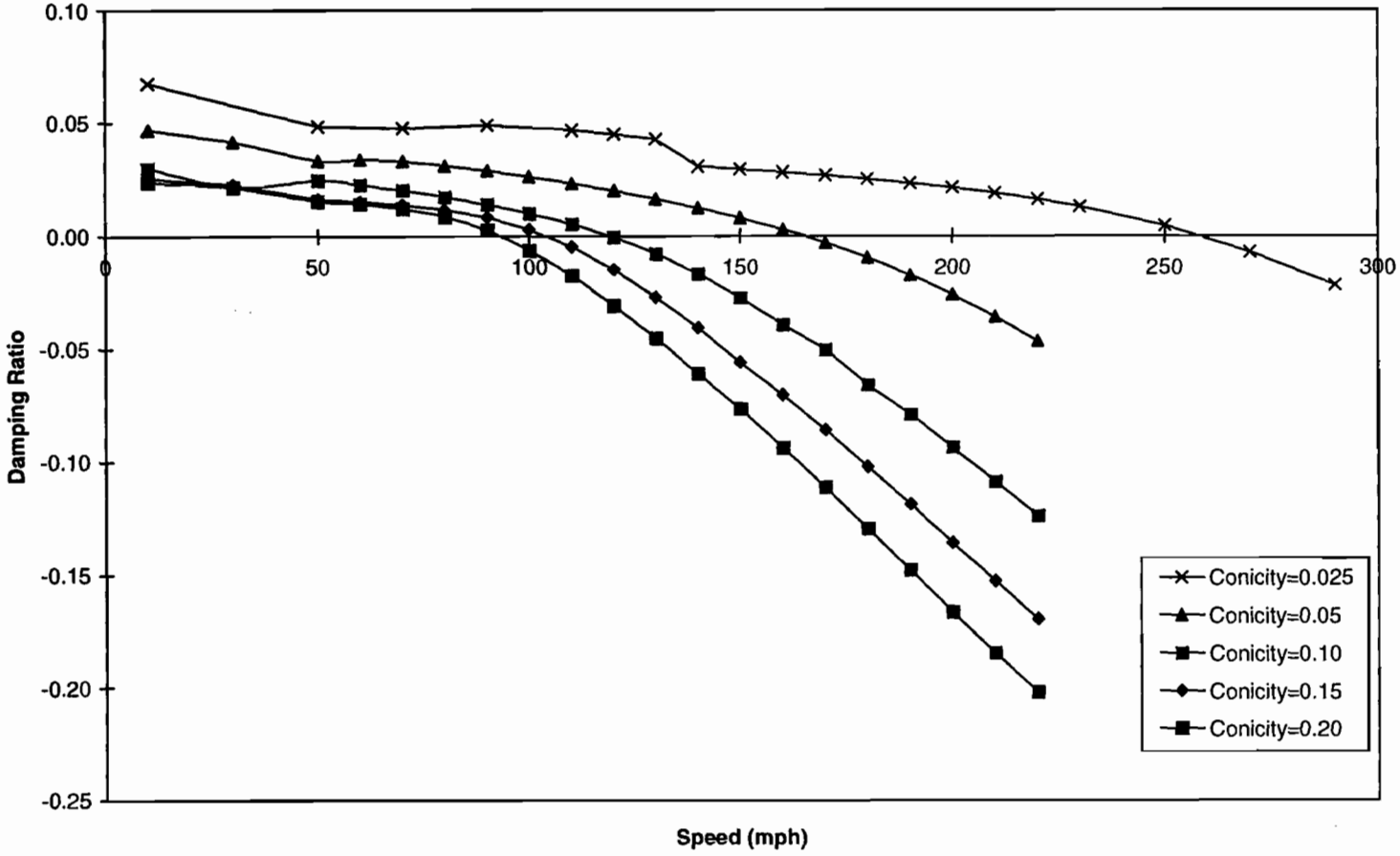

Figure 3-1. Truck hunting damping ratio versus speed (empty bi-level car, equalized trucks)

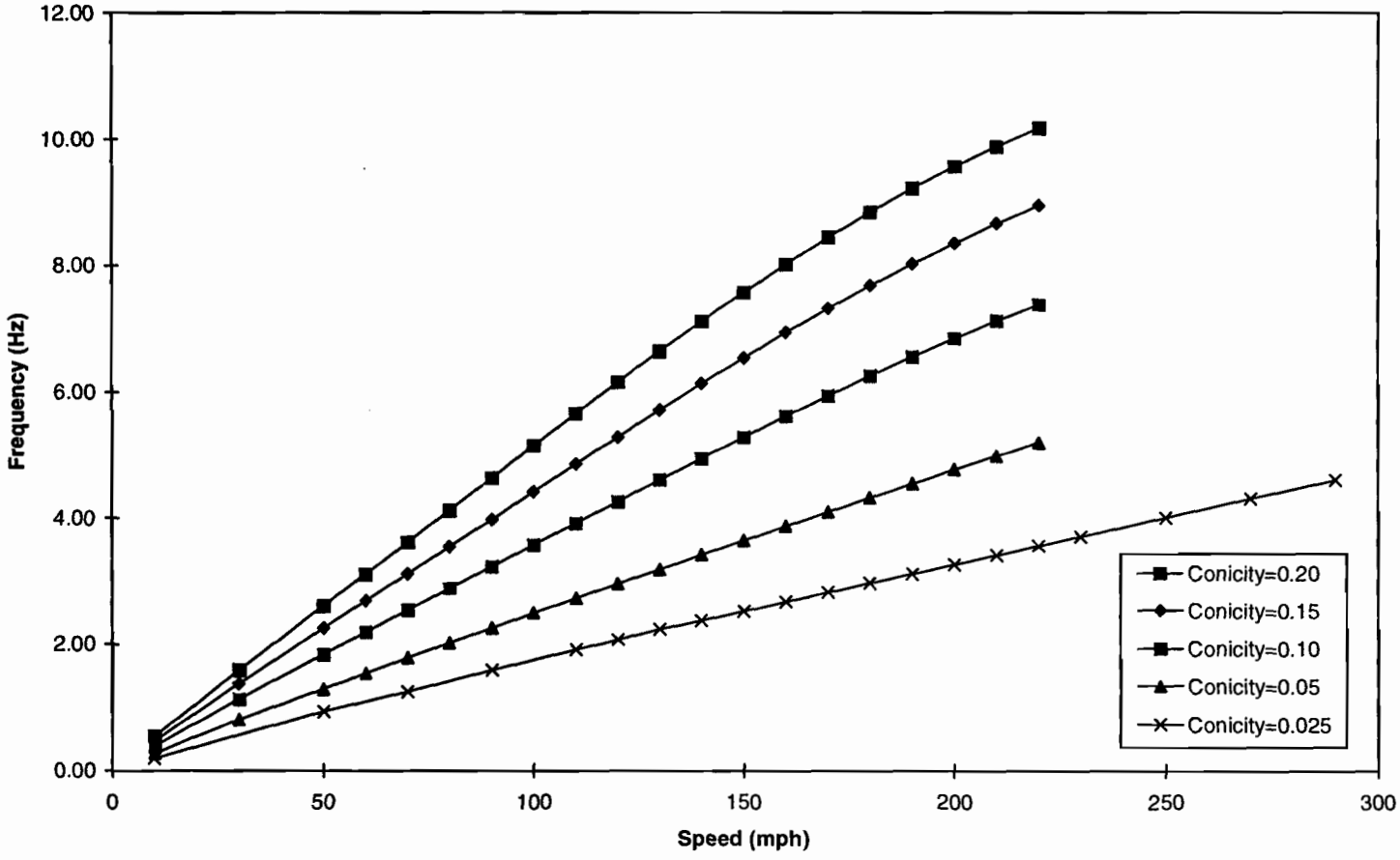

Figure 3-2. Truck hunting frequency versus speed (empty bi-level car, equalized trucks)

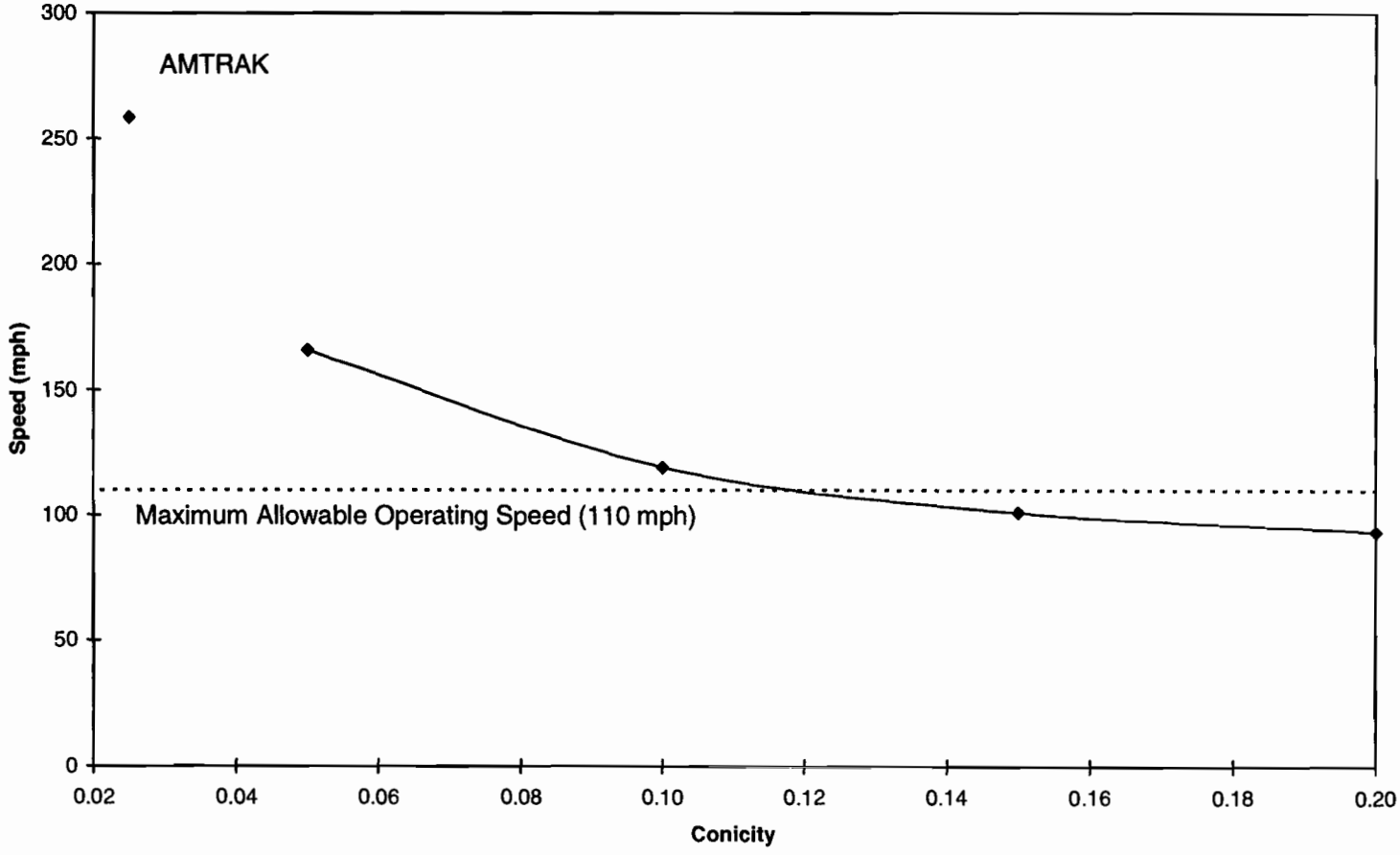

Figure 3-3. Critical speed versus conicity (empty bi-level car, equalized trucks)

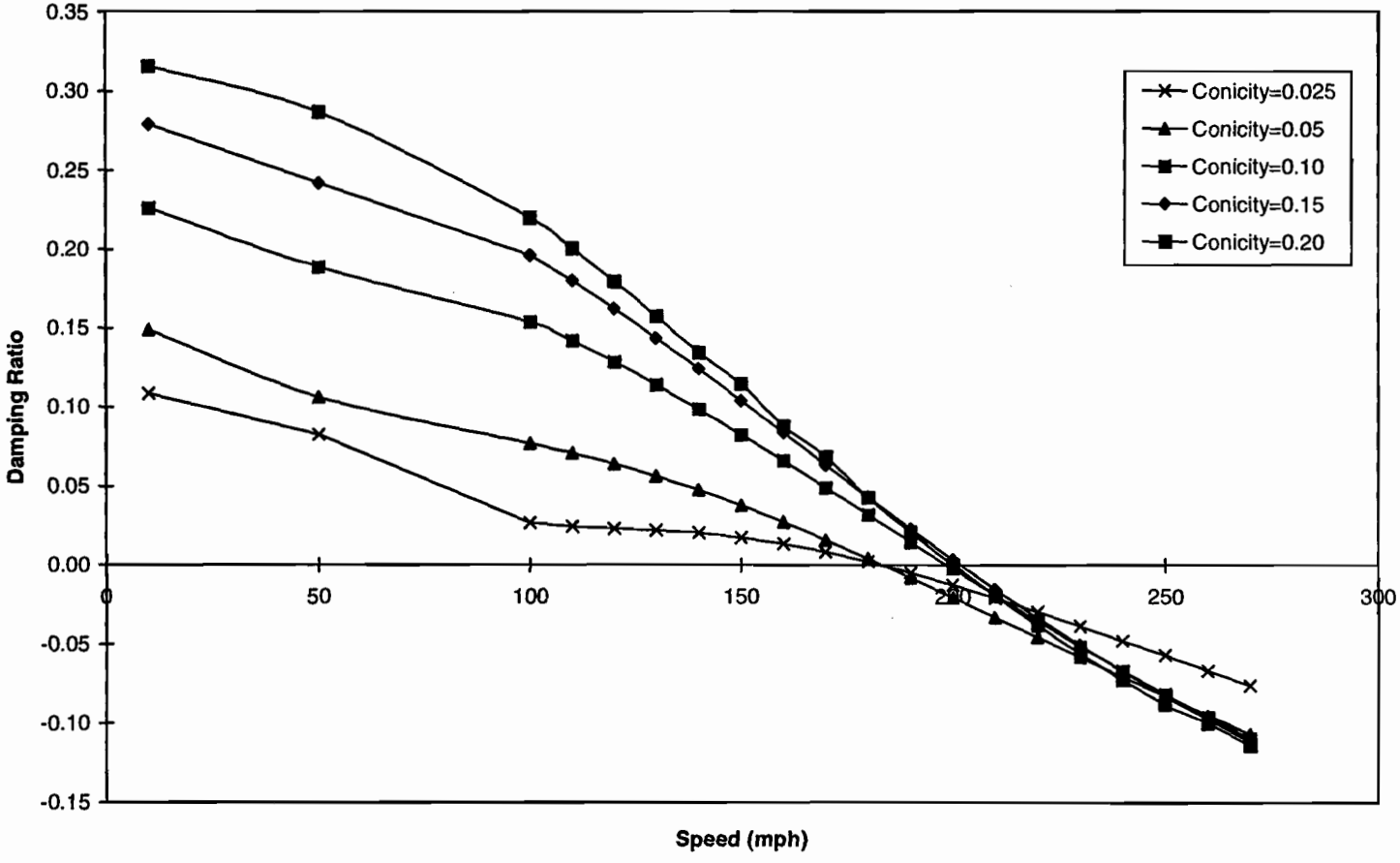

Figure 3-4. Truck hunting damping ratio versus speed (empty bi-level car, non-equalized trucks)

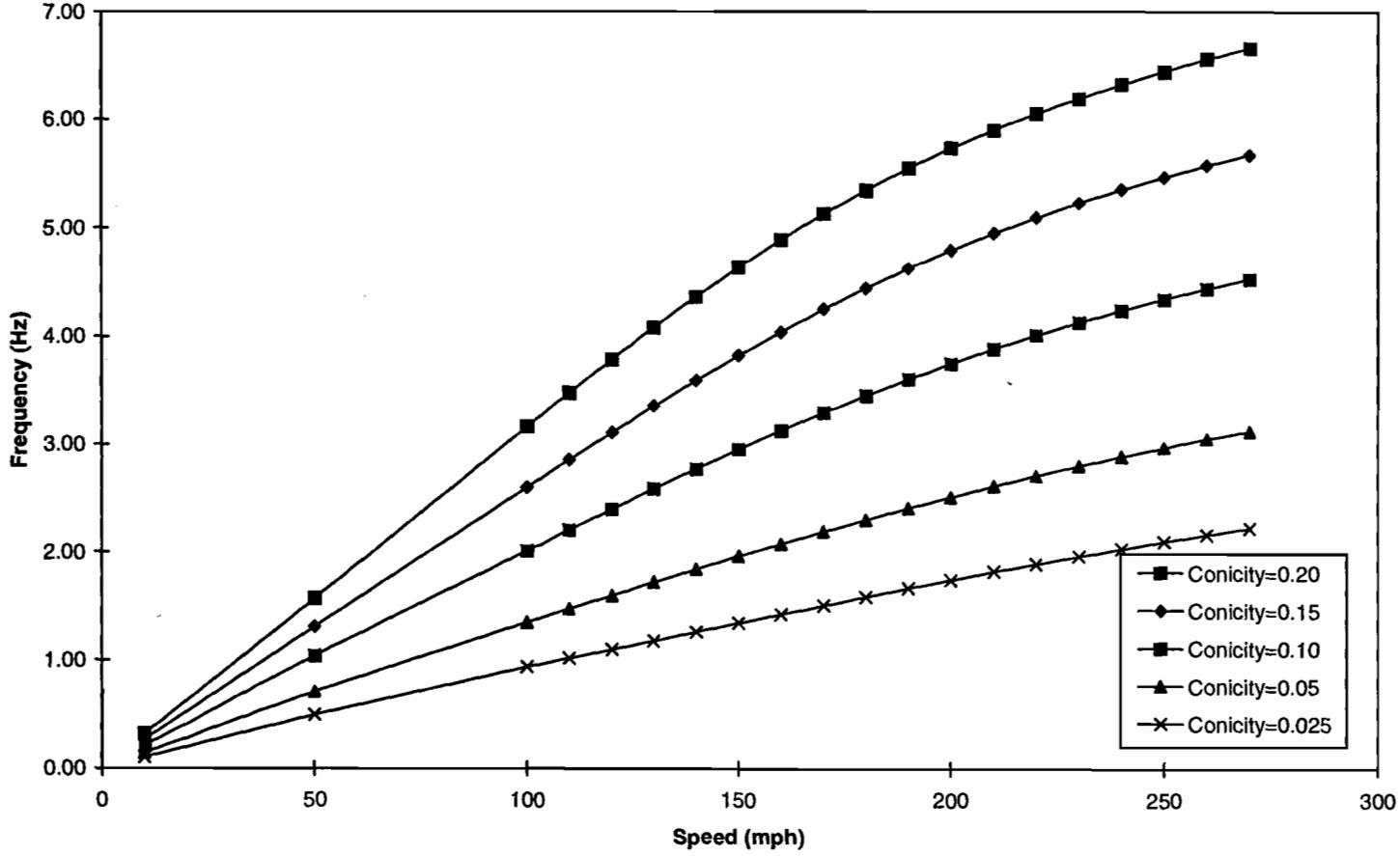

Figure 3-5. Truck hunting frequency versus speed (empty bi-level car, non-equalized trucks)

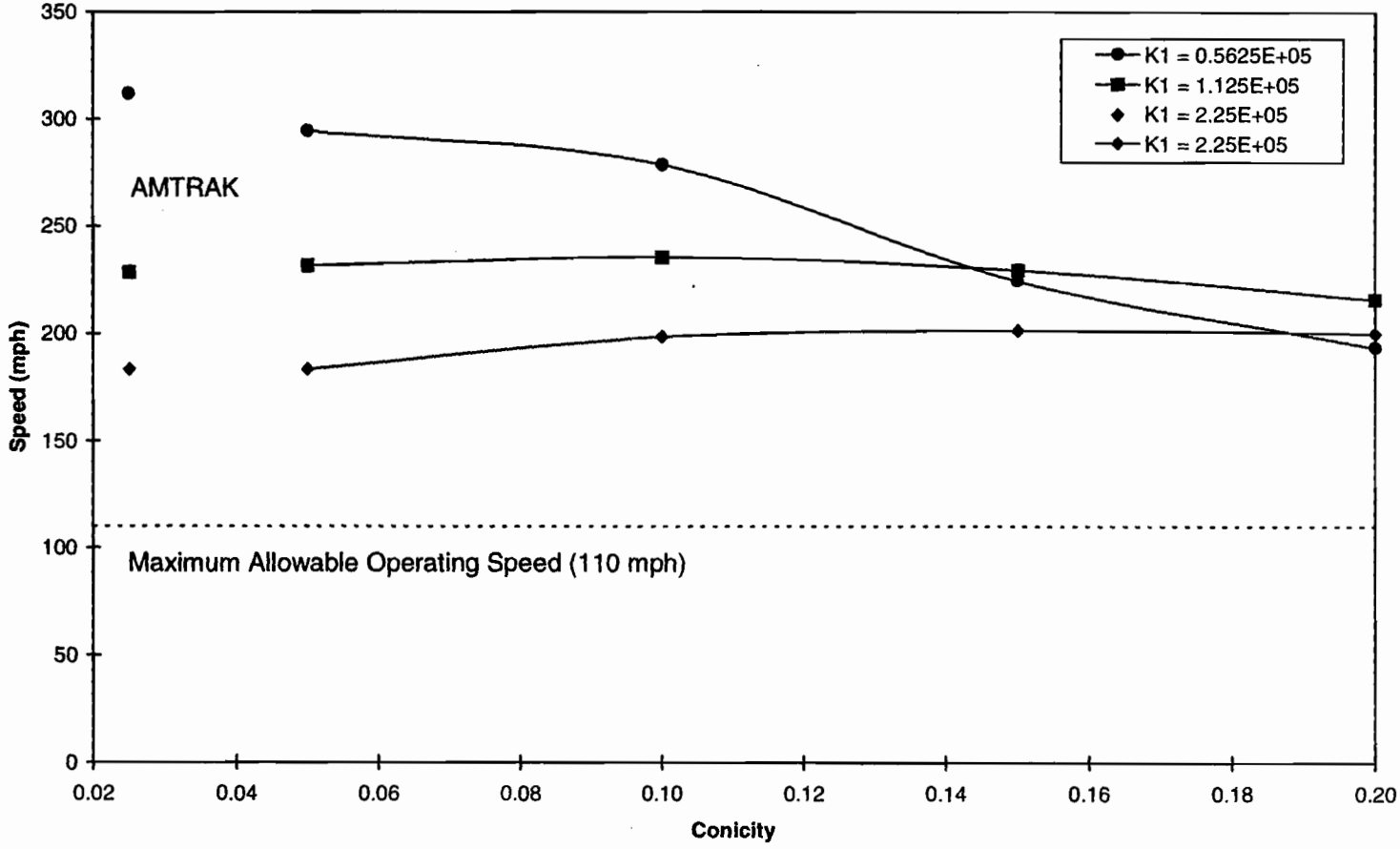

Figure 3-6. Critical speed versus conicity (empty bi-level car, non-equalized trucks)

In all of the cases, the critical speeds found are adequately above the typical operating speeds of commuter passenger rail vehicles for all effective conicities investigated, although the results for the equalized trucks show the lower critical speeds. However, vehicles with equalized trucks are found to have the critical speed decreasing with increasing wheel conicity, whereas the opposite is found with the non-equalized trucks where the change is quite small. This difference was subjected to further investigation and found to be influenced by the large nominal value established for the primary longitudinal suspension stiffness in the non-equalized truck. Figure 3-6 shows the critical speed as a function of conicity with the primary longitudinal stiffness varied for this car. Decreasing the original stiffness value by a factor of four causes the change with effective conicity to decrease. Figure 3-6 also indicates that it is possible to select a value for the truck primary longitudinal stiffness for this car that renders its critical speed little effected by effective conicity changes with wear.

Figures 3-7 and 3-8, for the equalized trucks, and Figures 3-9 and 3-10, for the non-equalized trucks, show the effect on the damping content and frequency of the variation of empty and loaded bi-level cars and the reduction in height to single-level. Since there is a difference for the single-level car and it has the lowest critical speed for the car with non-equalized trucks, its critical speed comparisons are shown with the bi-level for both equalized and non-equalized trucks in Figures 3-11 and 3-12. It is shown to have the higher critical speeds for the car with equalized trucks.

3.2 Comparison of Hunting Results from OMNISIM and NEWHUNT

OMNISIM is used to compare the predicted behavior, particularly the critical speeds against those from NEWHUNT. The results are given in Table 3-1. The files developed using PROFIT for the wheel profile fit on the rail and used in the OMNISIM runs deviated by up to 8 percent from the expected small motion effective conicities. The measured effective conicities for a lateral movement of 0.2 in. are compared with the nominal tread angle in Table 3-2. The inaccuracy was found difficult to correct in PROFIT. The small clearances in the pedestals laterally and longitudinally are not enough to allow a full range of axle movement as modeled in the NEWHUNT equations (Appendix A). This was cured by opening up the gap in the OMNISIM runs used only for comparison with NEWHUNT results. This emphasizes the limitation of linear analysis.

3.3 Detailed Hunting Analysis - OMNISIM

This detailed analysis is concerned with simulating the full nonlinear dynamic response of the commuter cars over the operational speed range up to any point of derailment which may be predicted to occur. The simulation program OMNISIM described in Appendix A was used to examine the potential for derailment beyond the critical speed up to full flange contact. Variations in effective conicity occur as the axle moves laterally and in yaw which are not modeled in the simulation. Thus the critical speed has a less precise meaning than that of the negatively damped root noted in the linearized results. In order to prevent confusion from too many variables, the coefficient of friction at the wheel/rail interface was held constant at 0.4. A full set of truck parameters was used throughout, including pedestal clearance where specified and sidebearer friction.

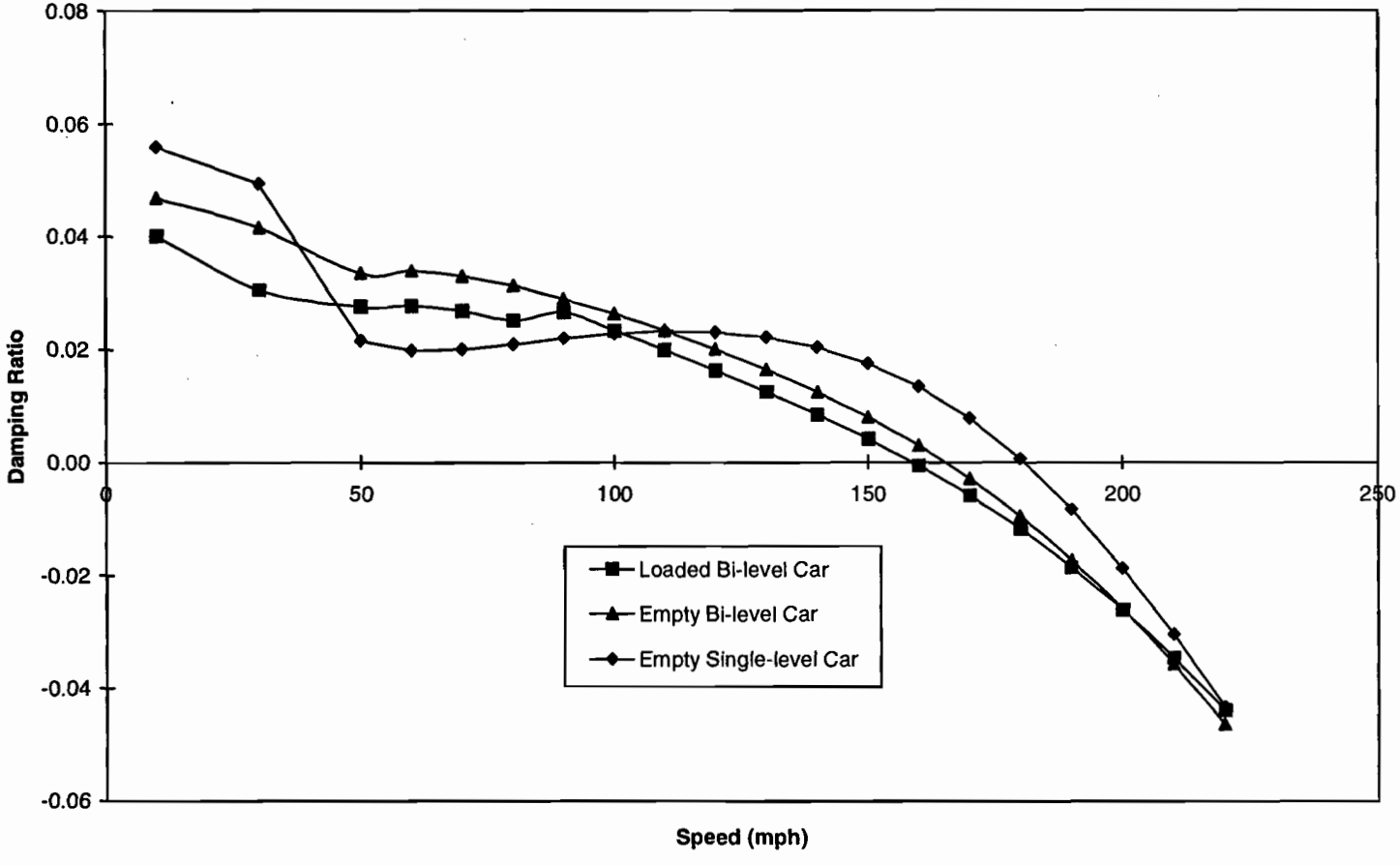

Figure 3-7. Truck hunting damping ratio versus speed (conicity = 0.05, equalized trucks)

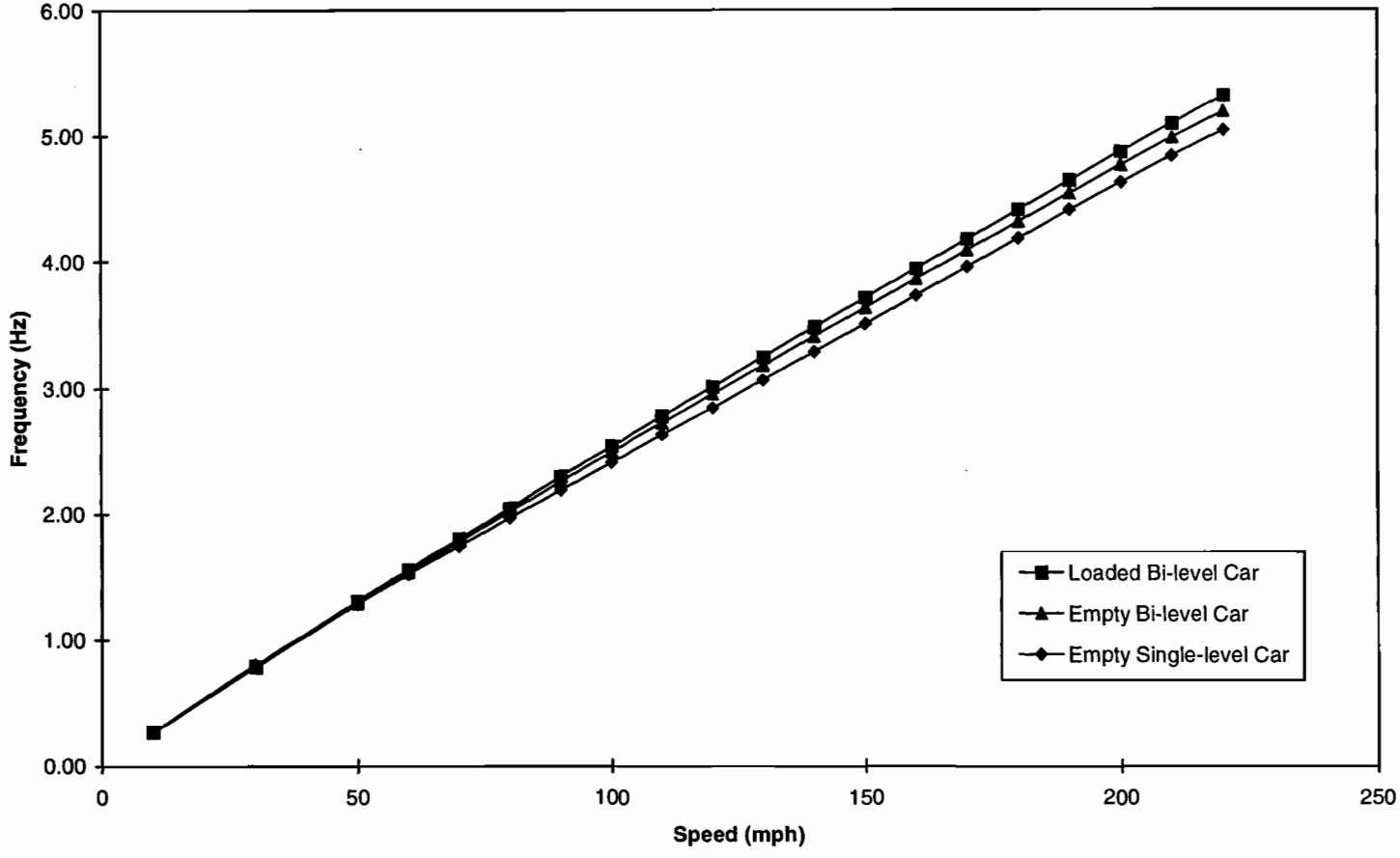

Figure 3-8. Truck hunting frequency versus speed (conicity = 0.05, equalized trucks)

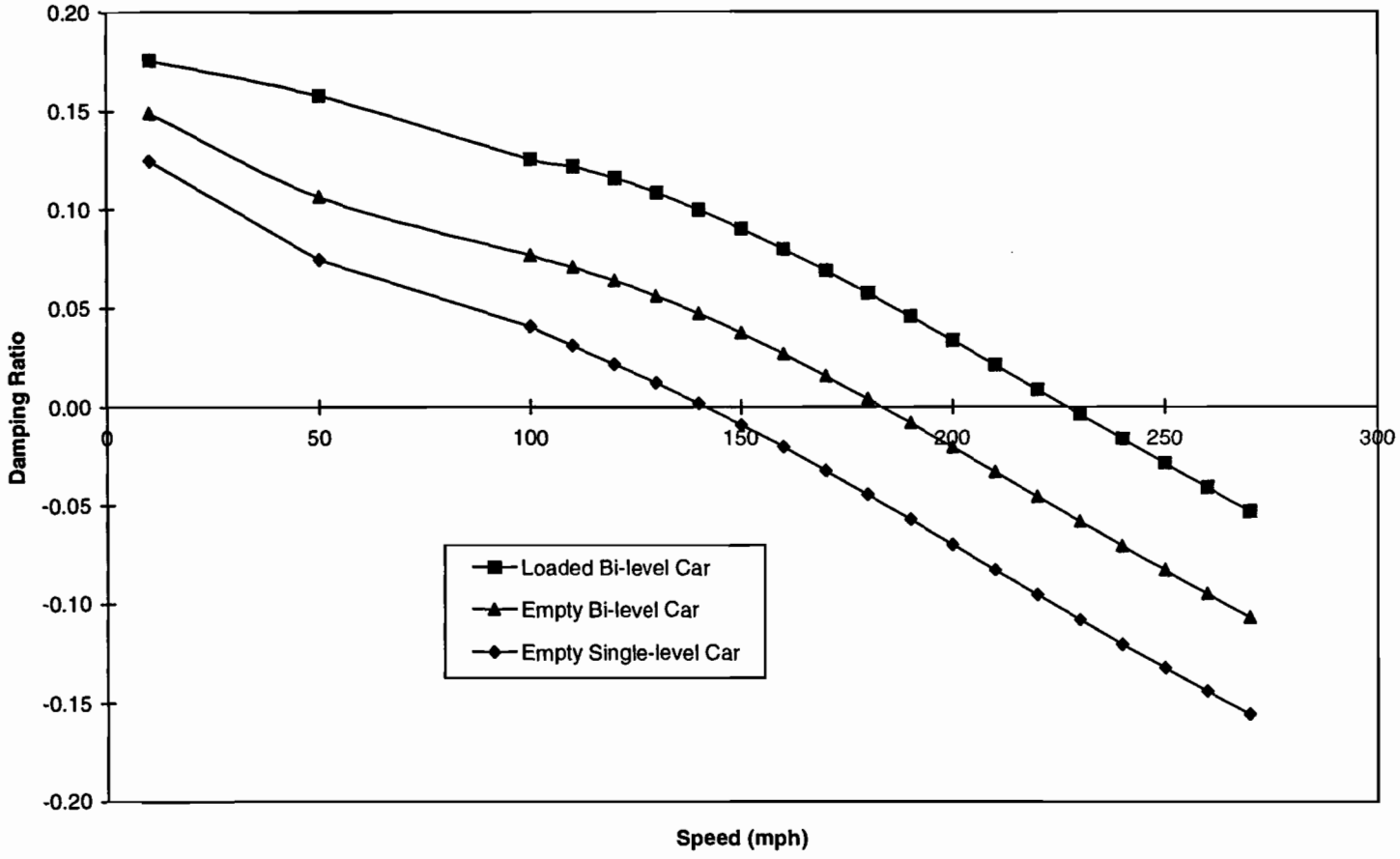

Figure 3-9. Truck hunting damping ratio versus speed (conicity = 0.05, non-equalized trucks)

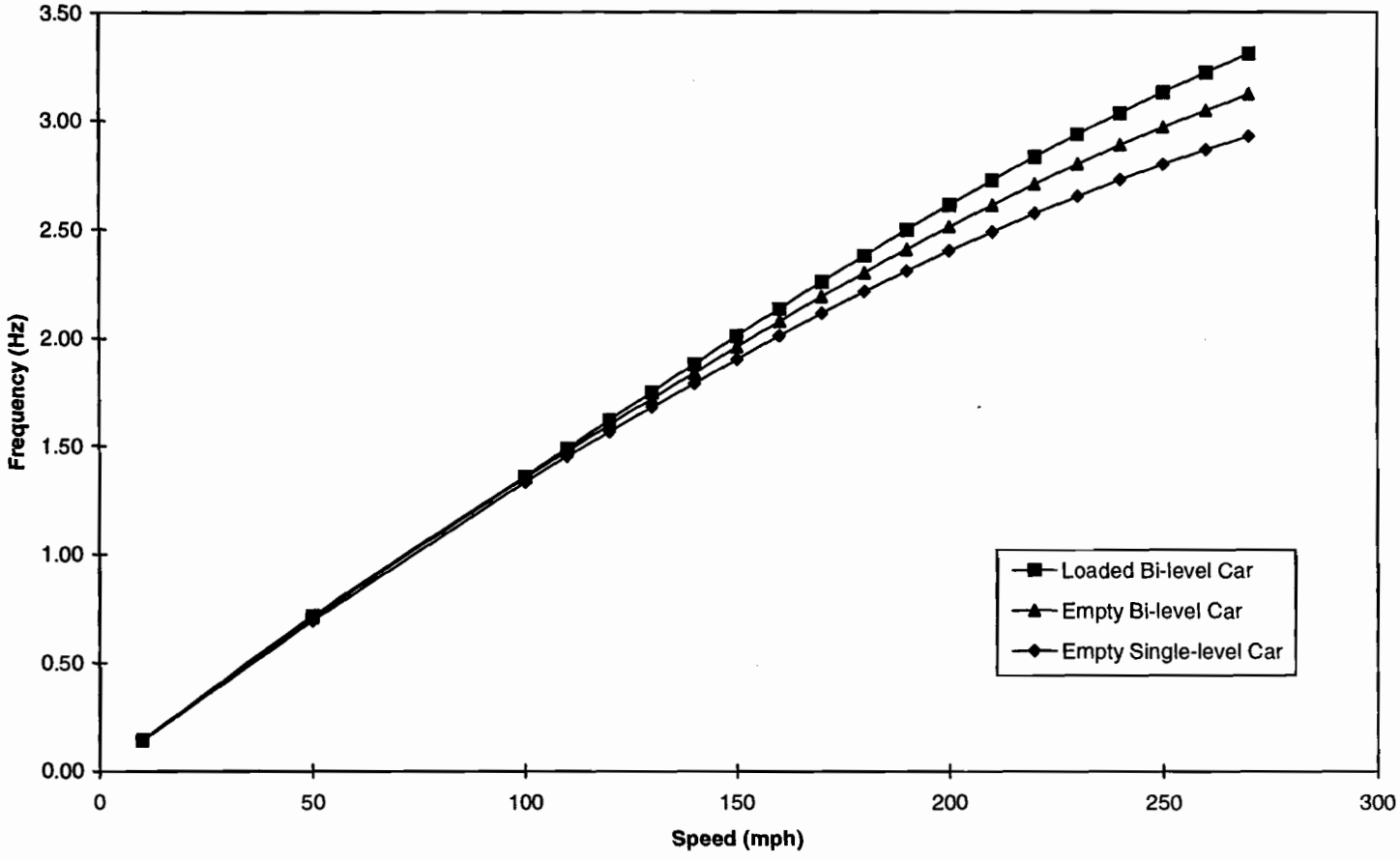

Figure 3-10. Truck hunting frequency versus speed (conicity = 0.05, non-equalized trucks)

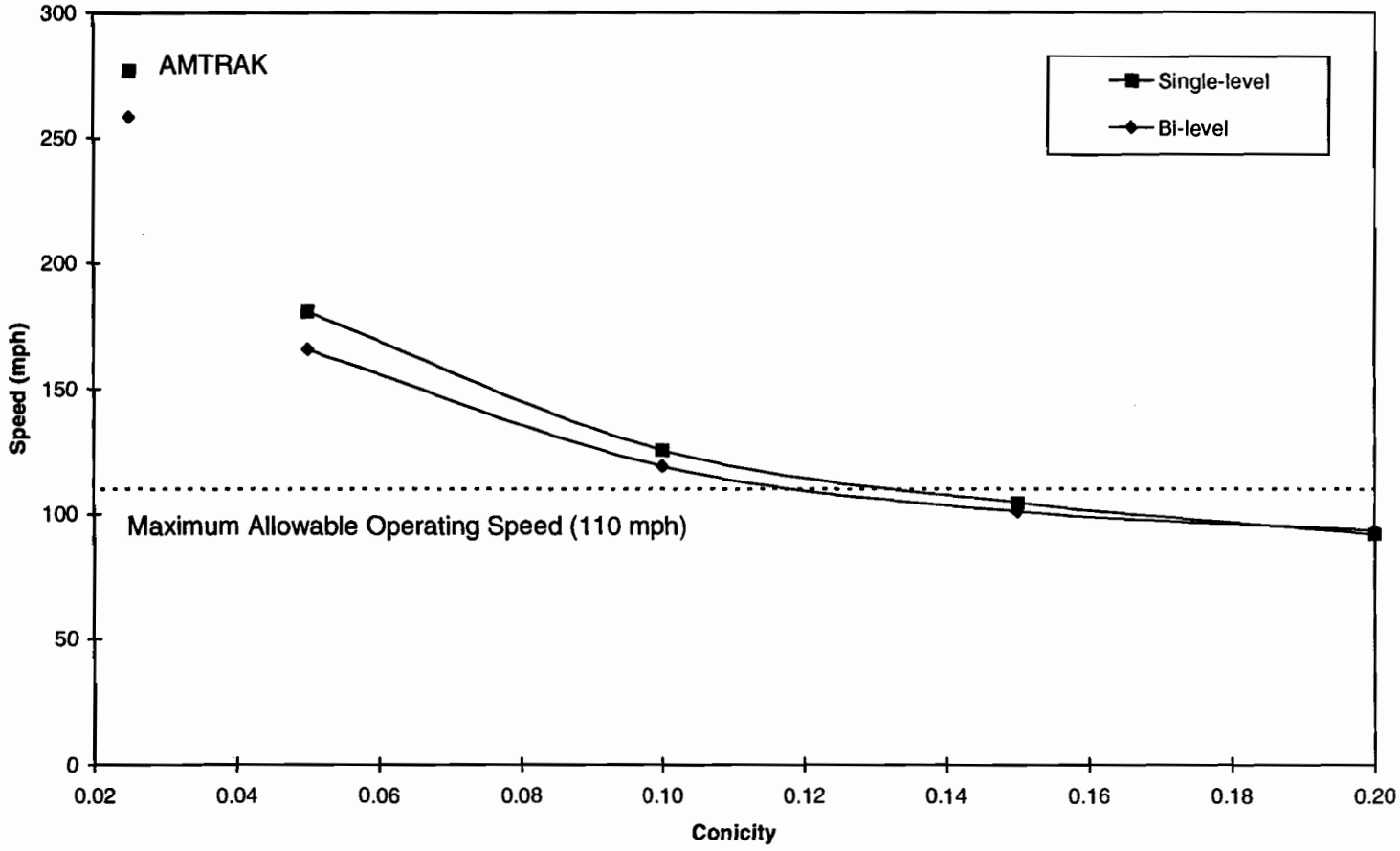

Figure 3-11. Critical speed versus conicity (equalized trucks, empty cars)

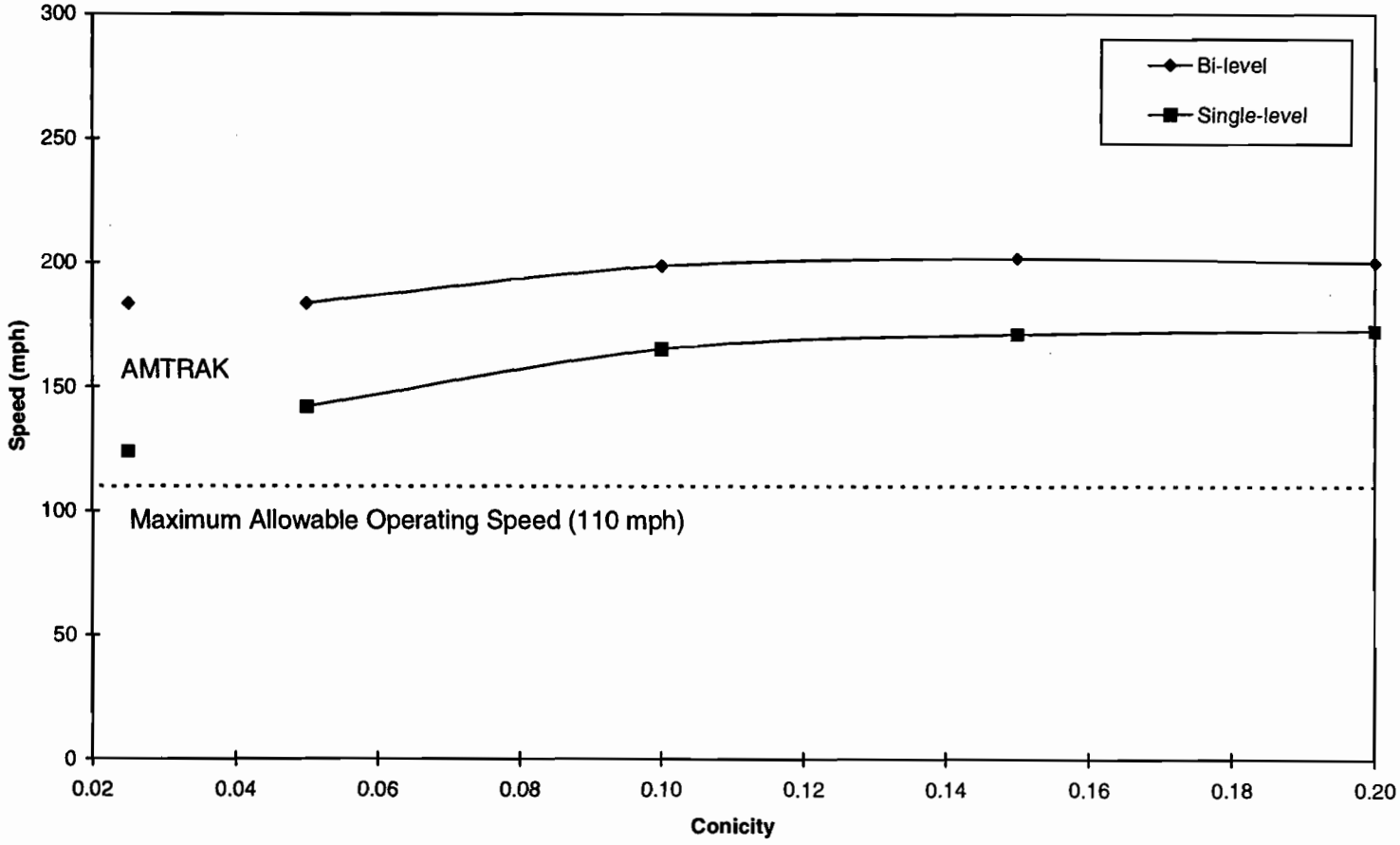

Figure 3-12. Critical speed versus conicity (non-equalized trucks, empty cars)

Table 3-1. Comparison of critical speeds between OMNISIM and NEWHUNT for the empty bi-level car on hard track

Truck Type	Profile Name	OMNISIM Crit Speed (mph)	NEWHUNT Crit Speed (mph)	Effective Conicity
Equalized	A1B	120 (155)[1]	150	0.06
Equalized	M1B	260	262	0.023
Equalized	W1B	105	107	0.12
Non-equalized	A1B	185	185	0.06
Non-equalized	M1B	160 to 180[2]	159[3]	0.023
Non-equalized	W1B	180	189	0.12

The notes in the table refer to behaviors noticed and shown below.

[1]The comparison of the continuing lateral oscillations following the initiating lateral shift in the rails, for sinusoidal shift amplitudes of 0.25 and 0.1 in. are given in Figures 3-13 and 3-14 for the car with equalized trucks. For an initial shift of 0.25 in. at 120 mph this car can be seen to hunt; yet for a shift of 0.1 in., a speed of 150 mph is just below the onset of hunting. The difference is significant and is clearly due to the nonlinearity of the contact geometry.

[2,3]Figure 3-15 shows the long wavelength response of the wheelset to the initiating shift in the OMNISIM results. The frequency is about 1.25 Hz and is clearly one of the body modes. The body motions show it to be an upper center roll mode which is lightly damped. In a long OMNISIM run there is a slight yaw coupling which shows as a cyclic beat frequency between the trucks. These results generally correspond well with the output from NEWHUNT at the same speed which shows the same mode with less body activity.

Table 3-2. Variations in the effective conicities as measured

Profile Label	Nominal Tread Cone Angle	Deduced Effective Conicity	Description
A1B	1:20	0.06	New AAR1B profile on 136 lb/yd rail
M1B	1:40	0.023	Amtrak AAR1B profile on 136 lb/yd rail
W1B	1:20	0.12	Worn AAR1B profile on 136 lb/yd rail

The response of the vehicle and particularly the axle varies with the initiating amplitude leading to the kinematic oscillation. Under these circumstances there may be limit cycles or amplitudes of the lateral oscillation that persist before the flange is contacted. In the case of the equalized truck, a limit cycle was observed for the wheelset oscillating in the pedestal gap. Flange contact itself defines a limit cycle within the flangeway clearance with repeated contact from one side to the other. The particular amplitude into which the oscillation stabilizes depends on the level of excitation from track misalignment. Variations in the rail gage also cause variation in the effective conicity and the potential for change in vehicle hunting behavior.

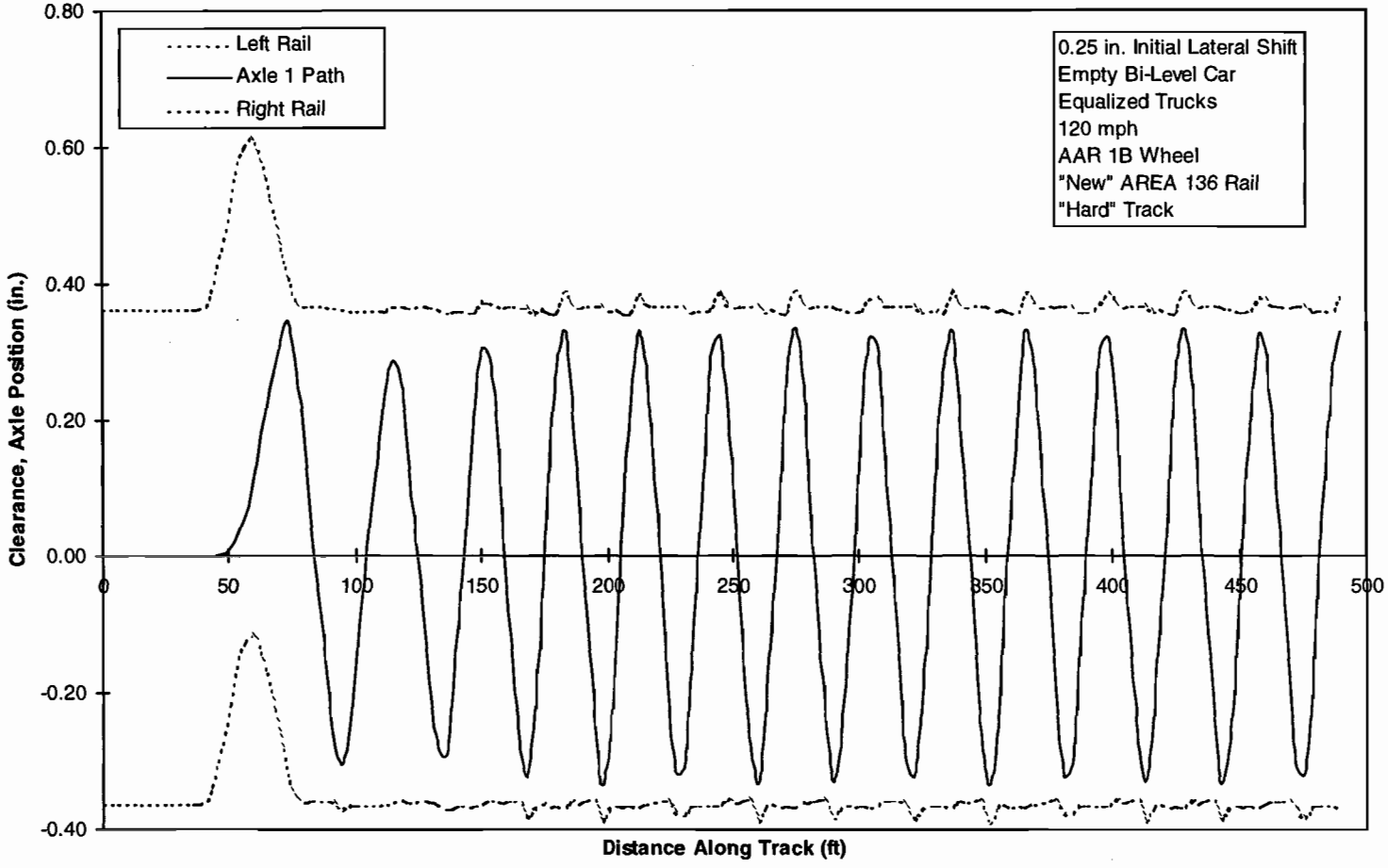

Figure 3-13. Lead axle lateral motion

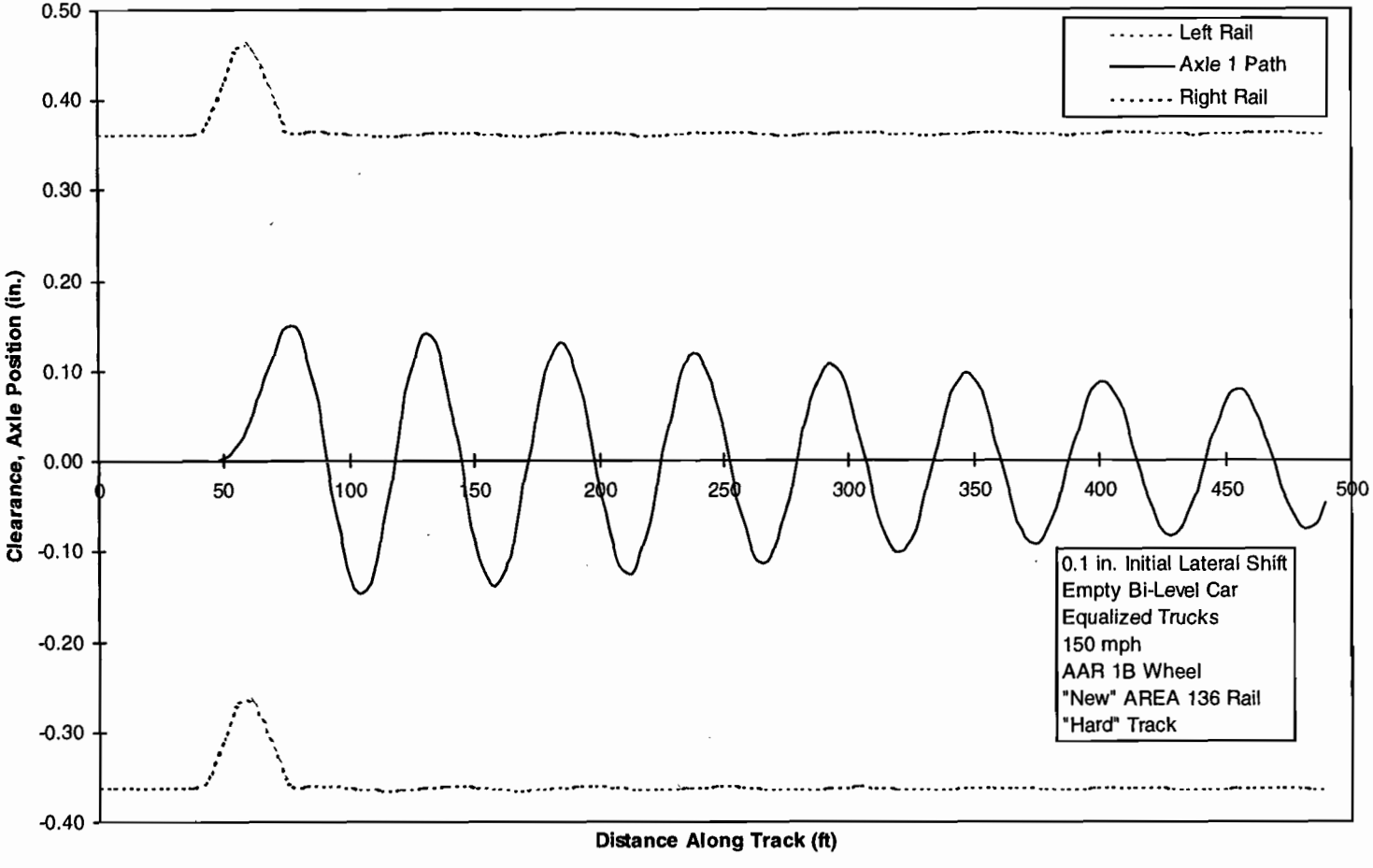

Figure 3-14. Lead axle lateral motion

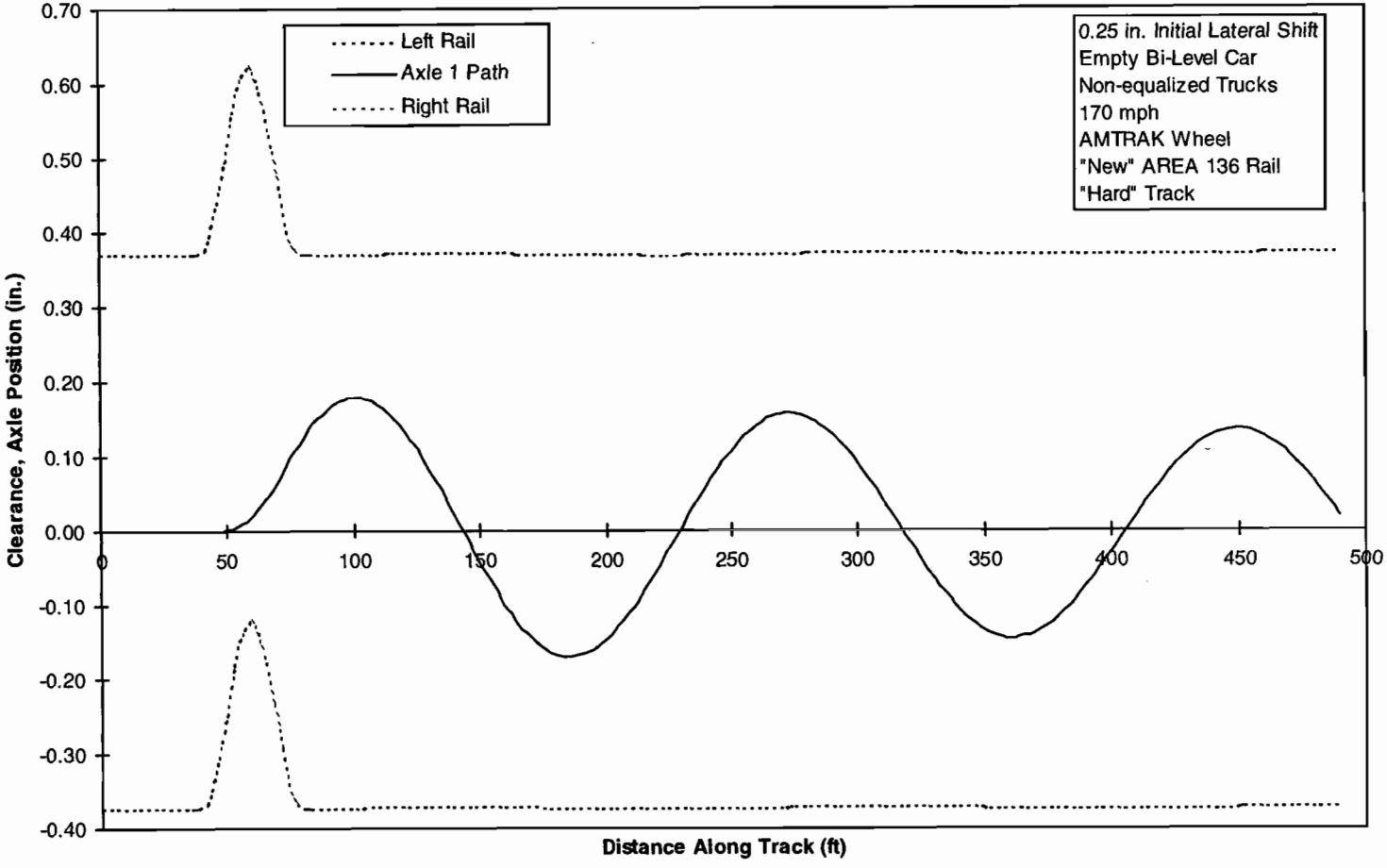

Figure 3-15. Lead axle lateral motion

Table 3-3 provides a summary of the speeds at which these limit cycles were observed for the various cars and cases examined. The lowest limit cycle oscillations are those of the cars with equalized trucks but they showed only a small lateral amplitude. Truck hunting or limit cycles occur at higher speeds well in excess of the operating range. The hunting speeds for the trucks with no equalization are also well above the operating range.

The "soft" track tends to give slightly higher critical speeds for the cars with equalized trucks and the increase in load from empty to loaded has little effect. However, the difference in track is more marked and in the opposite sense, "soft" track gives lower critical speeds, in the car with

Table 3-3. OMNISIM results - vehicle speed at limit cycle initiation

Body	Truck[1]	Prof.[2]	Load	Track	Axle Hunt Speed (mph)	Truck Hunt Speed (mph)
Bi-level	EQ	A1B	Empty	Hard	155	>300[3]
				Soft	175	>300
			Loaded	Hard	155	>300
				Soft	175	>300
		M1B	Empty	Hard	270	>300
				Soft	300	>300
		W1B	Empty	Hard	125	260
				Soft	145	>300
Bi-level	NE	A1B	Empty	Hard	n/a	190
				Soft	n/a	>300
			Loaded	Hard	n/a	215
				Soft	n/a	270
		W1B	Empty	Hard	n/a	185
				Soft	n/a	260
Single-level	EQ	A1B	Empty	Hard	155	260
		W1B			125	235
Single-level	NE	A1B	Empty	Hard	n/a	165
		W1B			n/a	160

NOTE - Limit Cycle Amplitudes were consistent with:
For Equalized truck axle - Contact with frame pedestal.
For Equalized truck - Contact of the rail with the wheel flange.
For Non-Equalized truck - Contact of the rail with the wheel flange.

[1] EQ - Equalized Truck; NE - Non-equalized Truck.

[2] A1B - New AAR 1B Std (1/20) on new 136 lb/yd rail.
M1B - Amtrak AAR 1B (1/40) on new 136 lb/yd rail.
W1B - Worn Tread on AAR 1B on new 136 lb/yd rail.

[3] No Speeds greater than 300 mph were run.

non-equalized trucks. For this car, the increase in load increases the critical speed on "hard" track slightly but decreases it on "soft" track. It is clear from these results, as it is in the examination using linear analysis, that the non-equalized truck has parameters which provide near maximum critical hunting speed for certain wheel and track variables. However, the body modes at these high speeds are not fully developed and should be treated with caution.

While a complete set of runs have been made to identify all unstable behaviors up to the hunting speed for all the car and track systems identified in Section 2, many of the results are of little consequence. However, certain particular cases and variables are now examined which describe the more important vehicle behaviors discovered. Since none of the cases suggested problems in the normal speed range, the speeds at the behaviors of interest discussed are high and would not be expected to be reached in normal operation.

Figures 3-16 to 3-21 show the behavior on "hard" track at 160 mph of the base bi-level car with equalized trucks, just above the onset of wheelset oscillations but well below any truck frame instability. The low amplitude lateral oscillation of the two wheels on each axle of the lead truck are shown in Figures 3-16 and 3-17. The lateral amplitude of this subcritical limit cycle at the rail is just under 0.1 in., well below flange contact, at a wavelength close to 55 ft. This is the theoretical wavelength for an unrestrained wheelset with a pure conicity of 1/20. The individual wheel L/V ratios are also small as shown in Figures 3-18 and 3-19 for the same axles. Finally for this case, the longitudinal motion in the pedestal clearance is given in Figures 3-20 and 3-21 for the two leading axles. The clearance in the pedestal is ±0.031 in. and is only taken up fully at the initial response for the 160 mph run shown. The stable limit cycle amplitude in this motion is just under 0.02 in.

Results for the bi-level car with non-equalized trucks at a speed of 220 mph, sufficient to give full flange contact, under otherwise similar conditions, are given in Figures 3-22 to 3-25. The lateral axle displacements in the flangeway clearance are given in Figures 3-22 and 3-23 and the wavelength appears to be slightly longer than the unrestrained wheelset at nearly 60 ft, due to their horizontal connection to the frame, which overcomes the effect of the increased conicity at the flanging amplitude. The L/V values for the individual wheels on each axle in Figures 3-24 and 3-25 are small and nowhere close to indicating a potential for derailment. Hunting needs to be very severe with other influences not seen here to cause wheel climb.

Figure 3-26 shows the lead lateral wheelset response for the same car when running at 190 mph, but with the tread conicity reduced to the 1/40 used in the Amtrak standard. There appears to be a stable limit cycle at less than full flange contact. This is somewhat misleading as the amplitude varies significantly with speed over a relatively wide range. It is the frequency which is of interest here. Unlike the previously observed limit cycles, this one has a wavelength of close to 180 ft or a frequency at the speed of 190 mph shown of about 1.7 Hz. This frequency is closer to those of the rigid body than that of the previously noted kinematic wavelength. The rigid body lateral, roll and yaw responses are given in Figures 3-27, 3-28 and 3-29 respectively. From these it may be deduced that the complex mode of behavior is that of a combined upper center roll with yaw. This mode is often referred to as the sway mode. In short, the low wheelset conicity has lead to low amplitude body hunting at this speed which is well above the normal operating range.

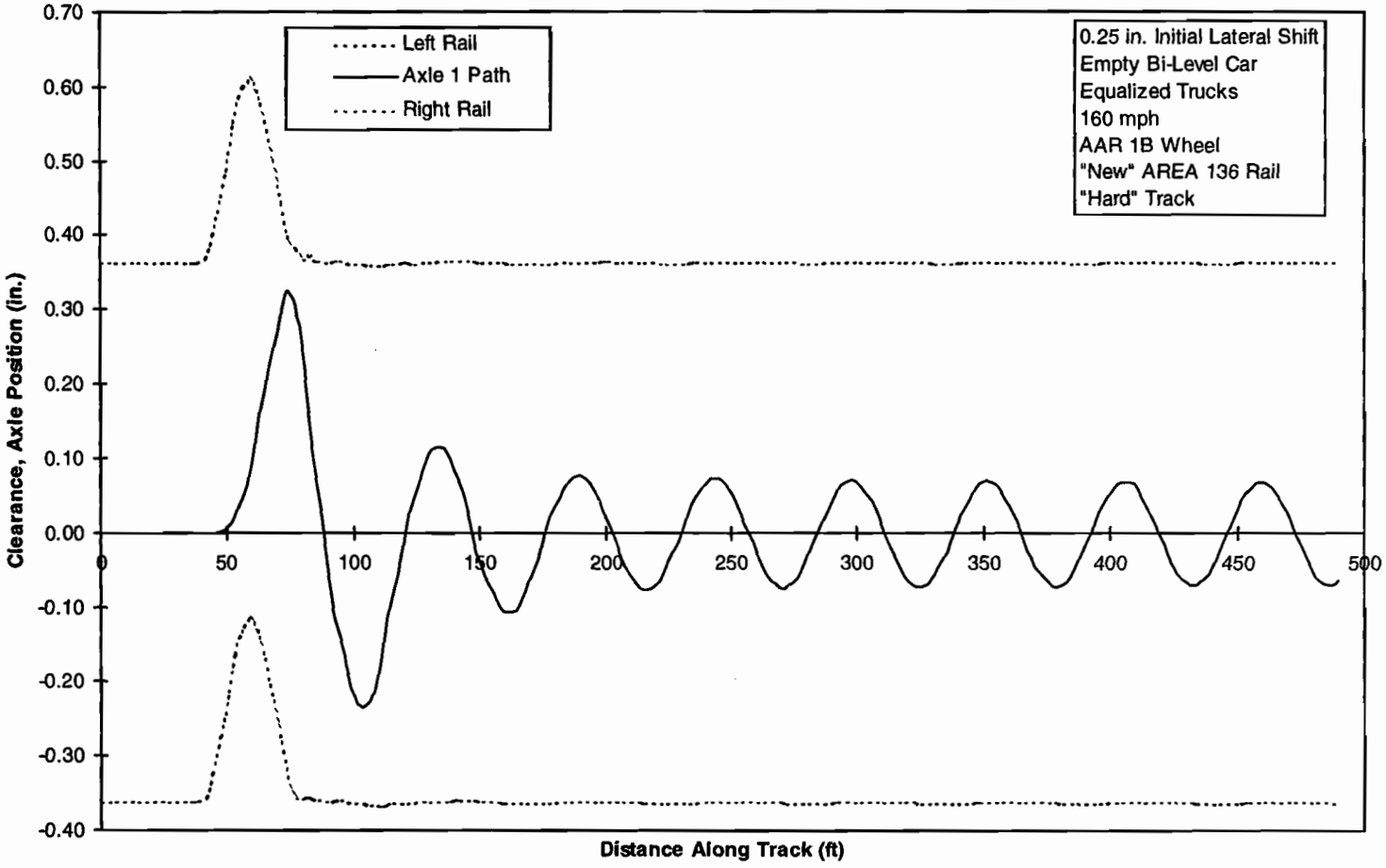

Figure 3-16. Lateral motion of lead axle

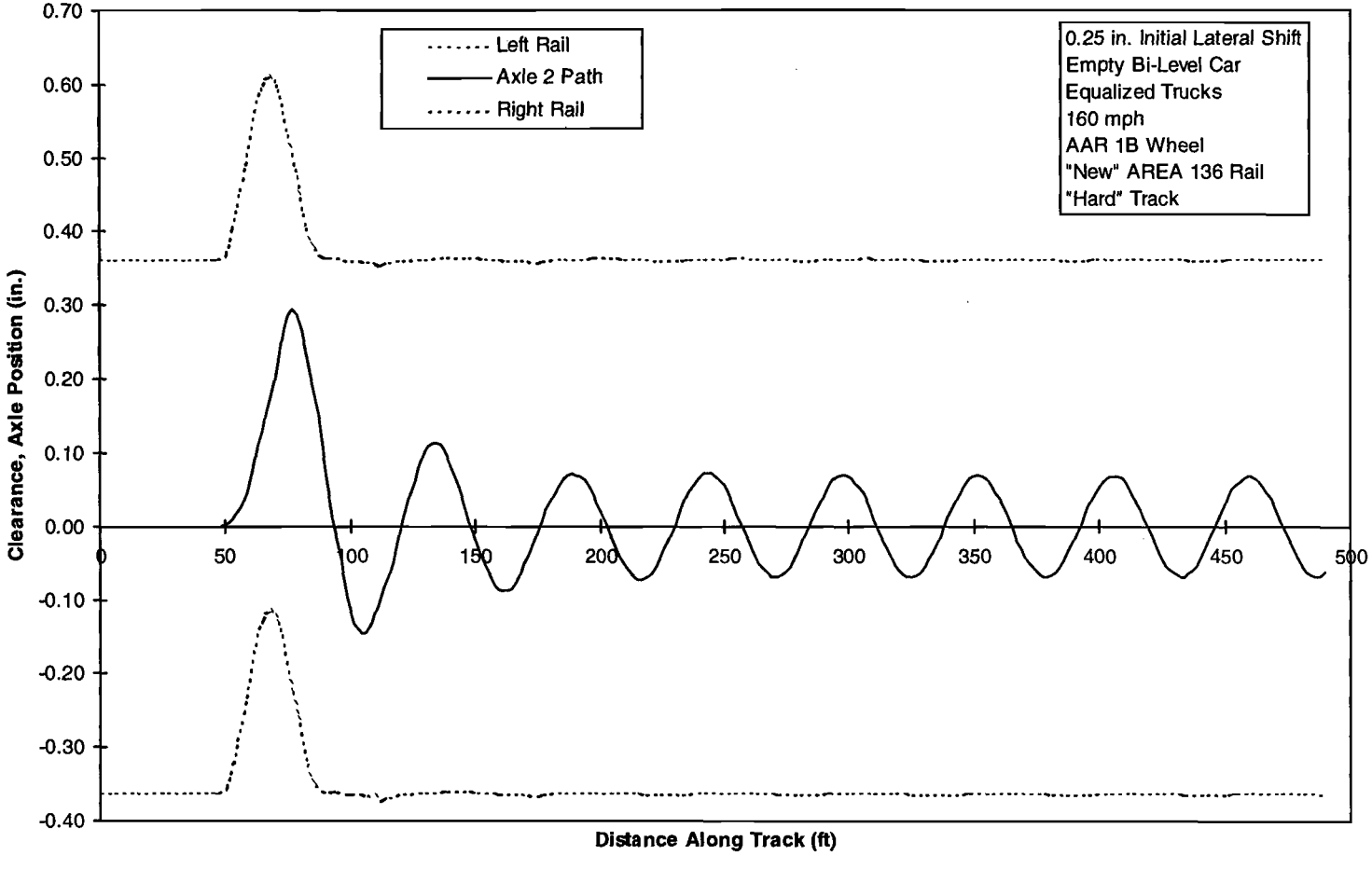

Figure 3-17. Lateral motion of second axle

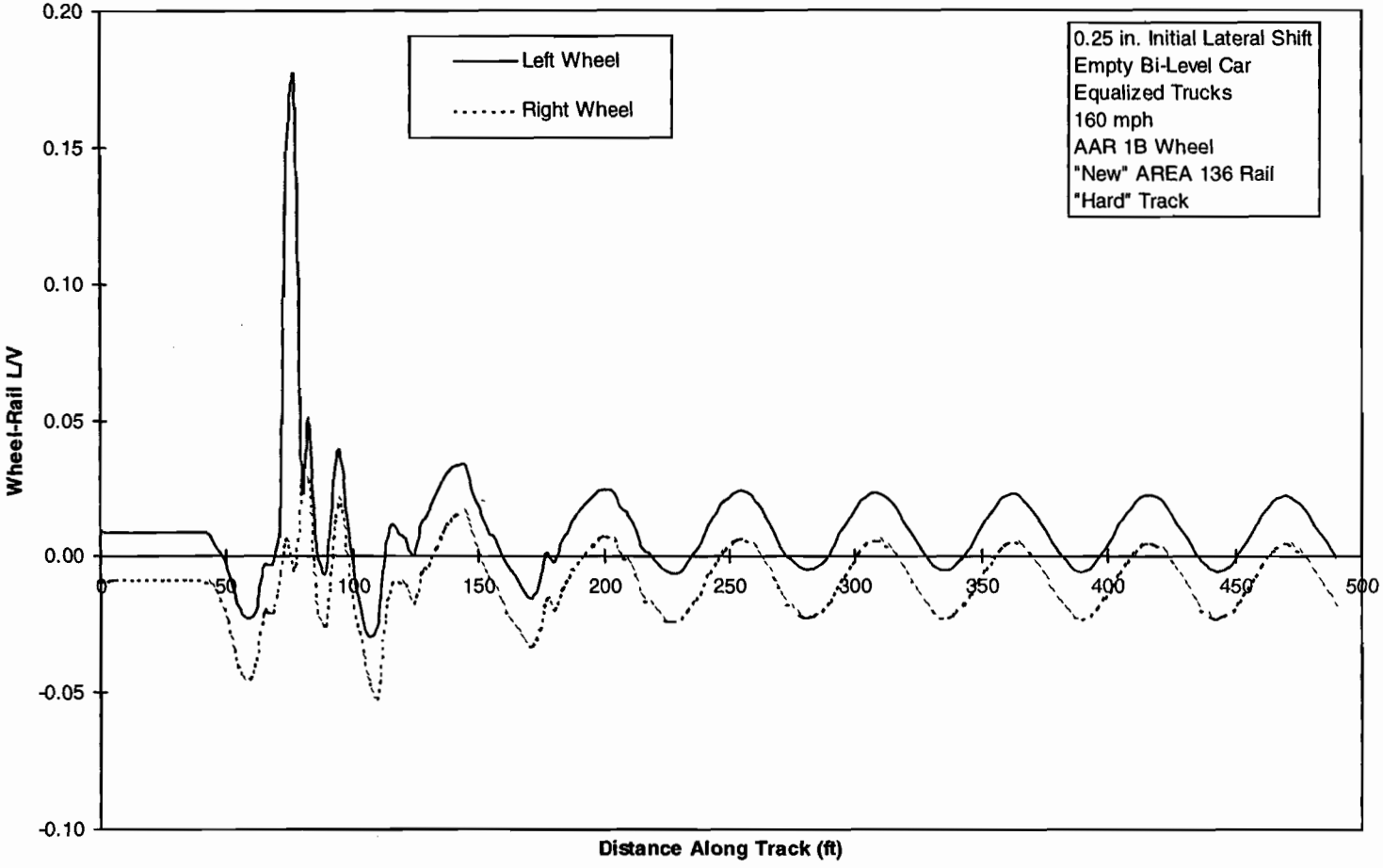

Figure 3-18. L/V ratios on individual wheels of lead axle

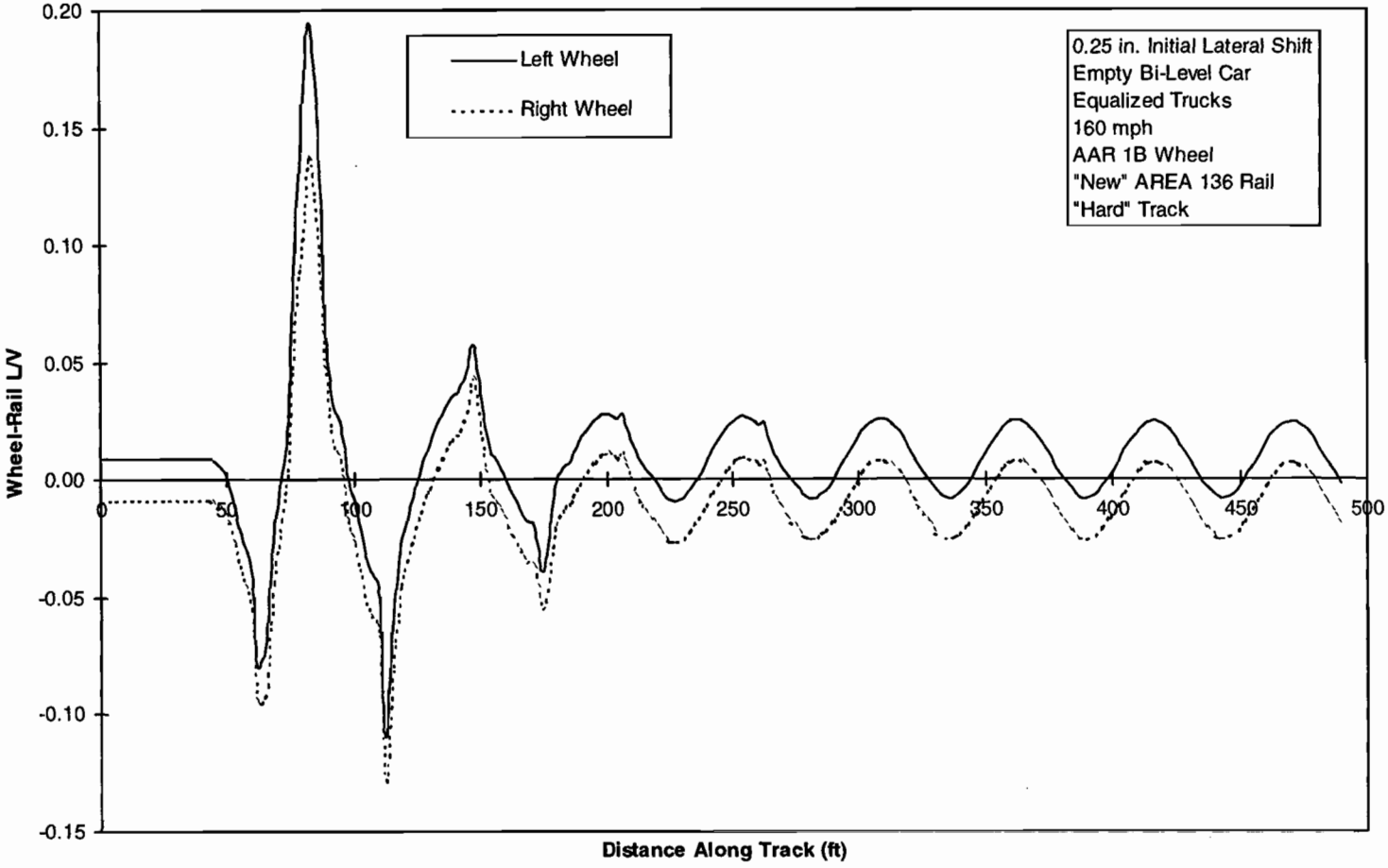

Figure 3-19. L/V ratios on individual wheels of second axle

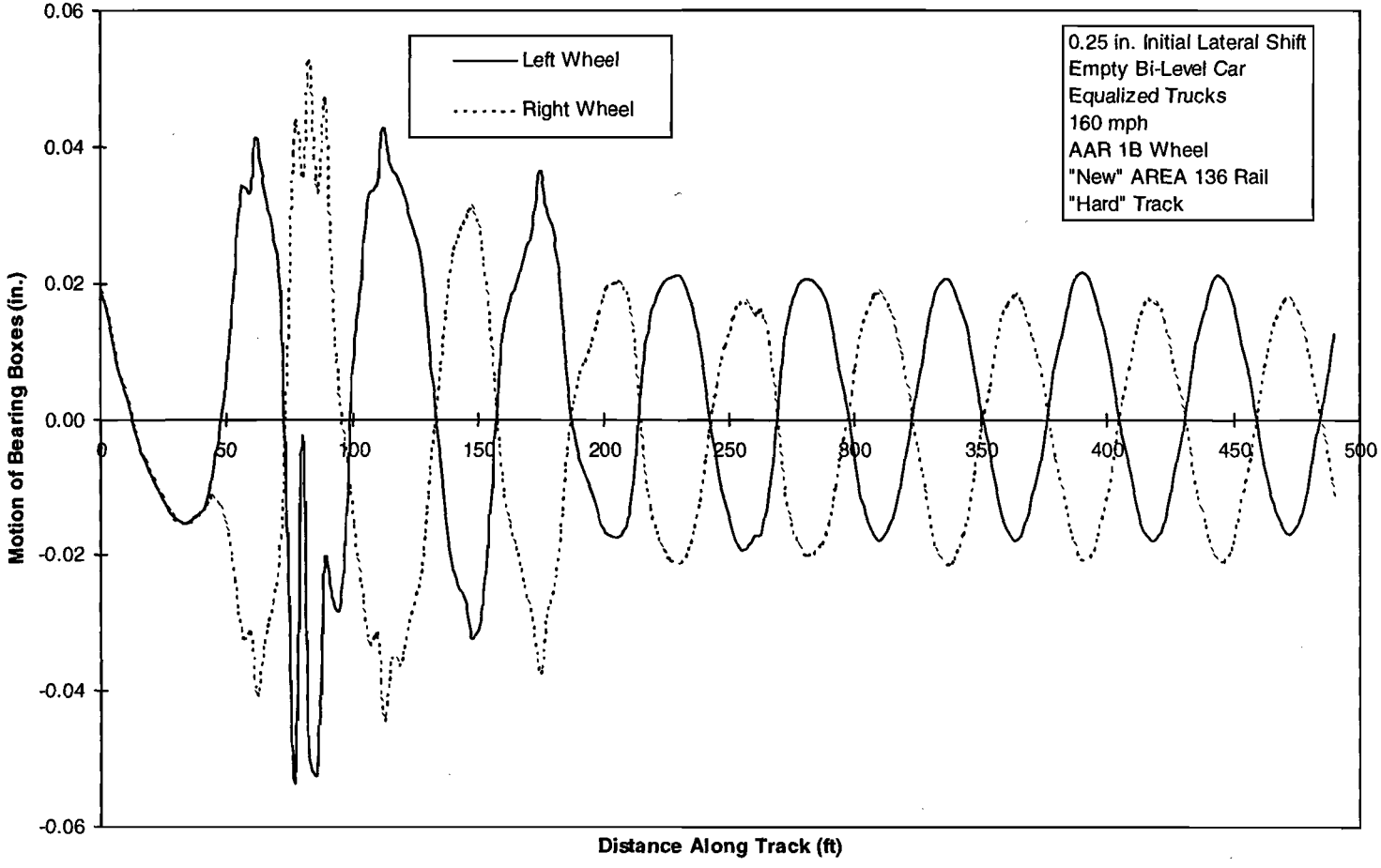

Figure 3-20. Motion of bearing boxes in pedestal clearance of lead axle

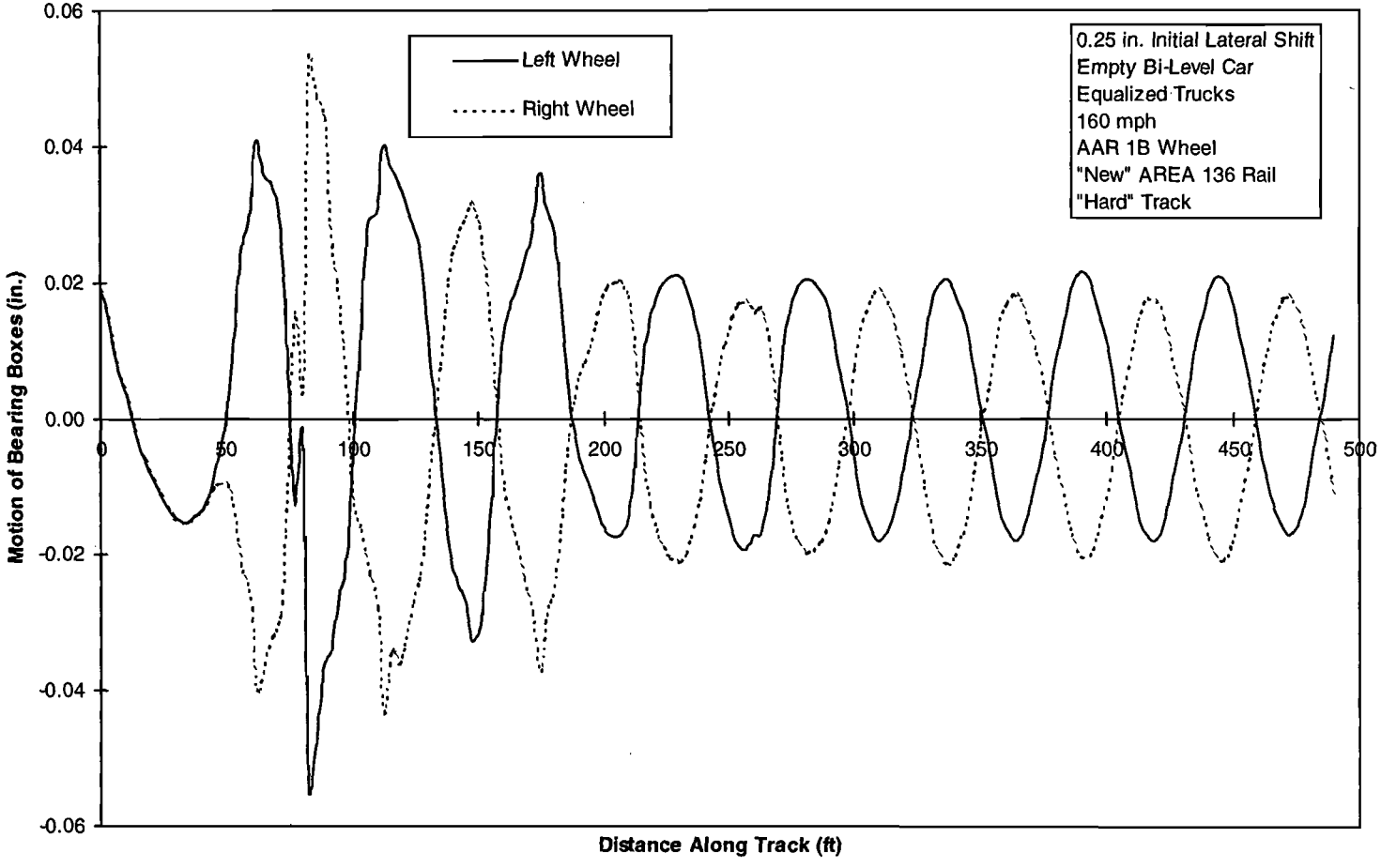

Figure 3-21. Motion of bearing boxes in pedestal clearance of second axle

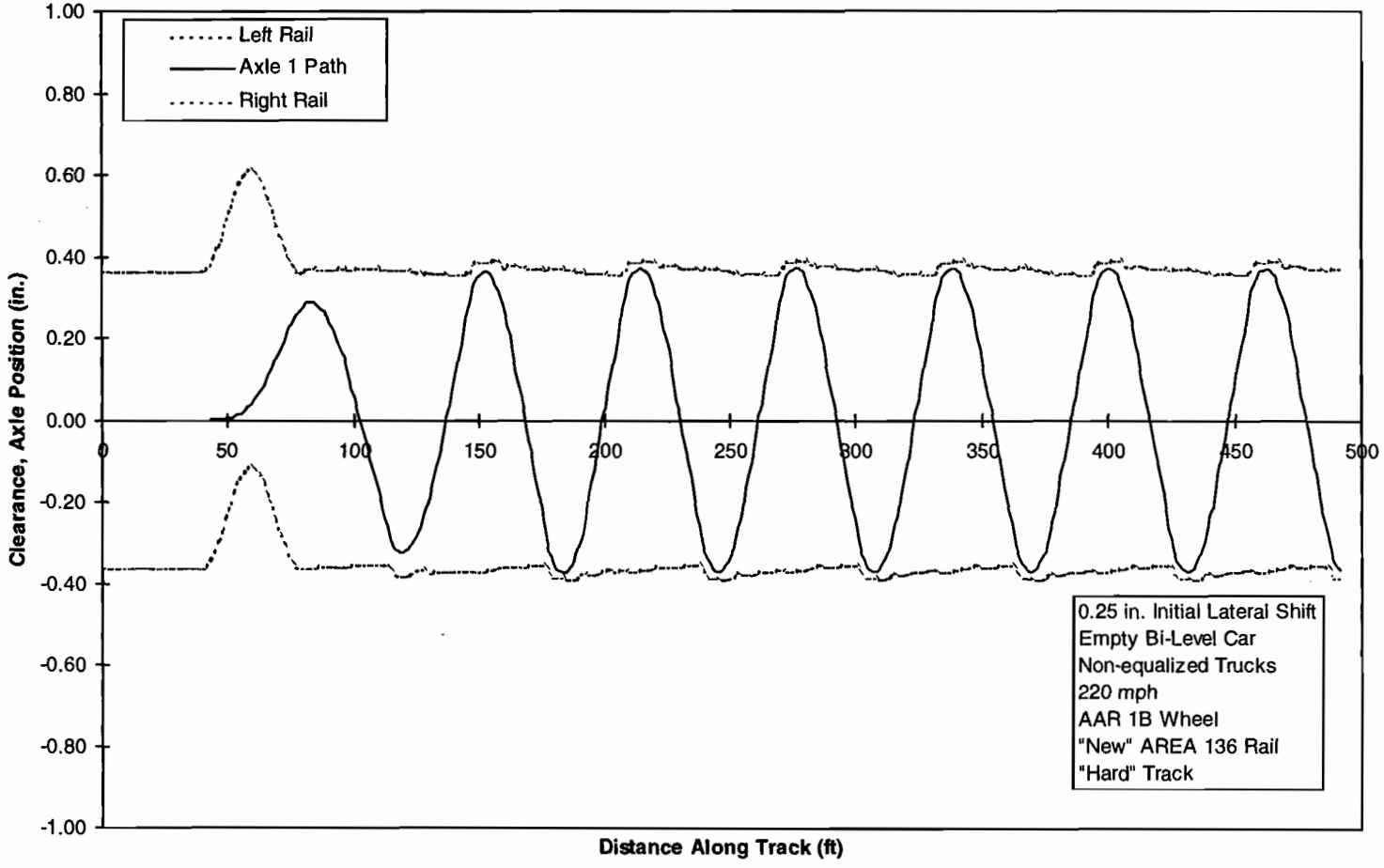

Figure 3-22. Lateral motion of lead axle

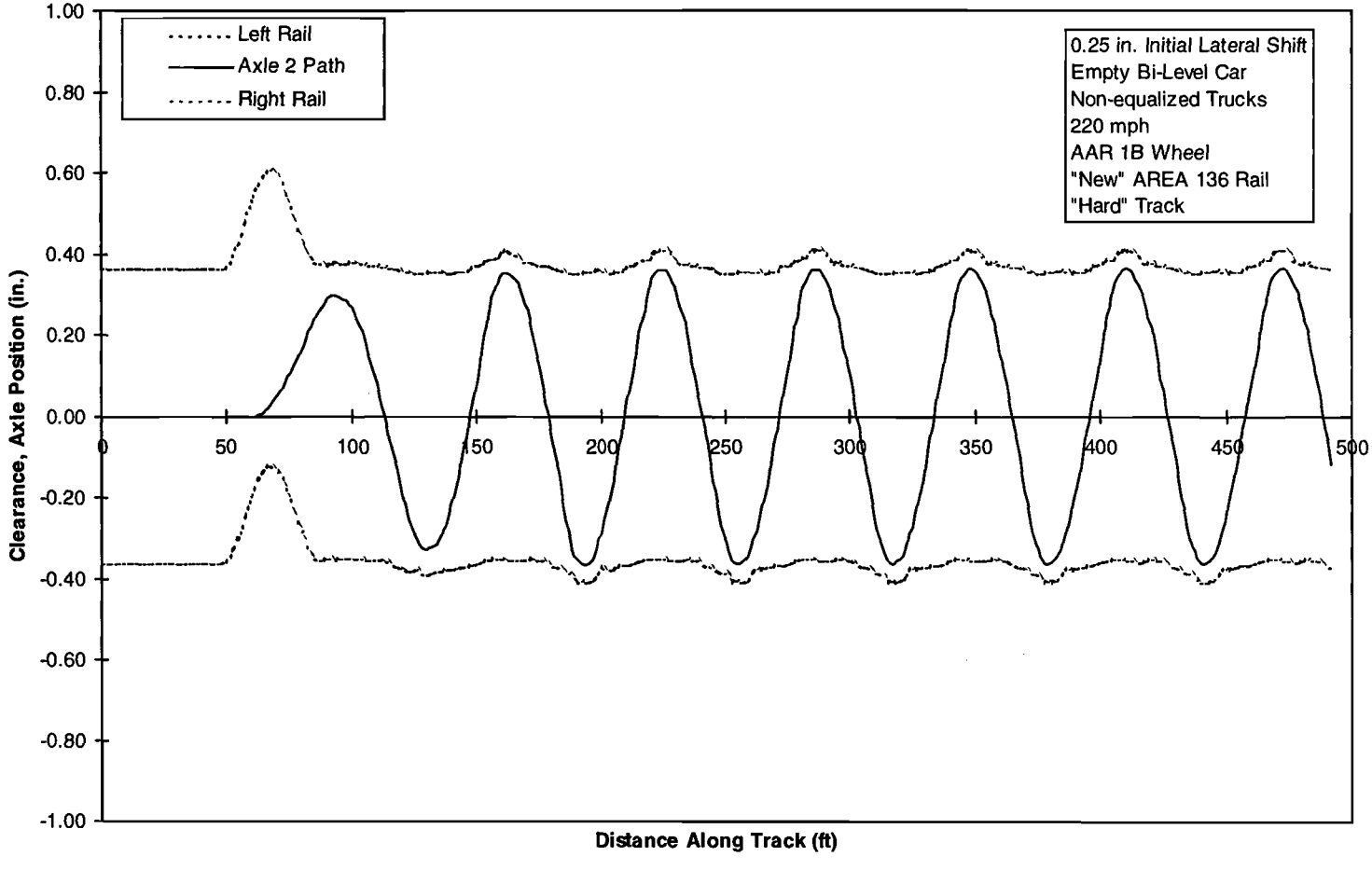

Figure 3-23. Lateral motion of second axle

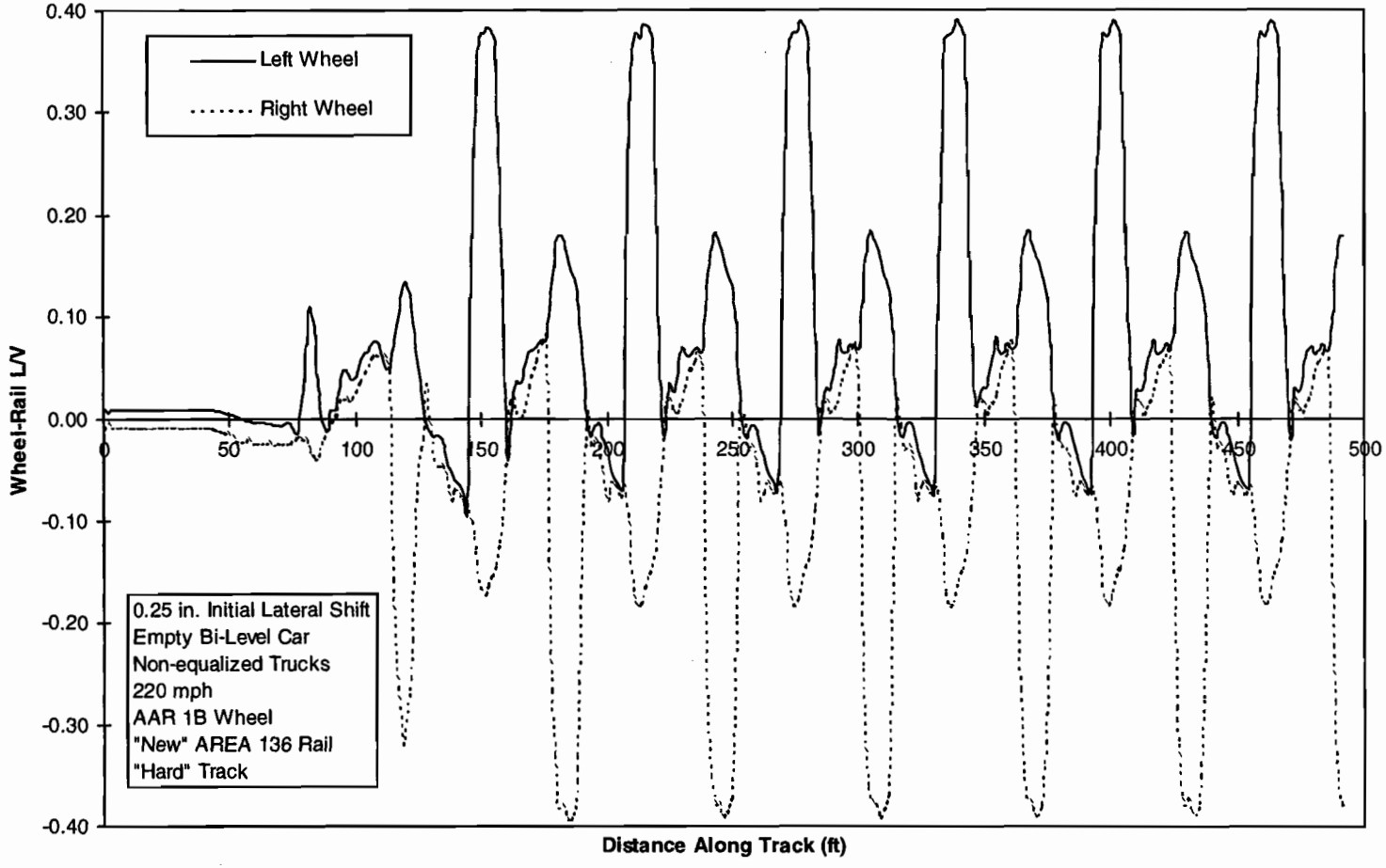

Figure 3-24. L/V ratios on individual wheels of lead axle

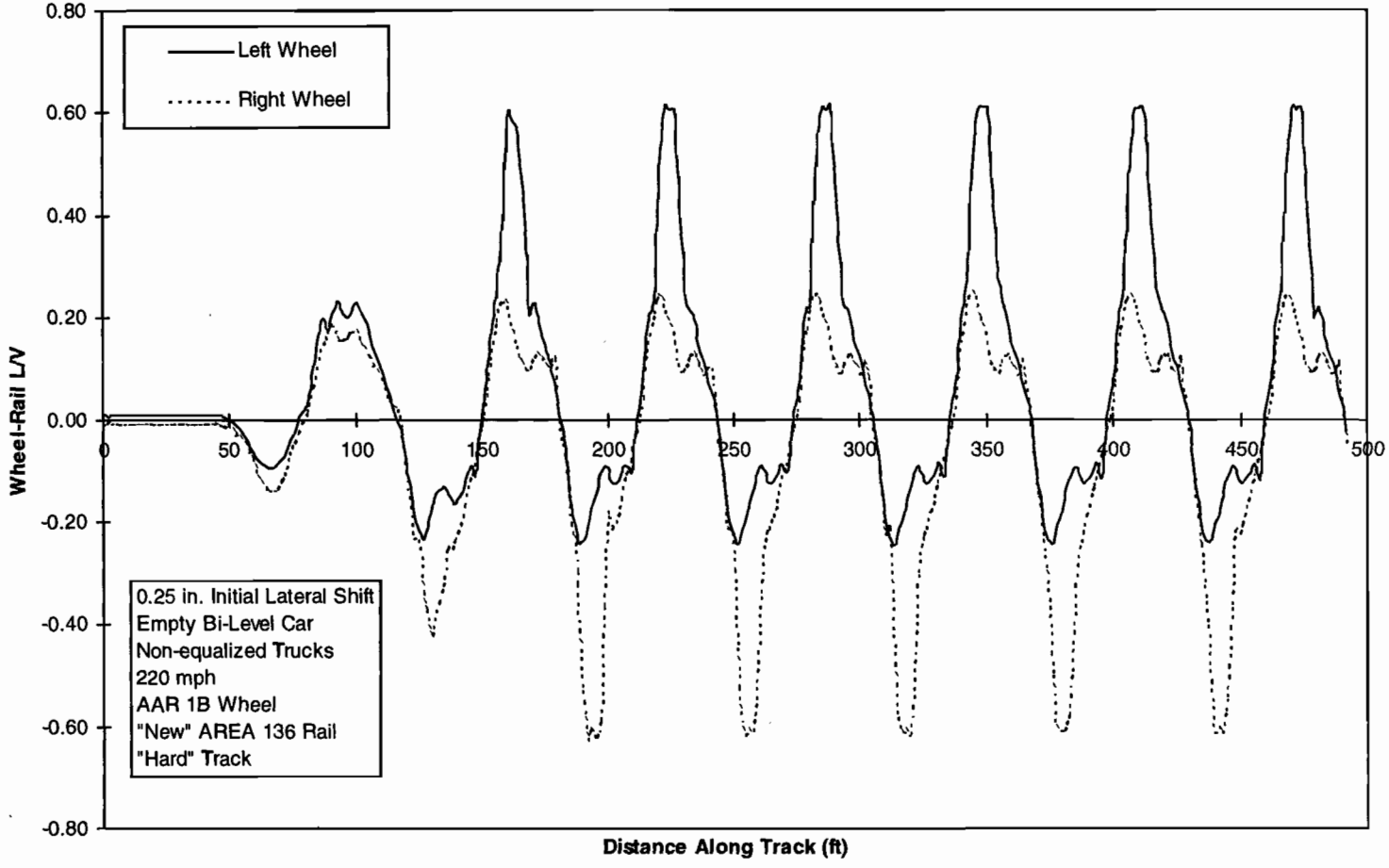

Figure 3-25. L/V ratios on individual wheels of second axle

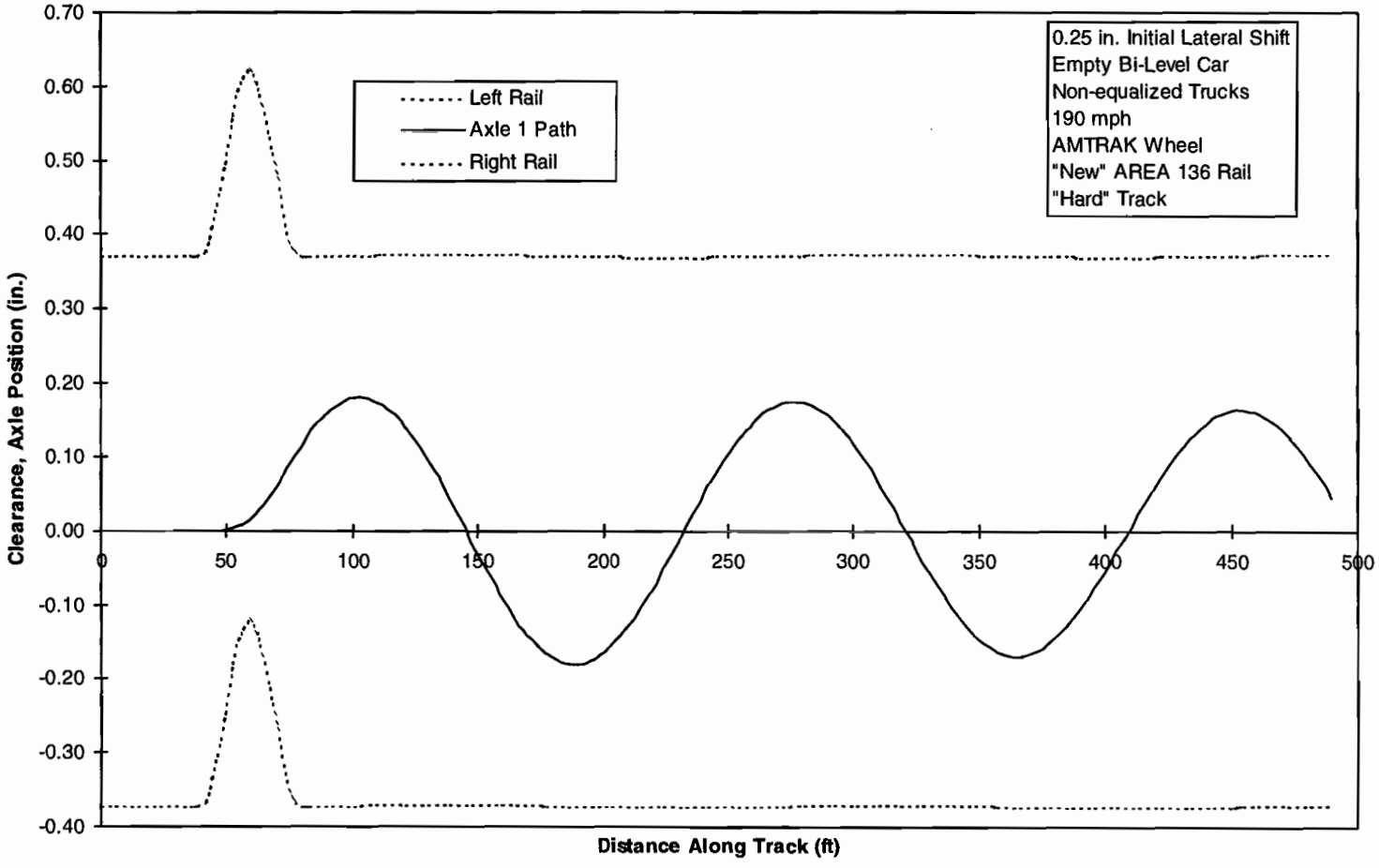

Figure 3-26. Lateral motion of lead axle

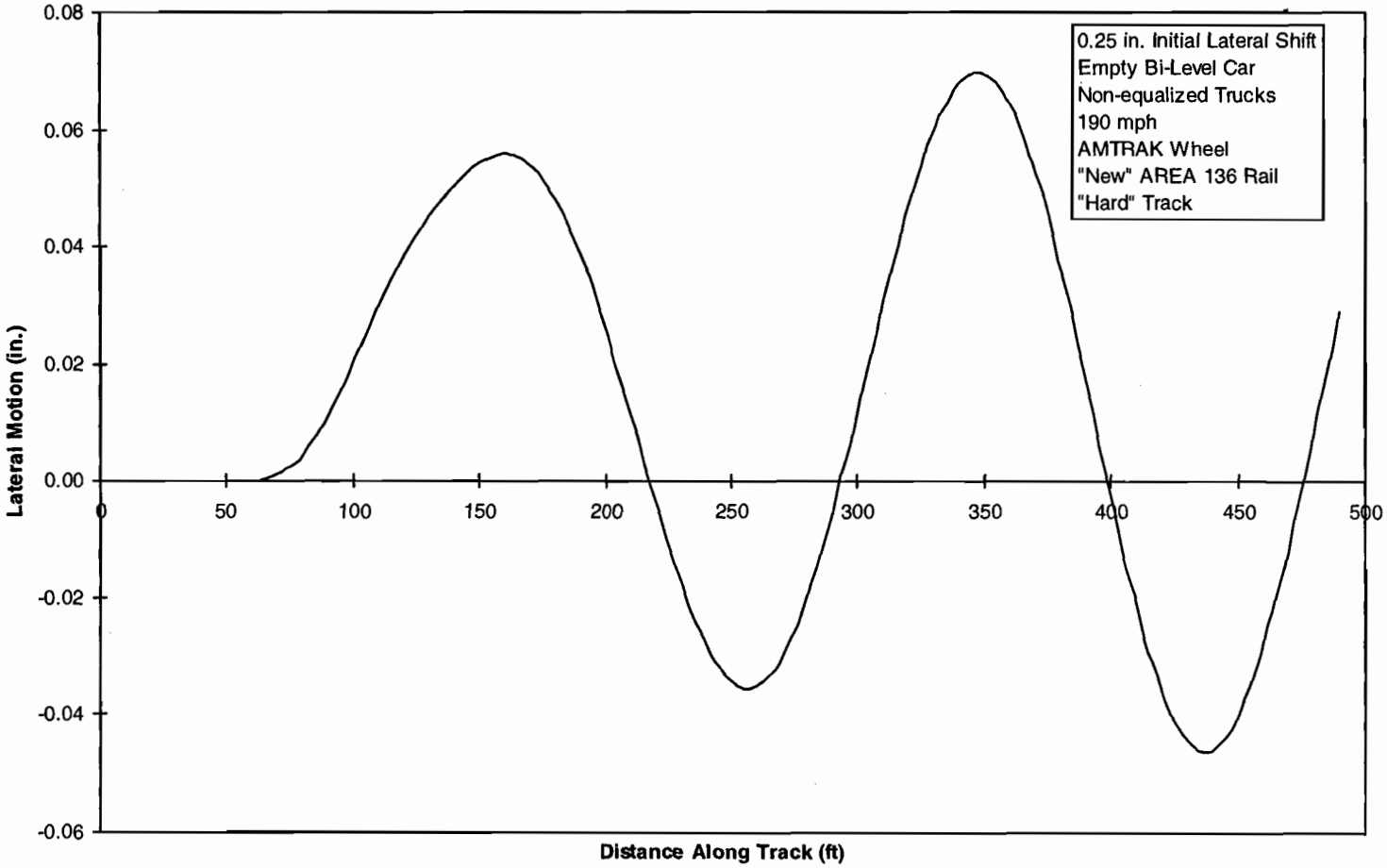

Figure 3-27. Lateral motion of car body

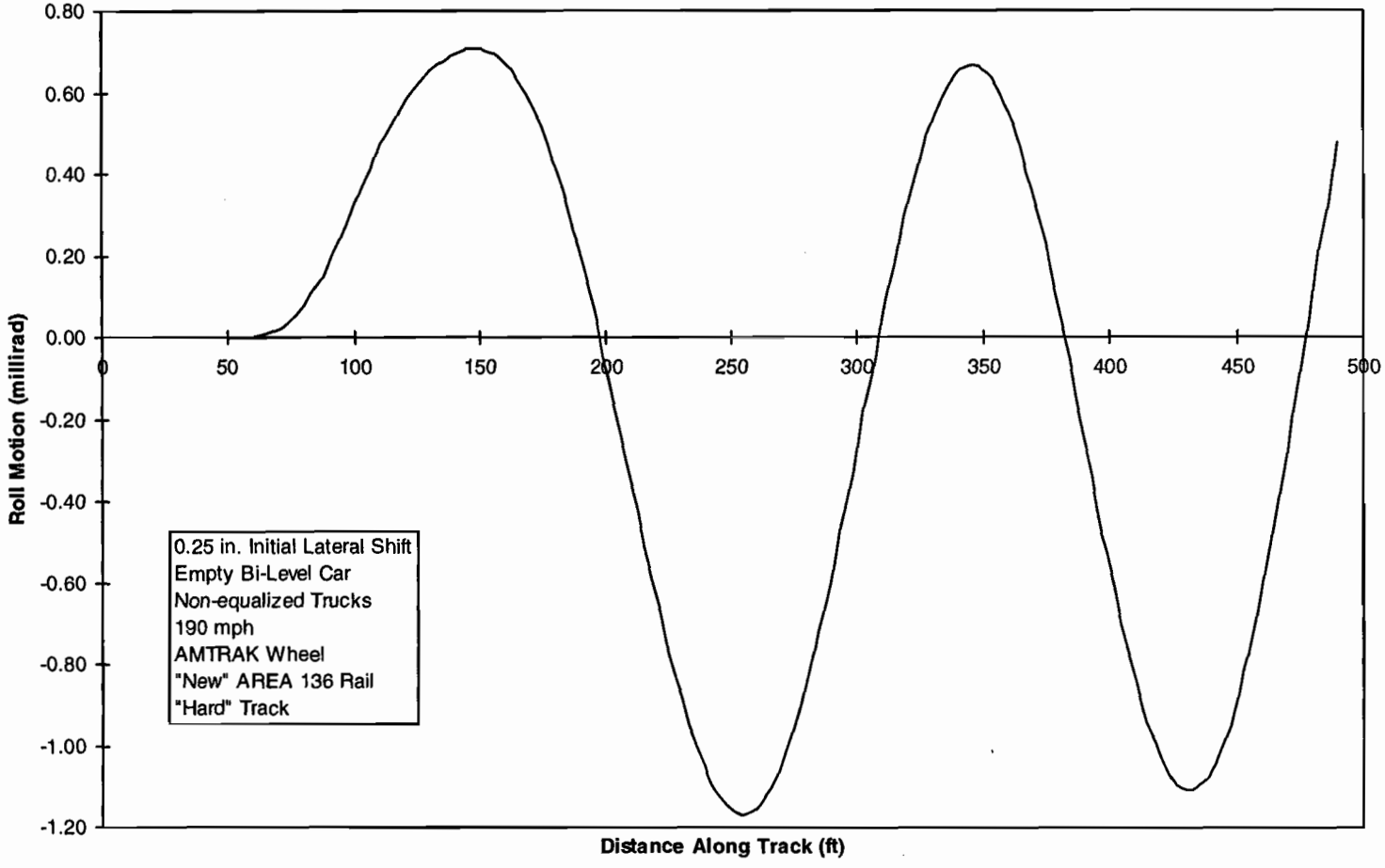

Figure 3-28. Roll motion of car body

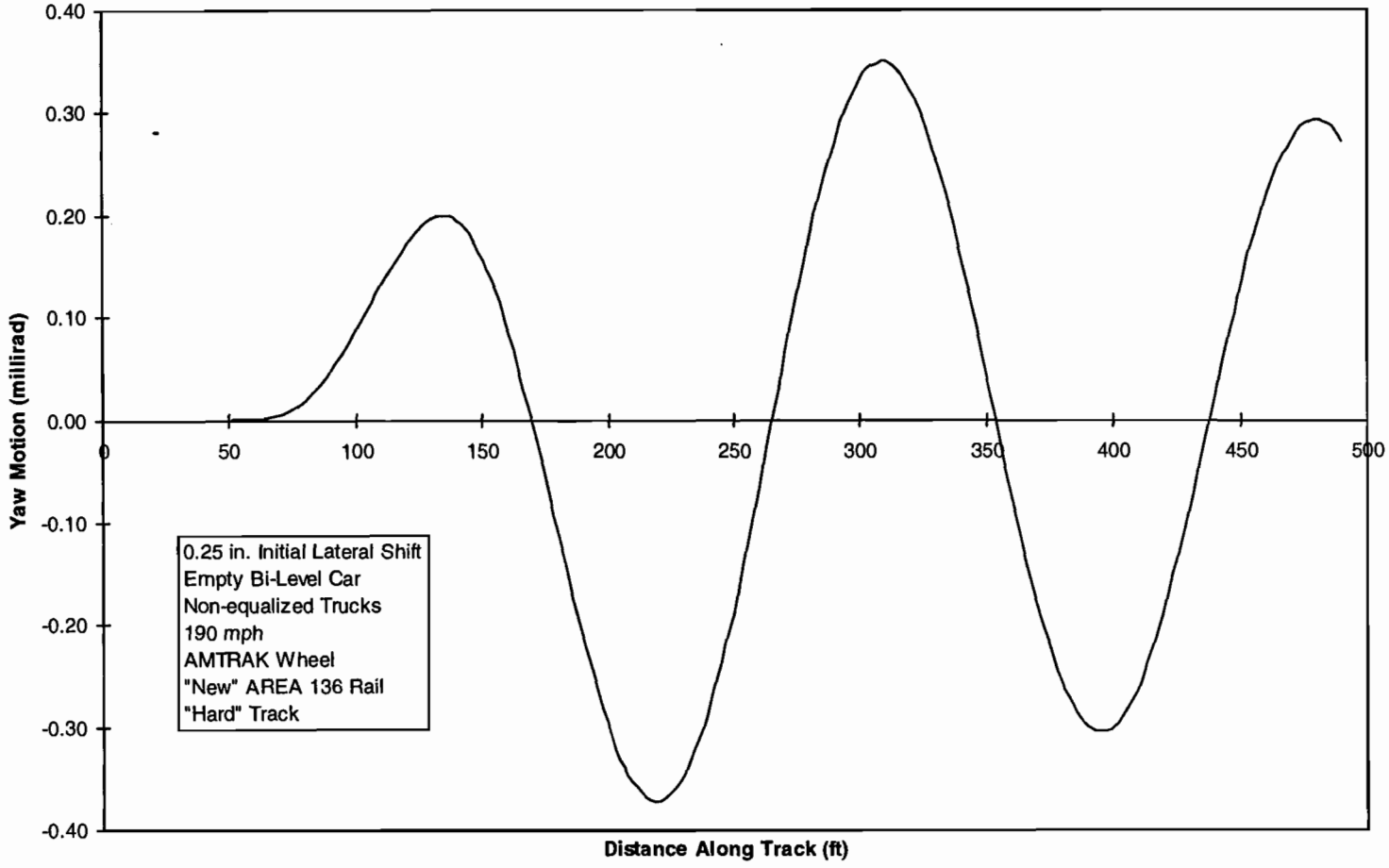

Figure 3-29. Yaw motion of car body

The response of the single-level car with AAR1B wheel profiles and non-equalized trucks at 140 mph is shown in Figures 3-30 to 3-33. This speed is just below that identified as critical, and shows the decaying lateral oscillation and small decreasing L/Vs. This is the vehicle with the lowest critical speed simulated. It is stable to speeds well above the present operating range and the results do not suggest a problem.

The results for the single-level car with equalized trucks, given in Figures 3-34 to 3-39, show the same low amplitude limit cycle of the wheelsets in the pedestal clearance at 200 mph as had been seen and discussed in the bi-level at 160 mph. At this higher speed, the impact with the pedestals are greater and continue into the stable limit cycle. The resulting L/Vs for the individual wheels are also slightly larger but remain small relative to any unsafe condition.

The final results demonstrate the effect of the "soft" track. The chosen results are for the base car with non-equalized trucks at the top speed investigated of 300 mph. Figures 3-40 to 3-43 show the lead and second axle lateral displacements. More importantly, however, they also show the significant motions of the rails under the wheels which increase during the run duration up to a total peak/peak motion of 1 in. at the lead axle and nearly 2 in. at the second axle, significantly larger than the axle lateral motion. The rail motions seem to be in phase, indicating for this extreme case that the tie is moving on the ballast. Further investigations of the effect of validated track movement at high speed may be desirable but is clearly beyond the range of speeds of importance to commuter cars.

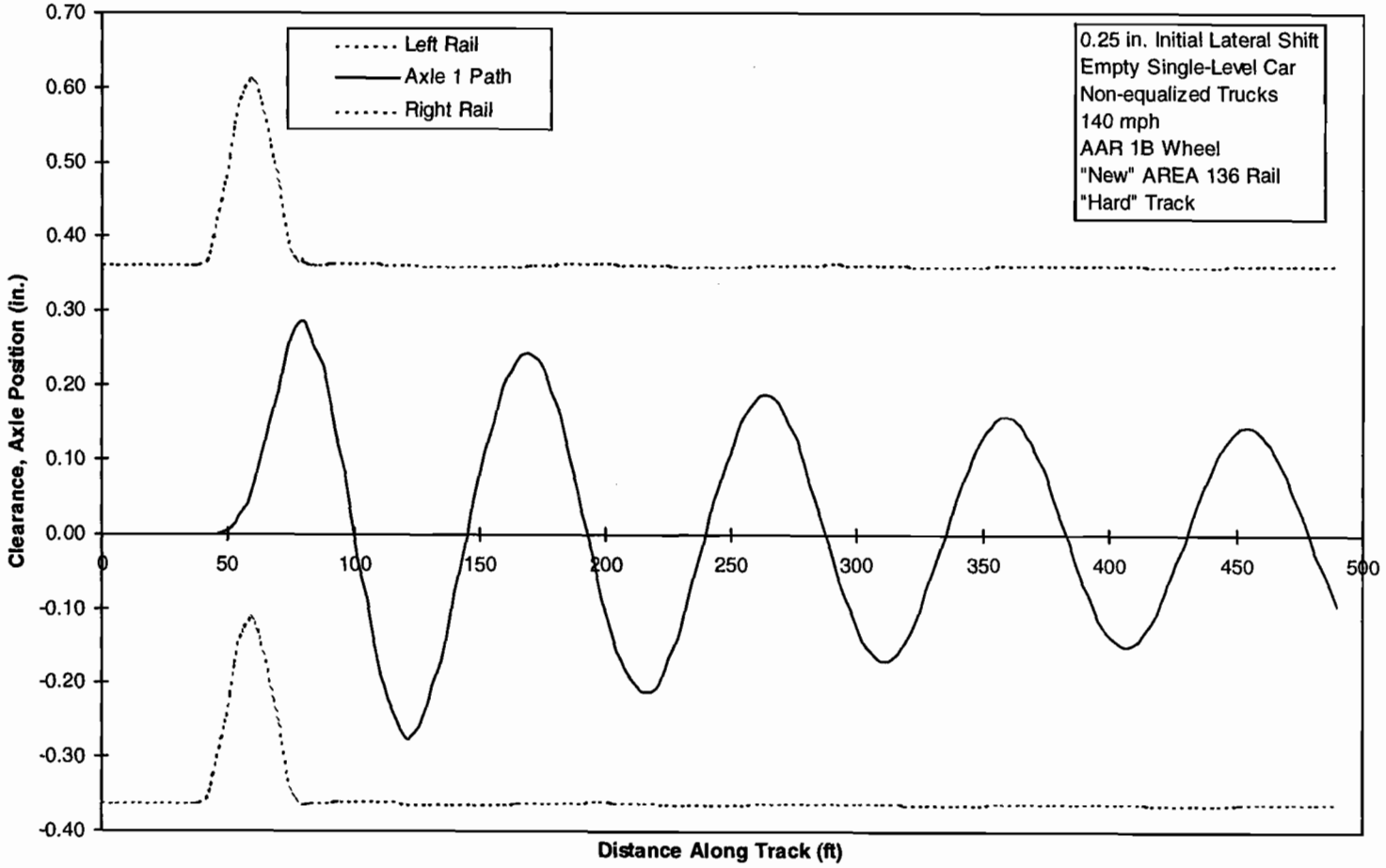

Figure 3-30. Lateral motion of lead axle

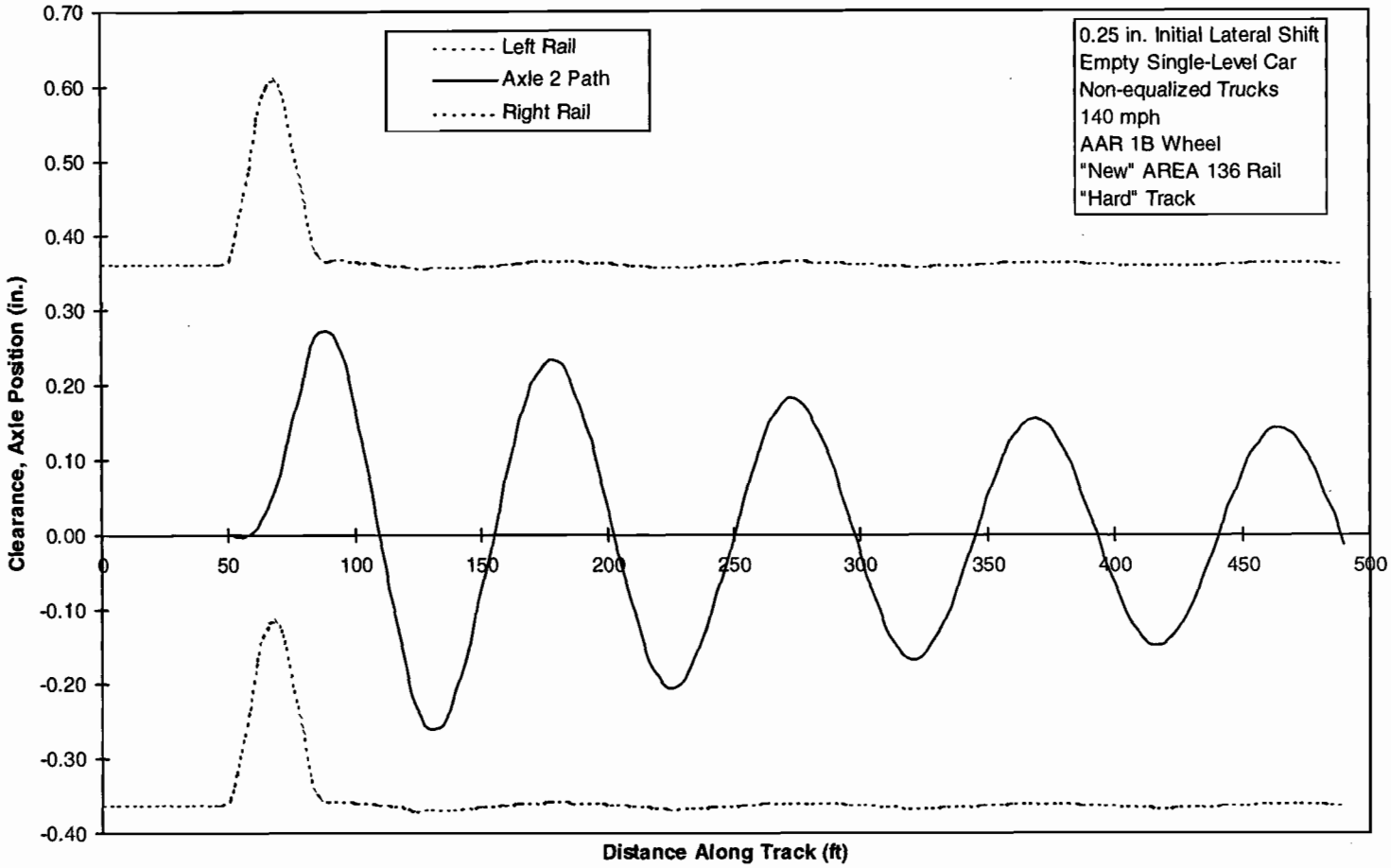

Figure 3-31. Lateral motion of second axle

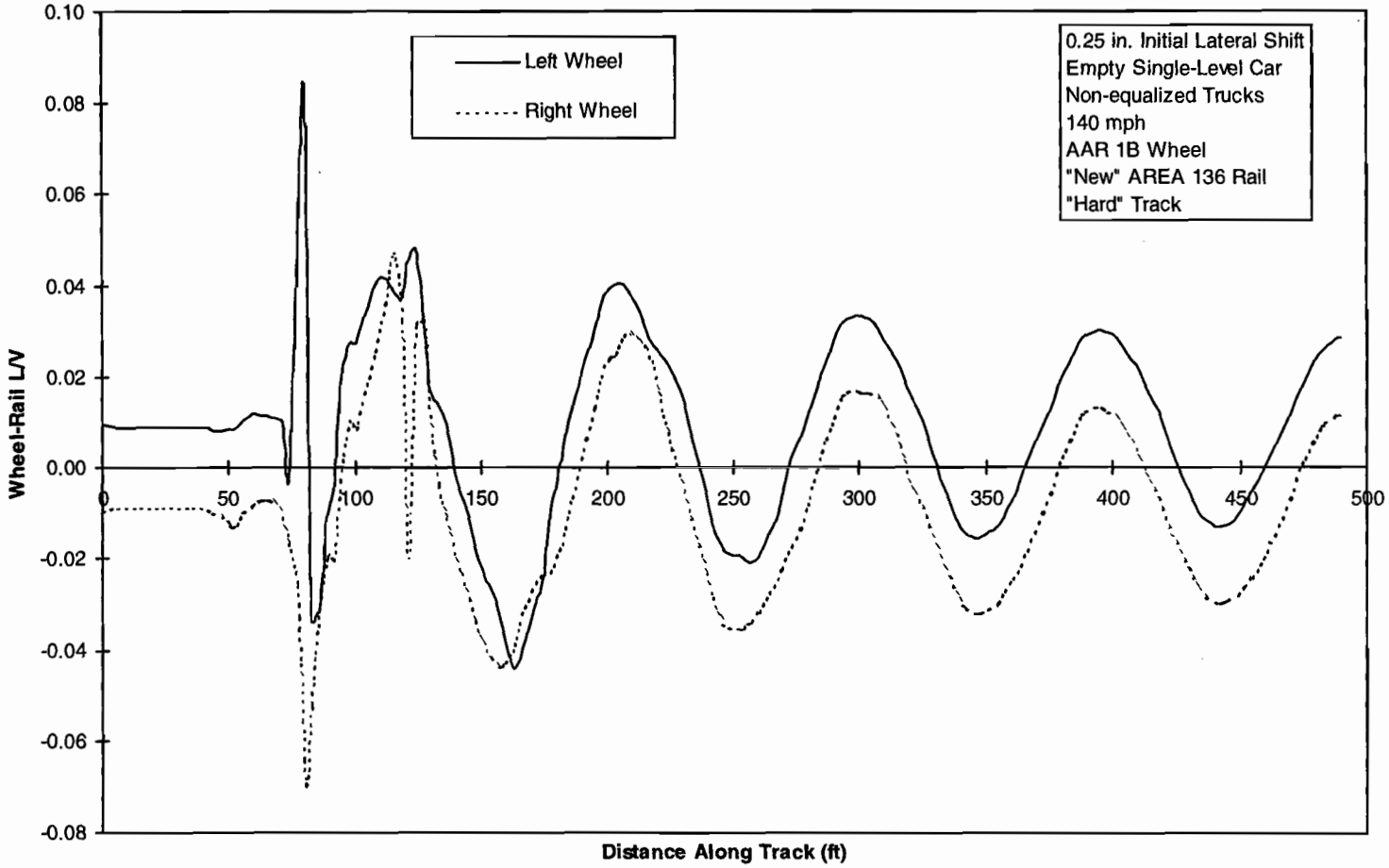

Figure 3-32. L/V ratios on individual wheels of lead axle

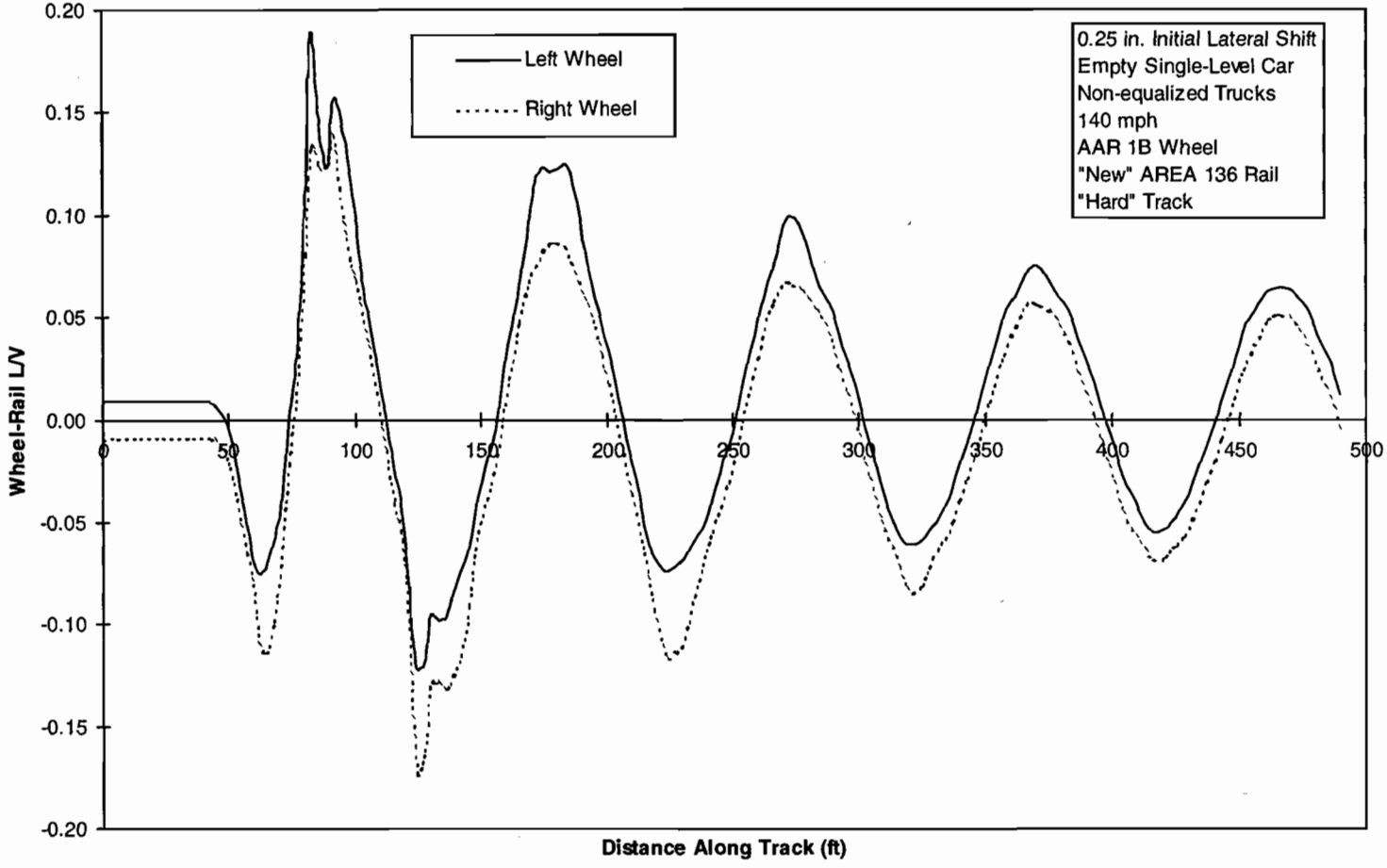

Figure 3-33. L/V ratios on individual wheels of second axle

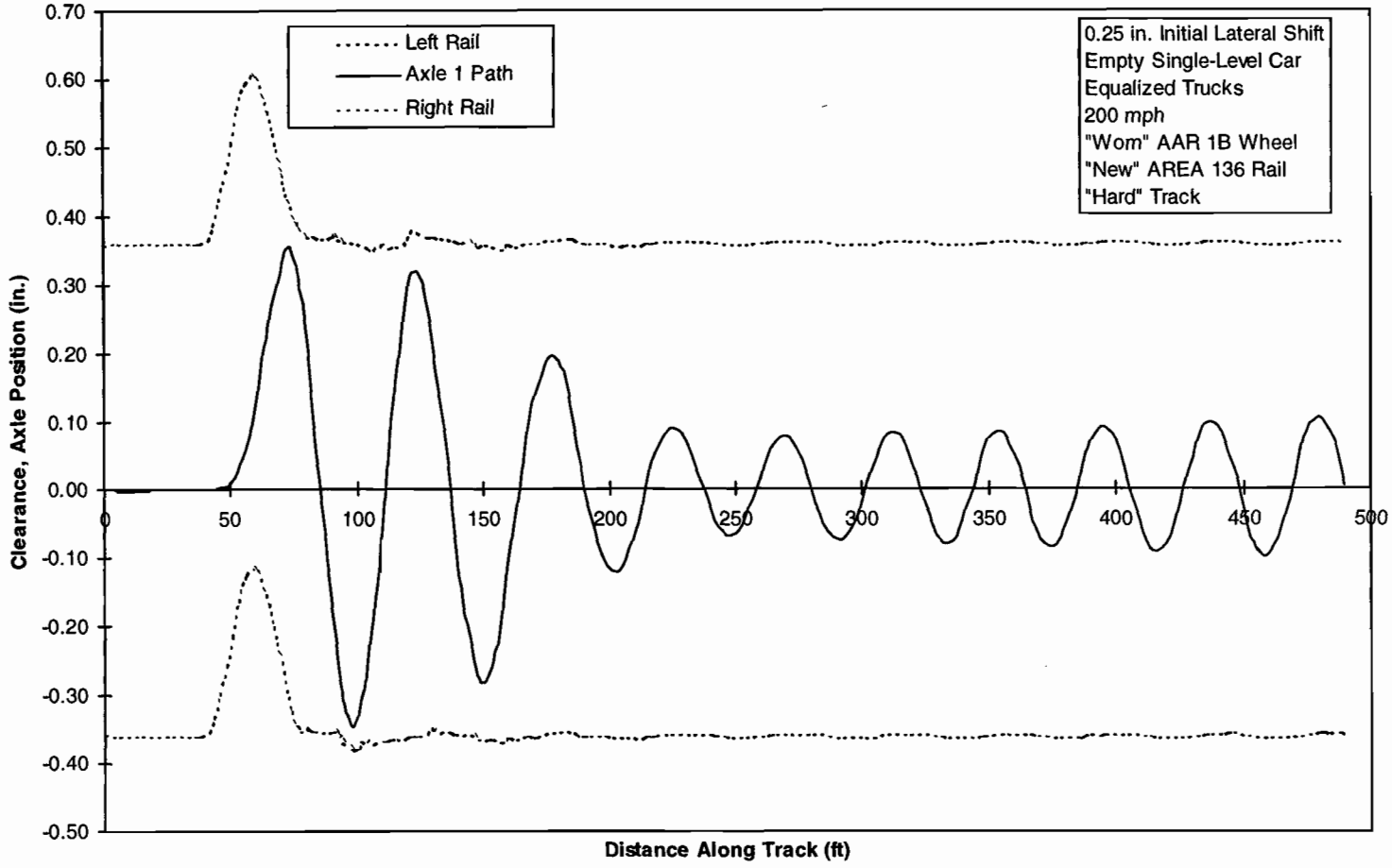

Figure 3-34. Lateral motion of lead axle

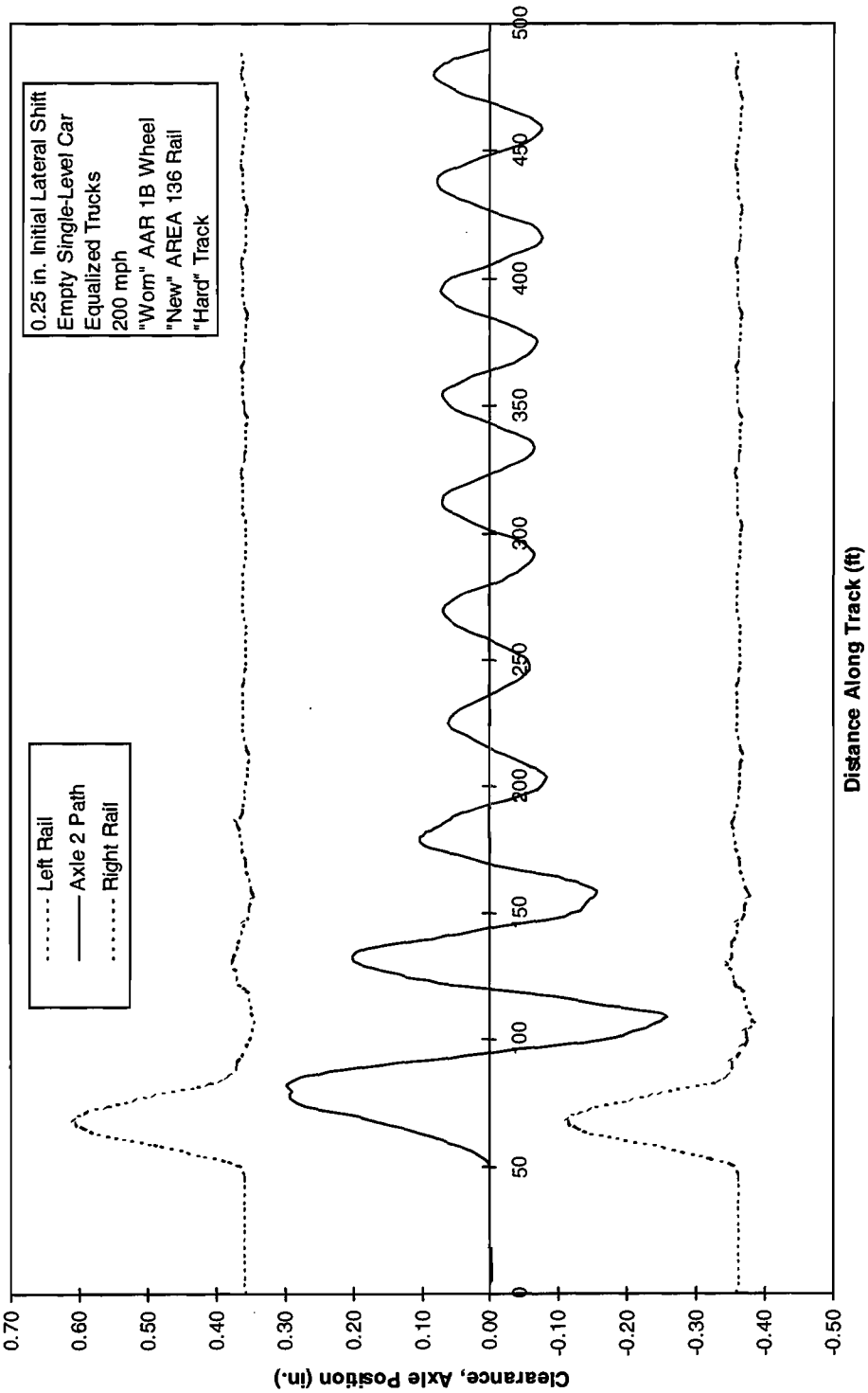

Figure 3-35. Lateral motion of second axle

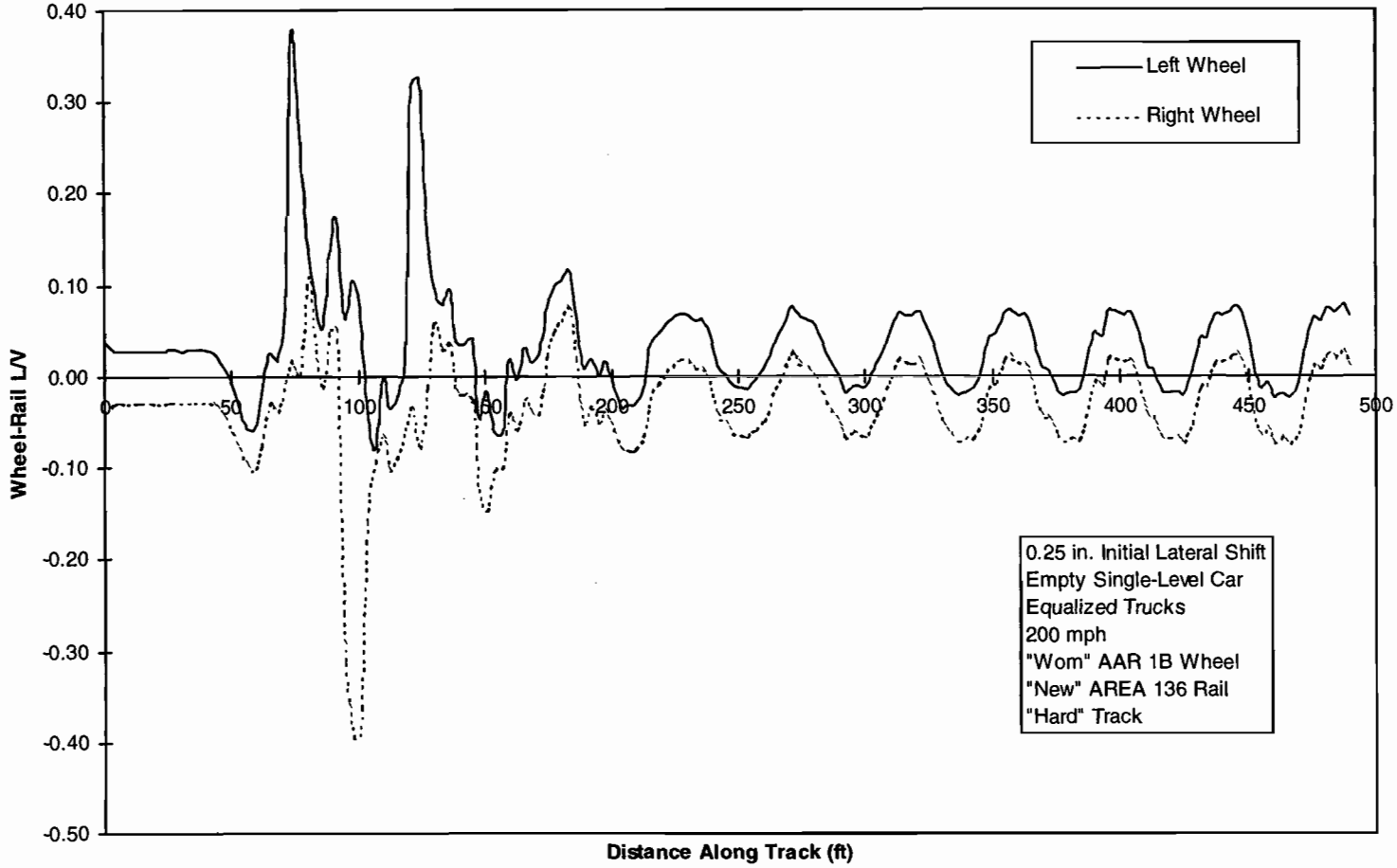

Figure 3-36. L/V ratios on individual wheels of lead axle

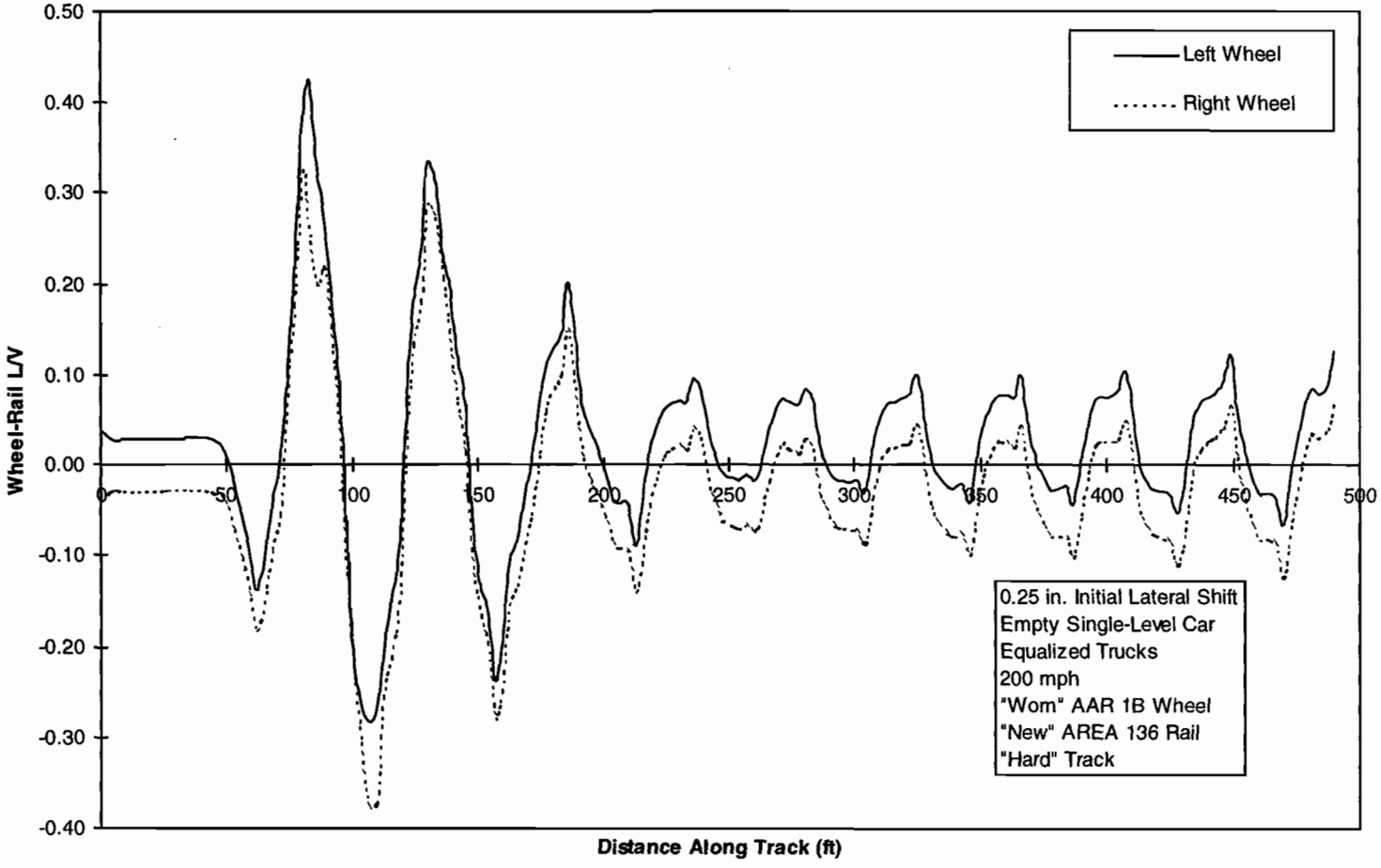

Figure 3-37. L/V ratios on individual wheels of second axle

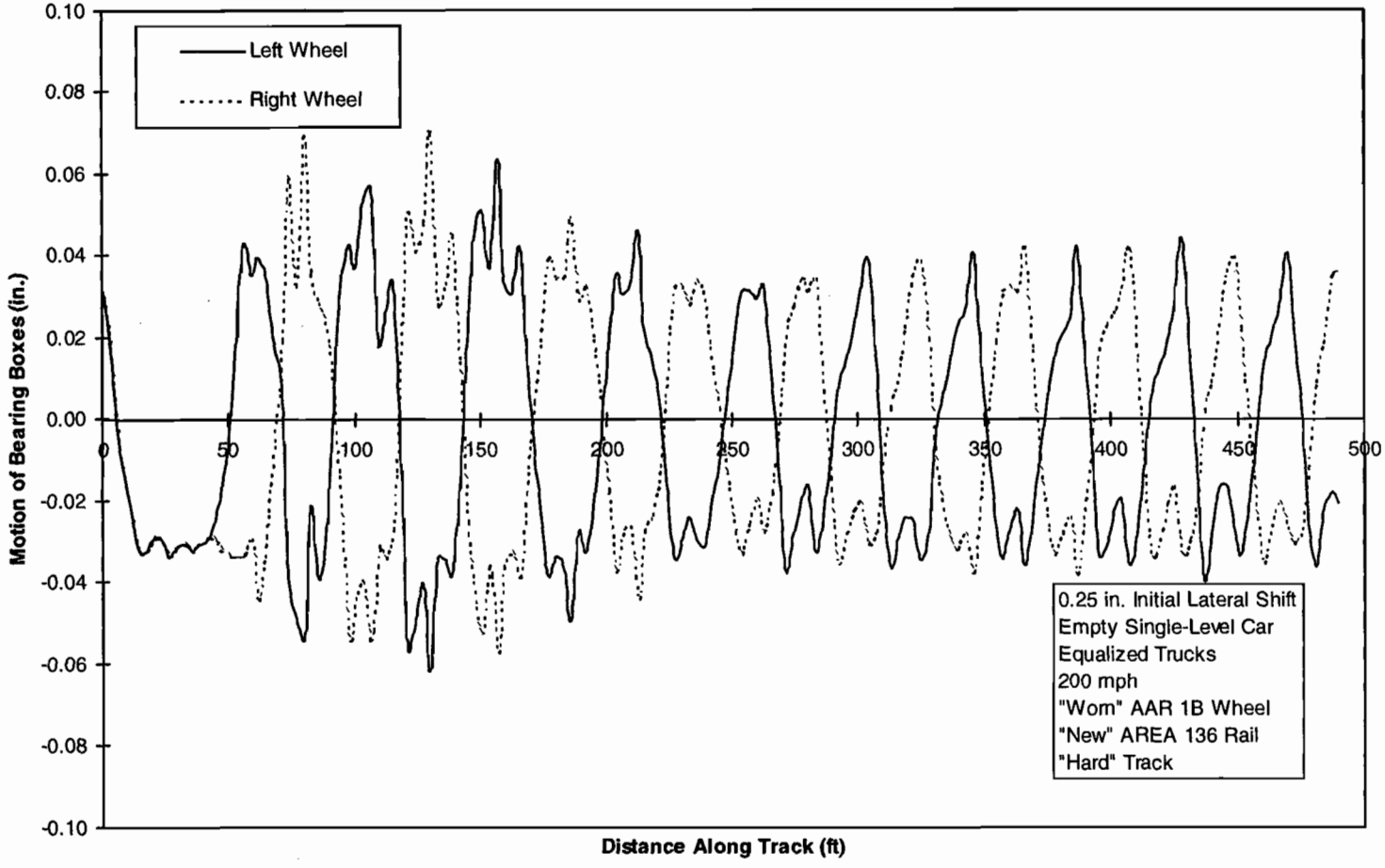

Figure 3-38. Motion of bearing boxes in pedestal clearance of lead axle

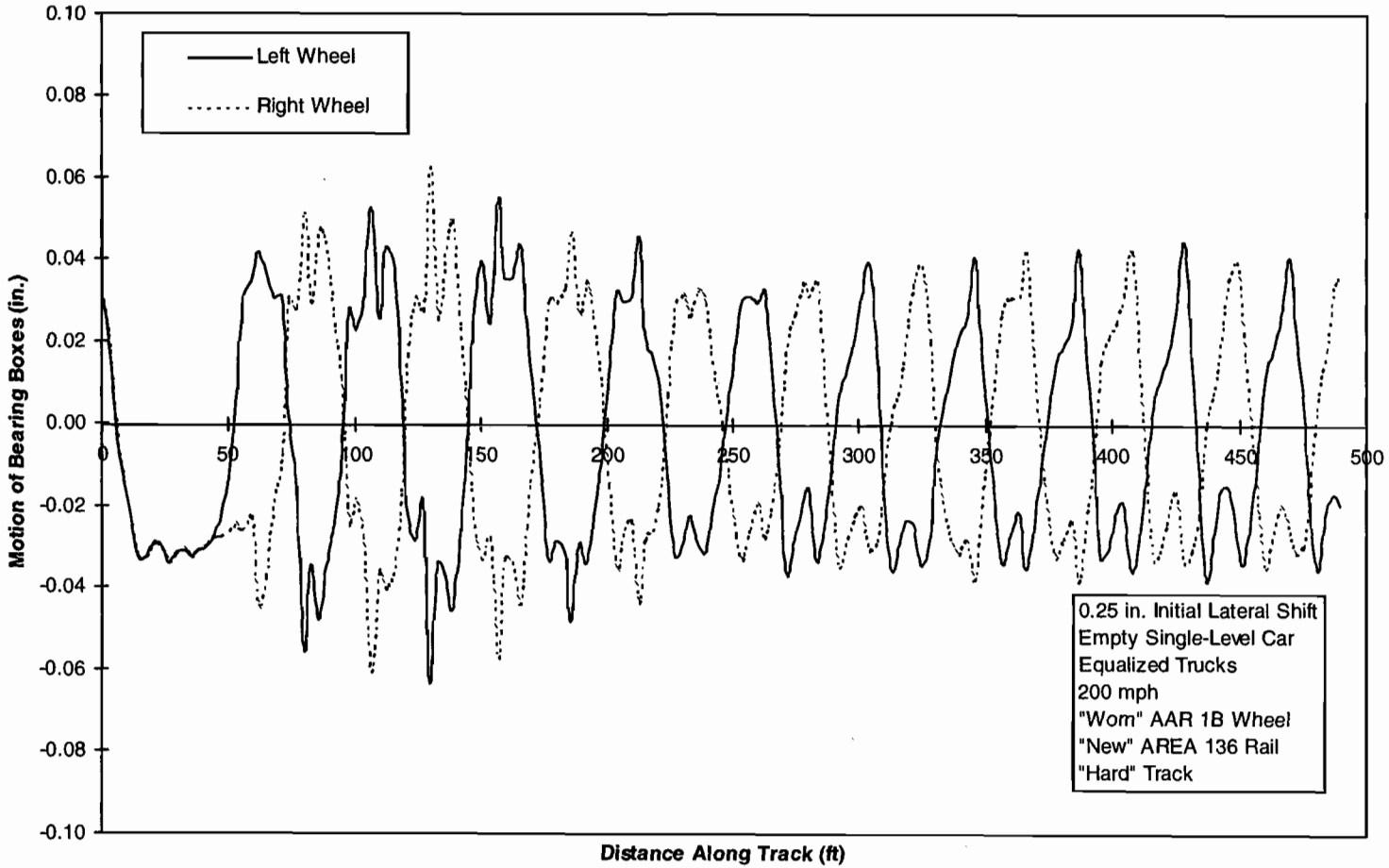

Figure 3-39. Motion of bearing boxes in pedestal clearance of second axle

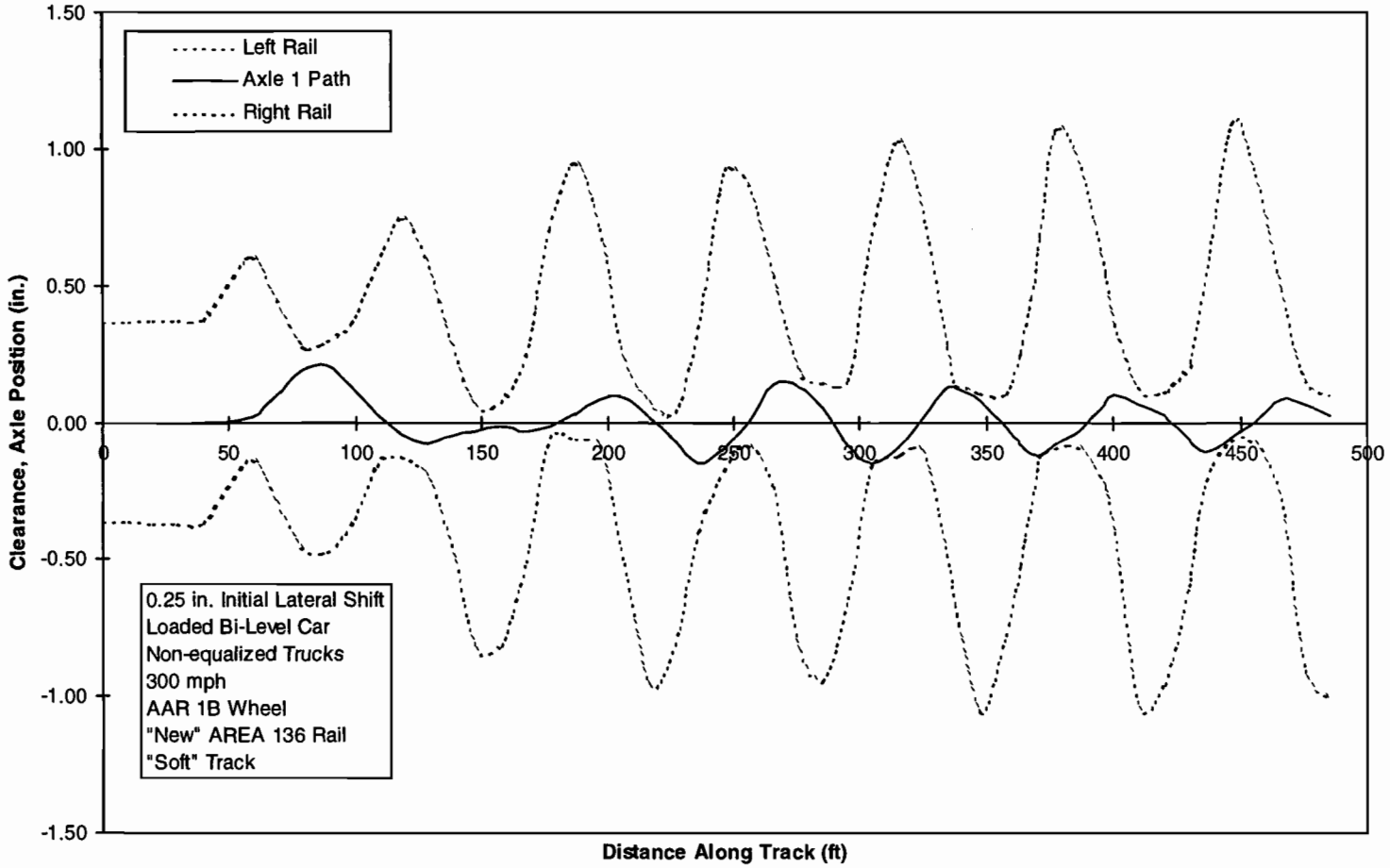

Figure 3-40. Lateral motion of lead axle - filtered

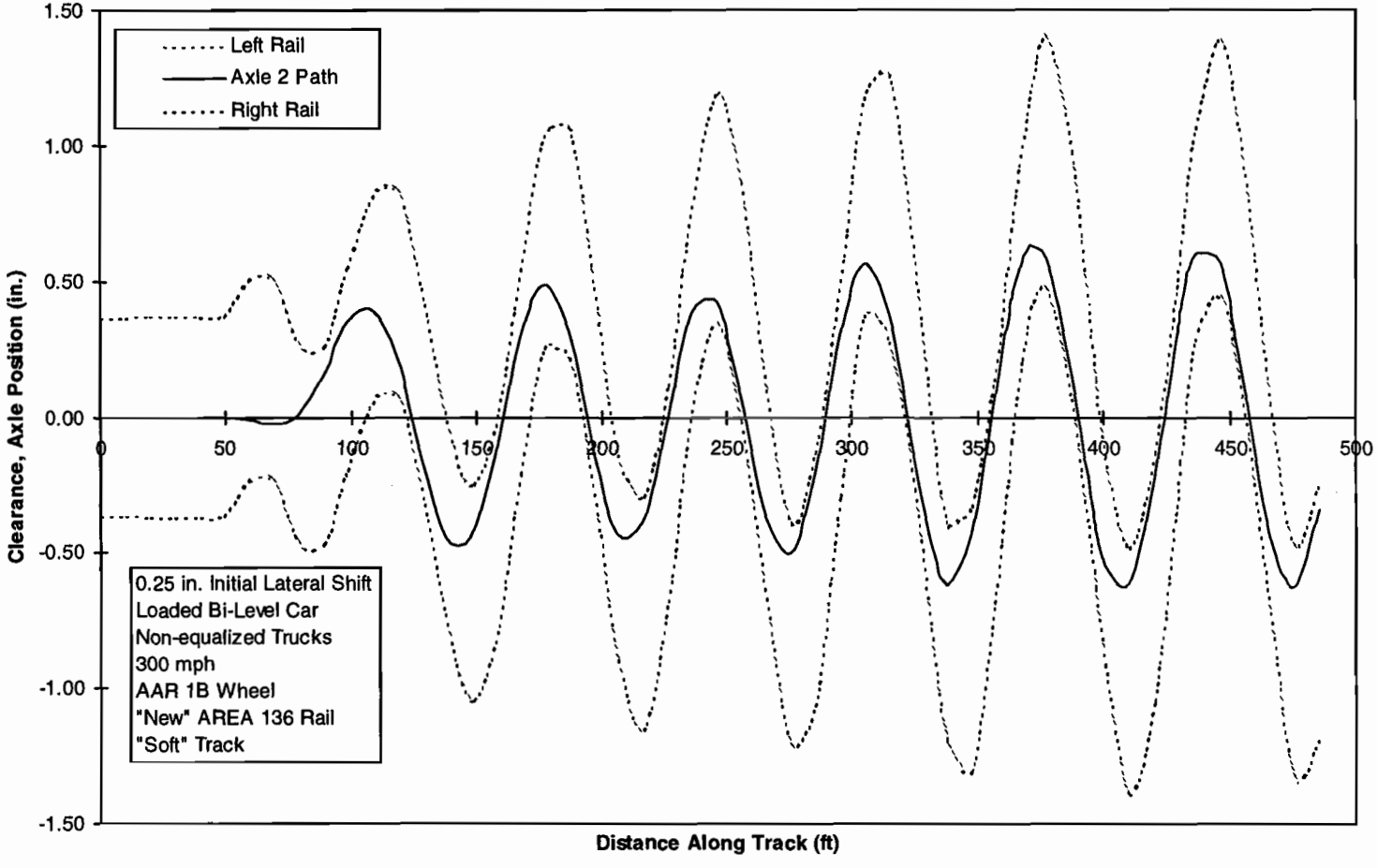

Figure 3-41. Lateral motion of second axle - filtered

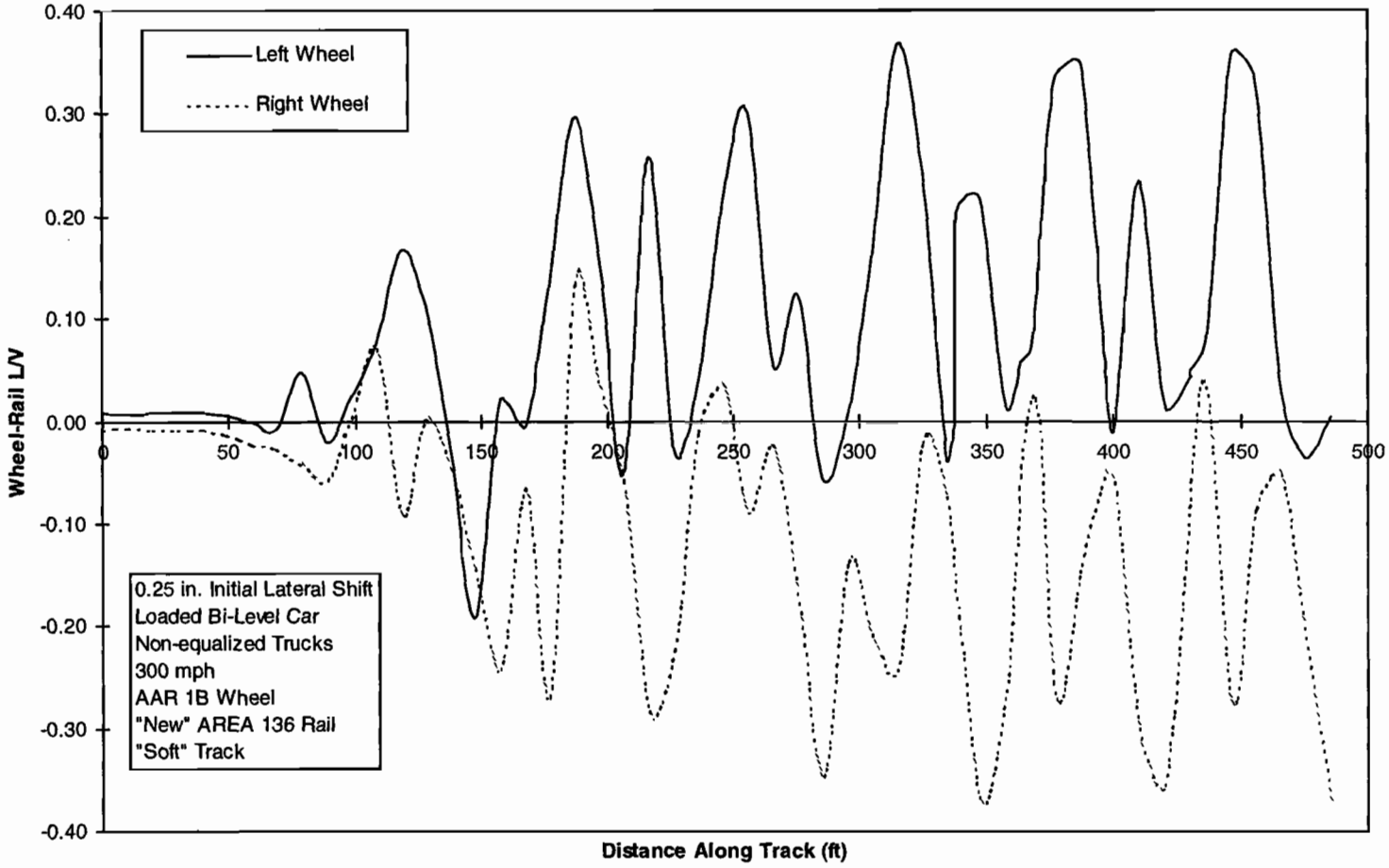

Figure 3-42. L/V ratios on individual wheels of lead axle - filtered

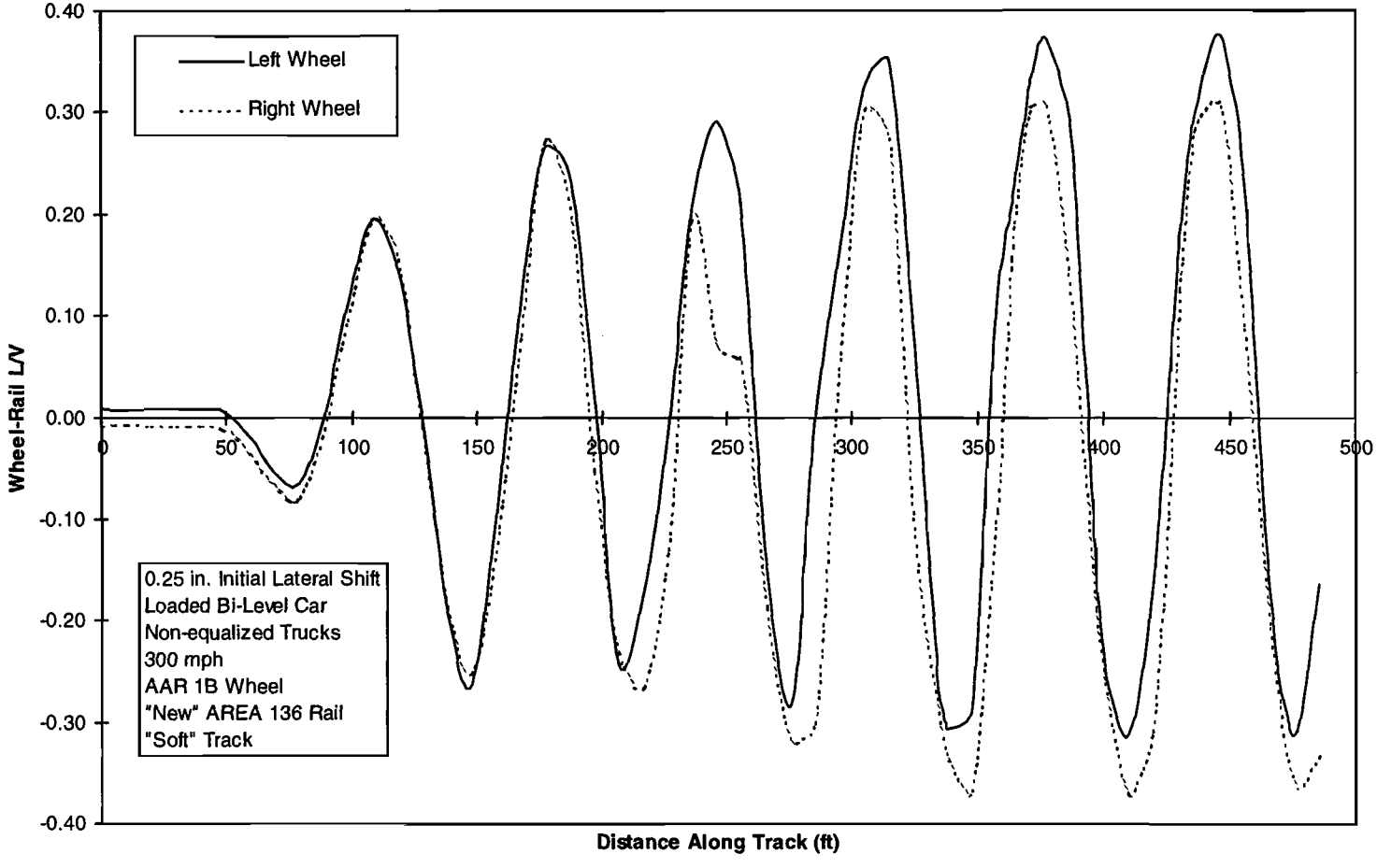

Figure 3-43. L/V ratios on individual wheels of second axle - filtered

4. RESPONSE TO CROSSLEVEL IN CURVES

In this work, OMNISIM was used to examine the detailed response of the system in a combined curving and twist situation up to and including derailment. The principal concerns are to verify the predicted pseudo-static behavior discussed in Appendix B and to extend this to the observation of the transient behavior in situations of large crosslevel in curves of 2.5, 5, 10, 15 and 20 deg. Two crosslevel perturbations are used. They are of short and long symmetric cusps of lengths from start to finish of 10 ft and 39 ft, respectively. The latter is selected to represent a rail length. Various amplitudes are tested to find those which can cause derailment in a significant number of cases. Those chosen for complete investigation have a 1.5 in. amplitude over the short length and a 3 in. amplitude over the long length, in the outer rail, in the body of the curve. The latter is consistent with the lowest level of track quality identified in FRA class 1. The track input is preprocessed with a filter to prevent the existence of wavelengths below 30 in. Further discussion of the effect of short wavelength inputs may be found in Section 6.

4.1 Behavior Over the 39 ft "Long" Length Cusp in a 2.5 deg Curve

This section begins with a complete description of the simulated response of the base vehicle and track system as investigated in the 2.5 deg curve. The deflected rail cusp is shown in Figure 4-1 for the commuter car on "hard" track. The first case studied is that of the bi-level car with equalized trucks. Figure 4-2 shows the lateral motion of the lead axle in the curve at the cusp. It is initially close to the outer rail in the steady curve and is pushed to flange contact at the cusp where the resulting lateral force generates a small lateral rail deflection. The lateral and vertical forces on the lead outer wheel are shown in Figure 4-3. Although there is some unloading of this wheel, it has not lifted as shown by the remaining vertical load and guidance remains just adequate as shown in Figure 4-4 in the L/V ratio.

The cusp point amplitude occurs at 359.5 ft, before the maximum L/V shown. It appears that, in this truck, the axle "bounces" on the rail after hitting the deepest point in the cusp, showing first a large vertical load followed by an unloading. The static vertical load is never less than 25 percent, as shown in Figure 4-5. This is further demonstrated in the two final graphs provided for this vehicle and track. Figures 4-6 and 4-7 are plots of the lead outer wheel L/V and percentage wheel unloading, respectively, against two roll angle differences in each case. The first difference is the roll difference across the axles in the lead truck and the second is the roll difference across the truck frames. As can be seen in Figure 4-6, the L/V remains small until after the maximum relative roll angles have been passed. The same can be said of the percentage wheel unloading shown in Figure 4-7. The latter graph also provides a comparison with calculated static values for unloading a leading wheel assuming both full shear and no shear. However, the connection is not direct as can be seen from the following discussion.

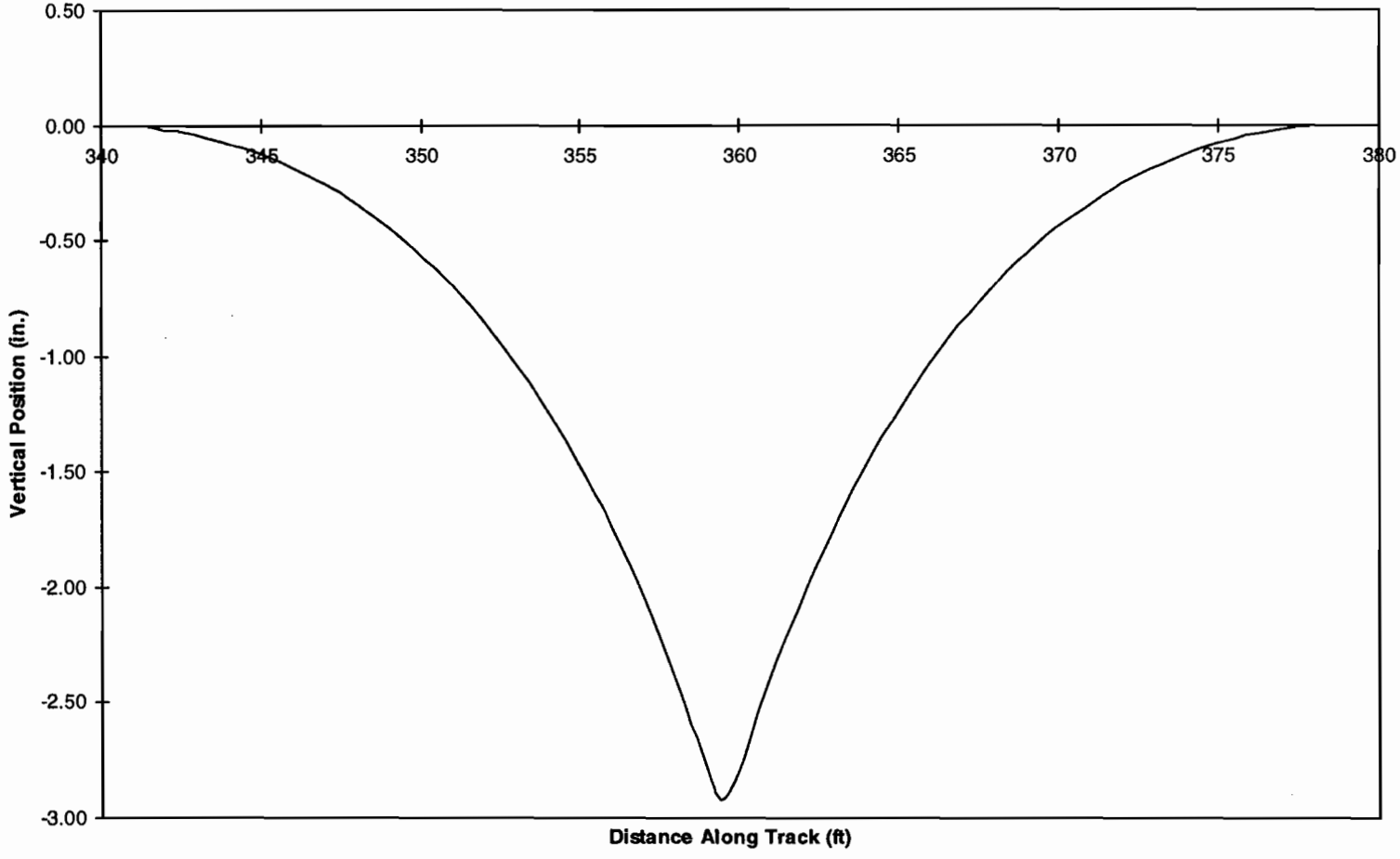

Figure 4-1. Vertical motion of left wheel

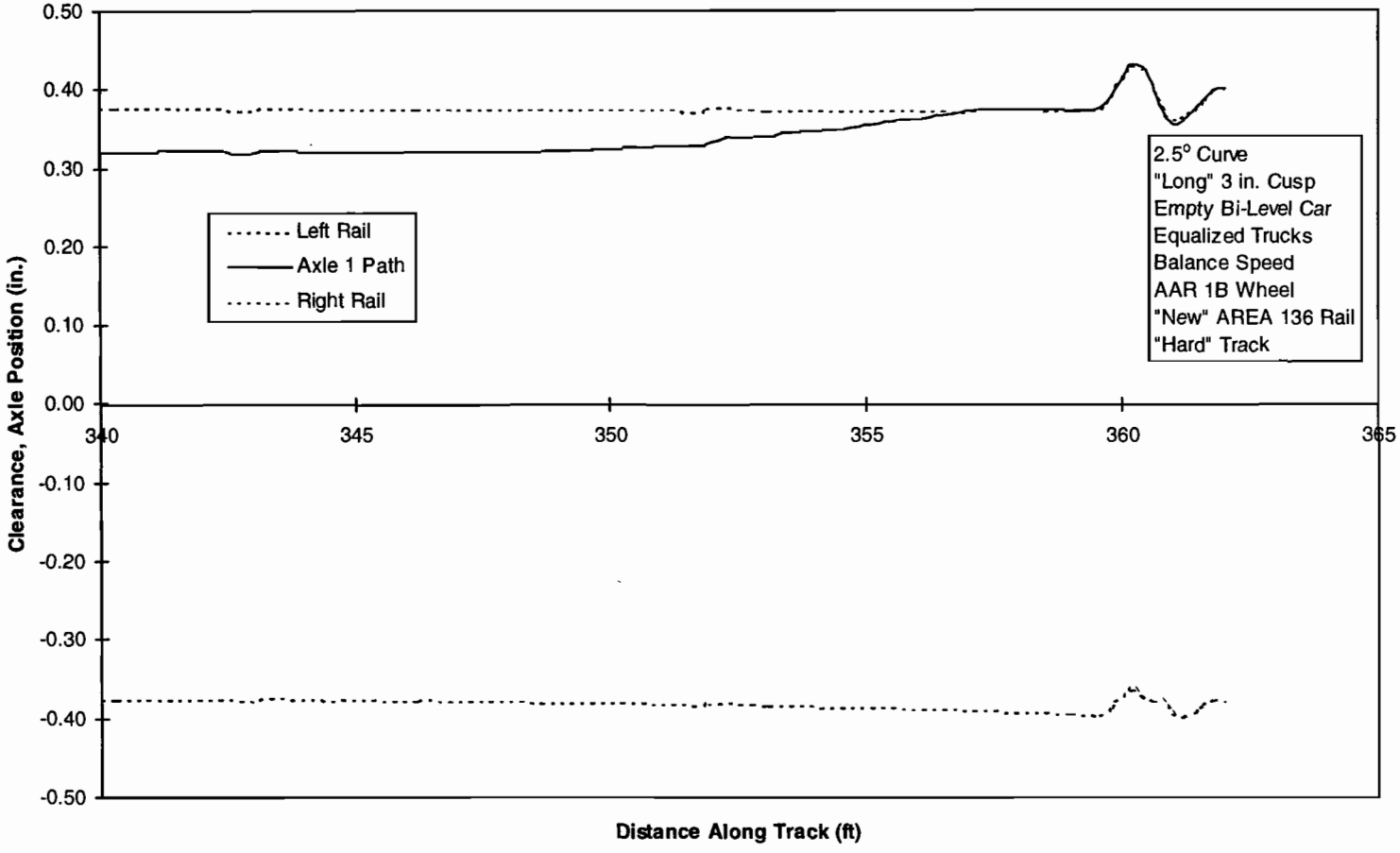

Figure 4-2. Lateral motion of lead axle

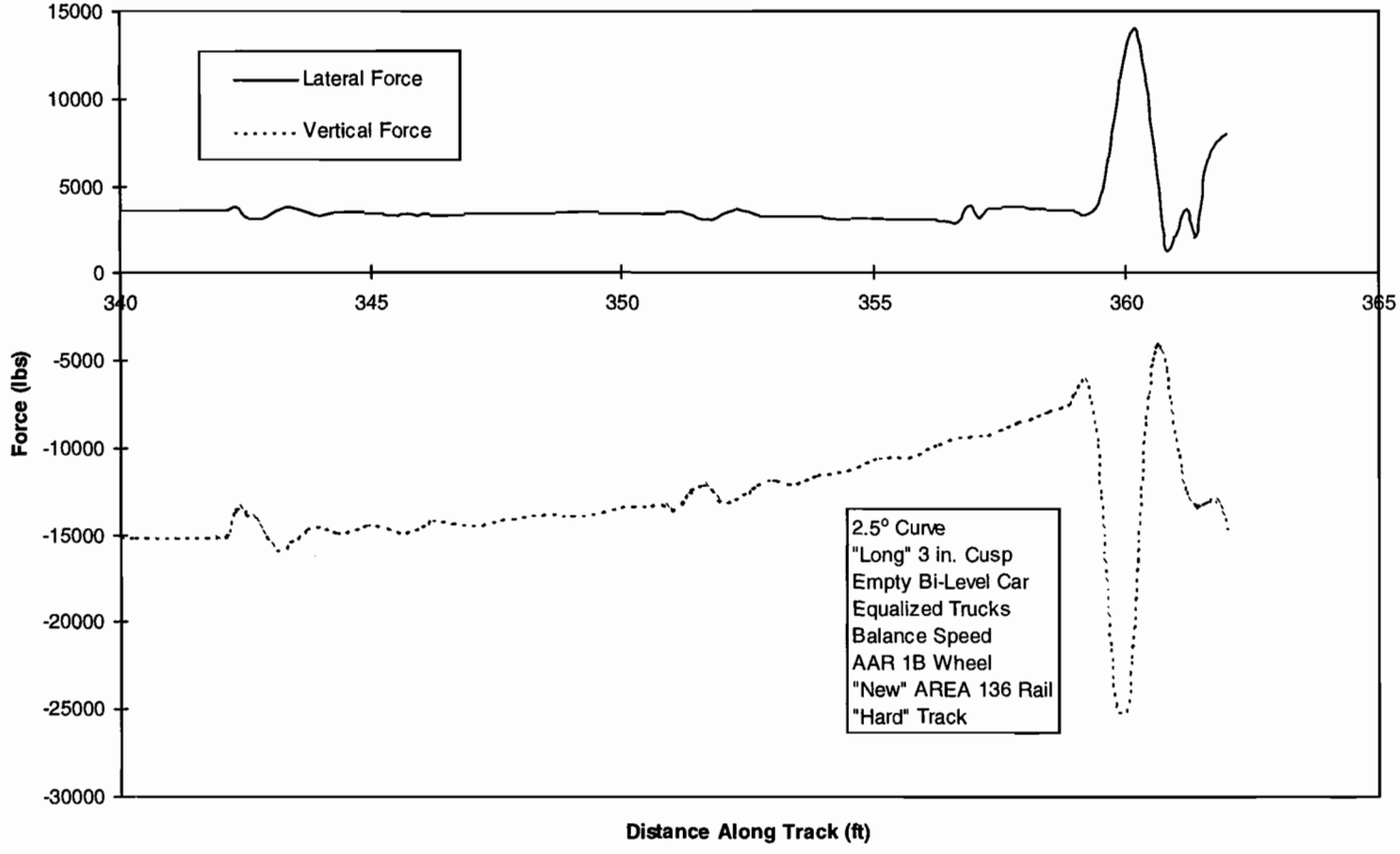

Figure 4-3. Lateral and vertical forces on lead outer wheel

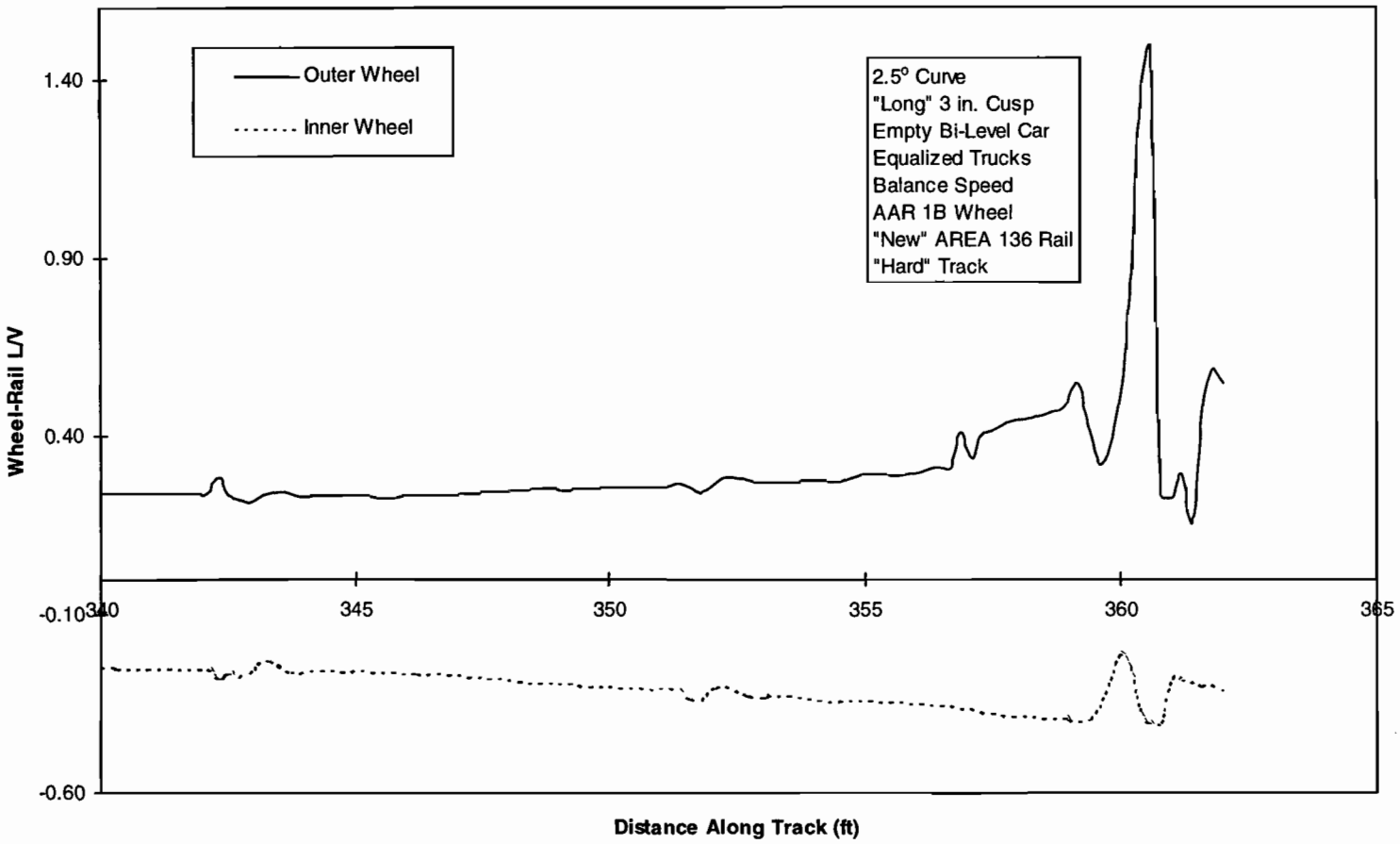

Figure 4-4. L/V ratios on leading wheels

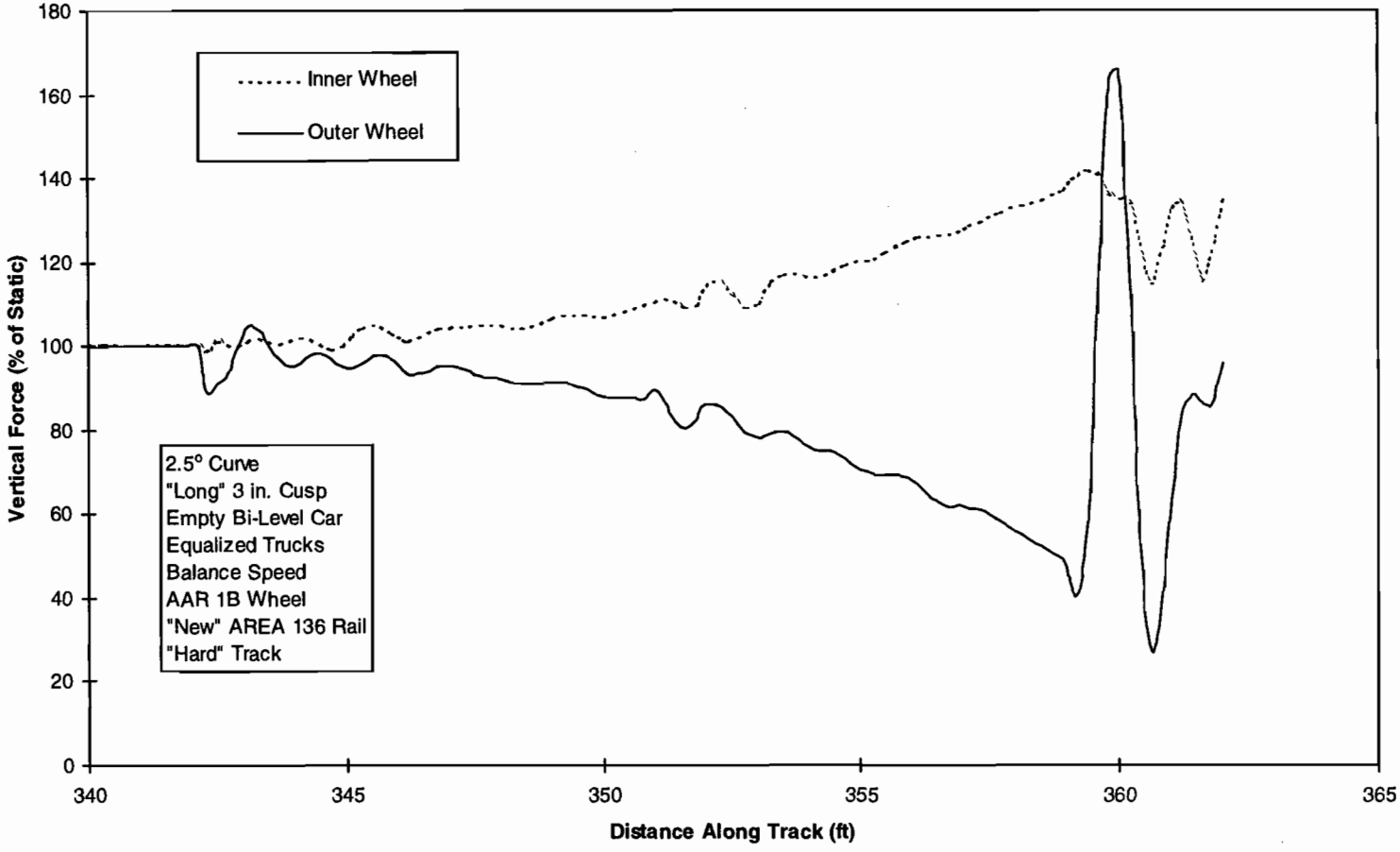

Figure 4-5. Vertical force reduction on leading wheels

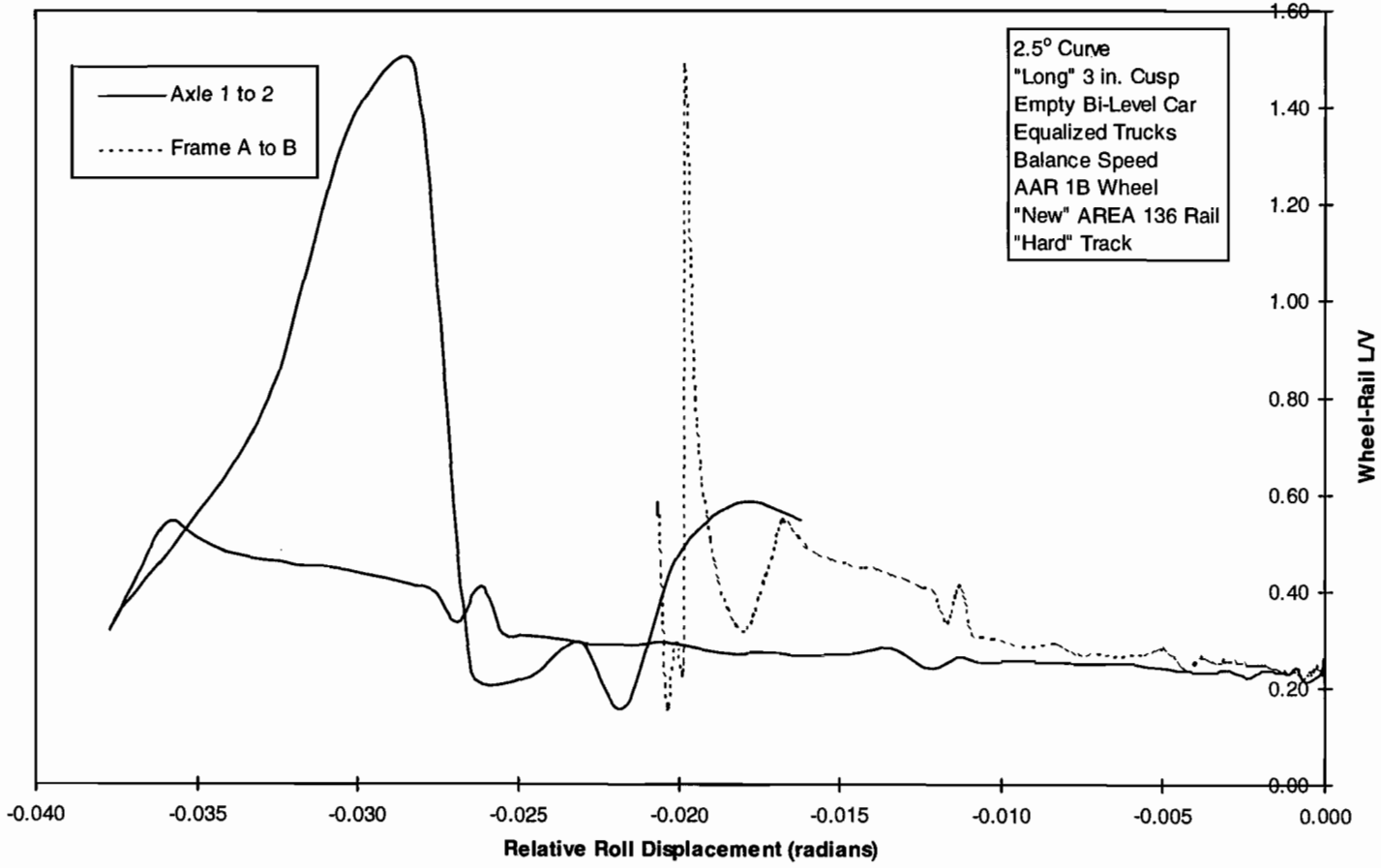

Figure 4-6. L/V ratios on lead outer wheel versus relative roll displacement

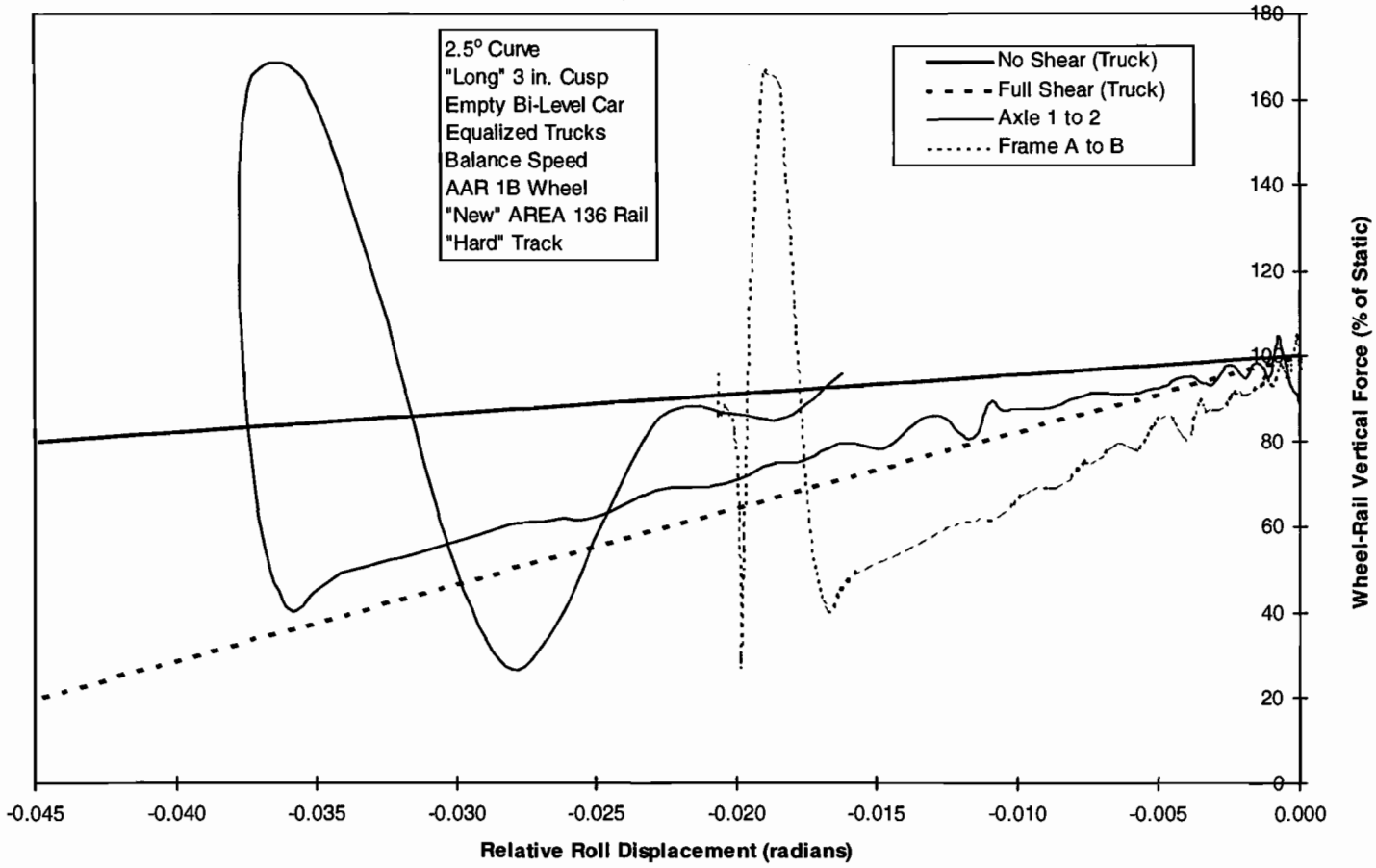

Figure 4-7. Percentage leading outer wheel vertical load versus relative roll displacement

The expressions for the relative roll stiffness are taken from the analysis in Method B of Appendix A. However, the wheel unloading suggested in this section initially used an assumption which is now shown to be inadequate. Both methods, A and B, assume that a satisfactory model for individual or truckside wheel unloading can be obtained by examining only the effect of the vertical forces and vertical and roll degrees of freedom. Initial comparisons between the static and dynamic behavior, showed that this was not valid. The following analysis makes no such assumption and adds the effect of the truck "shear" to wheel unloading. The lateral movement between axle centers due to differential roll over the crosslevel between axles gives rise to a "shearing" effect across the truck. This "shear" effect will only be negligible if the shear stiffness of the truck is small, such as in the three-piece truck used frequently for freight.

The shear stiffness of the commuter car trucks is a function of the primary lateral and longitudinal stiffnesses. In terms of these values the expression for shear stiffness, K_s, becomes,

$$K_s = \left\{ \frac{1}{1/K_{py} + \left(b/d_p\right)^2 1/K_{px}} \right\}$$

Thus, the additional roll stiffness between the axles becomes $K_e = r_w^2 K_s$ where, r_w is the rolling radius of the wheel. The complete expression for the wheel unloading becomes that given in Appendix A and repeated here for convenience,

$$\%\text{static}F_v = \frac{100}{2aF_v}\left\{\left(K_e + \frac{r^2 K_a}{2}\right)\left(\phi_{i1} - \phi_{i2}\right) + \left(\frac{K_d}{2}\right)\phi_N\right\}$$

In order to compare the effect of the static unloading suggested by this expression and the dynamic variation due to the cusp, the expression is rewritten in two parts due independently to the roll across the axles in the truck and that between the frames. The former is a consequence of the primary suspension, including any equalization, and the latter the secondary suspension and twist of the body. Thus,

$$K_{12} = \frac{2K_e + r^2 K_a}{2}$$

and

$$K_N = \frac{K_d}{2}$$

where r is the equalization ratio defined in Appendix A. The ratio of the relative roll angles changes slightly with position on the track, ϕ_{12} and ϕ_N can be determined from the positions across the cusp shape. For accuracy and simplicity this was taken directly from the graphs. For the car investigated with equalized trucks at the cusp this ratio, p, is 2.385 and as used later for the non-equalized trucks at derailment, 1.804.

The graphs of percentage of static wheel load against relative roll angle, as shown in Figure 4-7, can now be compared directly with the values calculated from the vehicle suspension stiffnesses. The modified values for direct comparison on Figure 4-7 and subsequent comparisons are,

$$\overline{K}_{12} = K_{12} + \frac{1}{p} K_N$$

$$\overline{K}_N = K_N + pK_{12}$$

Assuming the body to be torsionally rigid, the slopes of percentage wheel unloading per unit relative roll angle are calculated to be, for the car with equalized trucks,

With no shear, $\overline{K}_{12} = 446.4$ and $\overline{K}_N = 1065$
With full shear, $\overline{K}_{12} = 1792$ and $\overline{K}_N = 4273$

and for the car with non-equalized trucks,

With no shear, $\overline{K}_{12} = 2170$ and $\overline{K}_N = 3915$
With full shear, $\overline{K}_{12} = 3626$ and $\overline{K}_N = 6541$

The result in Figure 4-7 is immediately apparent. The slope of the lines from the OMNISIM runs for inter-axle roll angle and frame to frame roll angle are only close to those calculated in the straight lines if the shear stiffness is included. It may therefore be concluded that the omission of inter-axle shear in the computation of wheel unloading leads to significant errors for both trucks. This represents a second example, added to that in subsection 3.2 in this report, in which the output from OMNISIM, as yet not formally validated, showed up inaccuracies in a simpler approach, assumed to be valid through frequent use.

A similar set of results is now presented for the bi-level car with non-equalized trucks, also on "hard" track with the "long" cusp. The lack of equalization results in the cusp point not being reached before derailment takes place due to wheel unloading. This is shown directly in Figures 4-8 and 4-9 where the path of the axle center moves outside the flangeway clearance, identified by the left rail path, before the point is reached. Figure 4-10 shows that the lead left wheel becomes completely unloaded immediately after the wheel climbs. Since this computation would cause an infinite L/V in Figure 4-11, a value of 2 is given to the L/V, having the negative sign of the ratio at this point. The complete unloading is also seen in Figure 4-12 as a percentage of the static load. Figure 4-13 shows that the maximum L/V exceeds 2 and is coincident with the

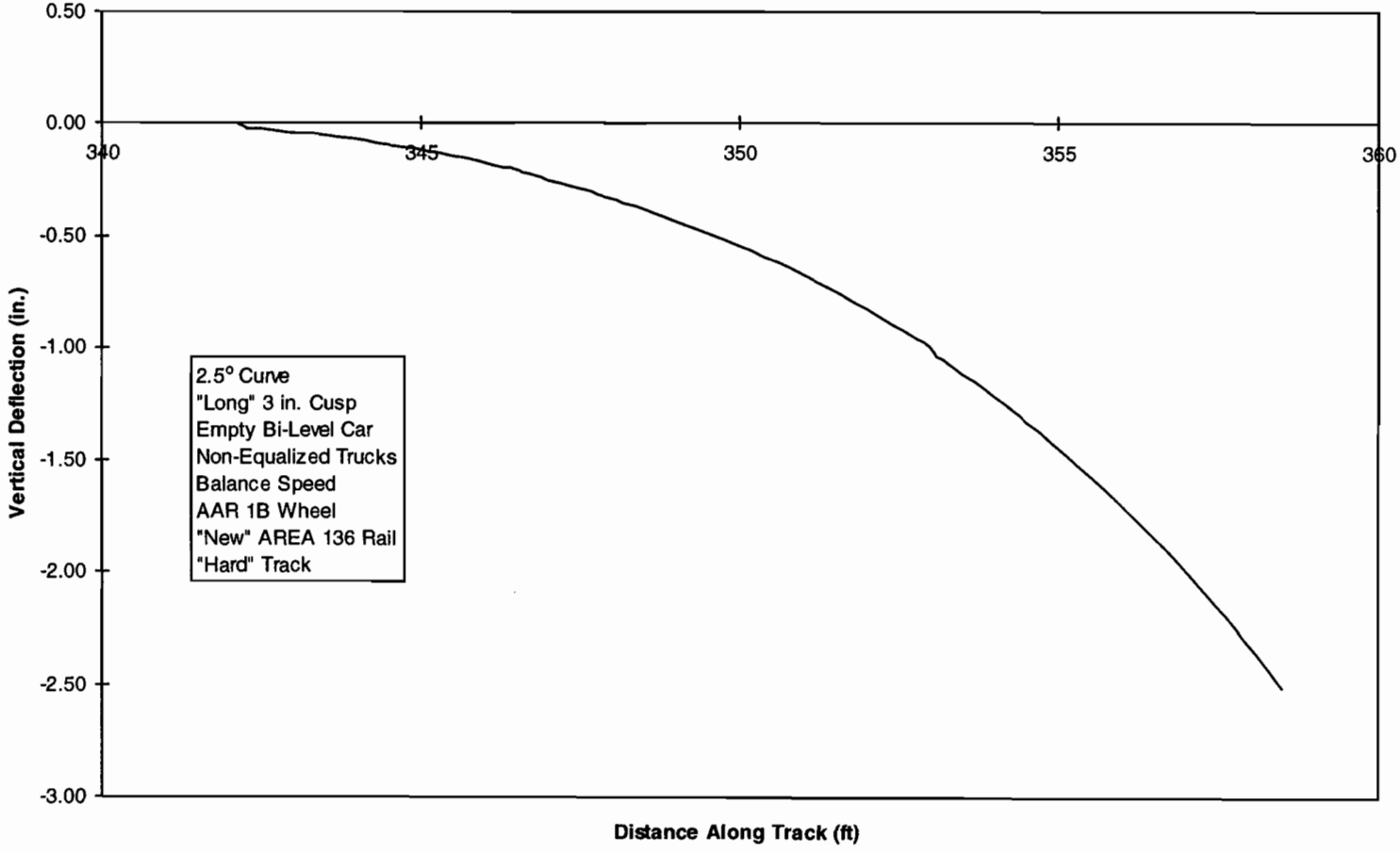

Figure 4-8. Vertical motion of left wheel

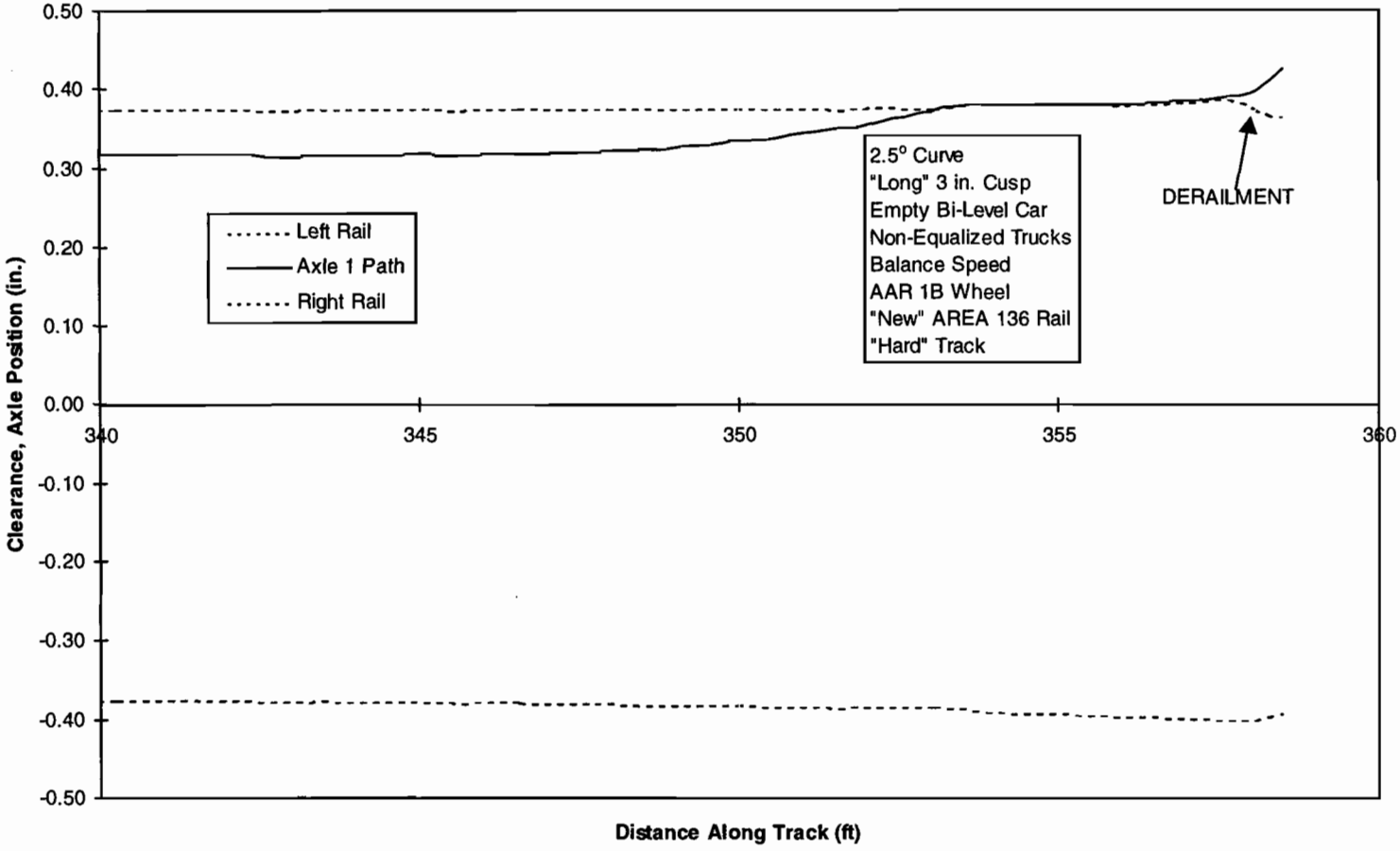

Figure 4-9. Lateral motion of lead axle

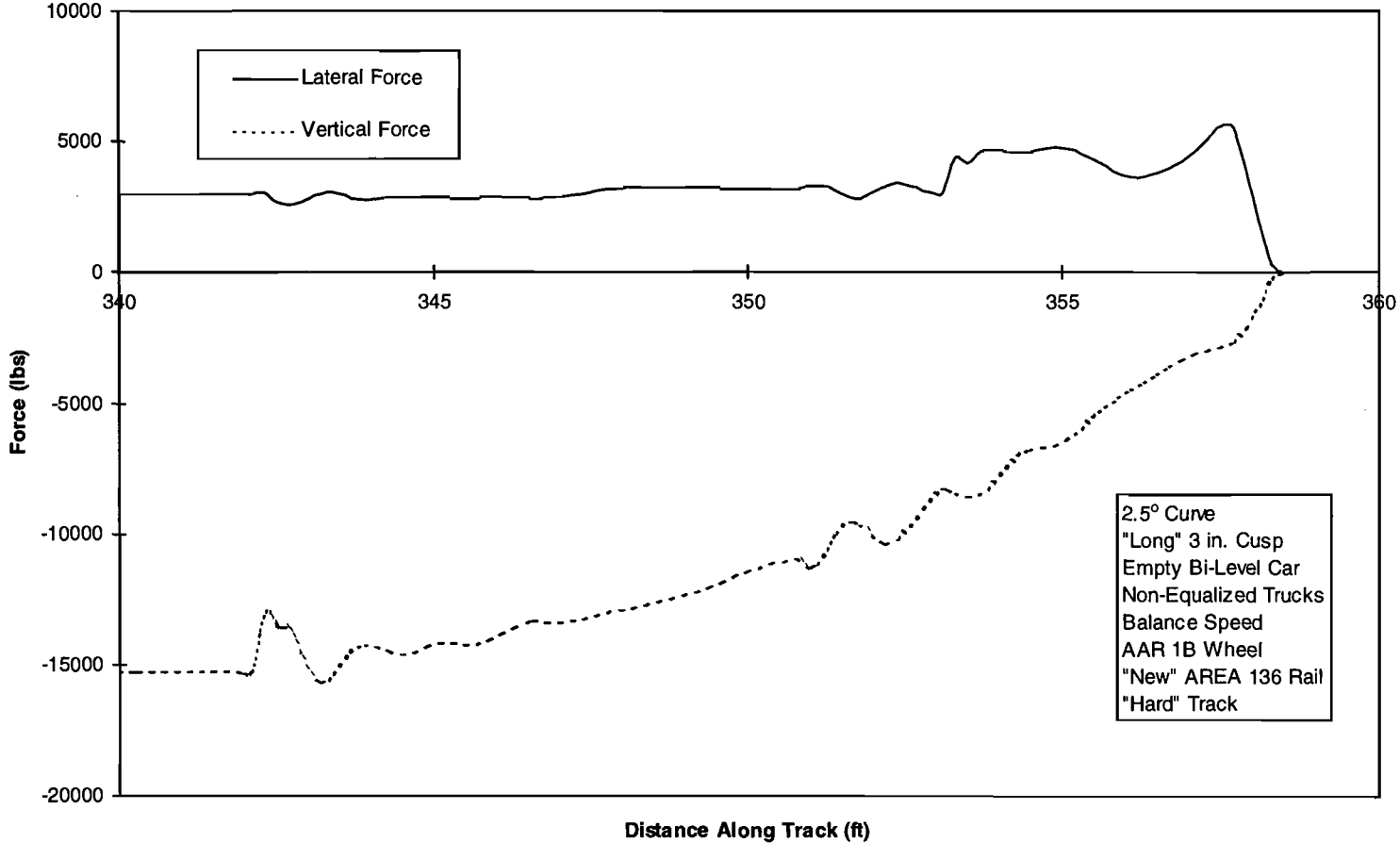

Figure 4-10. Lateral and vertical forces on lead outer wheel

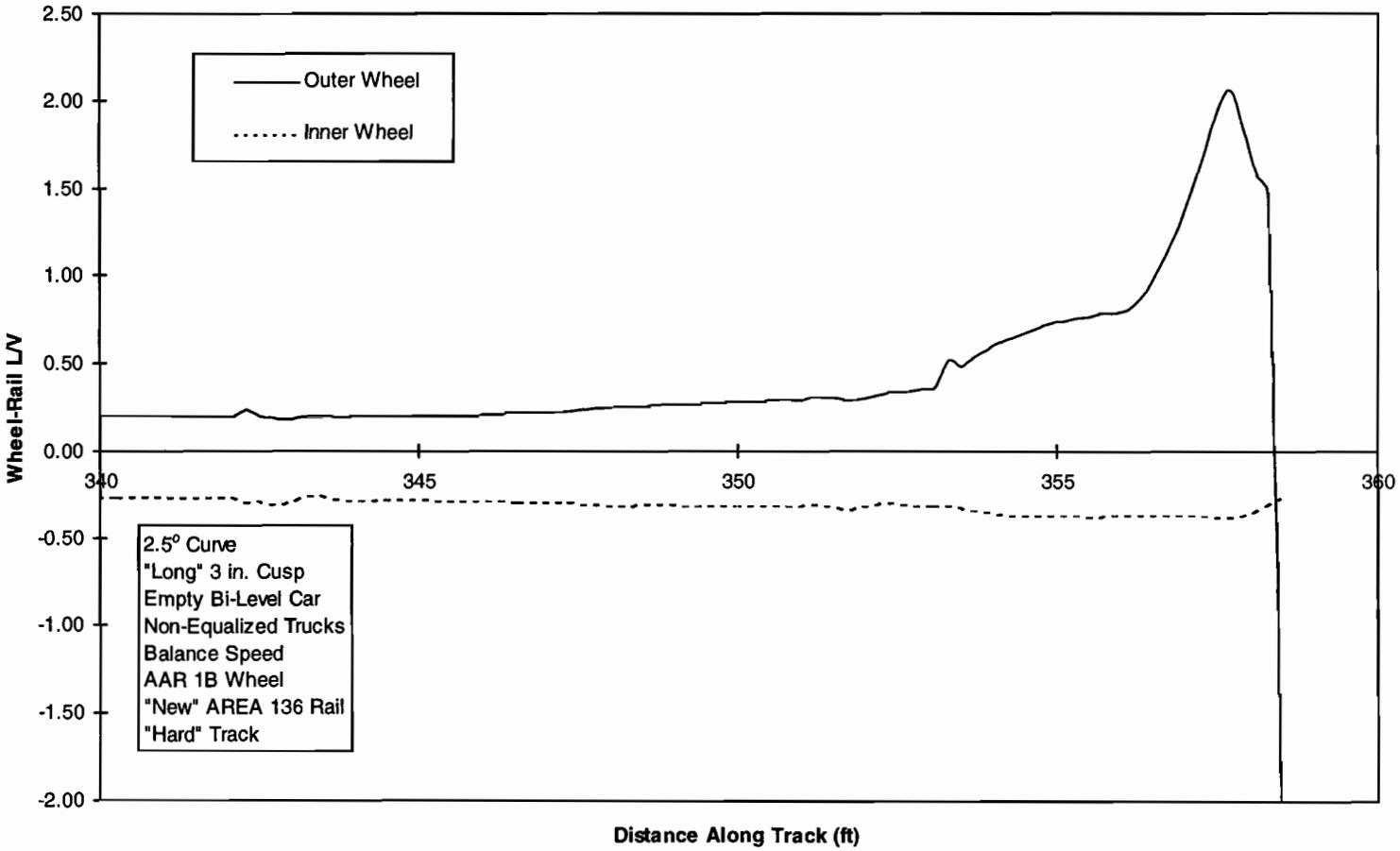

Figure 4-11. L/V ratios on leading wheels

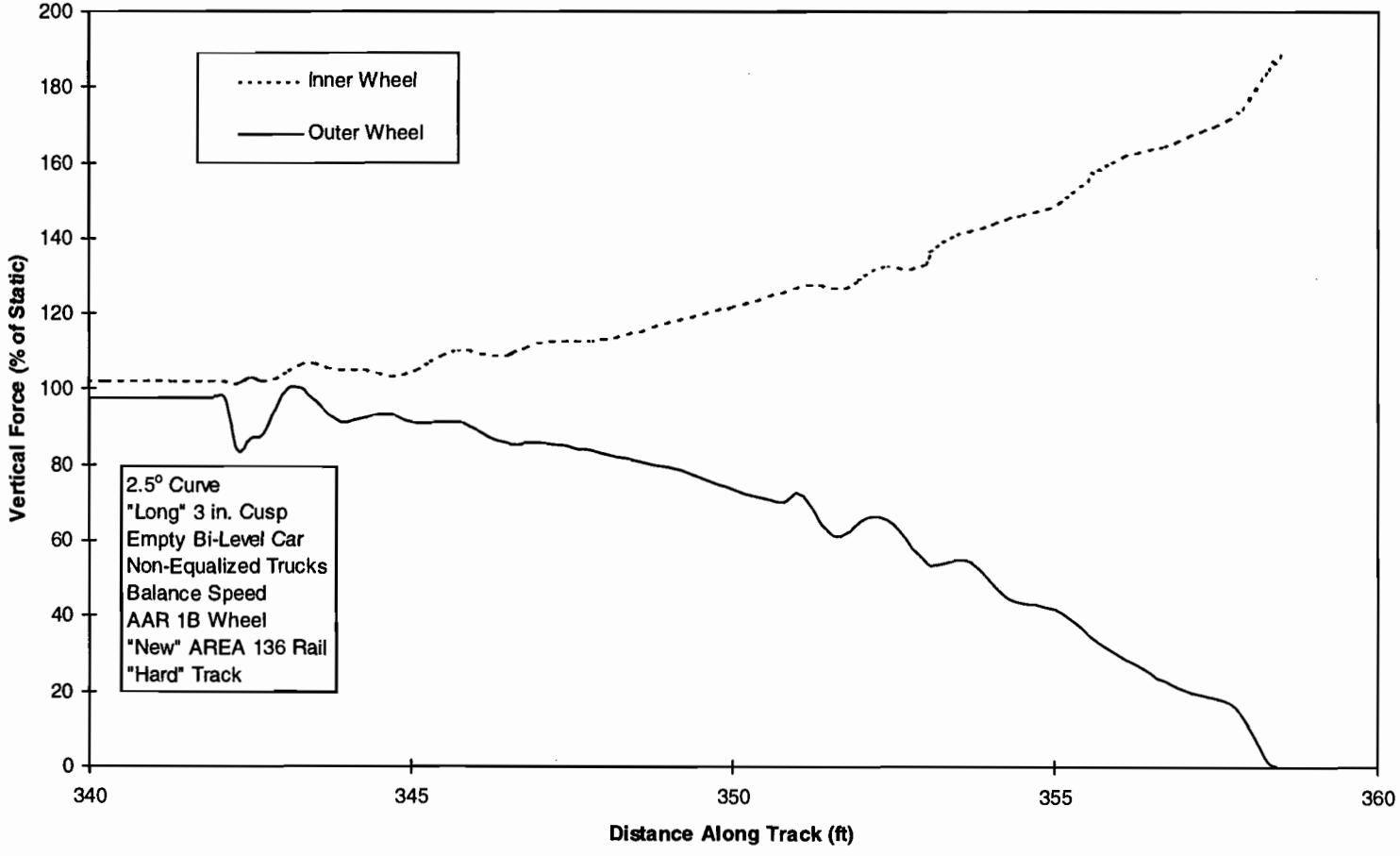

Figure 4-12. Vertical force reduction on leading wheels

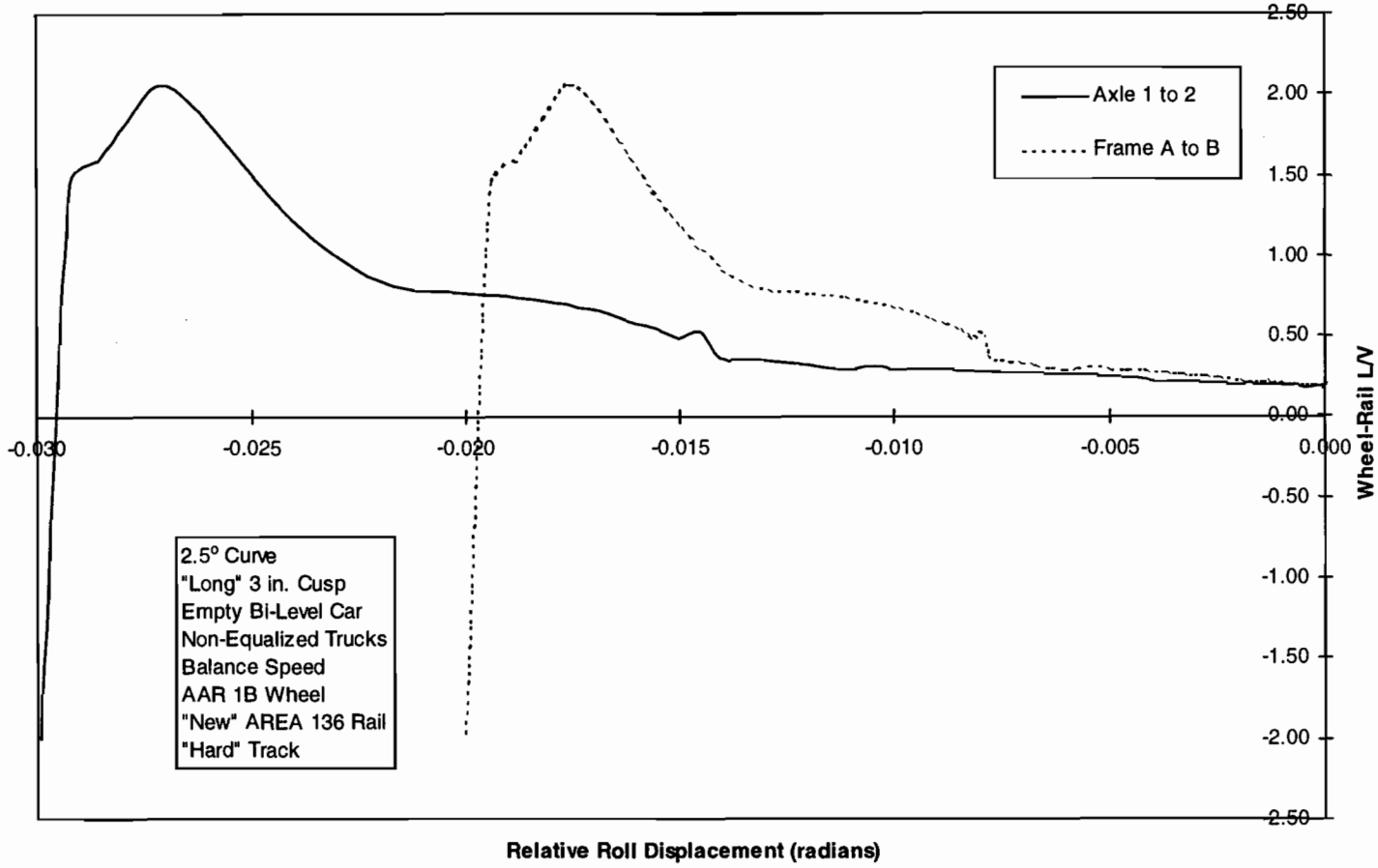

Figure 4-13. L/V ratios on lead outer wheel versus relative roll displacement

derailment, occurring before the cusp is reached. Figure 4-14 also shows the complete wheel unloading. The lines of static wheel unloading are also introduced into Figure 4-15 and again show the importance of truck shear in the result. The twist moment between the axles for full slippage at the wheel/rail interface is over 20,000 lb-in. This takes place at just over 10 mrads and leads to a small oscillation in the result shown previously in Figure 4-7 and for this car with non-equalized trucks in Figure 4-14.

The sets of results for the two base bi-level vehicles on "hard" track, shown above, indicate the significant difference in their behavior over the cusps. The car with equalized trucks retains sufficient vertical force under this very severe dip (FRA Class 1) and the resulting crosslevel, to continue steering through the cusp point, but is subject to a bounce following it. No derailment was noted however. On the other hand, the car with non-equalized trucks loses the vertical load on the lead outer wheel sufficiently to cause a wheel climb derailment due to loss of guiding forces. This behavior is adequately supported by a static model which includes the shear across the truck.

4.2 Effect of "Soft" Track and Low Body on the Results Over the 39 ft "Long" Length Cusp in a 2.5 deg Curve

Results from variations in the base cases are now discussed. The first variation is that of the "soft" track under the same cars. For the bi-level car with equalized trucks the lateral shift of the rails at the lead axle is shown in Figure 4-15. Being softer, the motion is larger than for the hard track, principally from lateral tie movement on the ballast of about 1/4 in. However, of greater importance, Figure 4-16 shows reduced wheel unloading and a much lower lateral force which leads to the lower L/V shown in Figure 4-17. Clearly there is a reduced danger from wheel climb on soft track. The percentage wheel unloading shown against roll angle difference in Figure 4-18, still indicates the importance of truck shear, and is generally less dynamic than the result on "hard" track. A similar set of results is shown in Figures 4-19 to 4-22 for bi-level cars with non-equalized trucks on "soft" track in the 2.5 deg curve.

The final variation for the "long" cusp in the 2.5 deg curve is for the single-level cars having a lower center of gravity and slightly lower weight. The track is again "hard." Since the static wheel load is less for this car, it might be expected that its results will be the worst from the point of view of safety from loss of guidance. This is confirmed by the results. For the equalized car, Figure 4-23 shows the lead outer wheel forces and Figure 4-24 the resulting L/V along the track. While no static wheel lift is apparent up to the cusp point, it is very close to lifting after at the "bounce," with a resulting brief, very large, L/V of over 2.3. The equivalent static slope for full interaxle shear in Figure 4-25 shows its importance in static analysis. A similar set of results is shown in Figures 4-26 to 4-28 for the single-level car with non-equalized trucks on "hard" track in the 2.5 deg curve. The results show a greater dynamic and earlier temporary wheel lift prior to the final derailment which occurs at a similar place to that of the bi-level car.

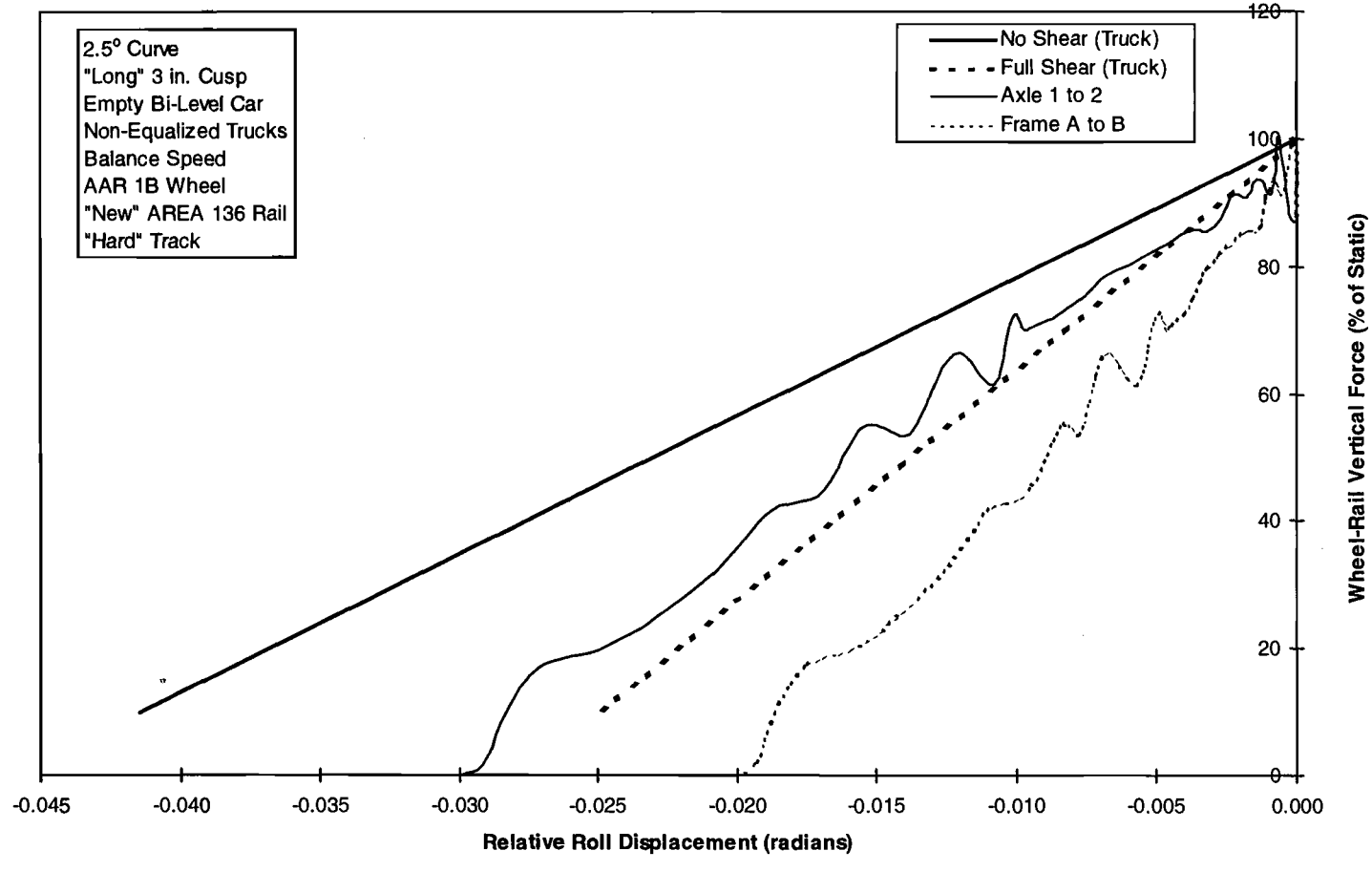

Figure 4-14. Percentage leading outer wheel vertical load versus relative roll displacement

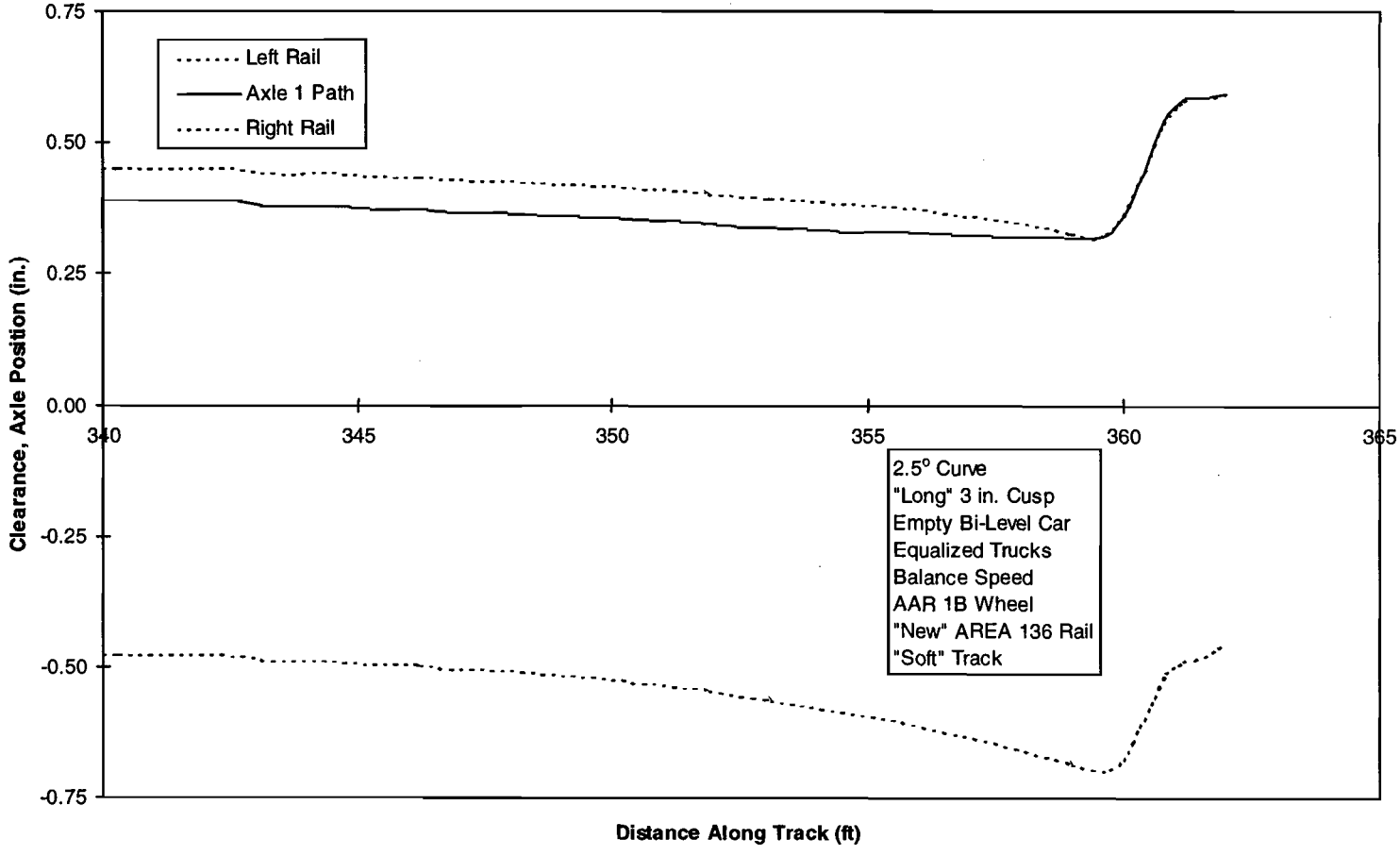

Figure 4-15. Lateral motion of lead axle

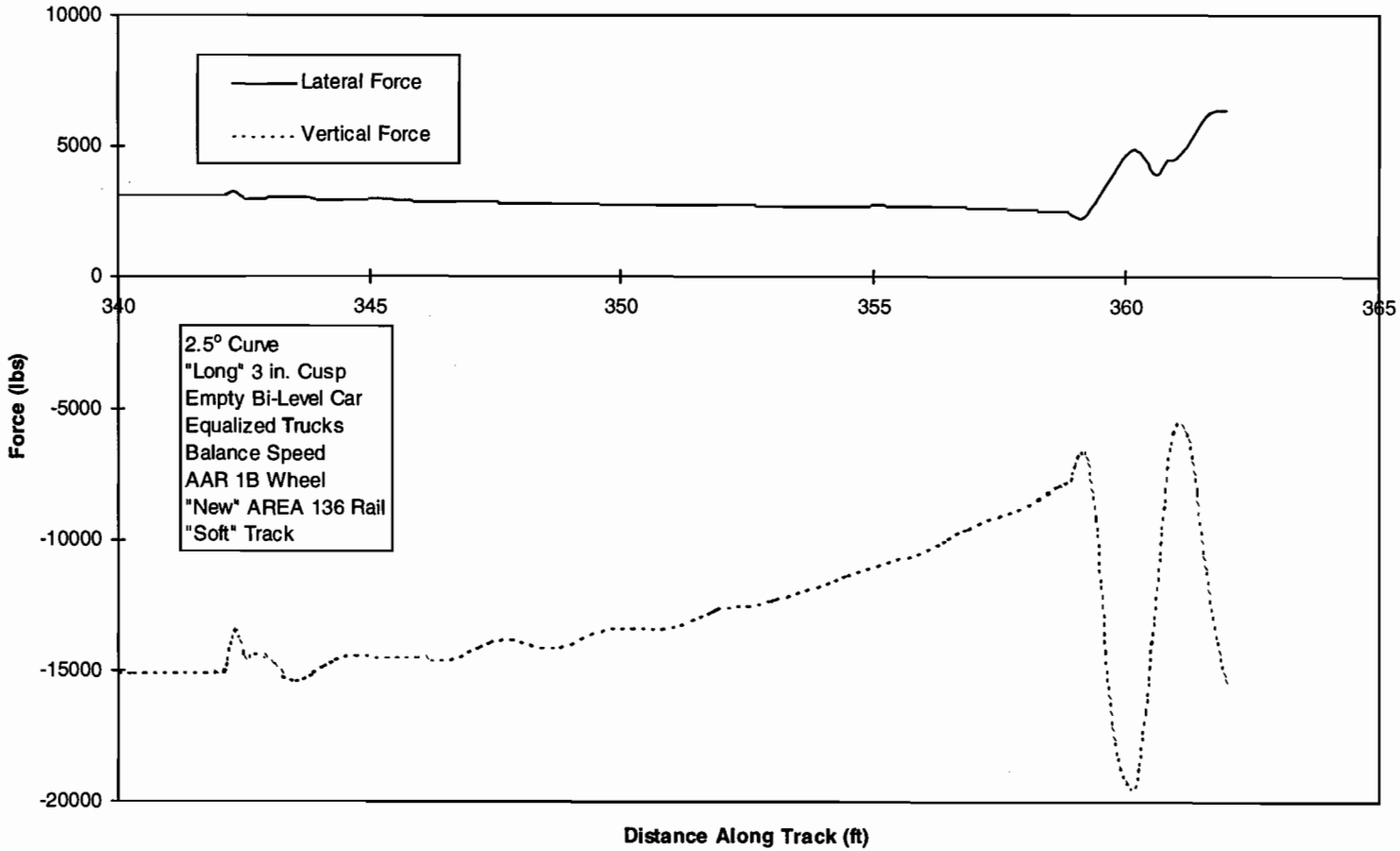

Figure 4-16. Lateral and vertical forces on lead outer wheel

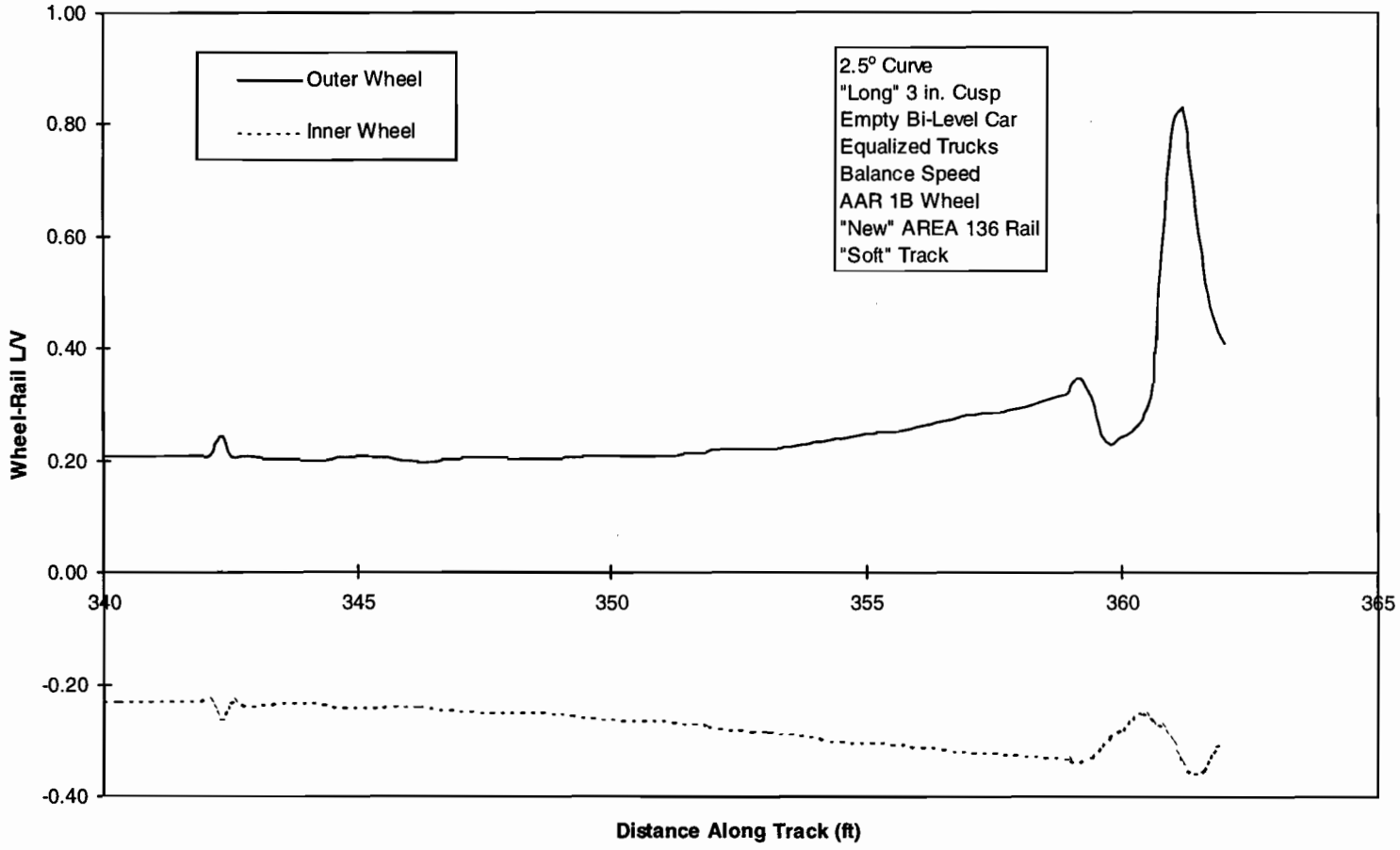

Figure 4-17. L/V ratios on leading wheels

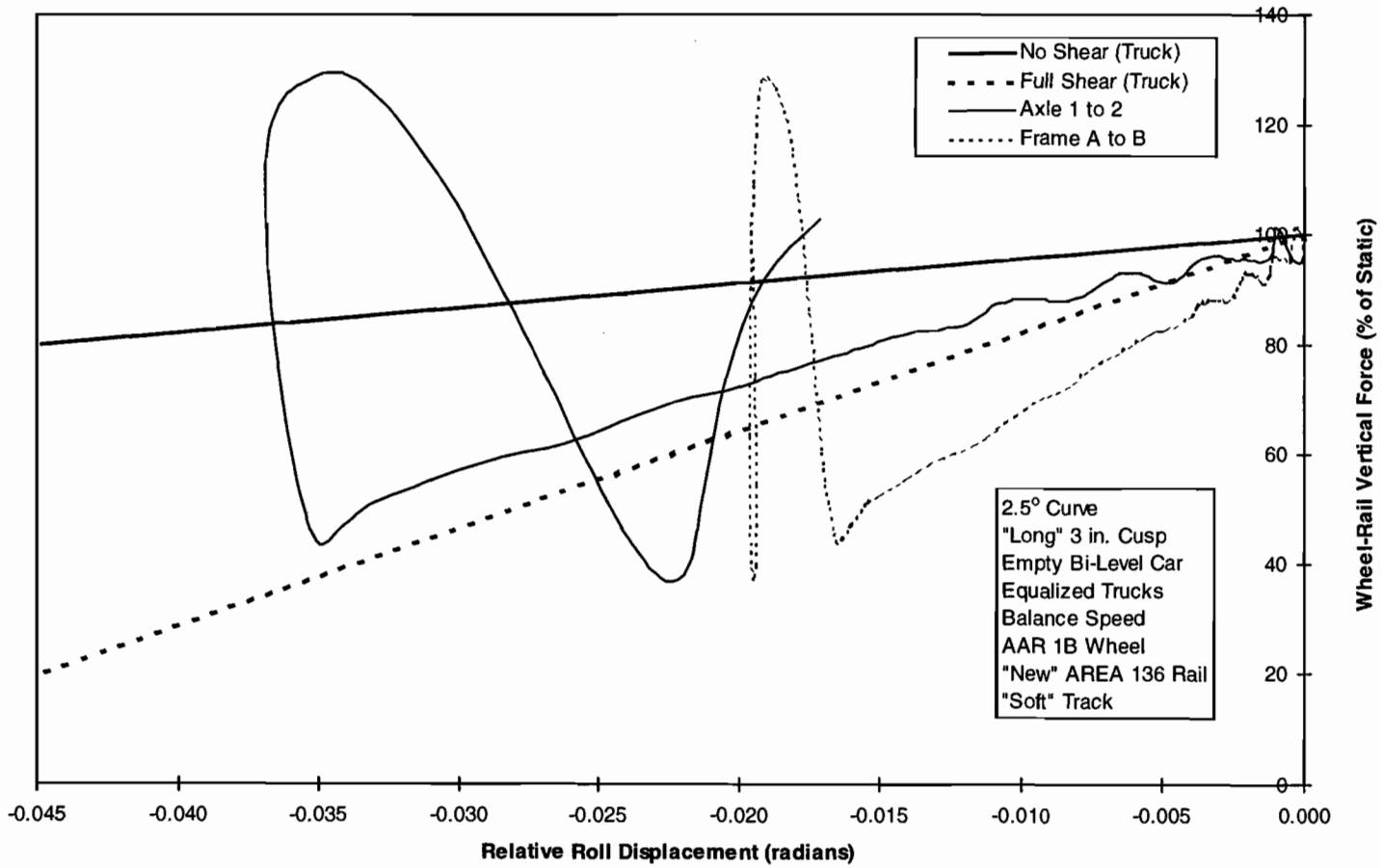

Figure 4-18. Percentage leading outer wheel vertical load versus relative roll displacement

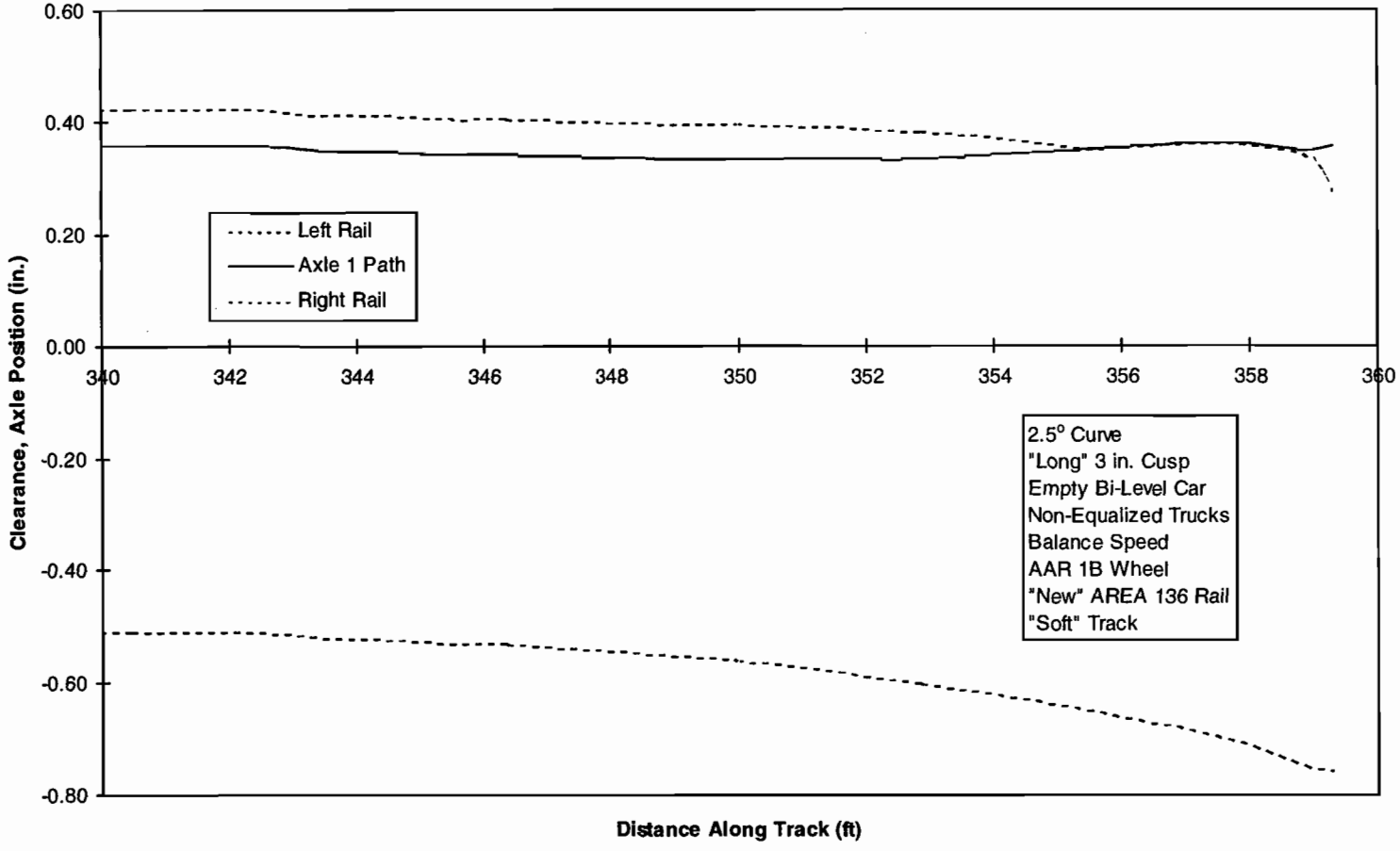

Figure 4-19. Lateral motion of lead axle

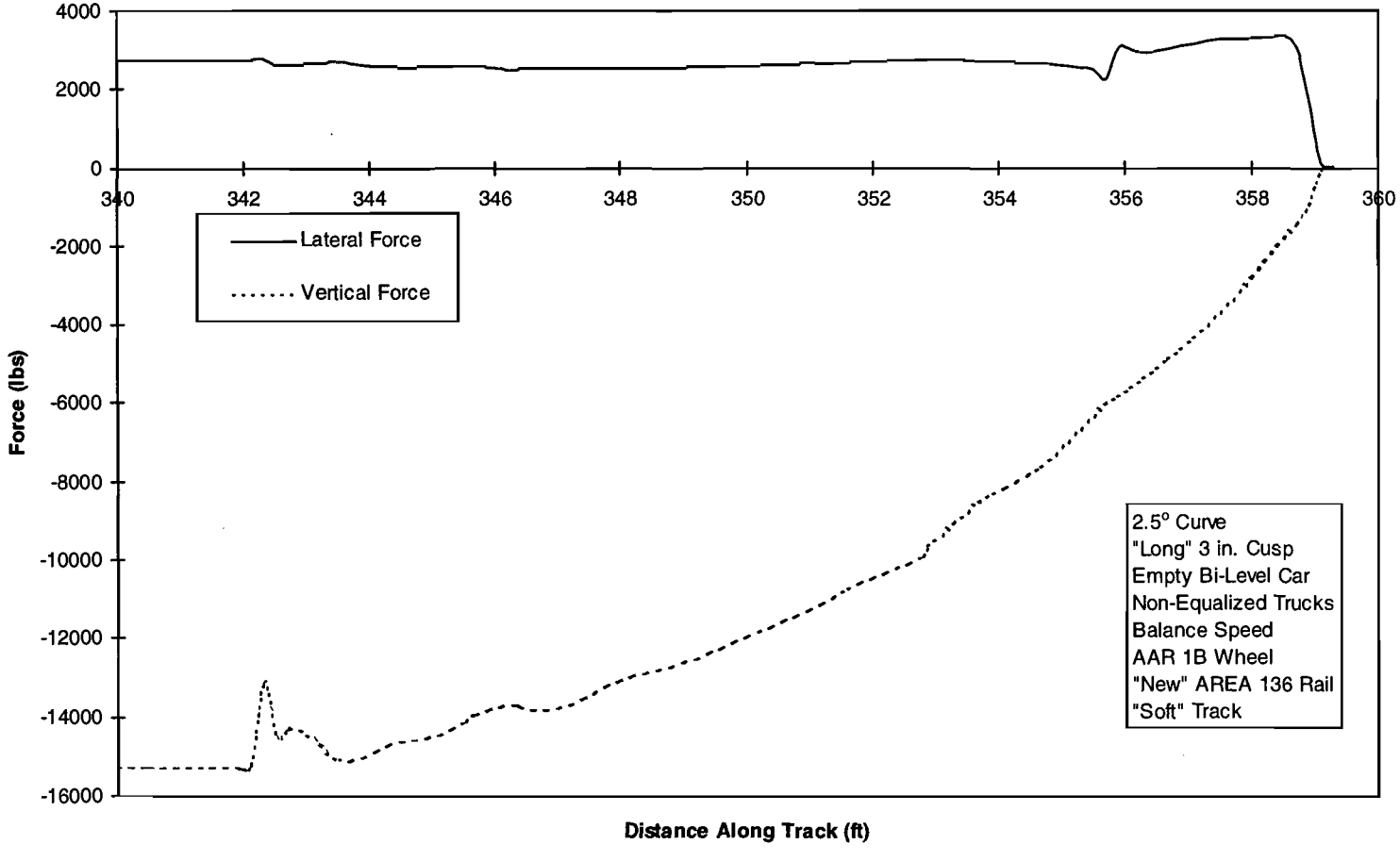

Figure 4-20. Lateral and vertical forces on lead outer wheel

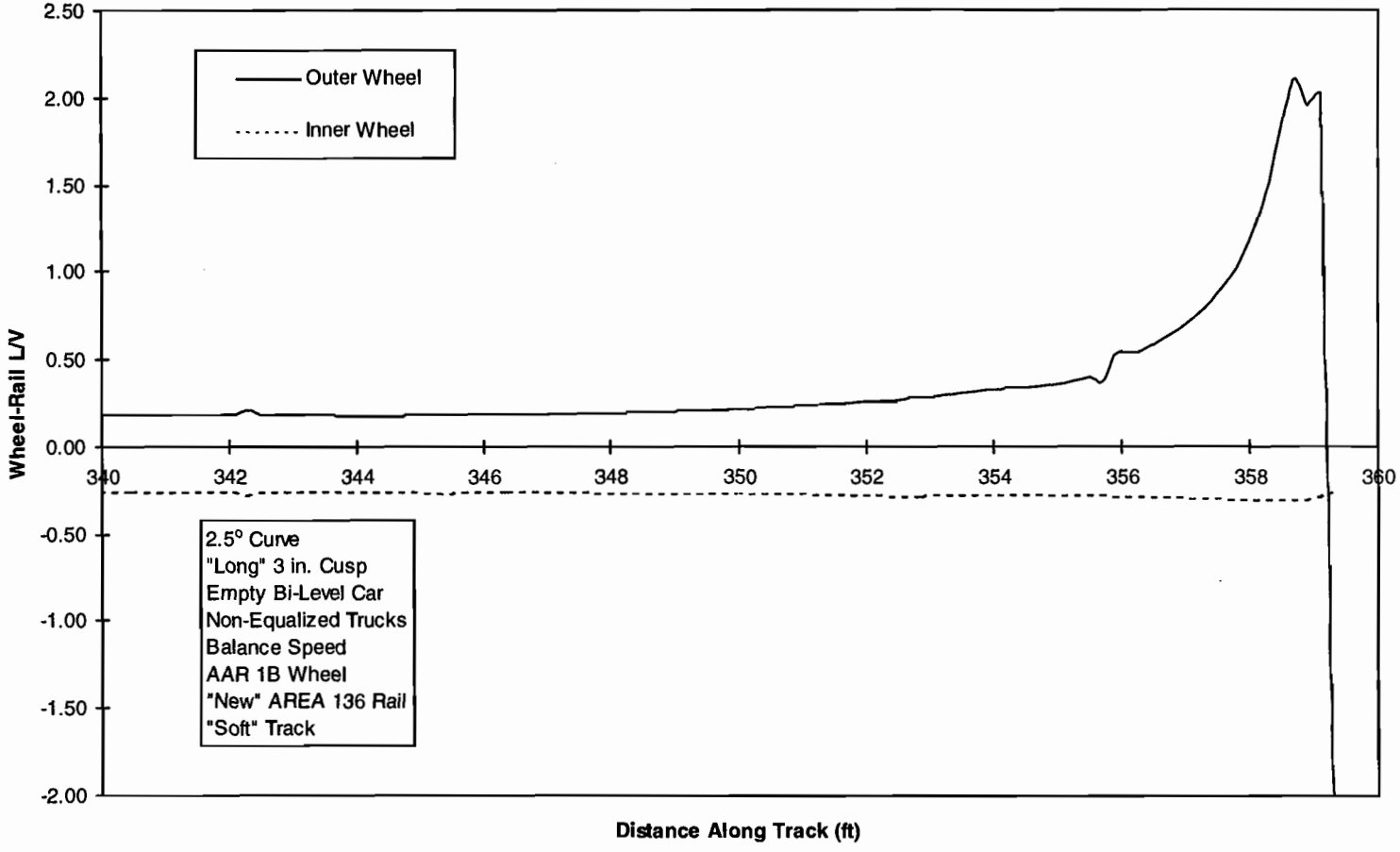

Figure 4-21. L/V ratios on leading wheels

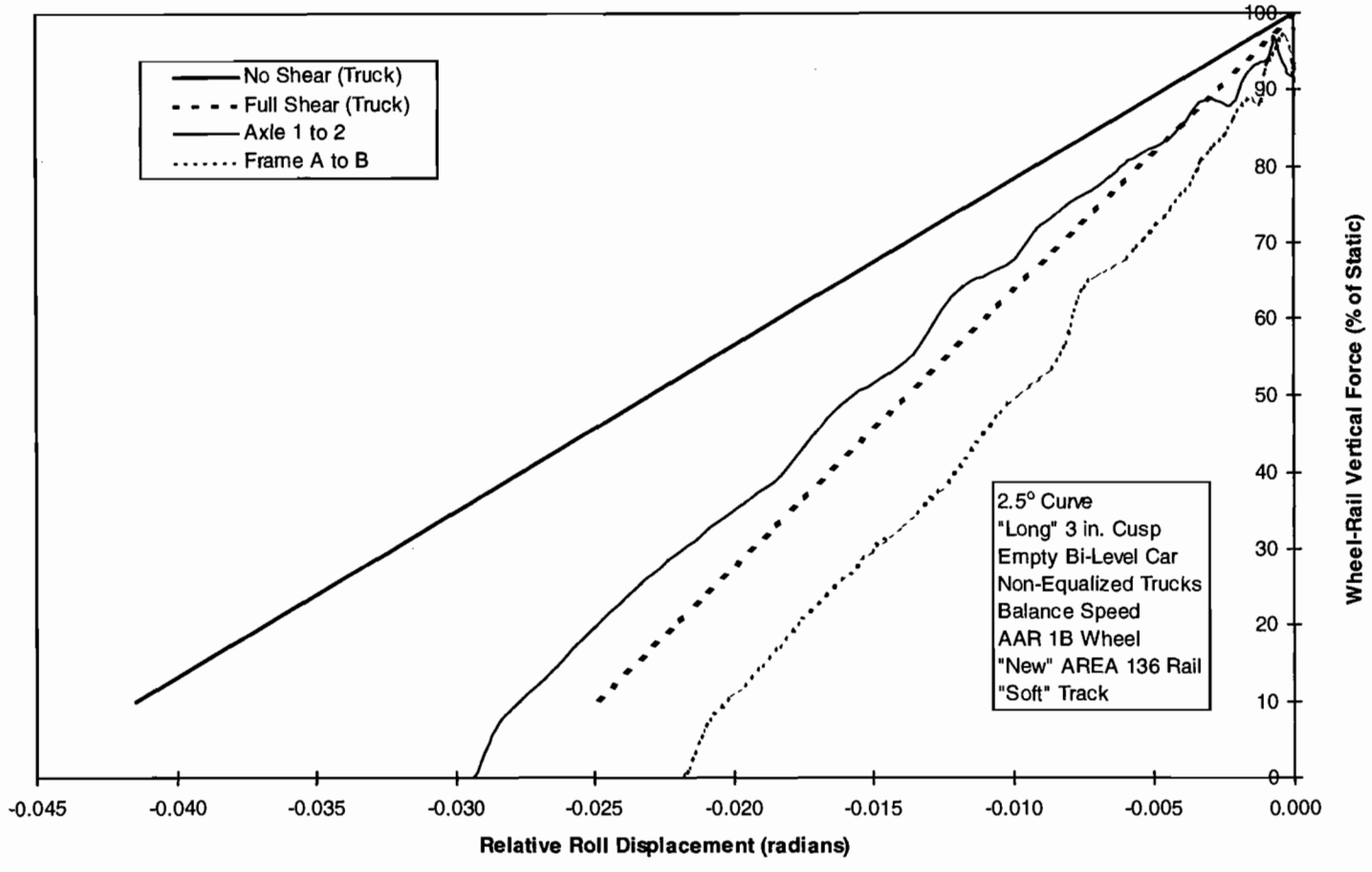

Figure 4-22. Percentage leading outer wheel vertical load versus relative roll displacement

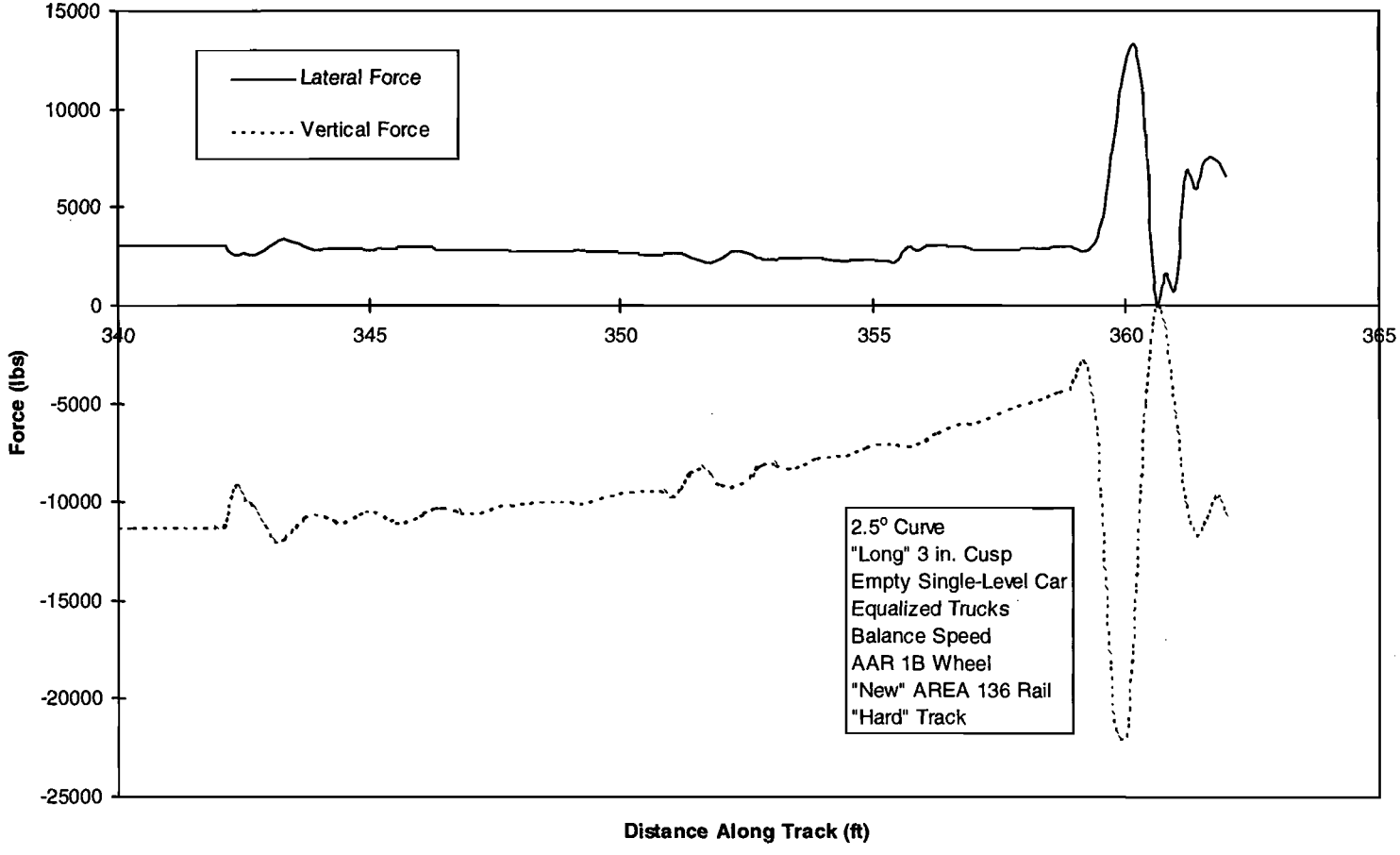

Figure 4-23. Lateral and vertical forces on lead outer wheel

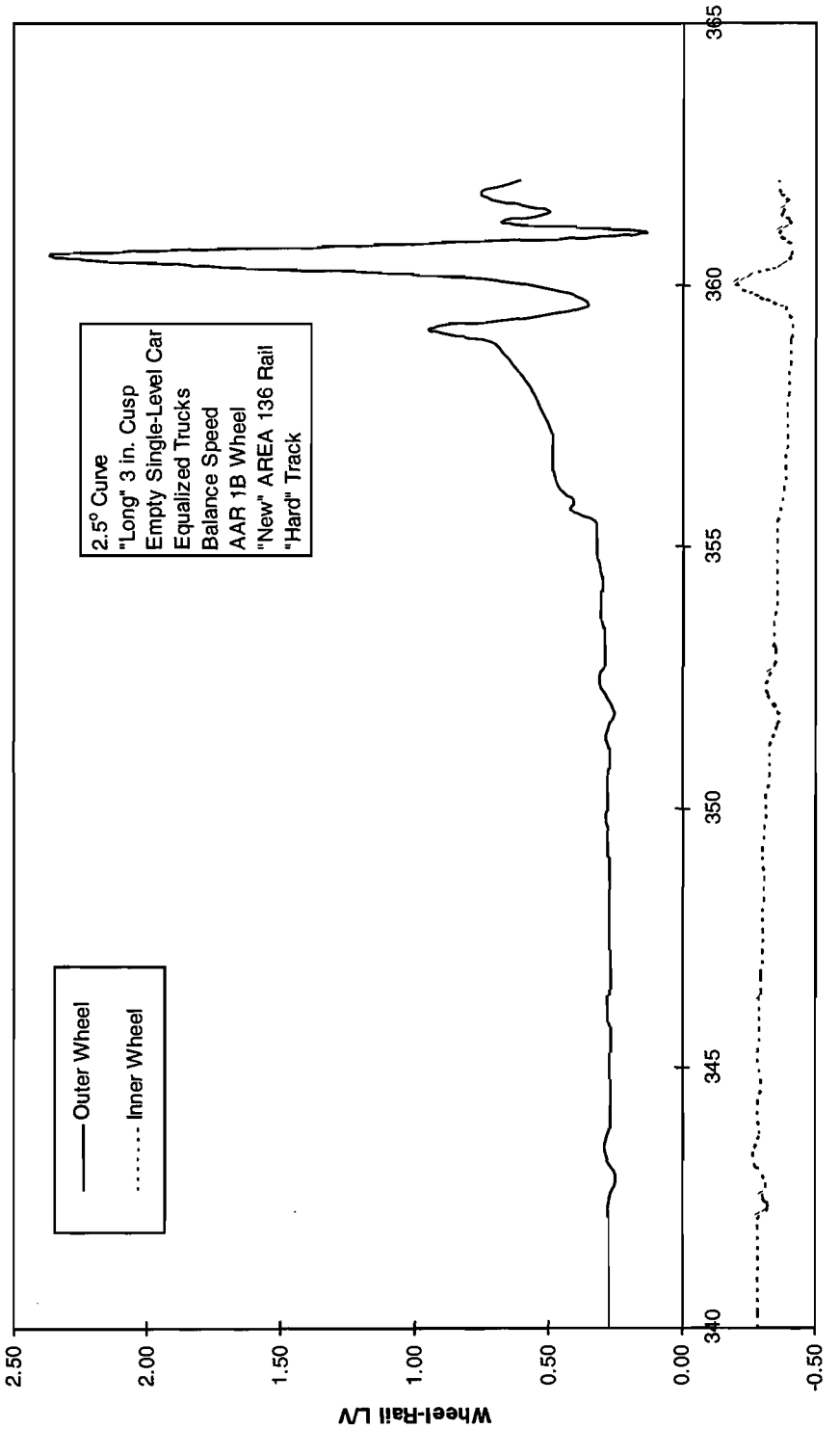

Figure 4-24. L/V ratios on leading wheels

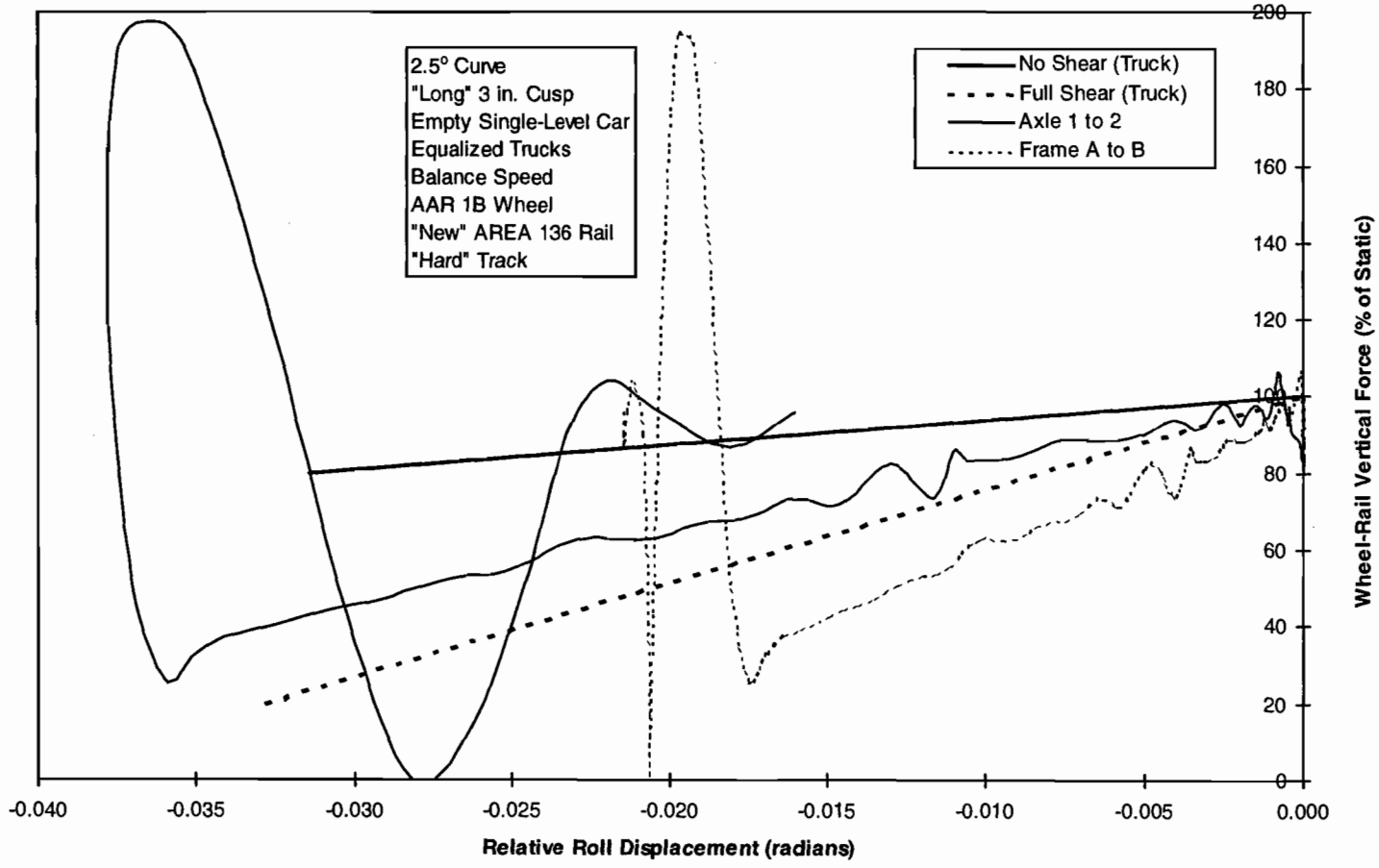

Figure 4-25. Percentage leading outer wheel vertical load versus relative roll displacement

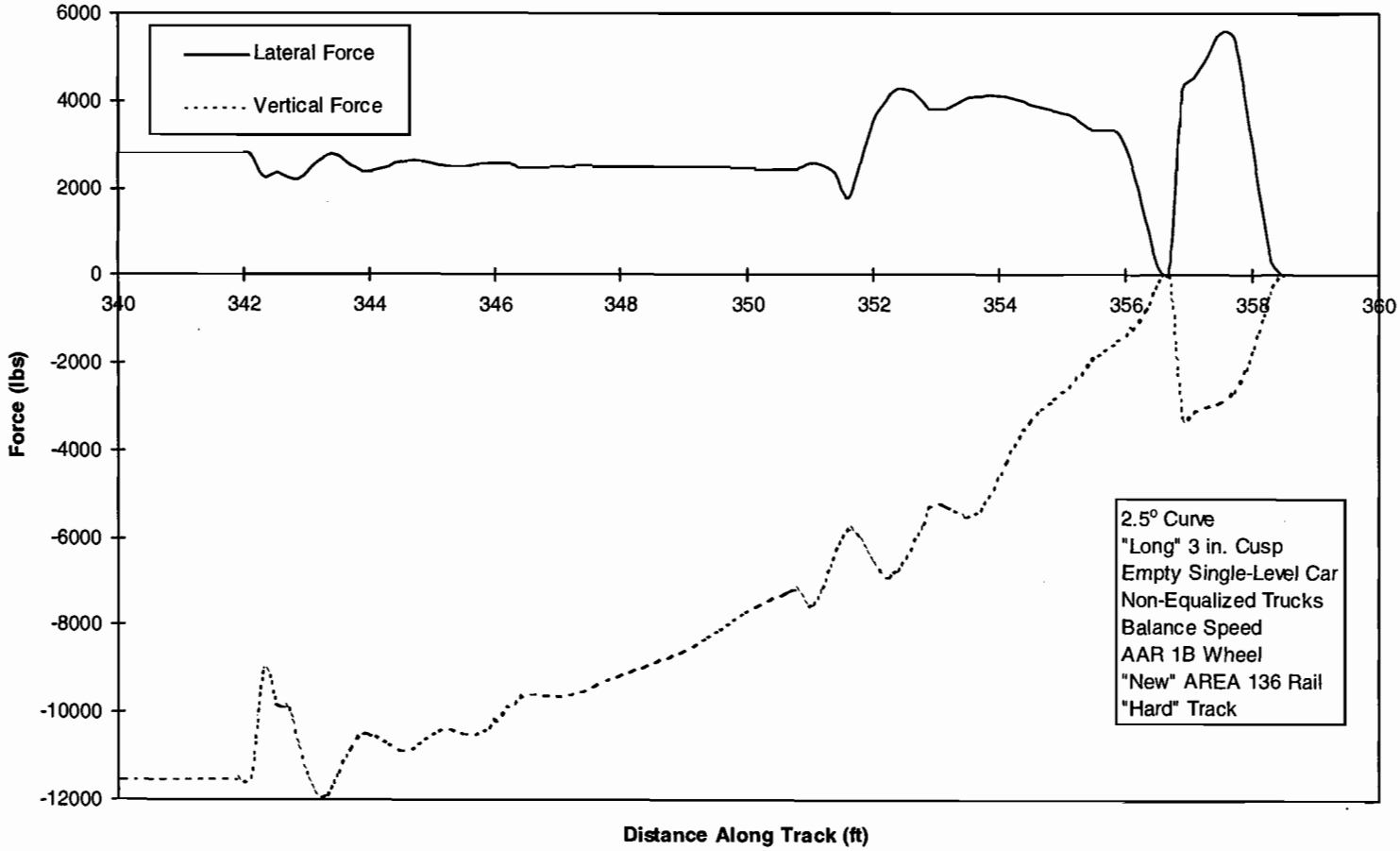

Figure 4-26. Lateral and vertical forces on lead outer wheel

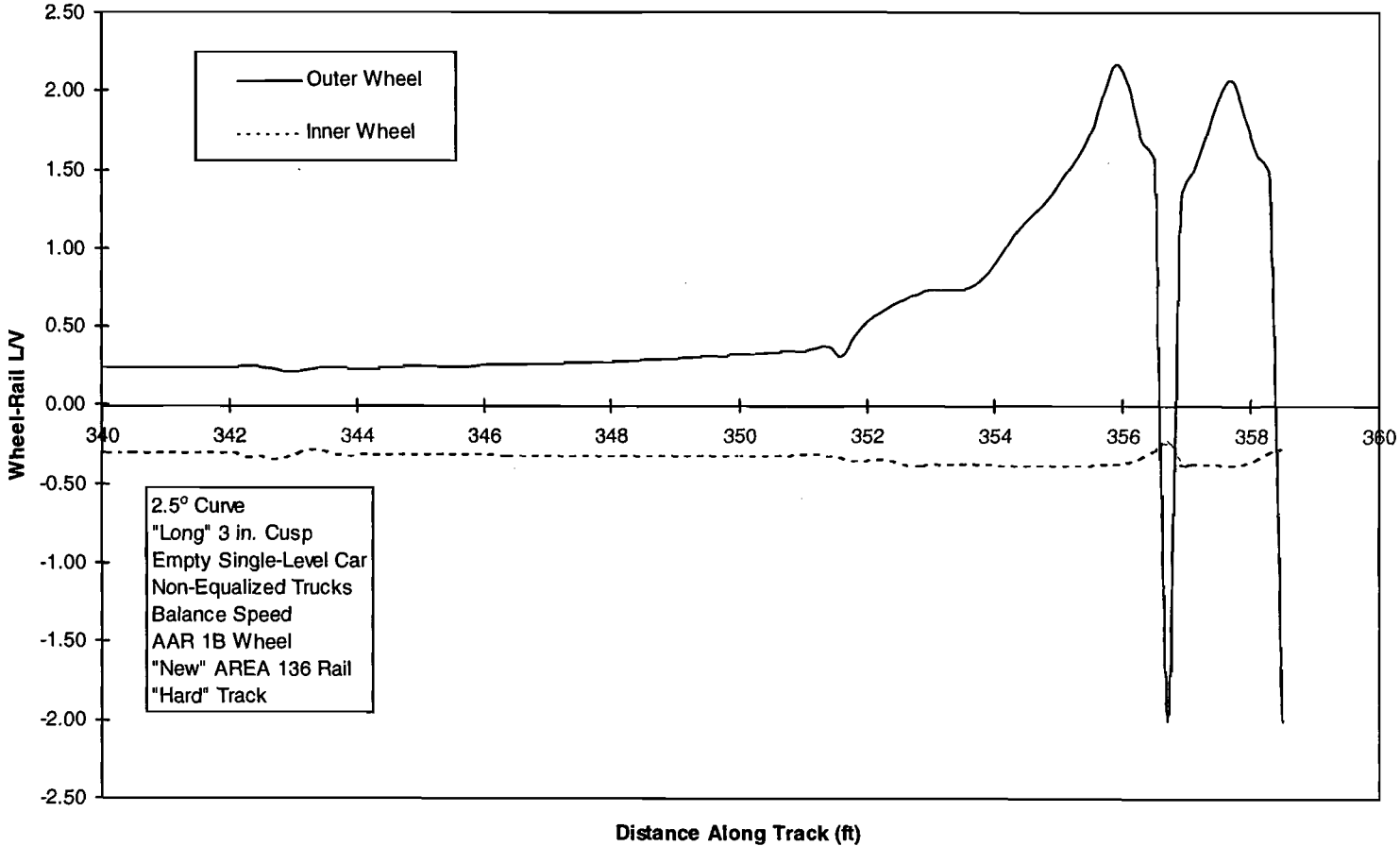

Figure 4-27. L/V ratios on leading wheels

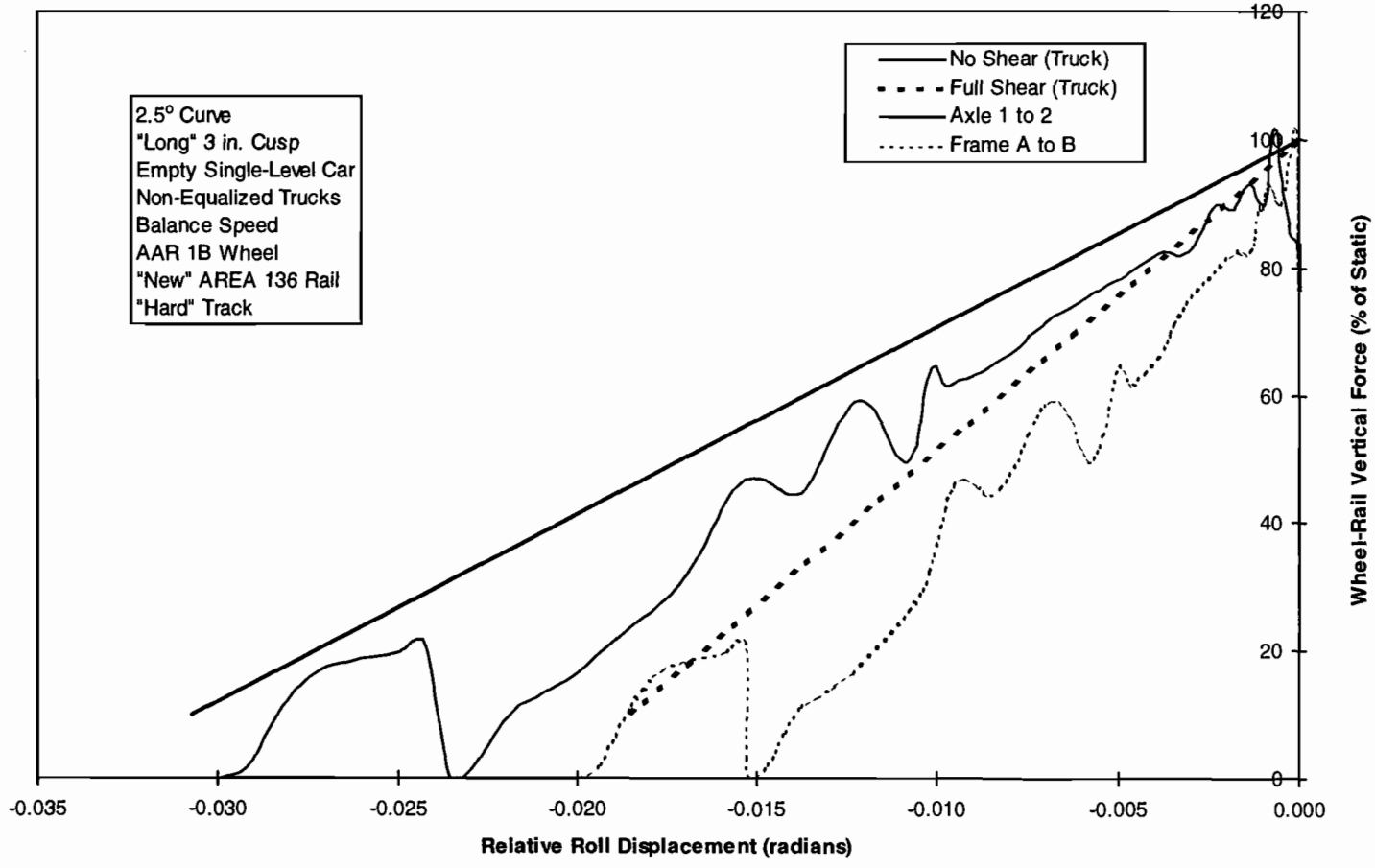

Figure 4-28. Percentage leading outer wheel vertical load versus relative roll displacement

4.3 The Effect of Track Curvature on L/V Values for Curves of 2.5 Up to 20 deg - Long Cusp

The first set of graphs are for the base car with equalized trucks on "hard" track. Figure 4-29 shows the lead outer wheel L/V as the vehicle moves over the cusp in the various curves. There is a small discontinuity at the commencement of the cusp which dies and is followed by the slow increase due to wheel unloading. This is further followed after the cusp point at 359 ft by the bounce giving a maximum L/V close to 1.6 for a very short duration, less than 2 ft, apparently insufficient to cause a loss of guidance. The numerical value at the apex of the graphs of L/V remains in doubt due to the step length. The lateral forces in the 10 deg curve and larger appear close to full slip and increase very little with curvature. This is also true for the car with non-equalized trucks shown in Figure 4-30. However, in this set of results, a derailment occurs at all curvatures before the cusp point is reached. It is reached earlier in the higher curvatures where full slip is apparent.

On "soft" track, the same results for the car with equalized trucks is shown in Figure 4-31. Full slip is relegated to curvatures above 15 deg and the peak L/V at bounce is significantly less than on hard track. The behavior appears safer from wheel climb. However, the difference is less apparent for the car with non-equalized trucks shown on "soft" track in Figure 4-32, derailments occurring in all cases.

Finally, for these plots of L/V, the single-level car with equalized trucks is shown in Figure 4-33 and with non-equalized trucks in Figure 4-34. Only the results for the 2.5 and 20 deg curves are given. Both are less safe than for the bi-level base case due to lower wheel loads. The behaviors are similar with the non-equalized trucks derailing earlier in the cusp. The higher L/V values of the equalized truck in the bounce following the cusp point are limited to the lower curvatures.

4.4 The Effect of Track Curvature on Percentage Lead Outer Wheel Unloading for Curves of 2.5 Up to 20 deg - Long Cusp

Figures 4-35 to 4-40 show the percentage unloading of the lead outer wheel versus the difference in roll across axles 1 and 2 for the same parameter variations and curvatures as in the previous six figures. The overall behavior shown is the same as that described previously with certain minor additions. For the car with equalized trucks on "hard" track, Figure 4-35 shows a slope close to that of the static line with full shear stiffness of the truck included. However, the graphs from OMNISIM show an offset which increases with curvature and saturates at the higher curvatures. This is due to the increase in net axle lateral force with curvature which introduces a vertical load shift to the outer wheel, even at balance in the curve. This important effect was not included in the static analysis. It can be seen to increase the safety from wheel climb slightly as the curvature increases by reducing the percentage unloading. Although the offset vertical load also exists in the car with non-equalized trucks in Figure 4-36, it has no advantageous effect on the derailments which occur slightly earlier.

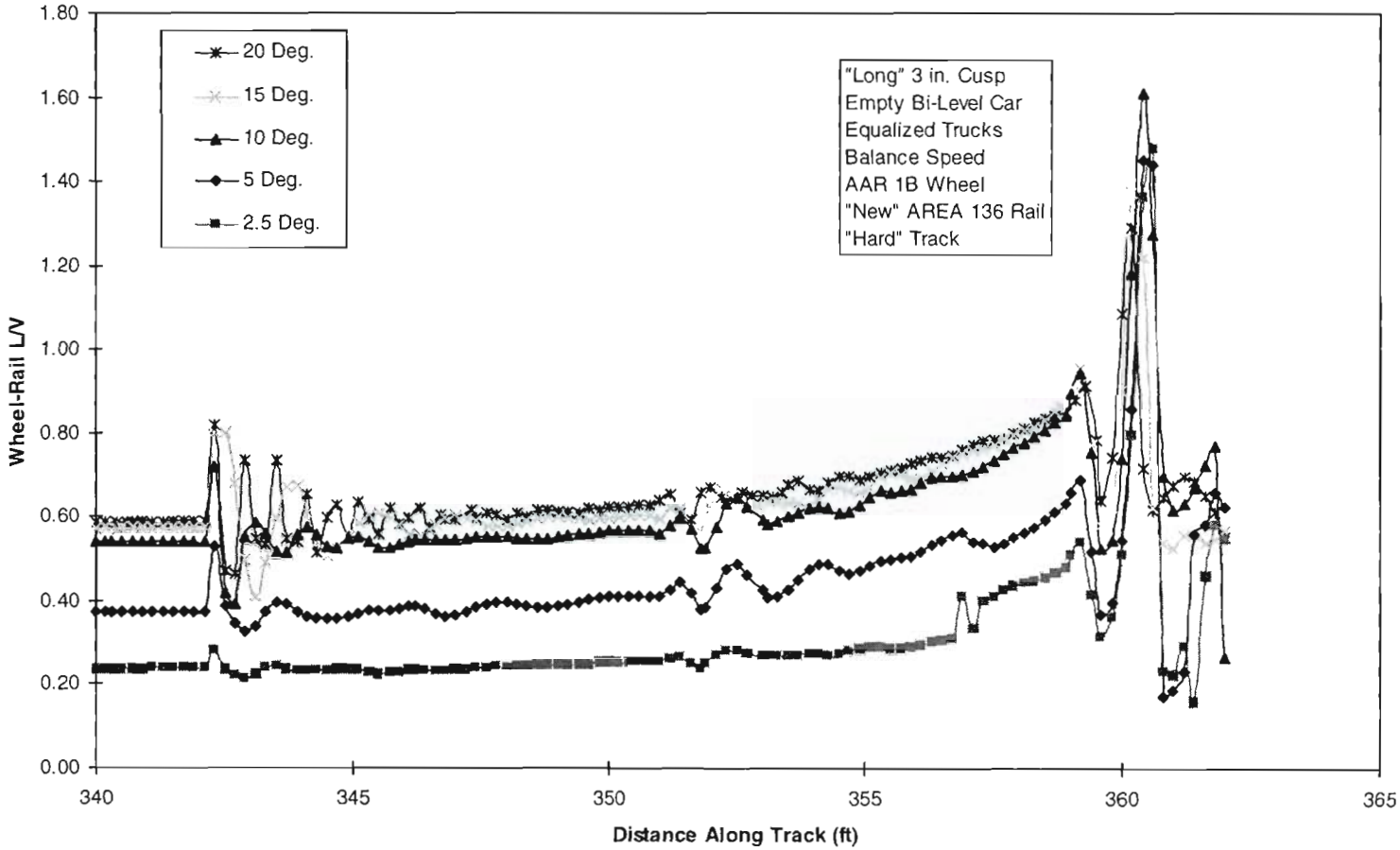

Figure 4-29. Comparison of L/V ratios on leading outer wheel

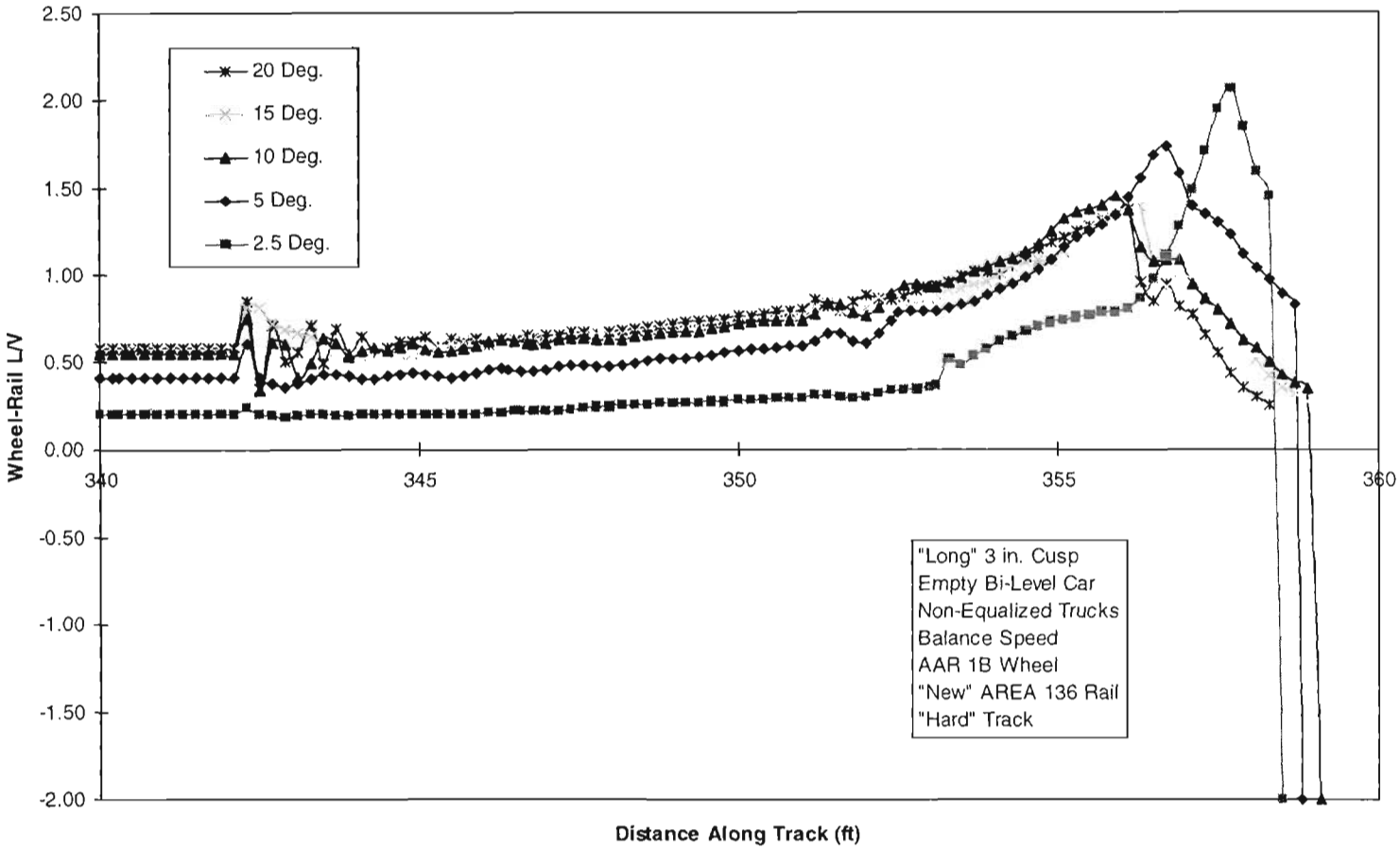

Figure 4-30. Comparison of L/V ratios on leading outer wheel

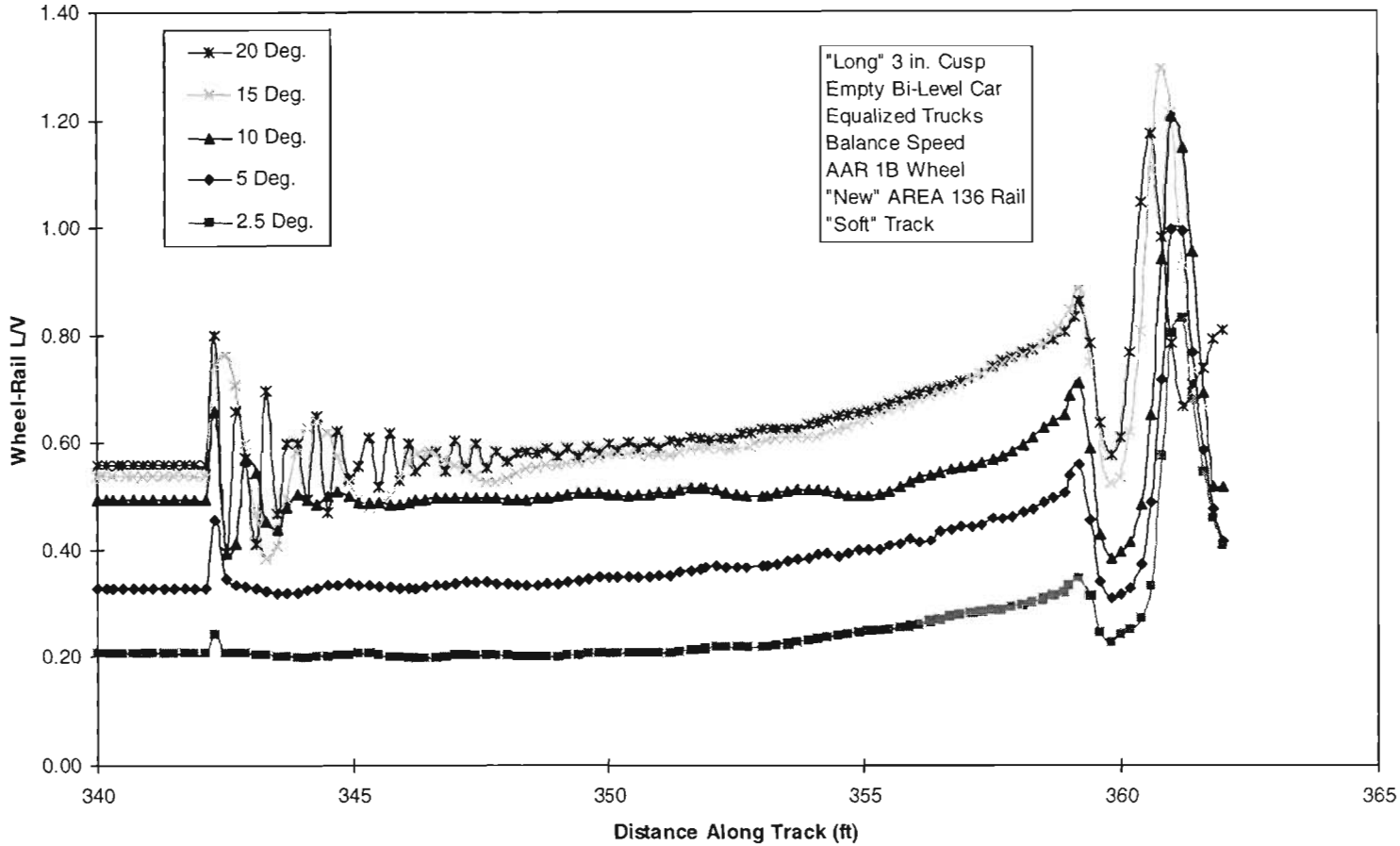

Figure 4-31. Comparison of L/V ratios on leading outer wheel

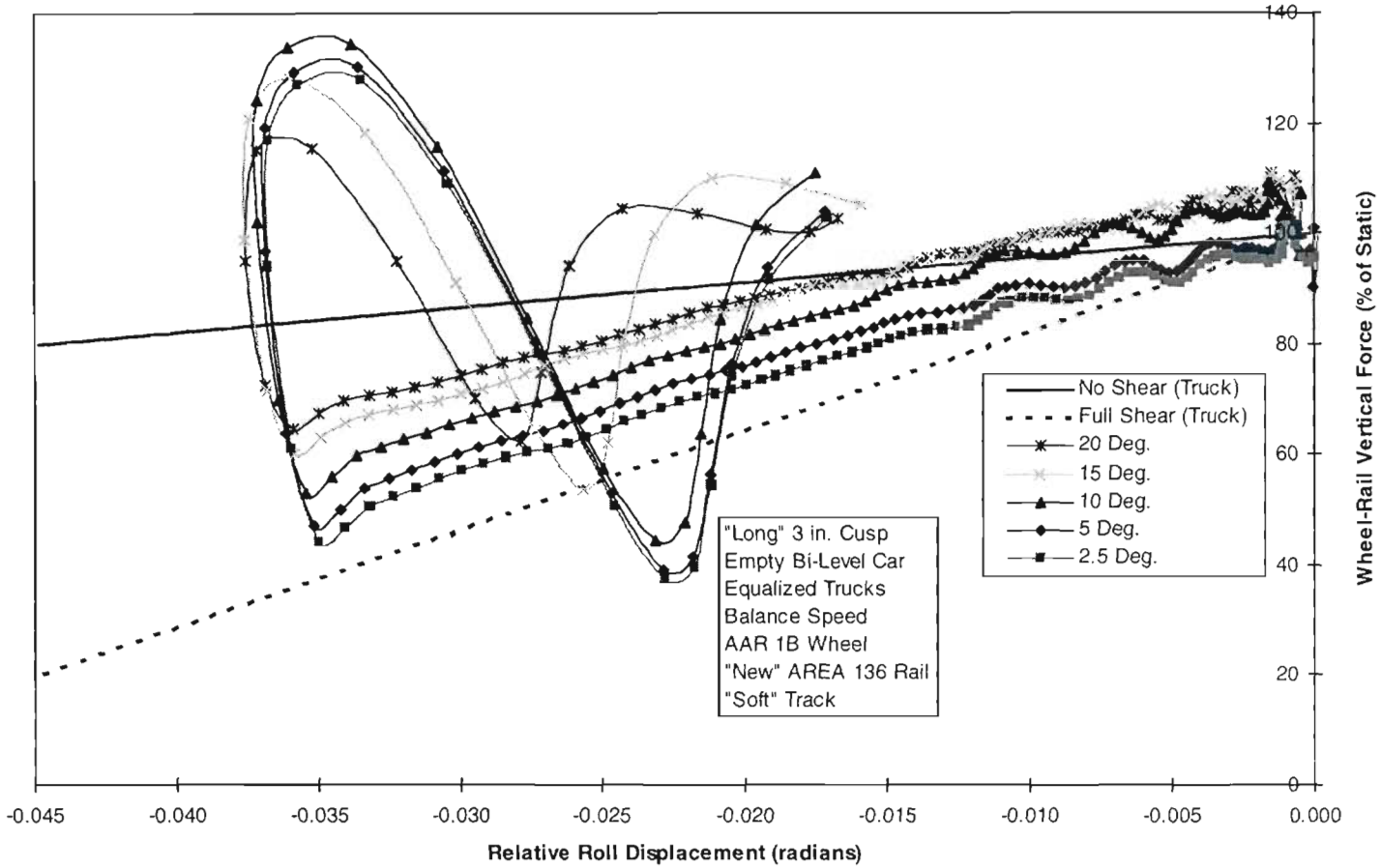

Figure 4-32. Comparison of L/V ratios on leading outer wheel

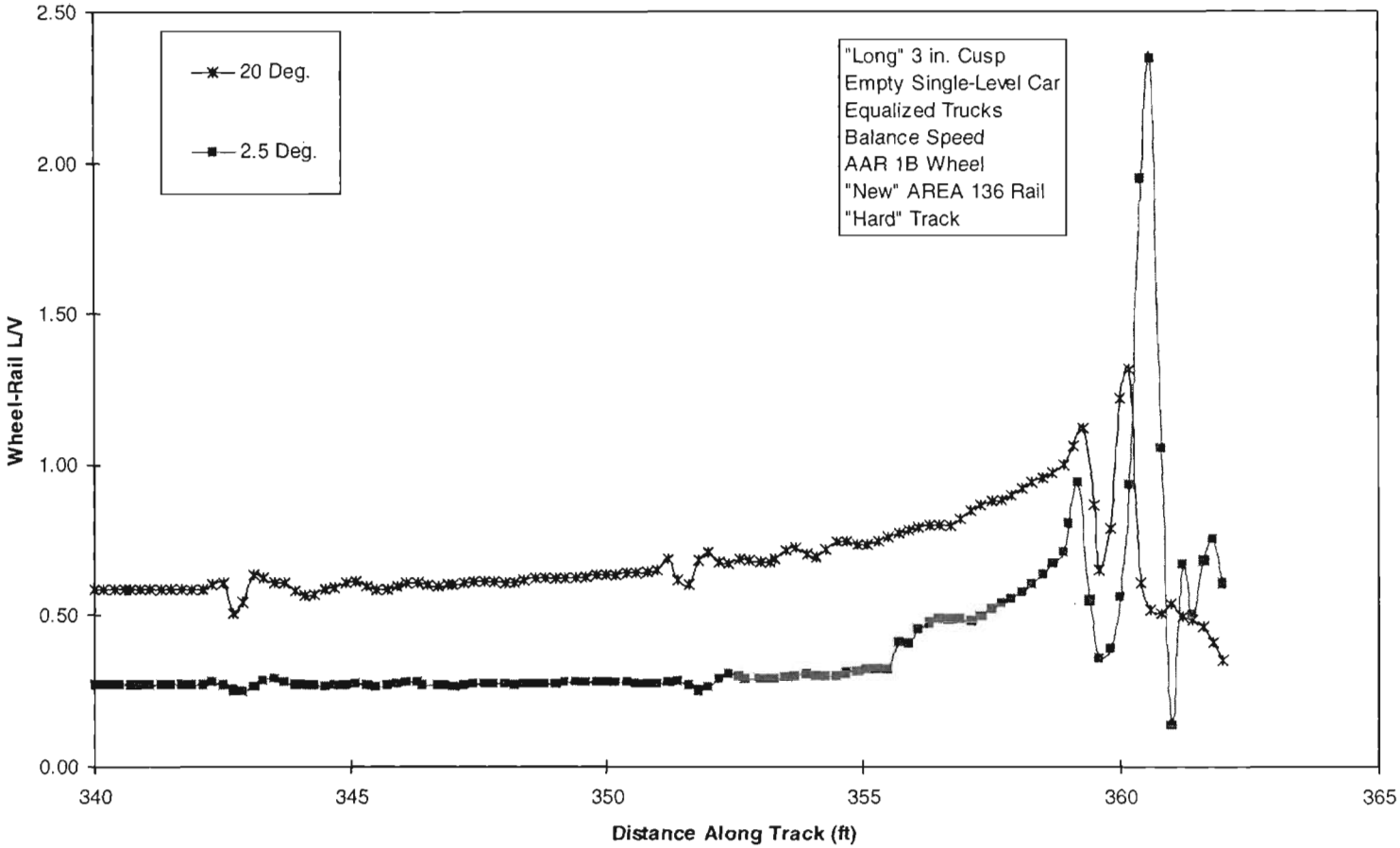

Figure 4-33. Comparison of L/V ratios on leading outer wheel

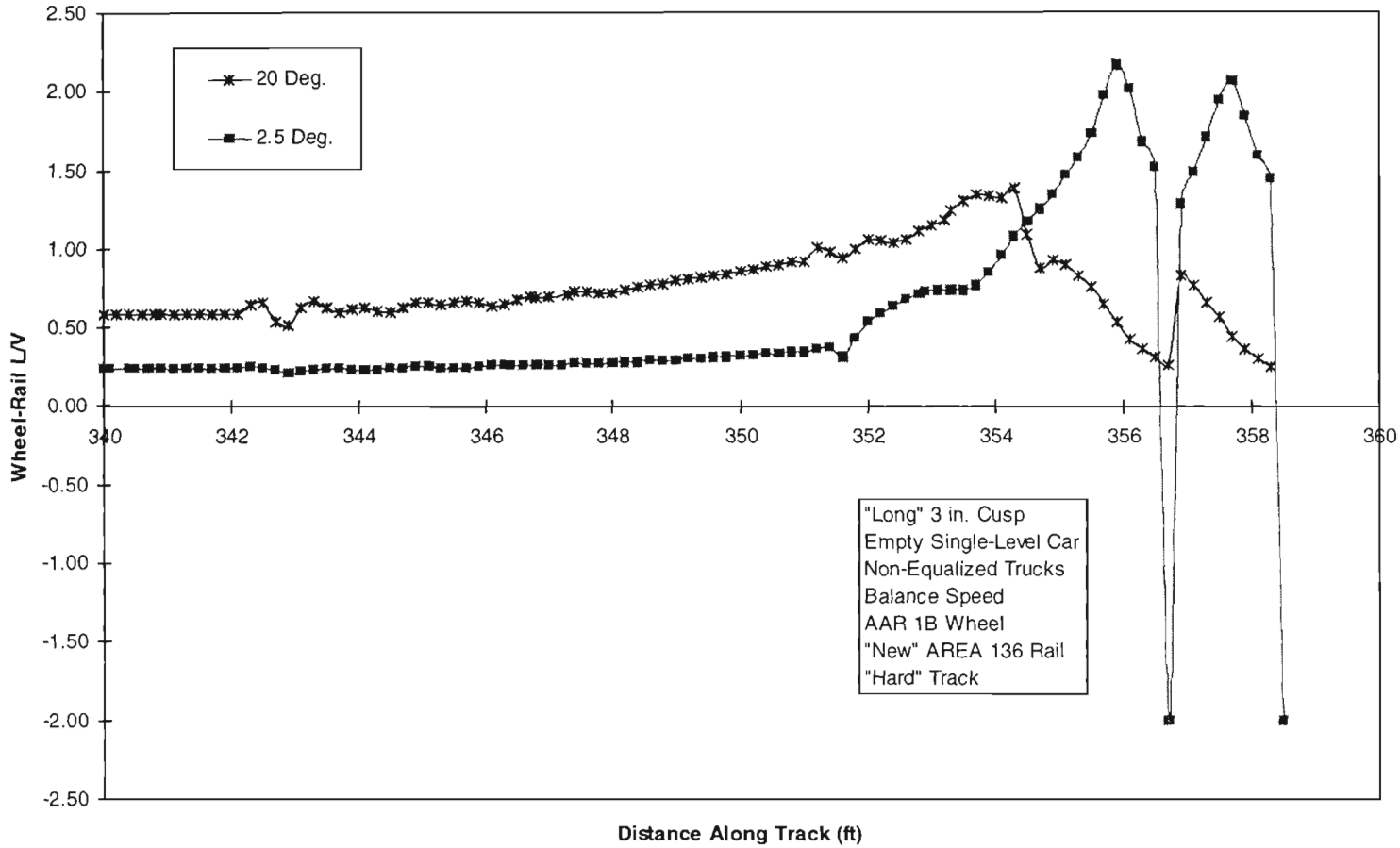

Figure 4-34. Comparison of L/V ratios on leading outer wheel

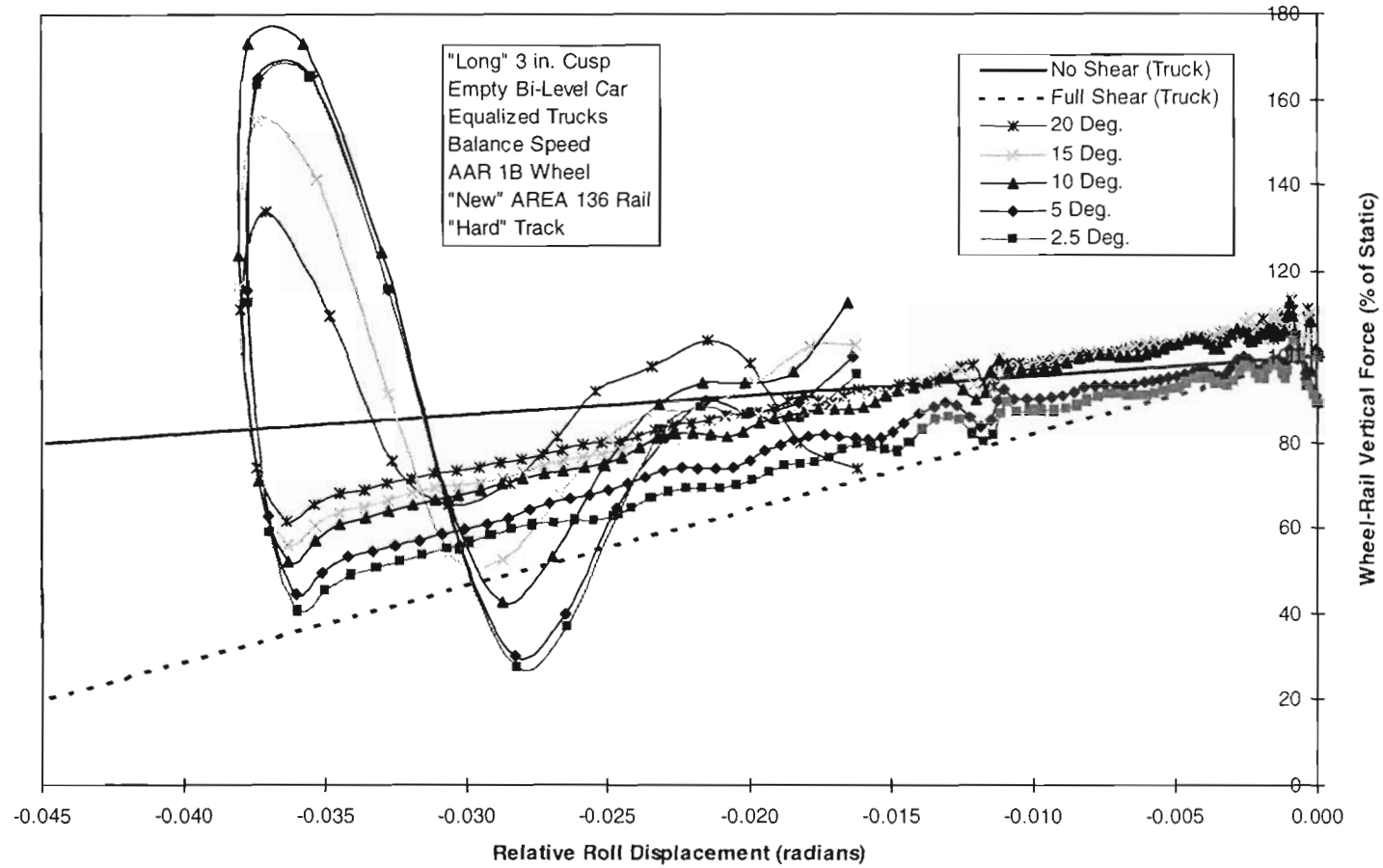

Figure 4-35. Percentage leading outer wheel vertical load versus relative roll displacement (axles 1 and 2)

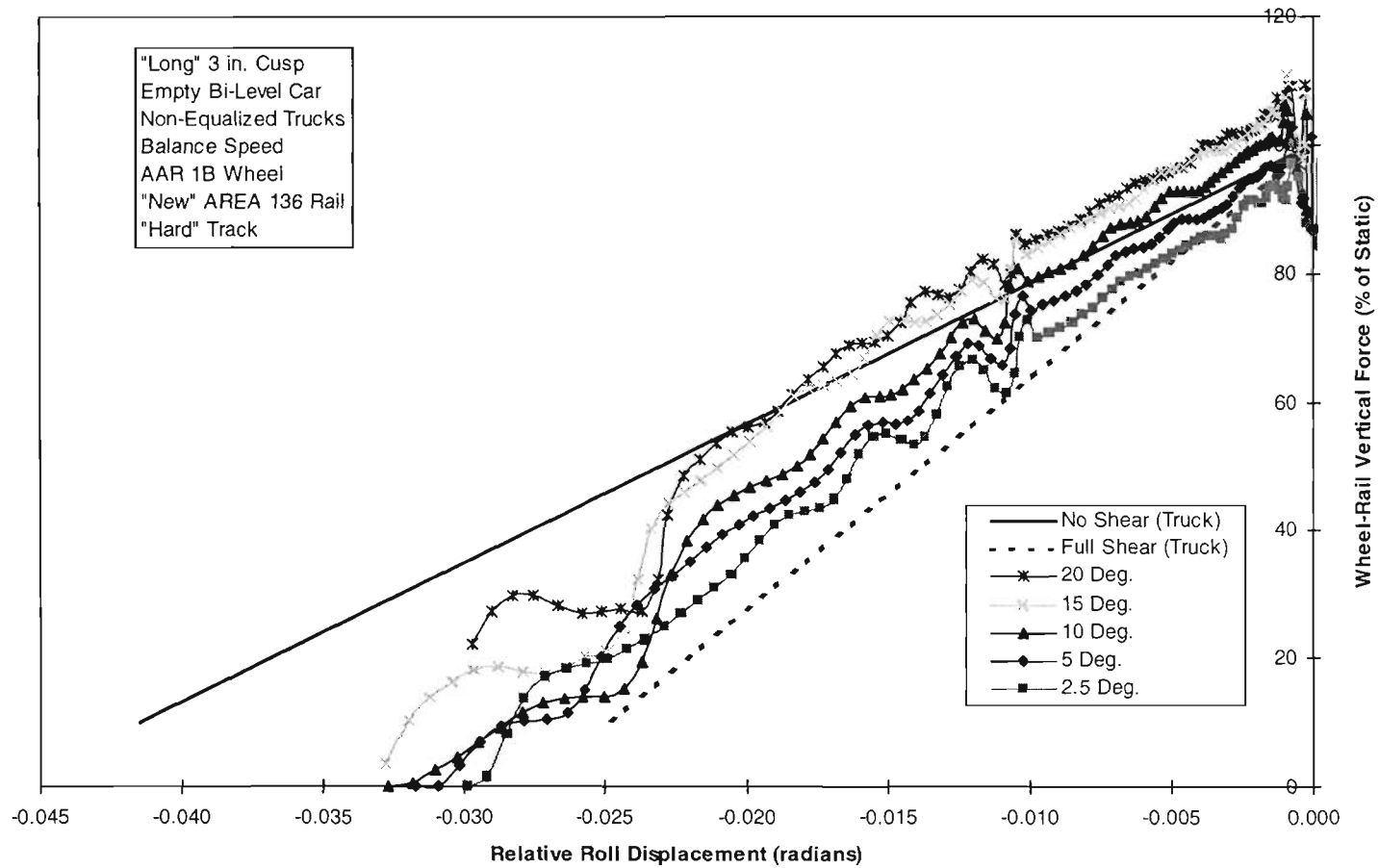

Figure 4-36. Percentage leading outer wheel vertical load versus relative roll displacement (axles 1 and 2)

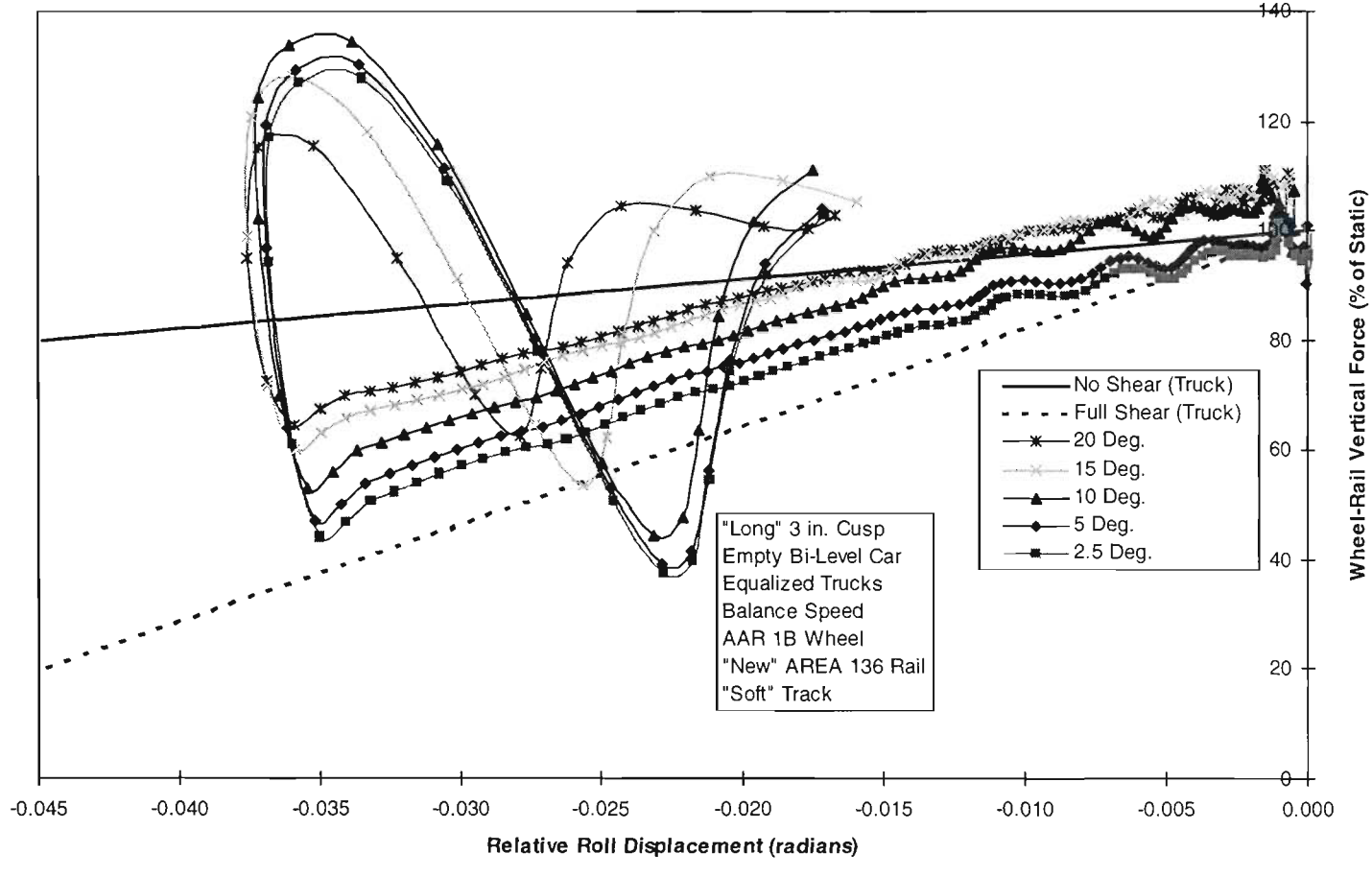

Figure 4-37. Percentage leading outer wheel vertical load versus relative roll displacement (axles 1 and 2)

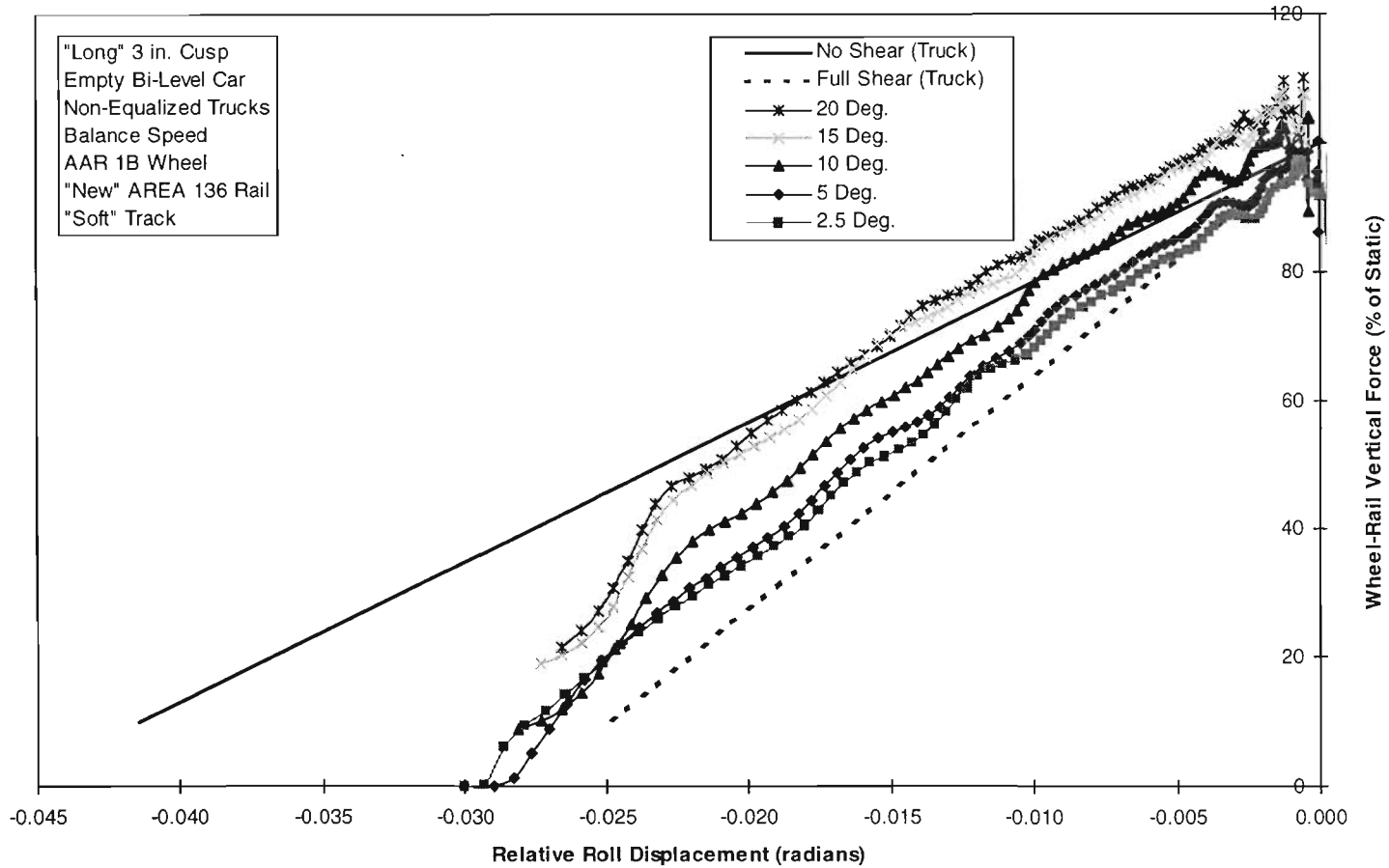

Figure 4-38. Percentage leading outer wheel vertical load versus relative roll displacement (axles 1 and 2)

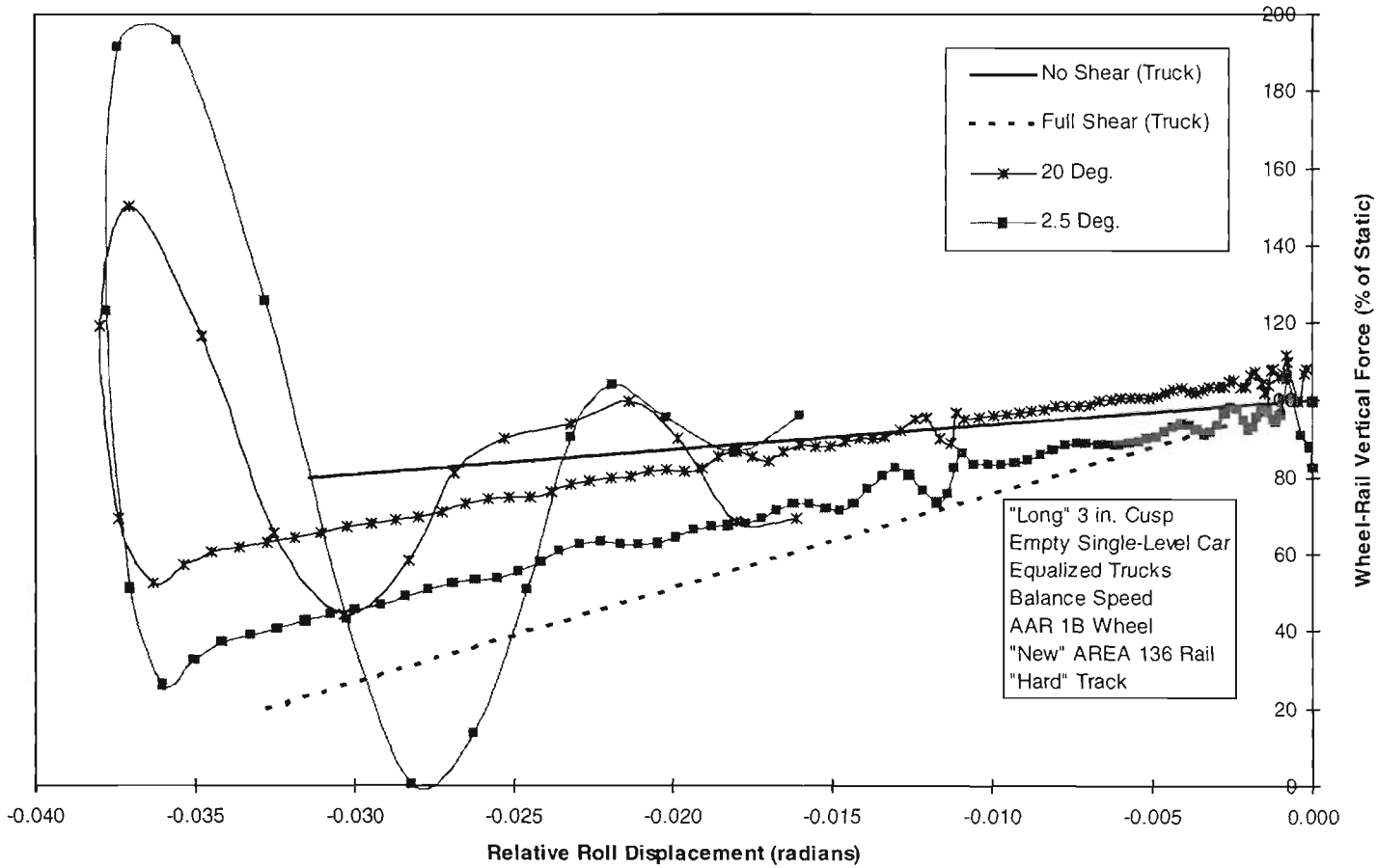

Figure 4-39. Percentage leading outer wheel vertical load versus relative roll displacement (axles 1 and 2)

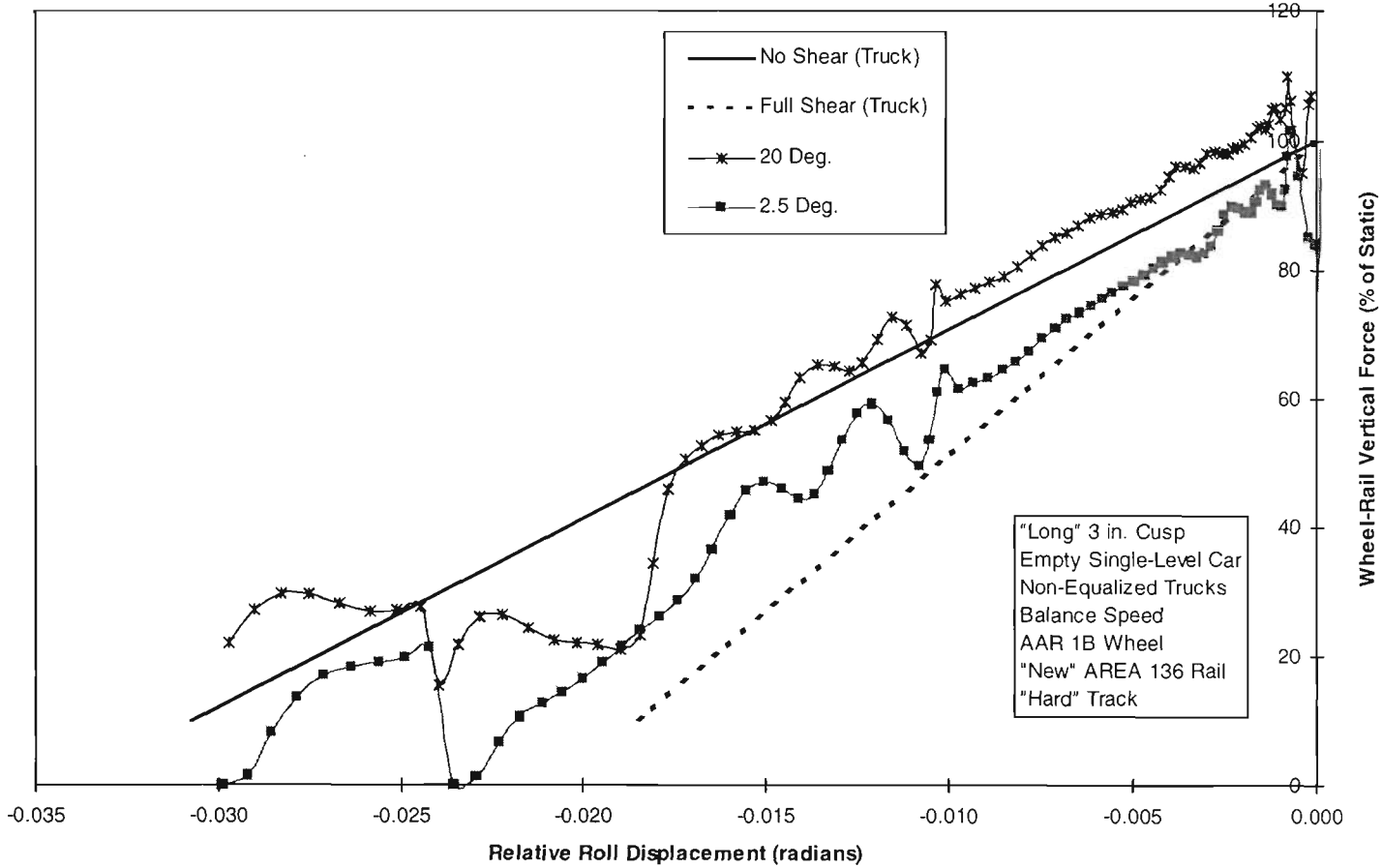

Figure 4-40. Percentage leading outer wheel vertical load versus relative roll displacement (axles 1 and 2)

The results for the "soft" track, given in Figures 4-37 and 4-38, show the same offsets in percentage load on the outer wheel for the higher curvatures as on "hard" track. However, the change is again only significantly beneficial with the equalized truck which does not derail. The results for the single-level car with equalized trucks on "hard" track, shown in Figure 4-39, indicate increased dynamic in bouncing past the cusp point but no derailment. The same body with non-equalized trucks, also dynamic as shown in Figure 4-40, derails as before prior to the cusp point, due to wheel unloading.

4.5 The Effect of Track Curvature on L/V Values for Curves of 2.5 Up to 20 deg - Short Cusp

Runs were also carried out over a short cusp of length 10 ft with a dip of 1.5 in. at the cusp point. The vertical cusp is shown in Figure 4-41. This amplitude was chosen as the maximum which showed the possibility of safety from derailment over this length in low curvatures. The first graphs are for the base cars with equalized and non-equalized trucks on "hard" track. Figures 4-42 and 4-43 show the lead outer wheel L/V as the vehicle with and without equalized trucks moves over the "short" cusp in the various curves. There is a steady value up to the beginning of the cusp followed by a dynamic variation through the cusp. For curvatures below 10 deg, this dynamic results in complete wheel unloading in both base car types, apparently insufficient to cause a loss of guidance.

4.6 The Effect of Track Curvature on Percentage Lead Outer Wheel Unloading for Curves of 2.5 Up to 20 deg - Short Cusp

Figures 4-44 and 4-45 show the percentage unloading of the lead outer wheel against the difference in roll across axles 1 and 2 for the same parameter variations and curvatures as in the previous two figures. The overall behavior shown is the same as that described previously with certain minor additions. For both base cars with and without equalized trucks on "hard" track, the figures show an initial slope close to that of the static line with full shear stiffness of the truck included. In the case of the non-equalized truck, the slope is almost sufficient to induce wheel unloading and loss of guidance. The offset in vertical loads due to the net lateral axle force is also apparent as before. However, the "short" cusp induces significantly greater amounts of dynamic activity, particularly at the lower curvatures, with very large overloads followed by complete unloading in both base car types.

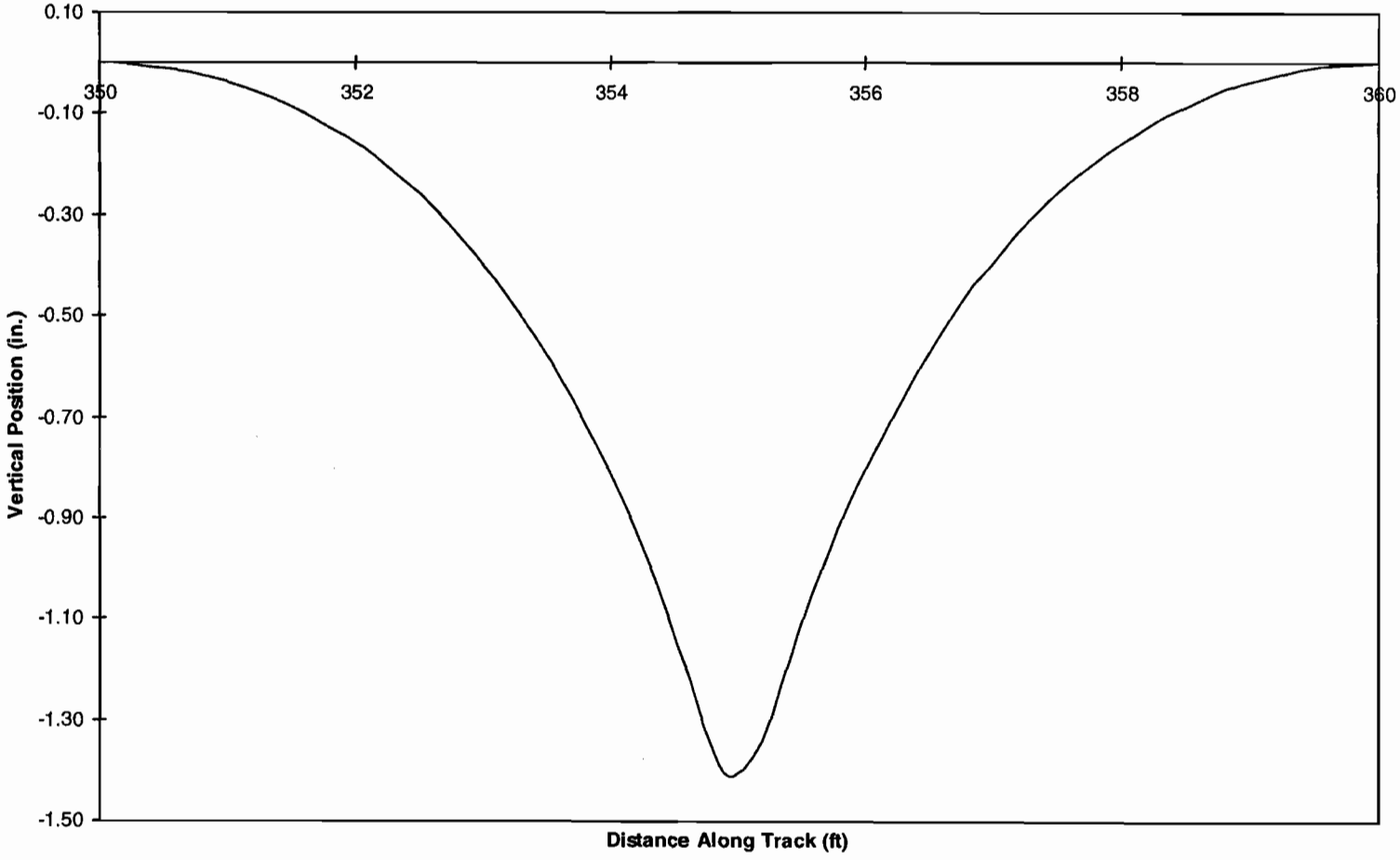

Figure 4-41. Vertical cusp

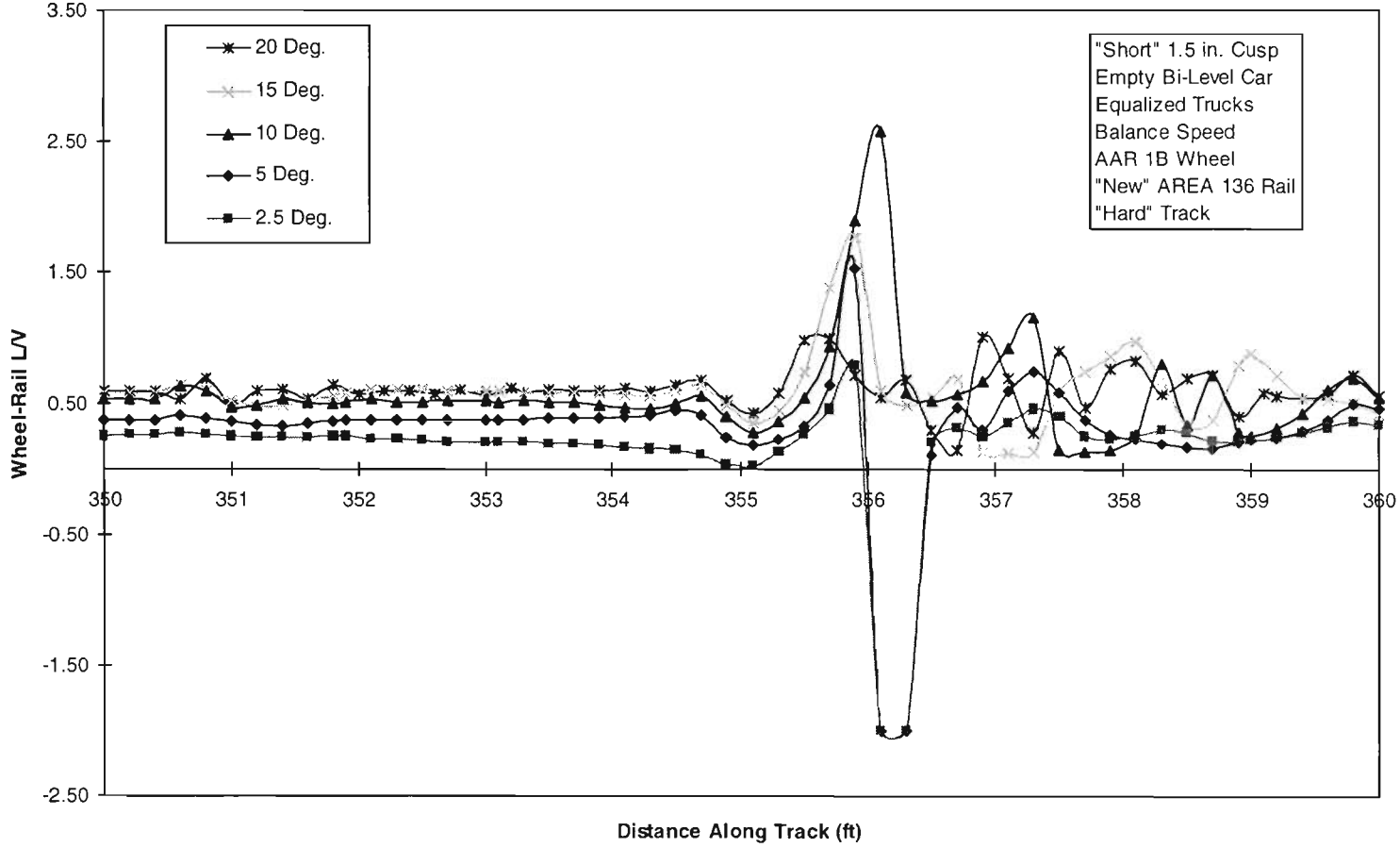

Figure 4-42. Comparison of L/V ratios on leading outer wheel

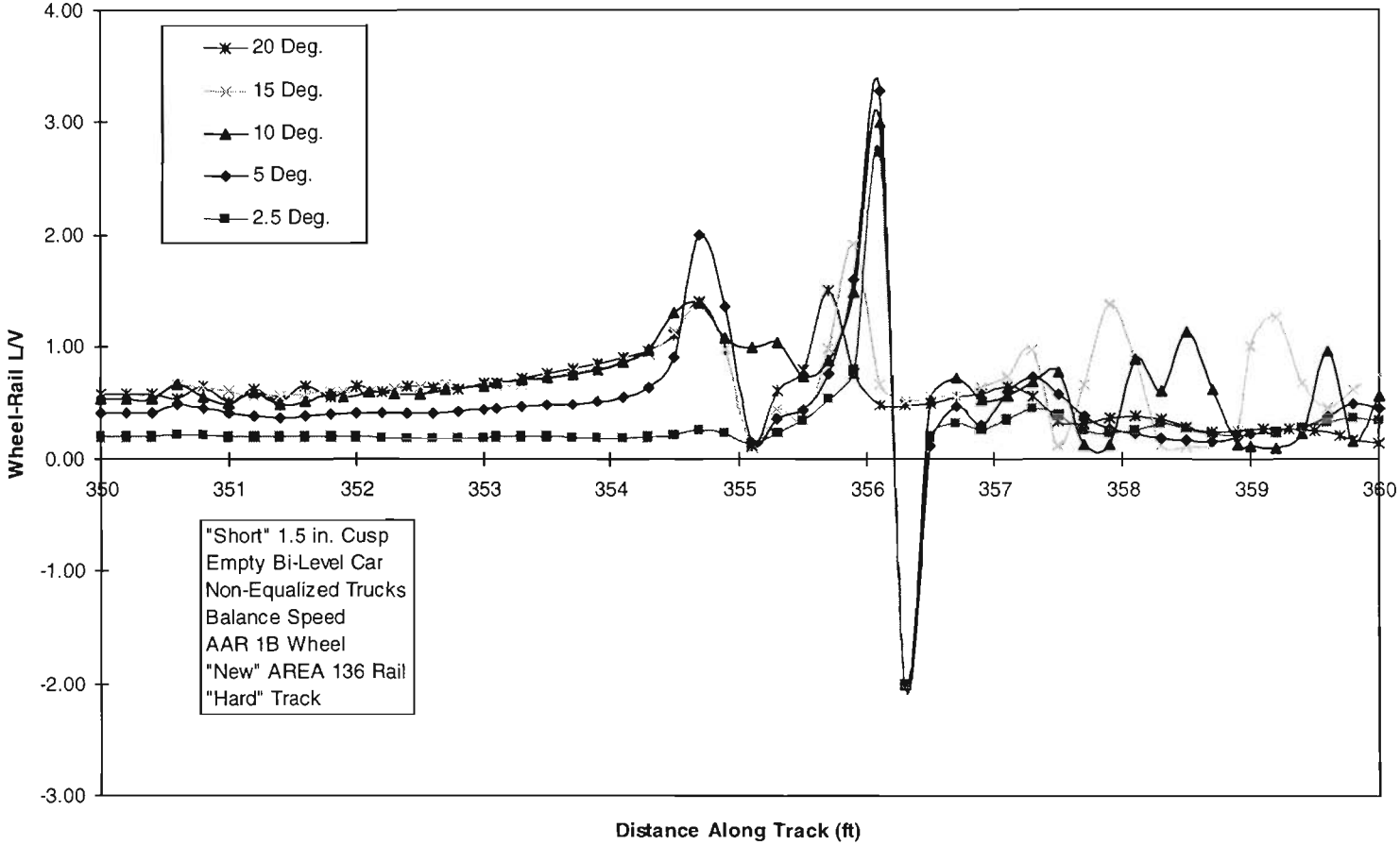

Figure 4-43. Comparison of L/V ratios on leading outer wheel

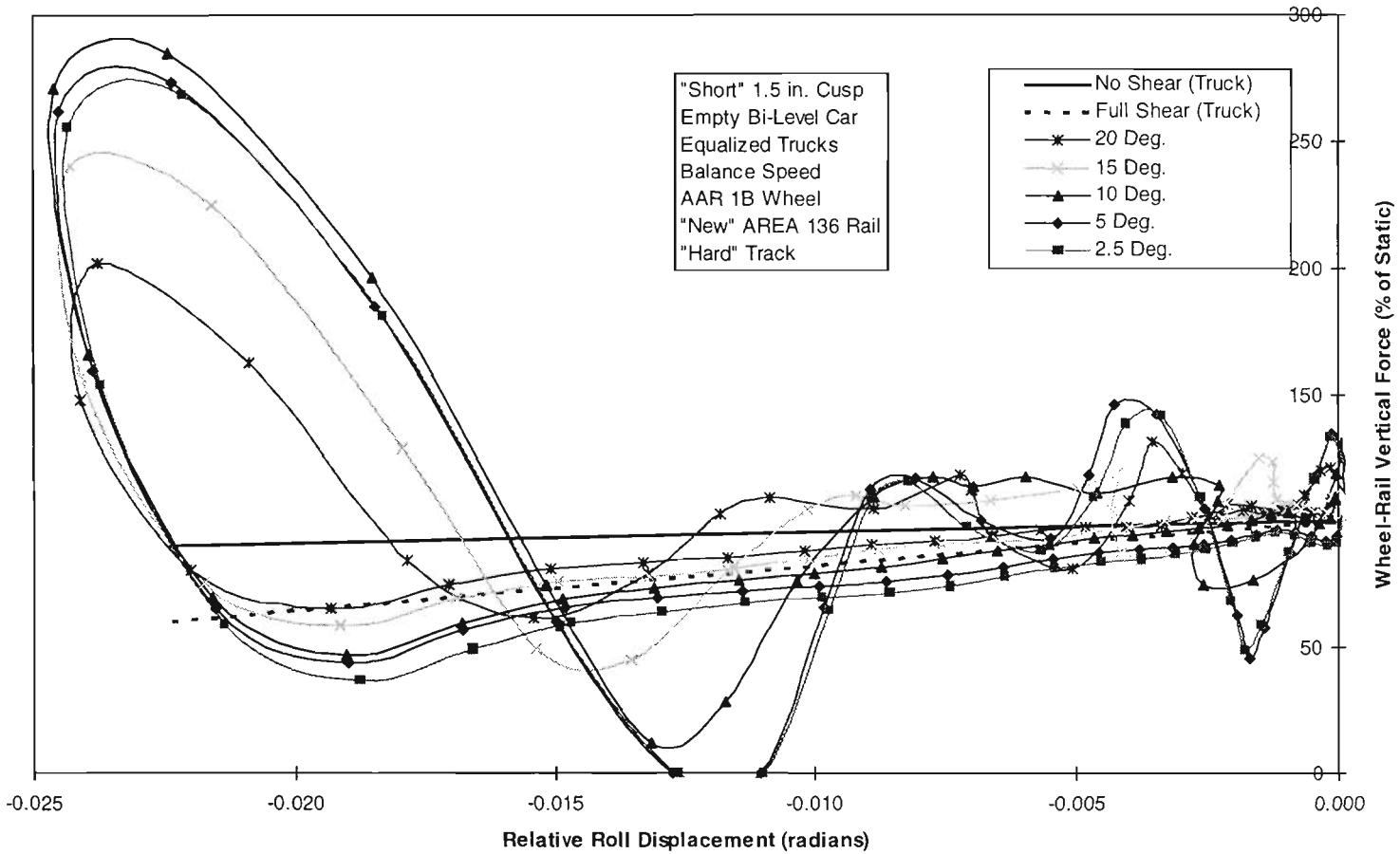

Figure 4-44. Percentage leading outer wheel vertical load versus relative roll displacement (axles 1 and 2)

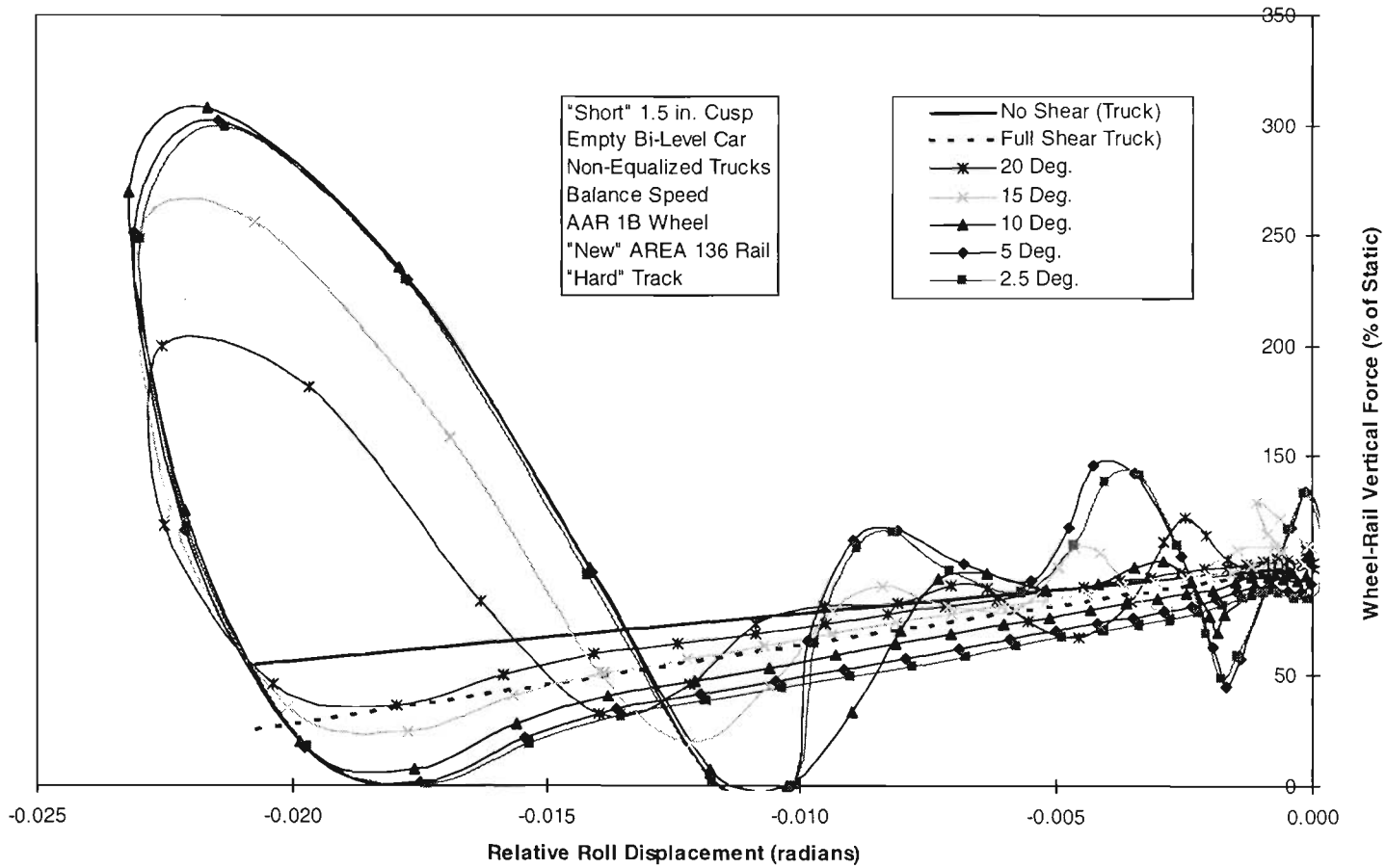

Figure 4-45. Percentage leading outer wheel vertical load versus relative roll displacement (axles 1 and 2)

5. RESPONSE TO VARIATIONS IN RAIL ALIGNMENT

Gage variation may occur in revenue service, and must be negotiated safely by the passenger vehicles. Figure 5-1 shows the basic track shape for the gage narrowing investigated. One of the rails is considered as a reference rail from which the effective gage can be determined based on the relative position of the other rail. This is regarded as providing the worst case in that it produces the largest slope of gage reduction. From Figure 5-1, it is seen that the slope of the gage narrowing is constant along the distance. The speed at which incipient wheel climb occurs, has been established here through OMNISIM simulations for vehicle and truck types considered in this work. The truck types have significant influence on the vehicle behavior in the gage narrowing scenario. In numerical work presented here, the inverse of the slope is used as a characteristic parameter in terms of which safe operational speeds can be expressed. This parameter is defined as the Gage Reduction Ratio (GRR). In addition to GRR, the track gage (G) is also important in the determination of wheel climb threshold speeds.

An alternative sinusoidal shape has been used in the past to examine the likelihood of wheel climb in gage narrowed track. This is shown in Figure 5-2. In this shape, the necessary

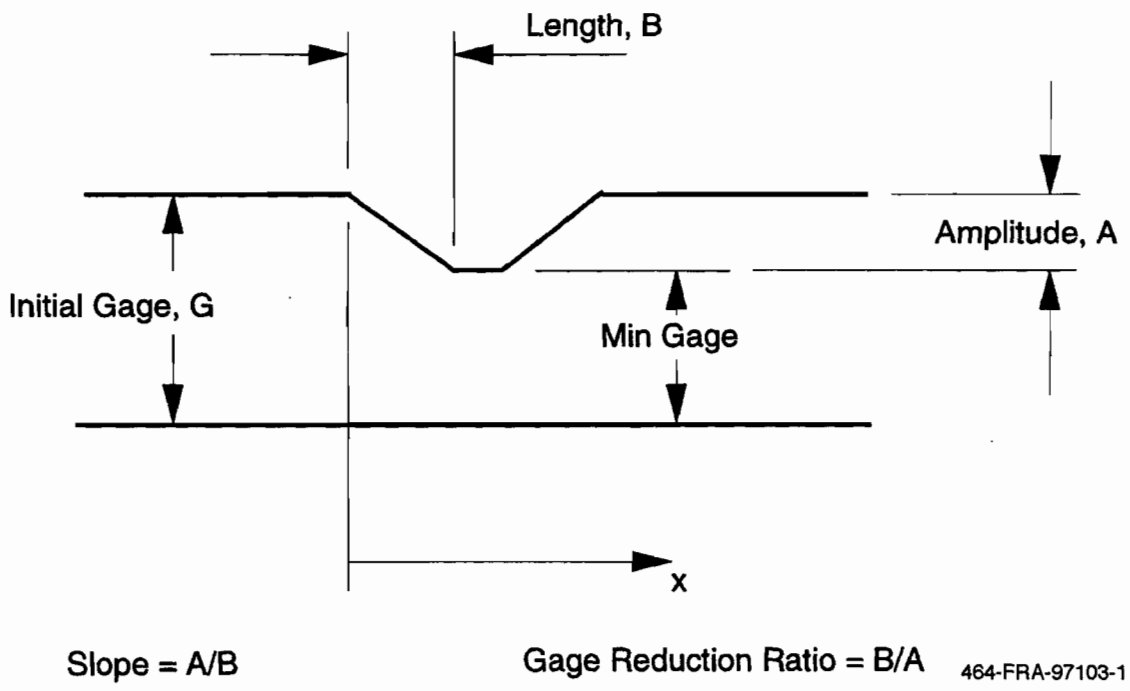

Figure 5-1. Constant gage narrowing scenario

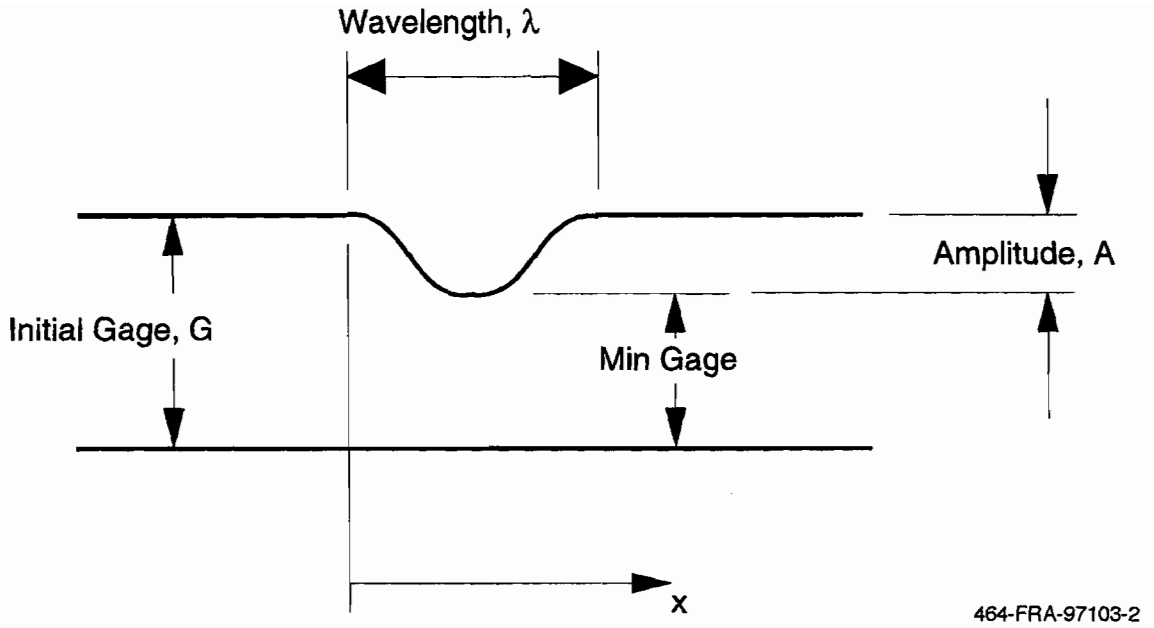

Figure 5-2. Sinusoidal gage narrowing scenario

parameters in gage narrowing are the initial gage (G) the amplitude (A) and the wavelength (λ). Since the slope of gage narrowing on the sinusoid at the point of flange contact varies with the axle initial lateral and yaw positions, the potential for derailment will similarly vary with these positions. The safety limits can be more conveniently expressed for the constant gage narrowing scenario rather than the sinusoidal scenario.

Using knowledge of track geometry, measured or simulated, it is possible to isolate the worst case of gage narrowing misalignment. This may be absolute or may be related to particular sinusoidal wavelengths in the track gage as measured. In either case the inverse of the largest slope or smallest GRR can be determined and plotted on the known graph for the car investigated and a maximum safe speed established.

Current FRA standards permit a maximum limit of 1/2 in. for the amplitude in gage narrowing in 31 ft for all classes of track. If this occurs sinusoidally over a wavelength of 6 ft, the worst GRR will be about 46; for a wavelength of 12 ft, it is 92. For these GRR's, the maximum permissible speed for the passenger vehicle with equalized trucks on track with a nominal gage of 56.5 in. are shown to be 40 mph and over 120 mph, respectively. The safety criterion implied here is that wheel climb derailment will occur if the vehicles operate at higher than the critical speeds identified.

The first case studied is that of the empty bi-level car with equalized trucks. The track chosen has an initial wide 59 in. gage with a sudden gage reduction at a rate of 1/40. The terminology has been adopted here of using the inverse and calling this a gage reduction ratio, N, of 40. Two speeds are examined, 55 mph and 58 mph. At 55 mph, Figure 5-3 shows that the left rail at the gage tightening moves laterally to the flange of the left wheel at which point the axle attempts to steer to prevent wheel climb. The L/V becomes large reflecting the 75 deg flange angle at climb, however, the wheel recovers, as seen in Figure 5-4, and begins to descend again towards tread contact with the rail. This result is labeled just safe from climb. The flangeway clearance is just under 0.4 in. for the profiles used in these runs. The same graphs are plotted in Figures 5-5 and 5-6 for the same system at a speed increased to 58 mph. In these no similar recovery takes place and the wheel continues over the rail head. This is labeled a wheel climb. In this manner the division was made between results indicating safe and unsafe behavior.

Figures 5-7 to 5-10 give similar results for the car with non-equalized trucks, an initial gage of the standard 56.5 in., and a sudden gage tightening ratio of 60. The speeds were again chosen to define the change from just safe to unsafe behavior. In this example, the distinction between safe and unsafe behavior is much more clear cut. However, it is worth noting that difference in the maximum L/V ratios between apparent just safe and unsafe behavior is very small. The L/V value, following the theory of Nadal, has often been used in the literature and in specifications to define safety from derailment. Where measurement is not a problem, such as in these simulations, wheel motion is the preferred indication of derailment.

The results of a large number of runs were examined to determine the behavior of the cars through sudden gage tightened track and an approach determined to provide an informative and useful graph of the results. The overall summary is shown in Table 5-1, which gives the just safe and unsafe speeds for both the base cars and various initial gage values. No speeds above 120 mph were investigated. These results are examined further in graphs of maximum safe speed against gage reduction.

5.1 Safe Speeds for Equalized Trucks

The maximum speeds, safe from wheel climb derailment, are determined for vehicles with equalized trucks, and are summarized in Figure 5-11. These results are applicable for both single and bi-level cars. The results are given for the nominal (initial) gage of 56.5 in. up to 59 in. As the GRR decreases, the allowable speed becomes considerably smaller. It may also be noted that initial wider gage allows higher speed for the same GRR.

Specific data for two sinusoidal gage narrowings are added. These are for a sinusoidal double amplitude of 2.5 in. with a wavelength of 20 ft and for a double amplitude of 3 in. with a wavelength of 40 ft. Each result is interpreted as a point on the plot of critical speed against gage reduction ratio and shown in Figure 5-11 for the initial gage of 59 in. The results are seen to be conservative and are due to the fact that the axle moves off the track centerline used in the calculation of GRR, prior to flange contact. The true value of GRR is therefore slightly larger than that used on the figure.

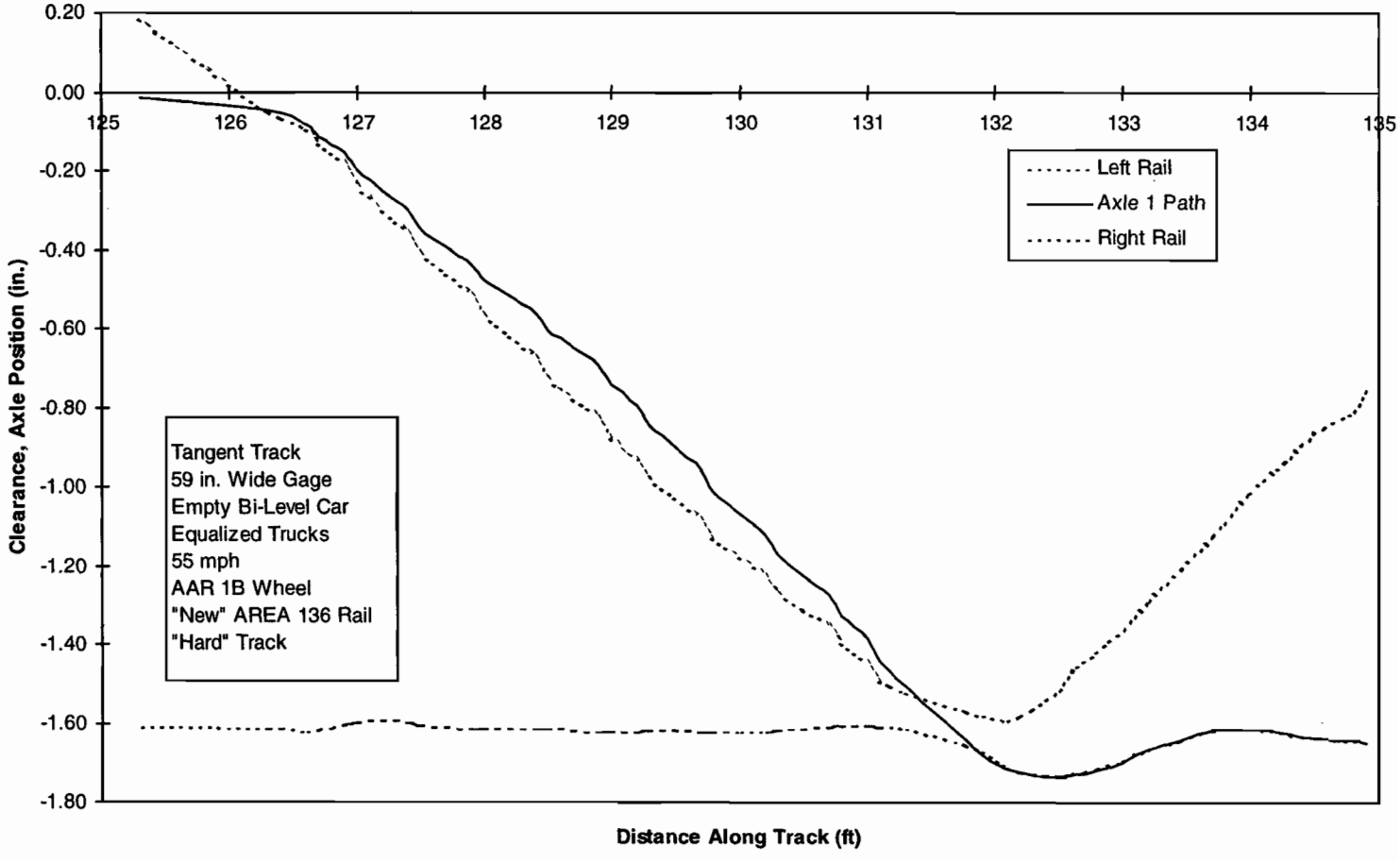

Figure 5-3. Lateral motion of lead axle - sudden gage tightening of 1/40

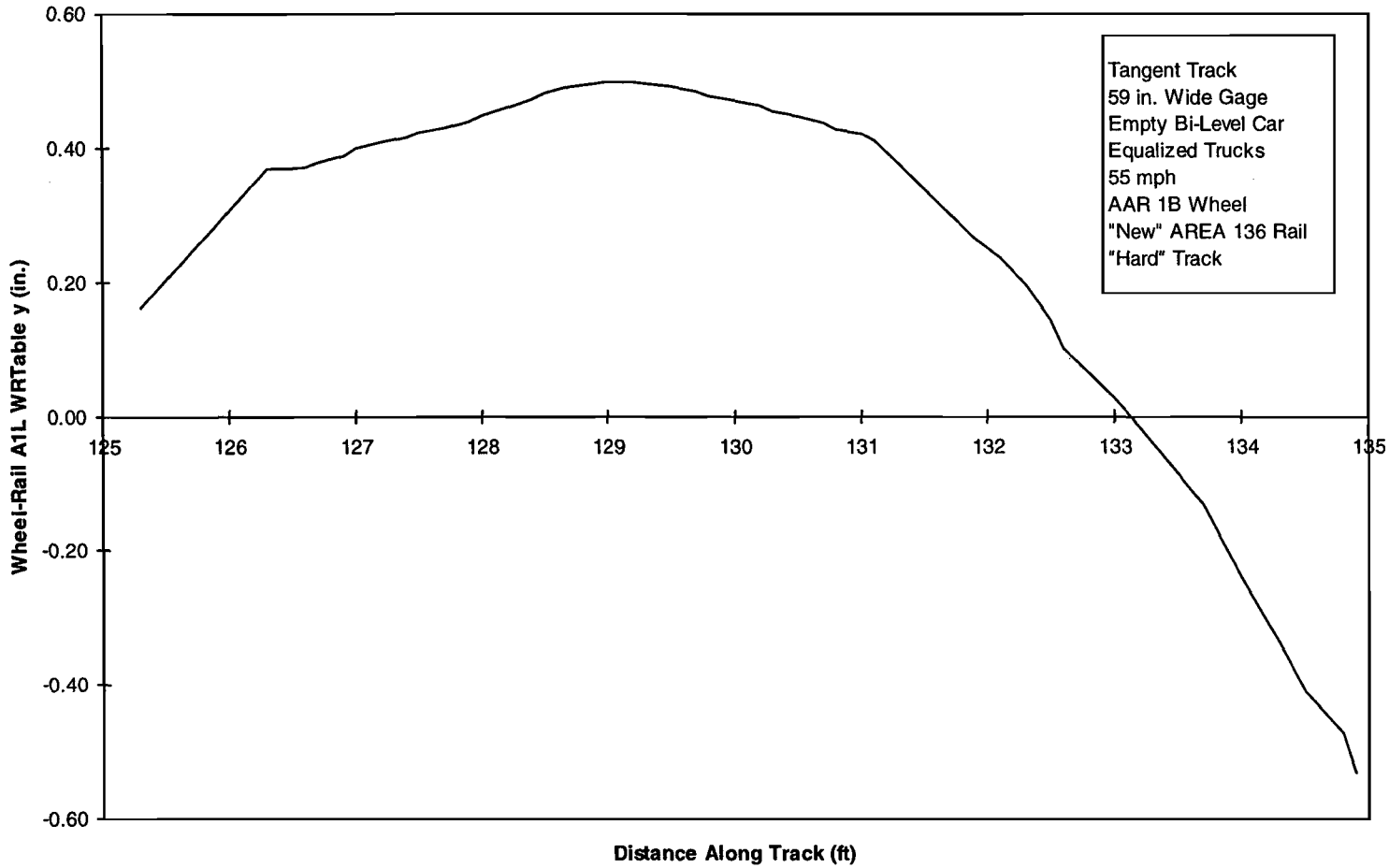

Figure 5-4. Wheel-rail relative lateral motion of lead left wheel - sudden gage tightening of 1/40

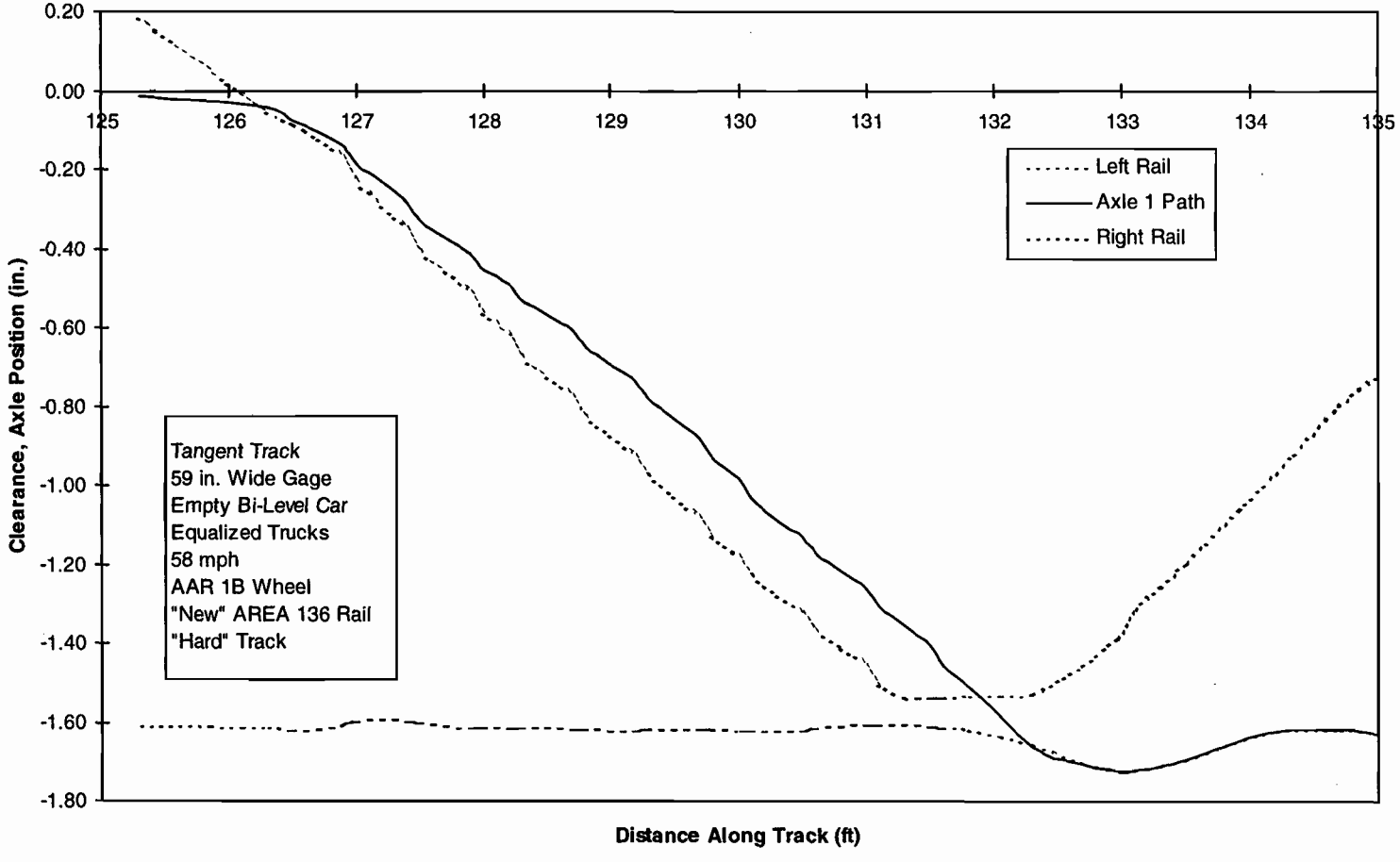

Figure 5-5. Lateral motion of lead axle - sudden gage tightening of 1/40

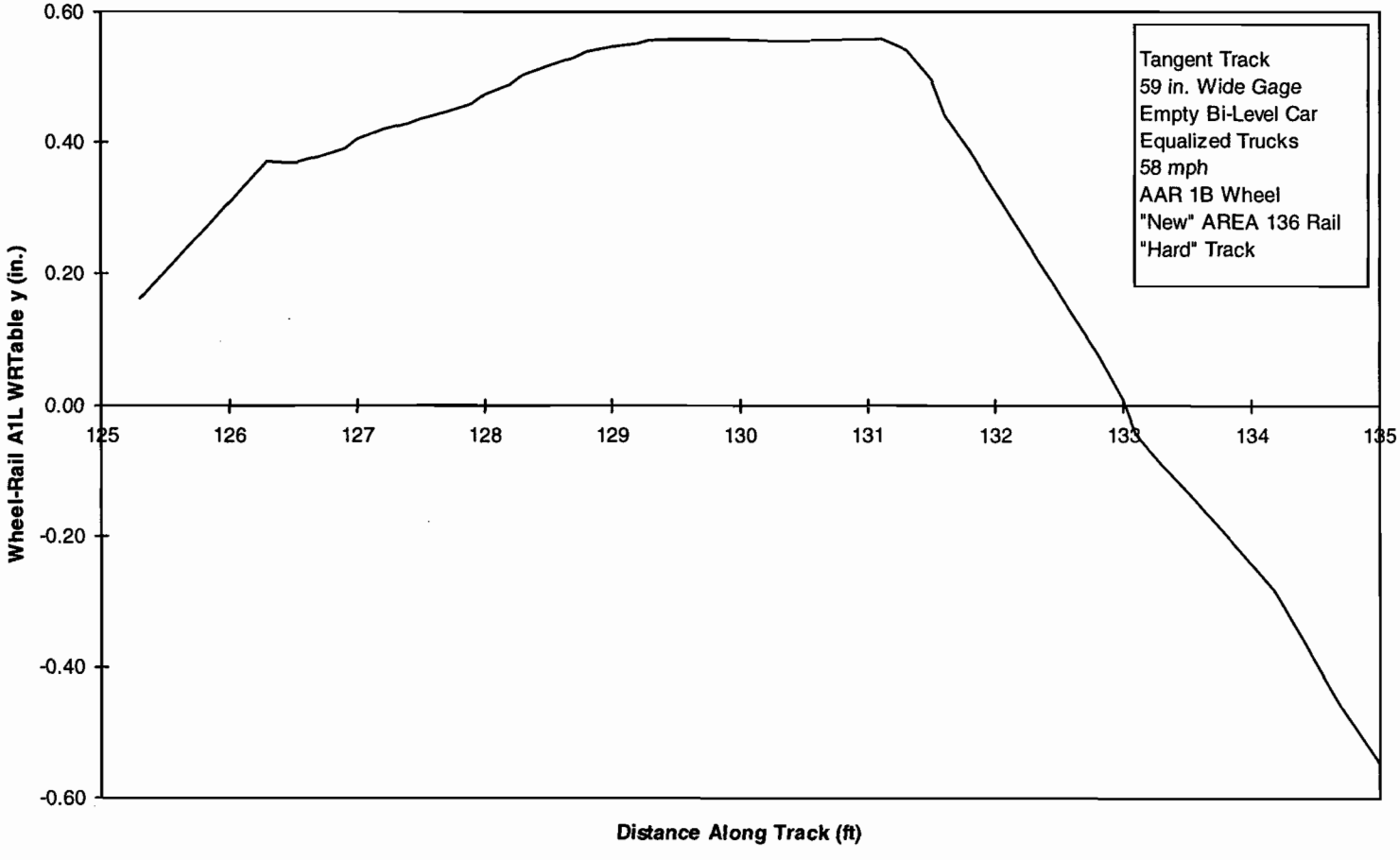

Figure 5-6. Wheel-rail relative lateral motion of lead left wheel - sudden gage tightening of 1/40

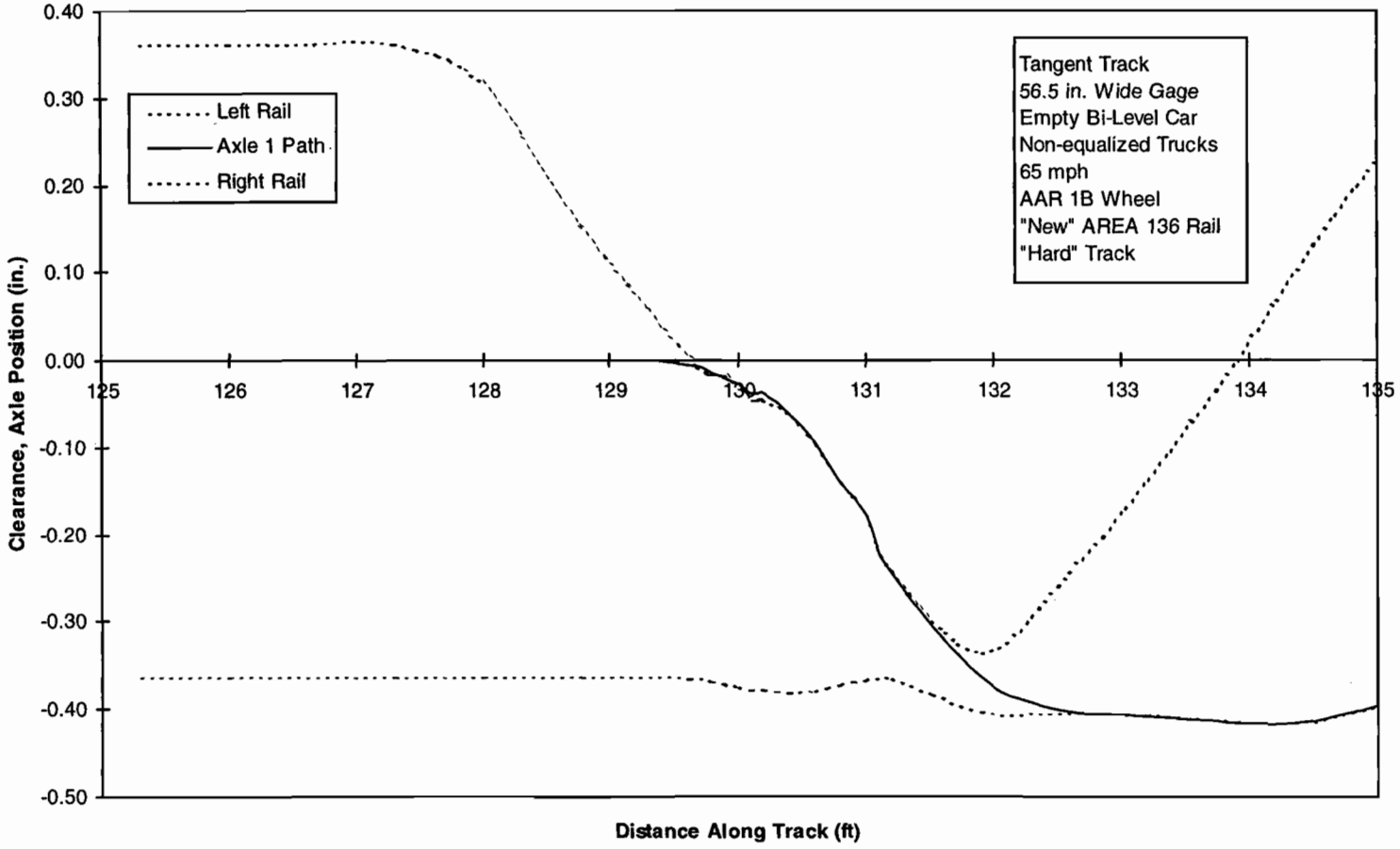

Figure 5-7. Lateral motion of lead axle - sudden gage tightening of 1/60

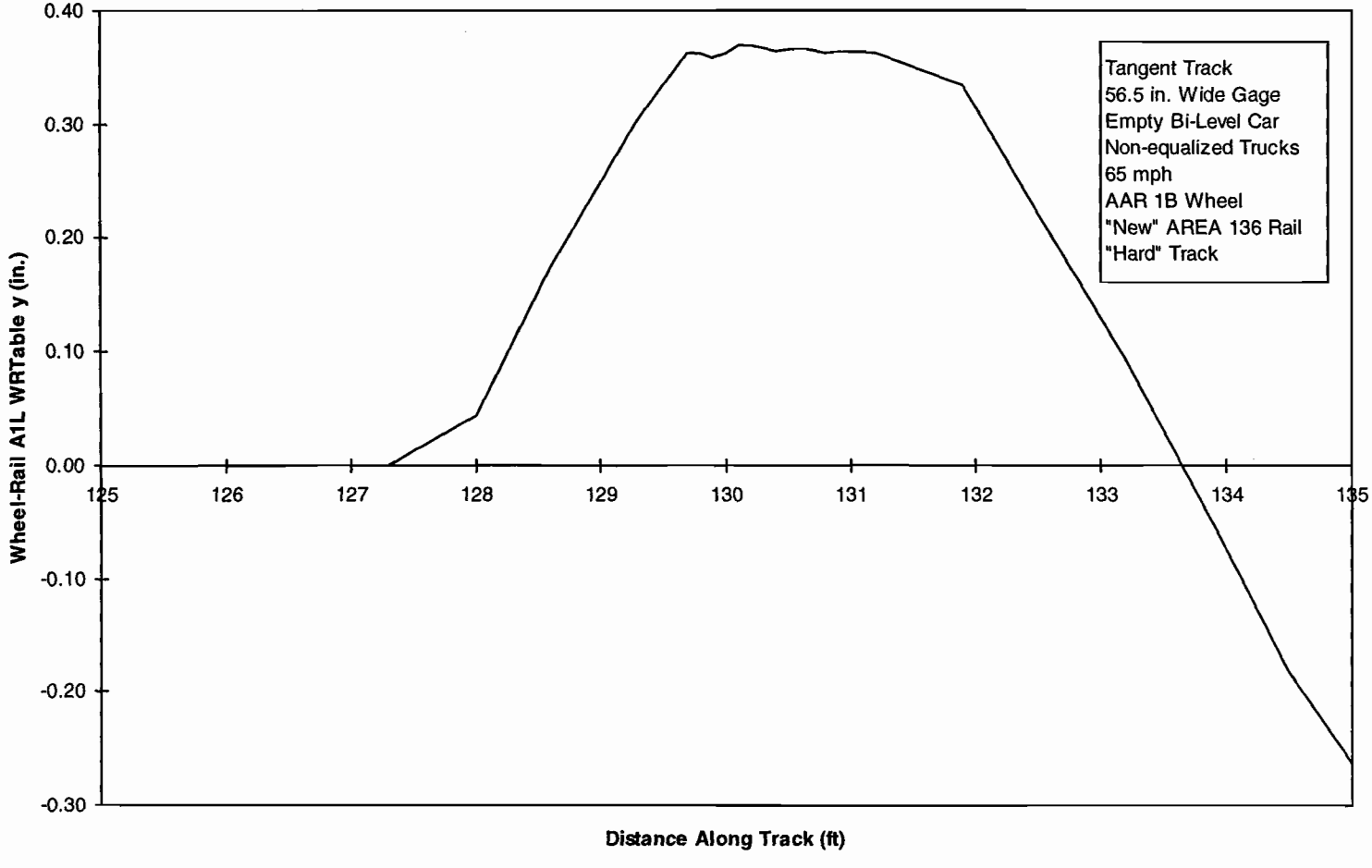

Figure 5-8. Wheel-rail relative lateral motion of lead left wheel - sudden gage tightening of 1/60

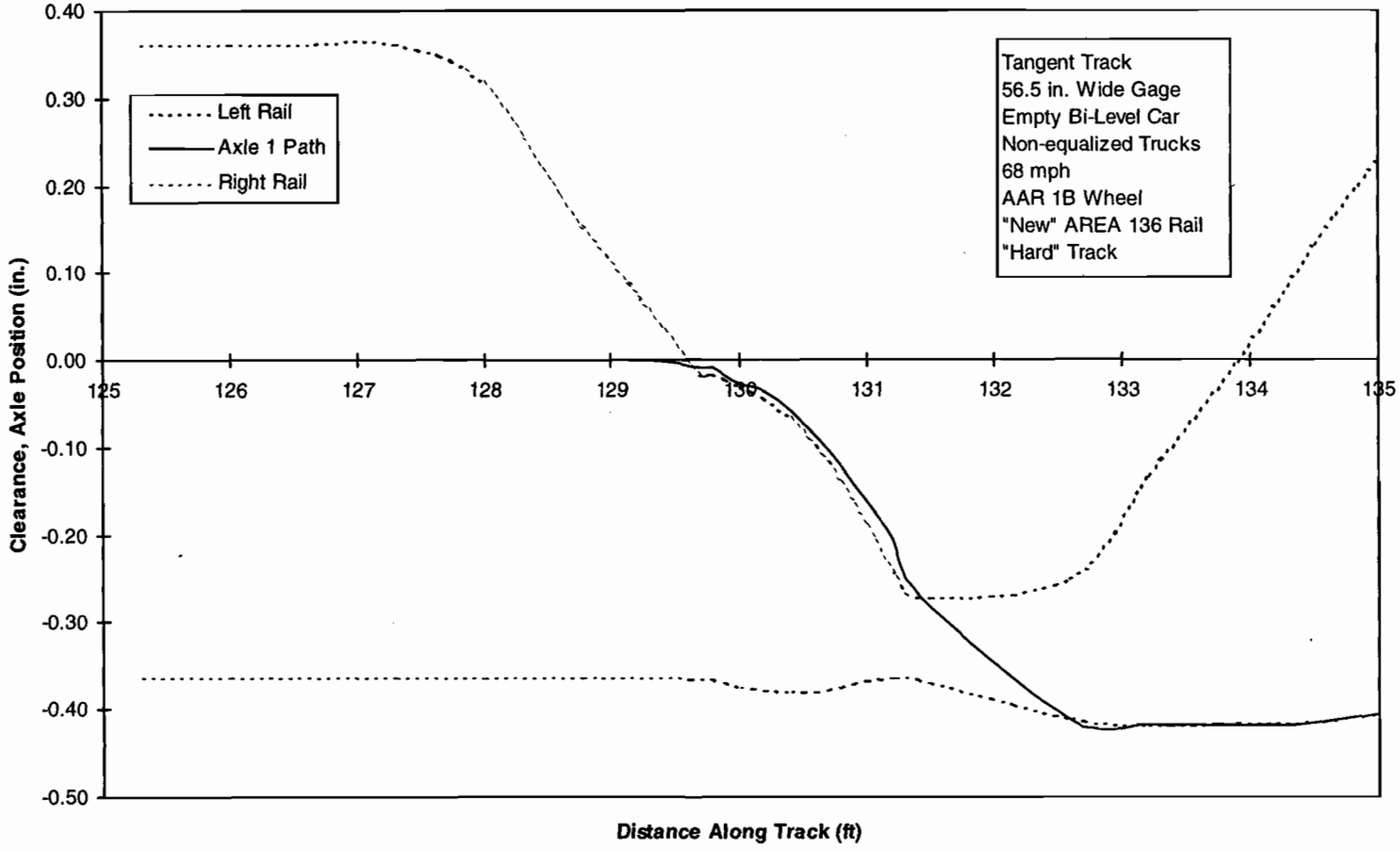

Figure 5-9. Lateral motion of lead axle - sudden gage tightening of 1/60

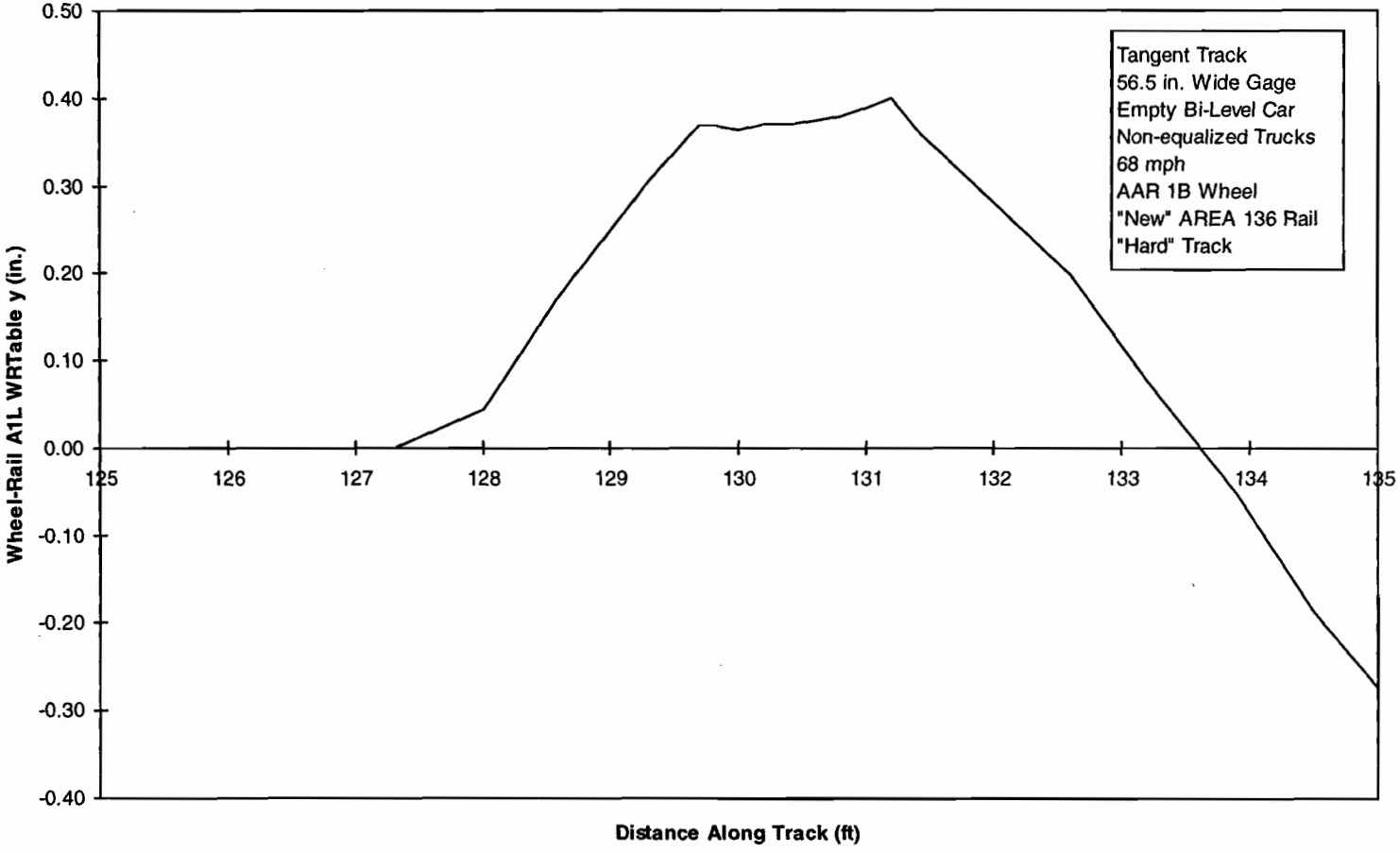

Figure 5-10. Wheel-rail relative lateral motion of lead left wheel - sudden gage tightening of 1/60

Table 5-1. Relationship between speed and safety from wheel climb for particular gage reduction ratios and initial gages

Initial Gage (in.)	Gage Reduction Slope (1/N) in./in.	Lowest Speed at Wheel Climb (mph)		Highest Speed without Wheel Climb (mph)	
		Equalized	Non-equal	Equalized	Non-equal
59	1/30	35	28	33	25
	1/40	58	48	55	45
	1/60	120+	90	120	88
	1/80	120+	120+	120+	120+
58	1/30	33	28	30	25
	1/40	53	43	50	40
	1/60	108	80	105	78
	1/80	120+	120+	120+	120+
57	1/30	30	28	28	25
	1/40	45	38	43	35
	1/60	90	68	85	65
	1/80	120+	110	120+	108
56.5	1/20	18	16	17	15
	1/30	30	28	28	25
	1/40	45	38	43	35
	1/60	85	68	80	65
	1/80	120+	105	120+	100

5.2 Safe Speeds for Non-Equalized Trucks

The maximum safe speeds for non-equalized trucks are shown in Figure 5-12, and are applicable for both single and bi-level cars. The same points for a sinusoidal gage reduction are also added. Comparing these results with those presented in Figure 5-11 for equalized trucks, the safe speeds are again lower with decreasing GRR. However, the results suggest that the critical speeds at incipient wheel climb for the equalized truck are higher than those for the non-equalized truck in this figure. As with the equalized trucks, an initial wider flangeway clearance allows higher speed for the same GRR without wheel climb.

5.3 Sinusoidal Gage Tightening

The sinusoidal gage tightening used was shown in earlier in Figure 5-2. The analytic expression for the lateral position of the left rail relative to the track center is given by,

$$y = y_c + \frac{G - 56.5}{2} - \frac{A}{2}\left\{1 - \cos\left(2\pi\frac{x}{\lambda}\right)\right\}$$

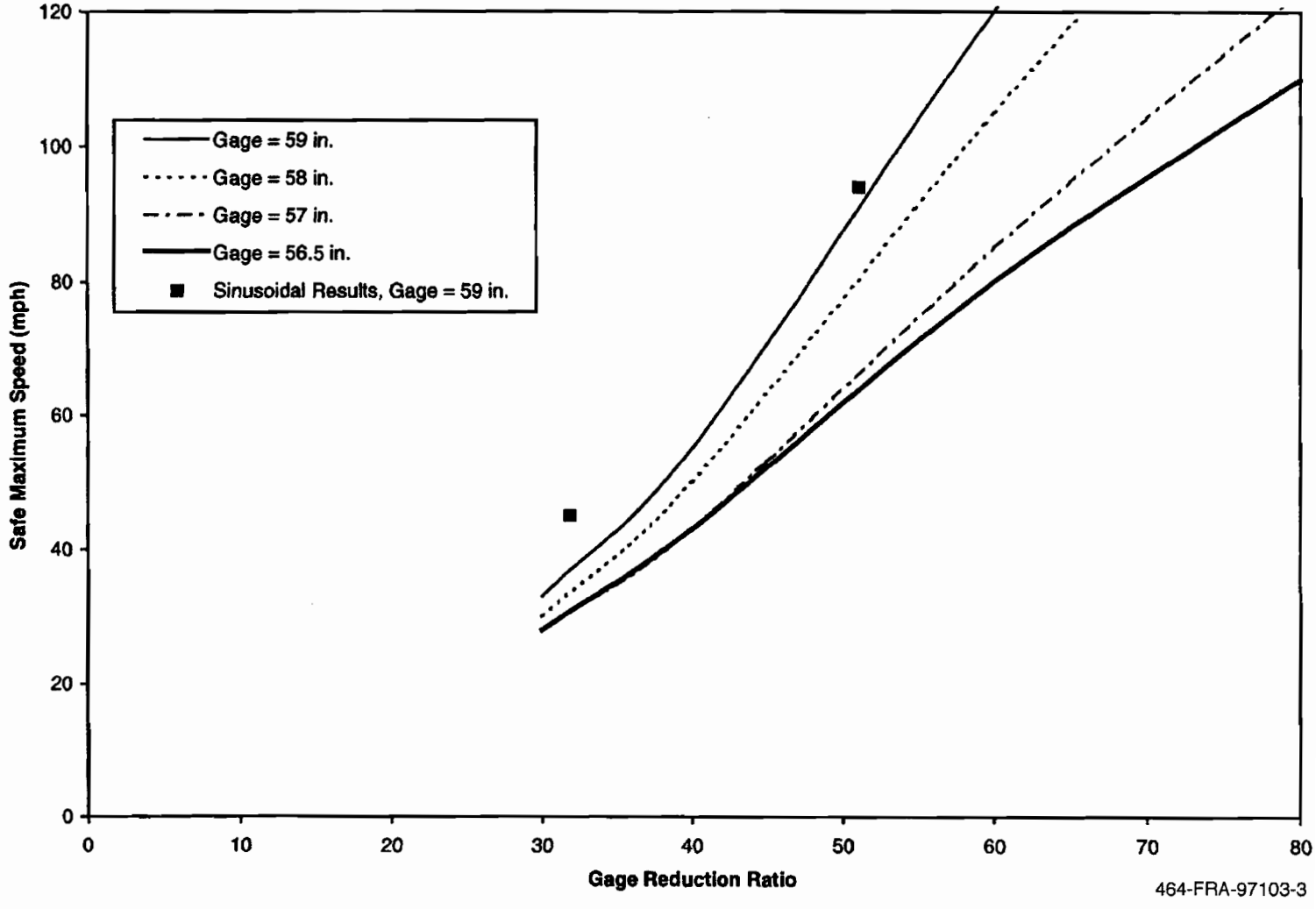

Figure 5-11. Maximum safe speed for equalized trucks

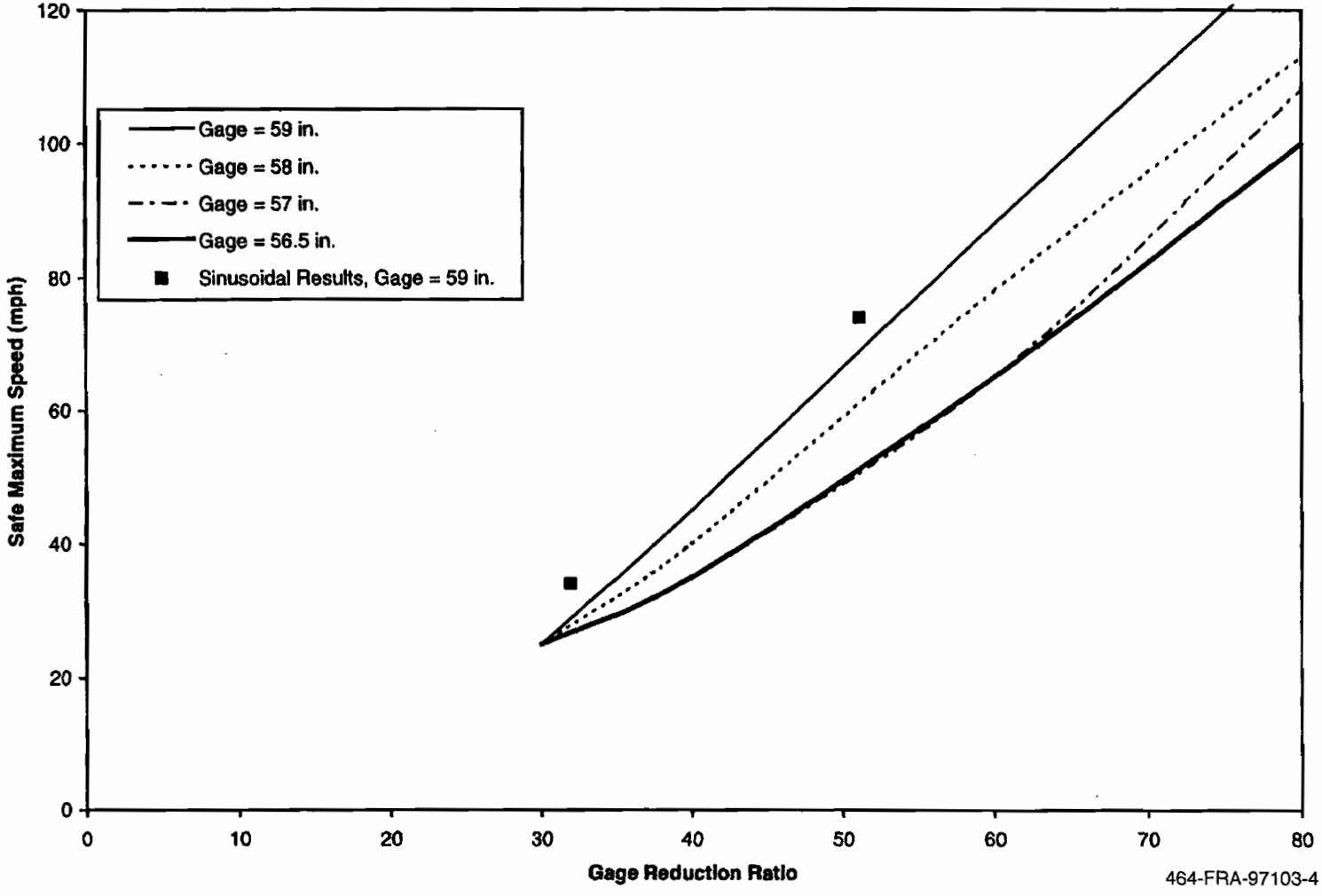

Figure 5-12. Maximum safe speed for non-equalized trucks

where

y_c is the flangeway clearance
G is the initial gage
A is the gage narrowing amplitude
λ is the gage narrowing wavelength
x is the distance along the track from its start.

This equation may be rearranged to give the inverse slope at the lateral position when the flange is contacted, or as defined in this work, the gage reduction ratio, N,

$$N = \left|\frac{dx}{dy}\right| = \left|\frac{1}{A\pi}\left\{\frac{1}{\sqrt{1-\left(1-\frac{2}{A}(C-y)\right)^2}}\right\}\right|$$

where, $C = y_c + (G-56.5)/2$

For the two wave shapes examined and added to Figures 5-11 and 5-12, the initial gage was 59 in. and the amplitudes were 2.5 and 3 in. for wavelengths of 20 and 40 ft respectively. Assuming that the axle remains on the track center at flange contact, i.e., y = 0, the gage reduction ratios are 31.9 and 51.1. The points given are at speeds which just show incipient wheel climb. It would seem that the methodology used to create the curves is slightly conservative. However, this is largely due to the fact that, in the simulation, the axle moves towards the right rail in advance of flange contact and y is not zero but slightly negative. The lateral axle motion in the flangeway clearance for the sinusoidal gage tightening cases added to Figure 5-11 and 5-12 are given in Figures 5-13 to 5-16. The gage reduction ratio is therefore slightly larger than that used from the simple analysis, and therefore safer. Also leading to conservatism is the fact that the sinusoidal shape eases the recovery, as the rail itself tends to cause the climbing wheel to return to tread contact. The approach suggested identifies a general methodology which can be used for all rail shapes and gages, even those from track measurements, to establish danger from wheel climb in gage reductions.

The results also suggest that the particular car design simulated with equalized trucks is safer, i.e., it can go faster than that with non-equalized trucks without wheel climb, over track with sudden gage narrowing.

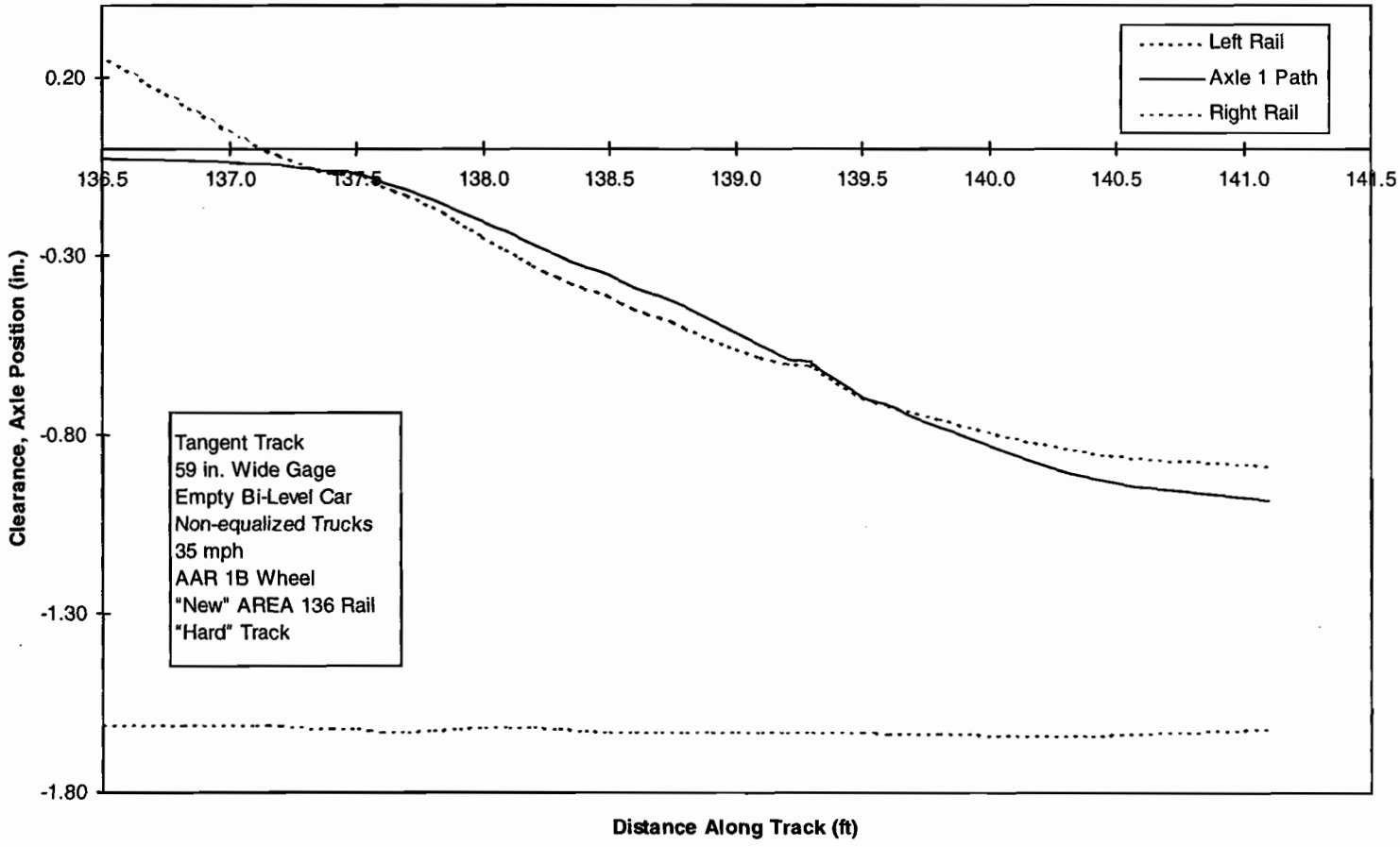

Figure 5-13. Lateral motion of lead axle - sudden gage tightening of 2.5 in.

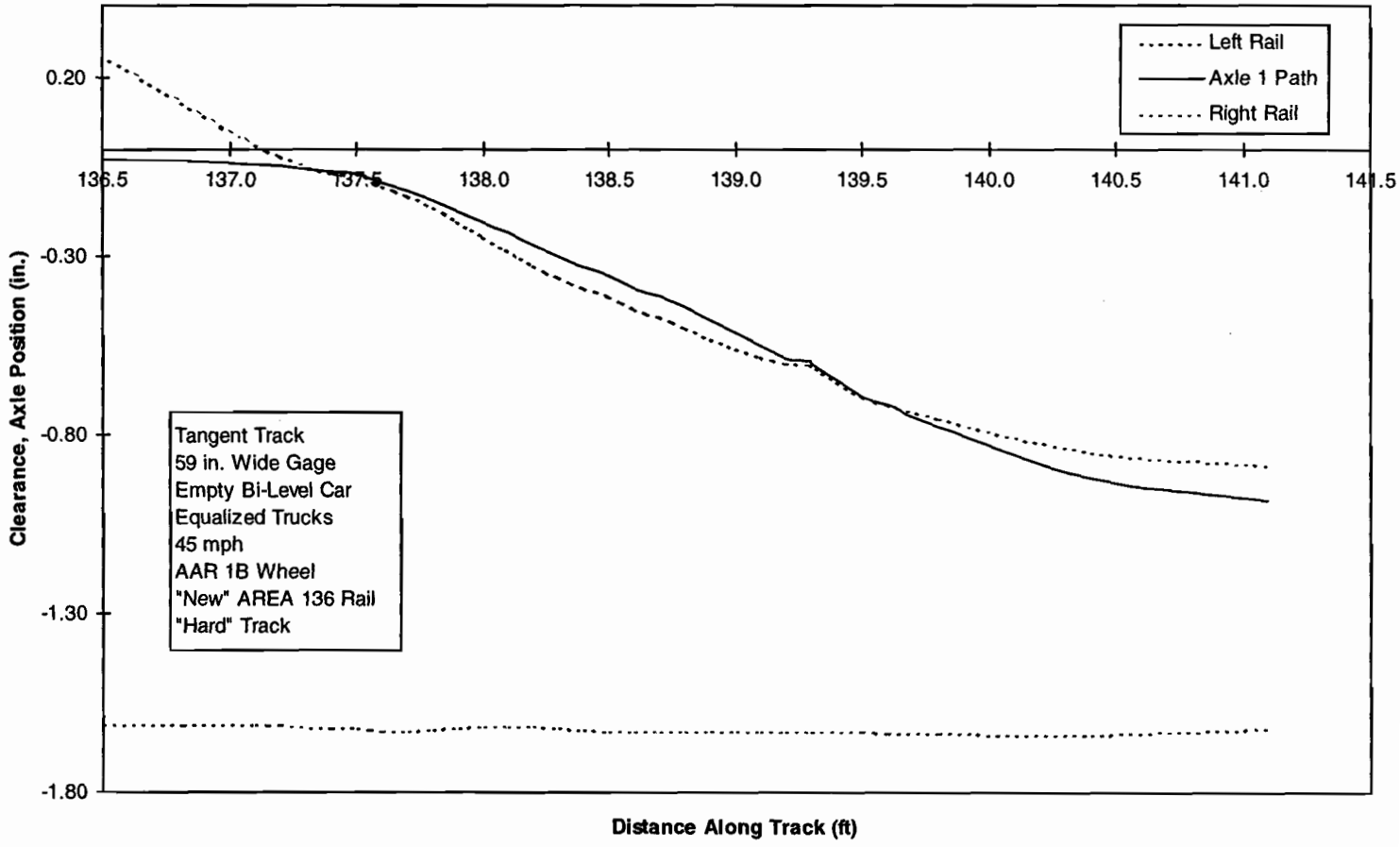

Figure 5-14. Lateral motion of lead axle - sudden gage tightening of 2.5 in.

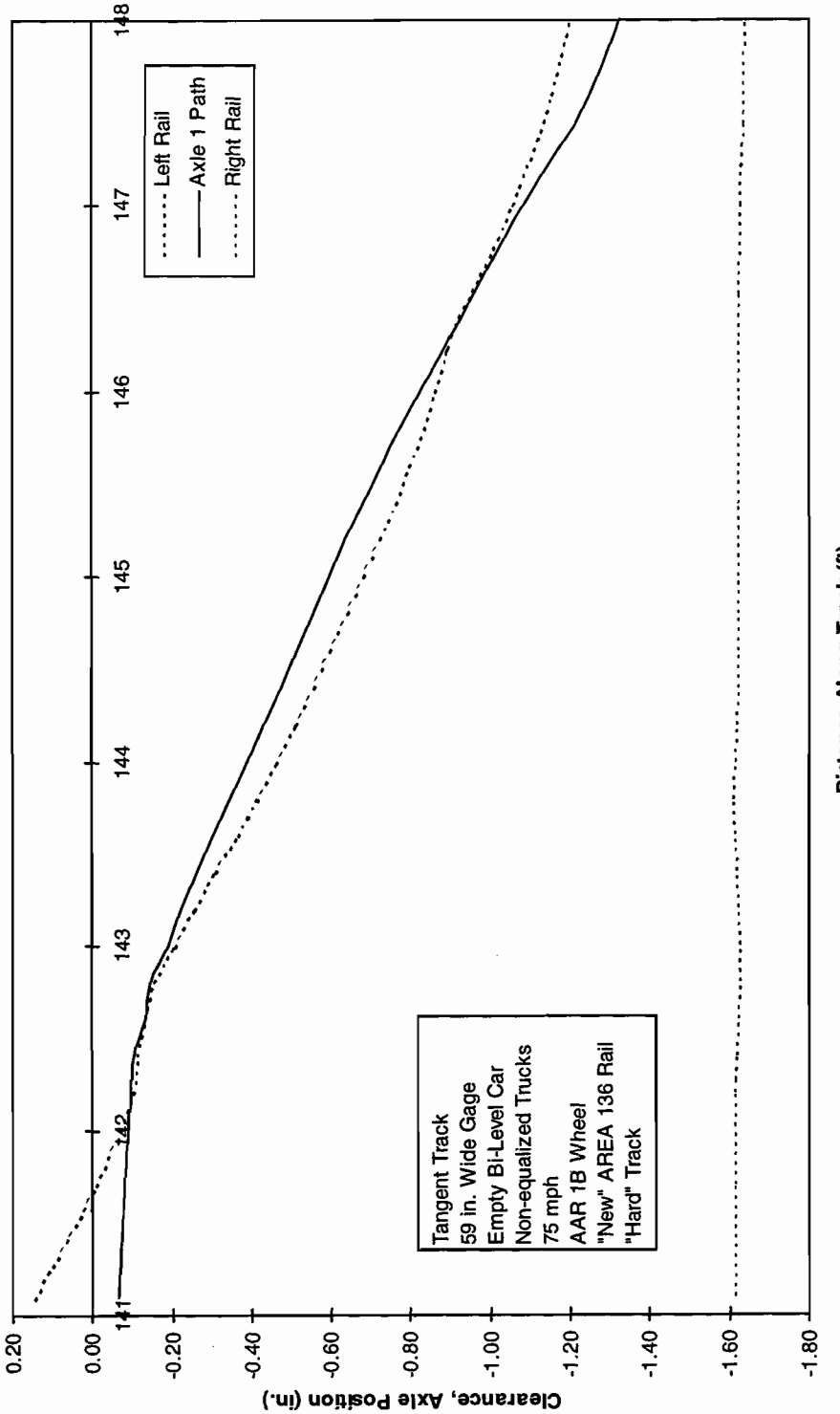

Figure 5-15. Lateral motion of lead axle - sudden gage tightening of 3.0 in.

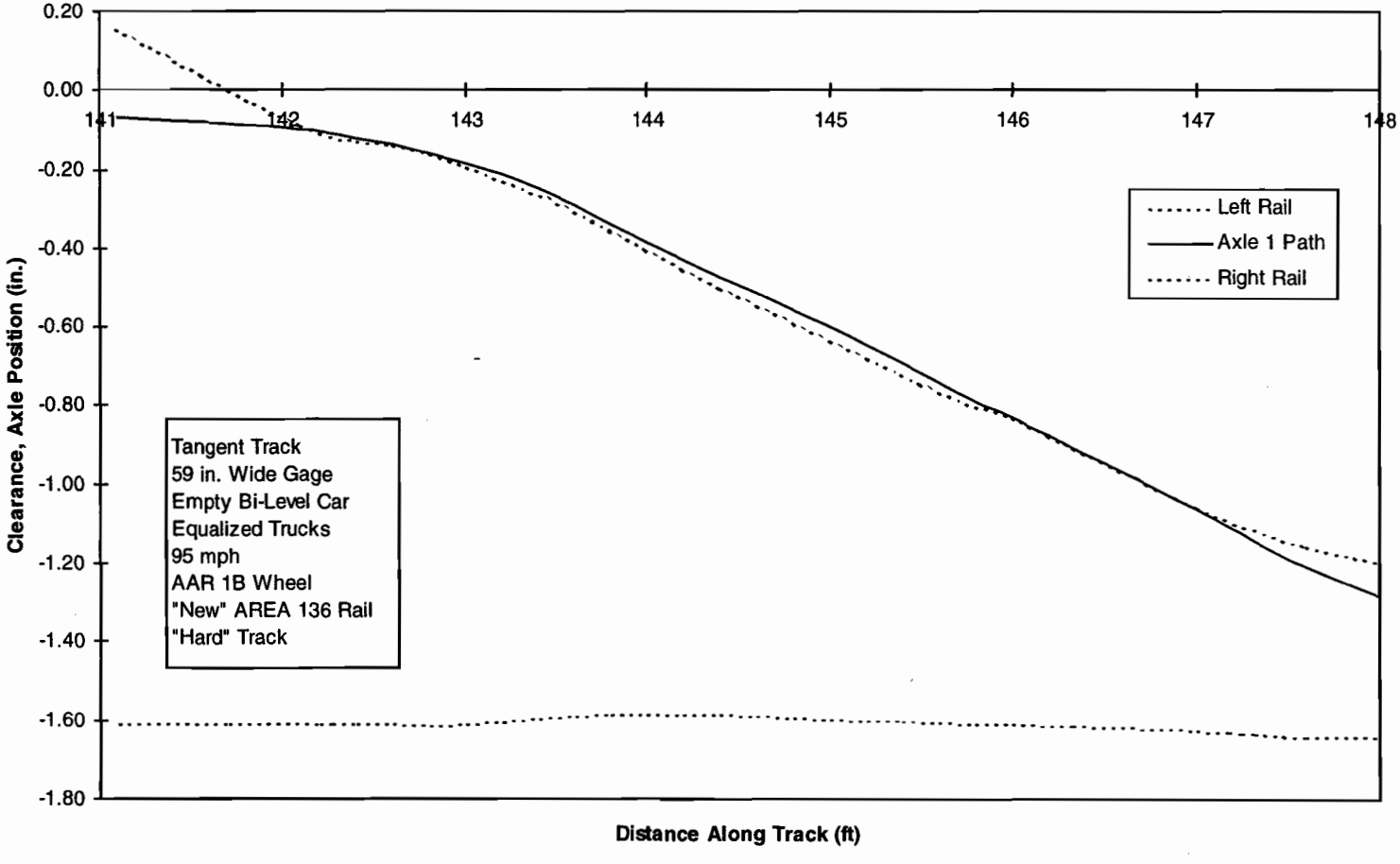

Figure 5-16. Lateral motion of lead axle - sudden gage tightening of 3.0 in.

6. RESPONSE TO COMBINED VARIATIONS IN ALIGNMENT AND CROSSLEVEL

As seen in Section 4, vertical perturbations provide the potential for dynamically unloading the wheels during guidance. This is especially important in curves, where lateral rail deviations may lead to large lateral forces as seen in Section 5. The combination of large lateral and small vertical forces from the "down-and-out" motion may lead to the potential for derailment. The forced response due to track irregularities, in both lateral and vertical directions, may include violent flanging and body roll. This behavior is closely related to body hunting through the forces at the wheel/rail interface and is especially important in a car with body steering. Thus combined alignment and crosslevel through curves may result in the loss of adequate guidance due to a combination of curving and dynamic response from rail irregularities. Both lateral and vertical wheel loads contain steady and oscillating components of force, which may result in derailment.

OMNISIM is used to evaluate the vehicle response in curved track with combined alignment and crosslevel perturbations. Perturbation amplitudes are chosen to provide near derailment conditions. Those selected are a 1 in. maximum outward cusp misalignment amplitude in the outer rail and downward cusps of 0.5 in. at the joints for crosslevel, the shapes being arranged to have the appearance of track with staggered jointed rails.

The vehicle response is determined from the simulations with particular attention being paid to axle and rail motions, wheel/rail forces and L/V ratios. Initial results are established for the same two base cars on "hard" track as used in previous sections. They are both empty bi-level cars but differ in having equalized and non-equalized trucks. Initial results were obtained without filtering and with track described by means of exponential functions previously used to represent jointed track. Figure 6-1 shows the development of the curvature and Figure 6-2 the superelevation for the 10 deg curve and a speed at balance of 30 mph. The vertical cusps are shown in Figure 6-3 and occur at each 39 ft rail length, out of phase between the left and right rails. The outer lateral rail shapes are given in the graphs of axle position in the clearance from the simulations, such as Figure 6-4.

The first results examined are those of the car with equalized trucks on track described analytically using exponentials, with a discontinuity at the cusps. The lateral position of the lead axle in the curve is shown in Figure 6-4 as it follows the outer rail. The resulting lateral and vertical forces on the lead outer wheel are shown in Figure 6-5 and the L/V ratios for both wheels on the leading axle in Figure 6-6. These graphs are shown for the full distance over the perturbations in the curve at the balance speed of 30 mph. The results for the same variables but for the car with non-equalized trucks are given in Figures 6-7 to 6-9.

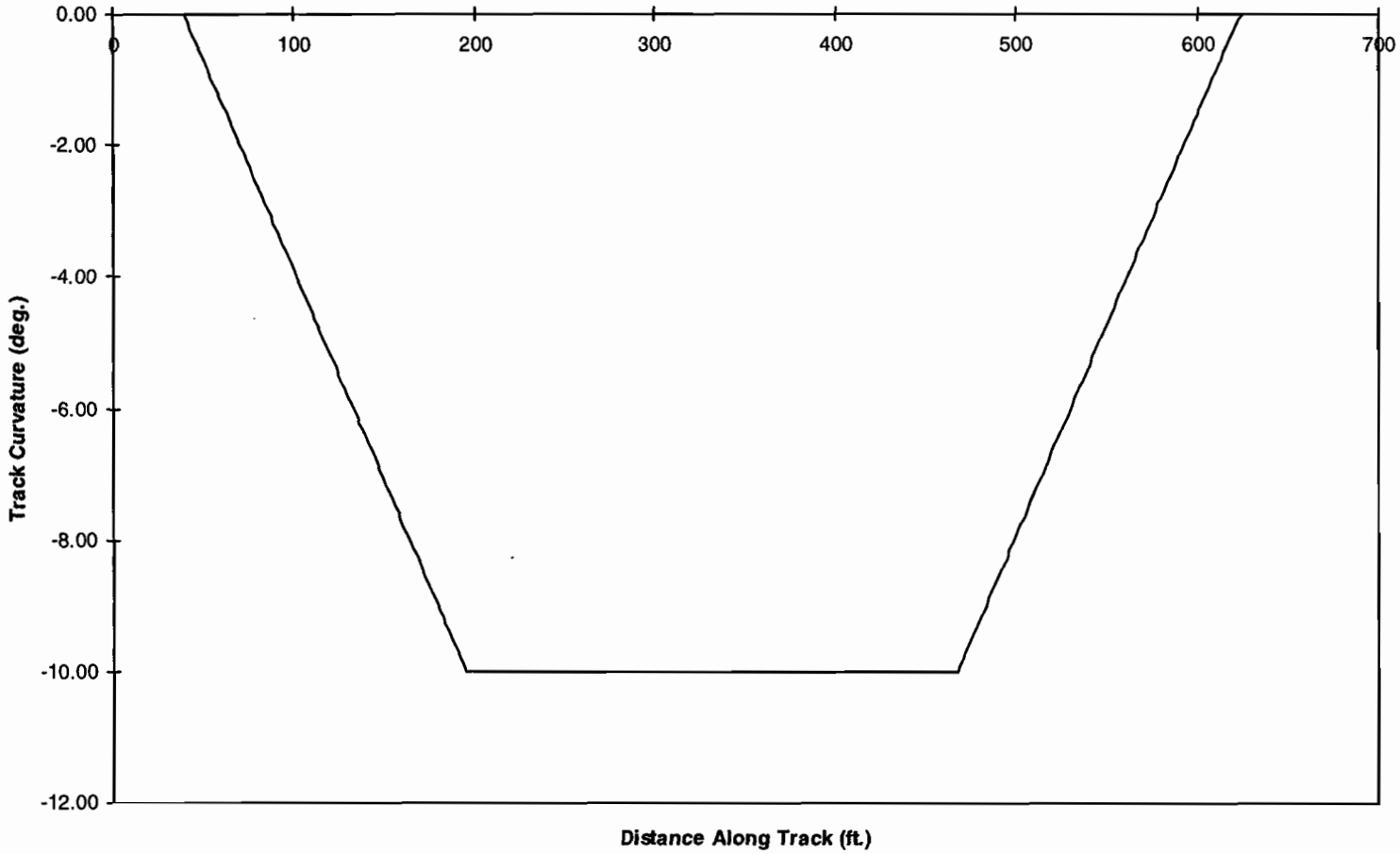

Figure 6-1. Development of the 10 deg curve

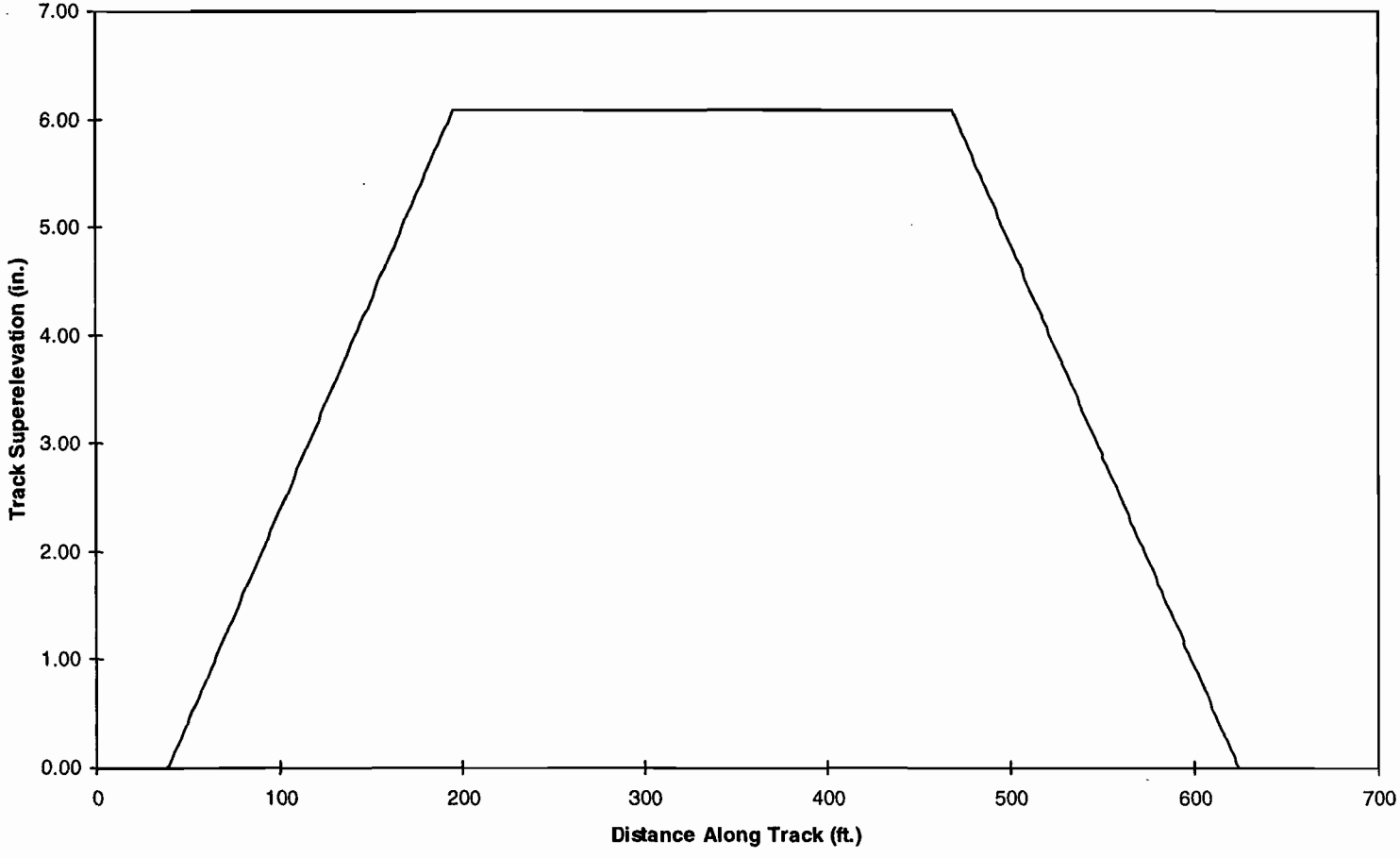

Figure 6-2. Development of the superelevation in the 10 deg curve

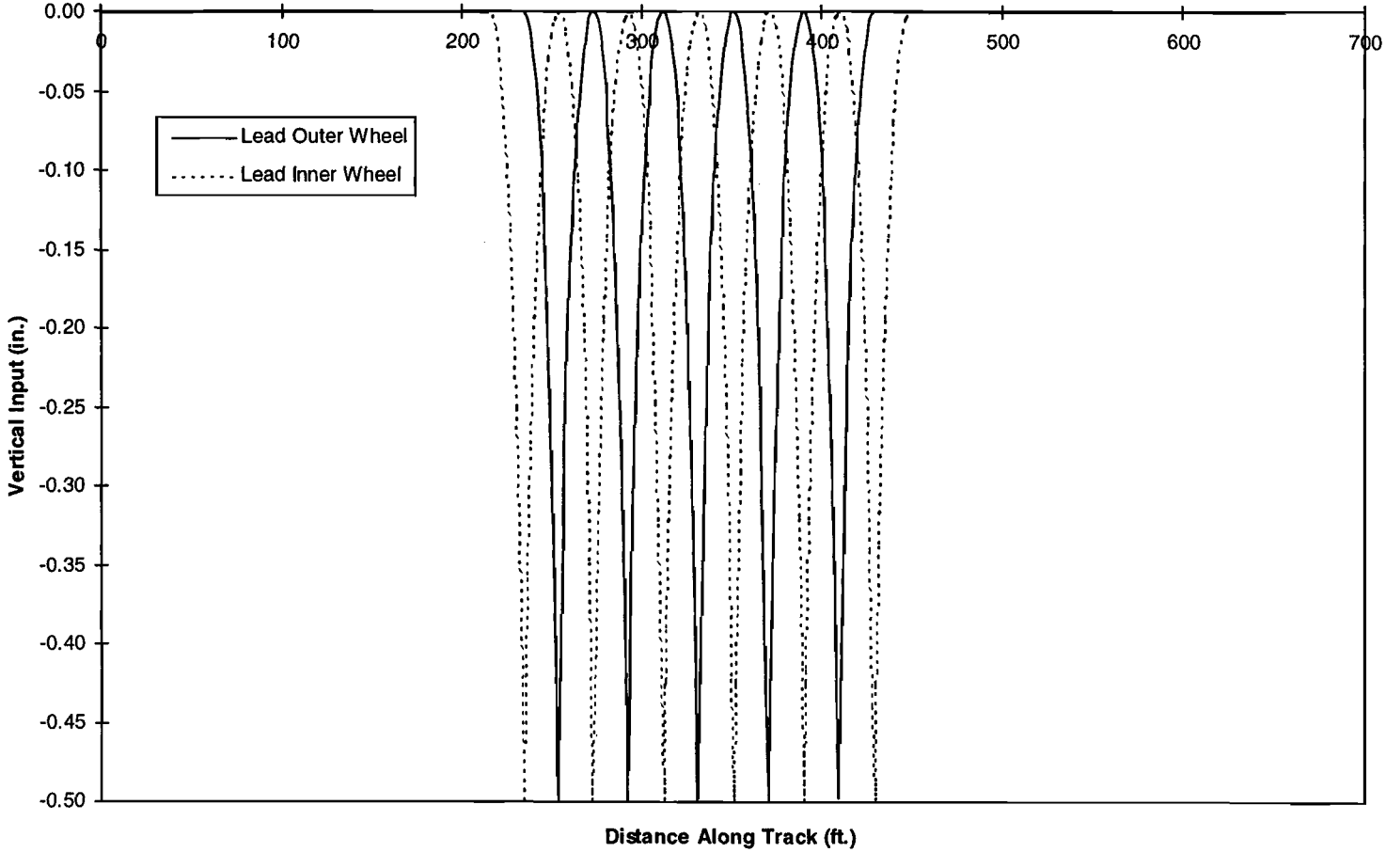

Figure 6-3. Shape of downward cusps in the 10 deg curve

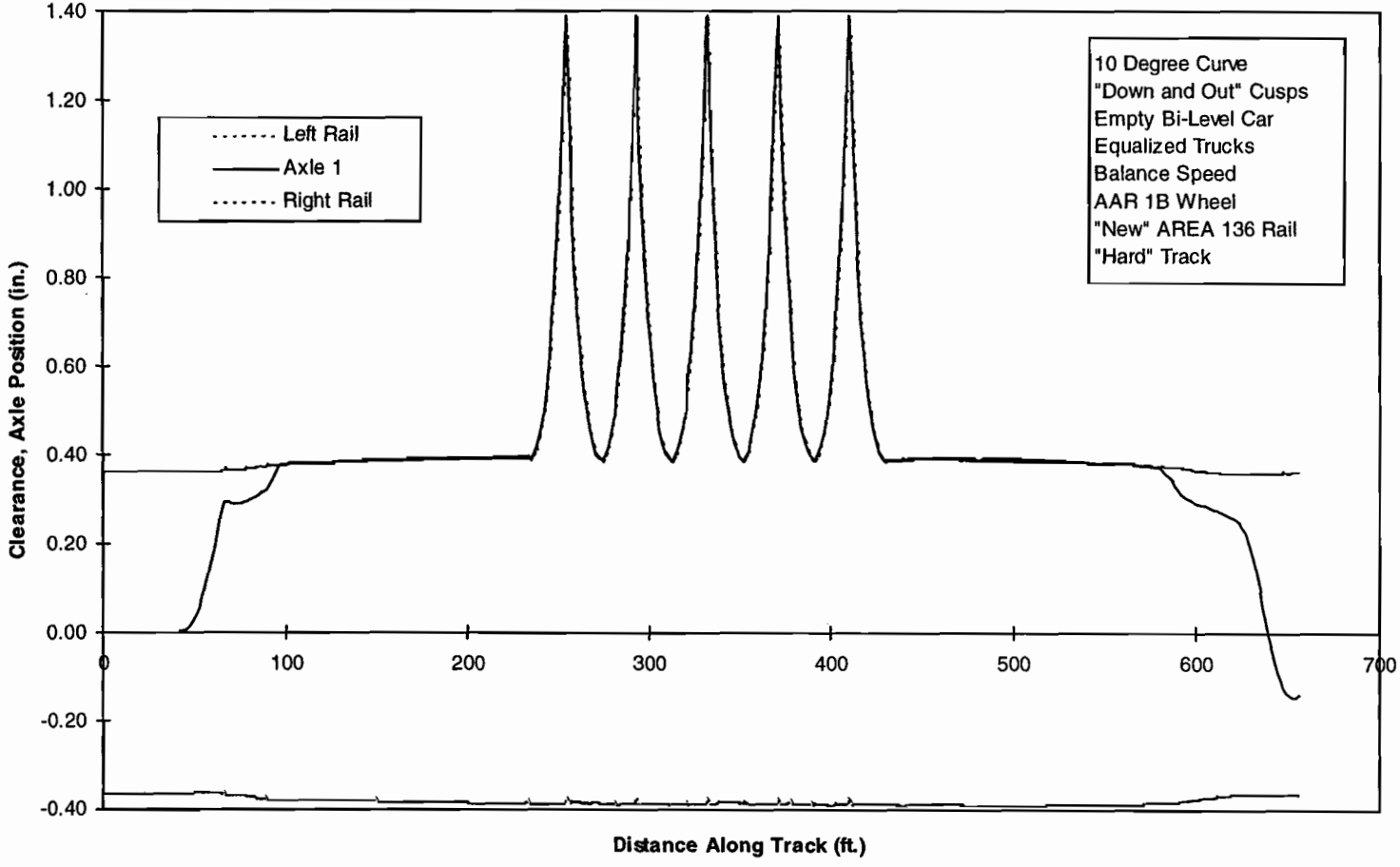

Figure 6-4. Lateral motion of lead axle in the flangeway clearance

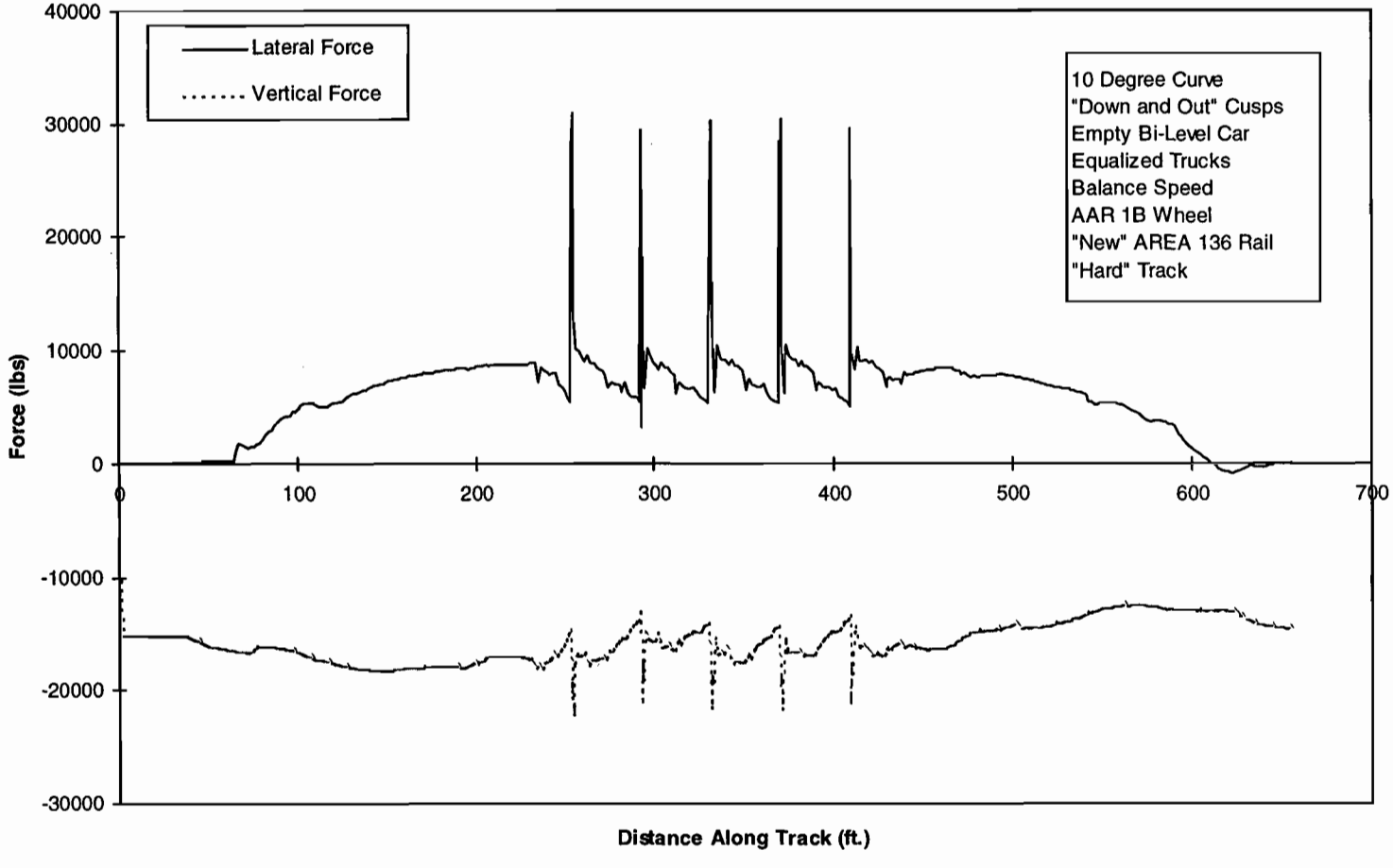

Figure 6-5. Lateral and vertical forces on lead outer wheel

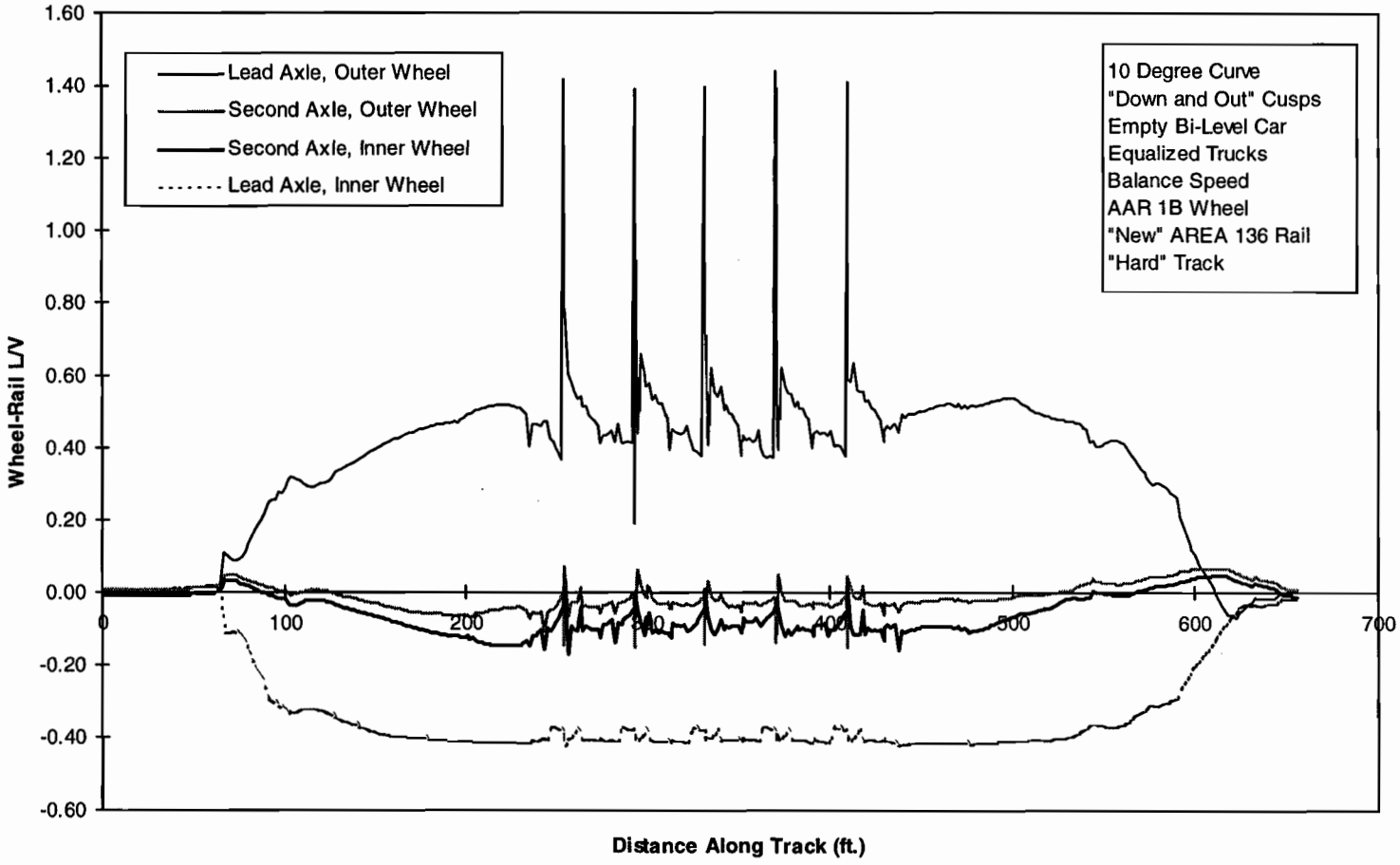

Figure 6-6. L/V ratios on leading wheels

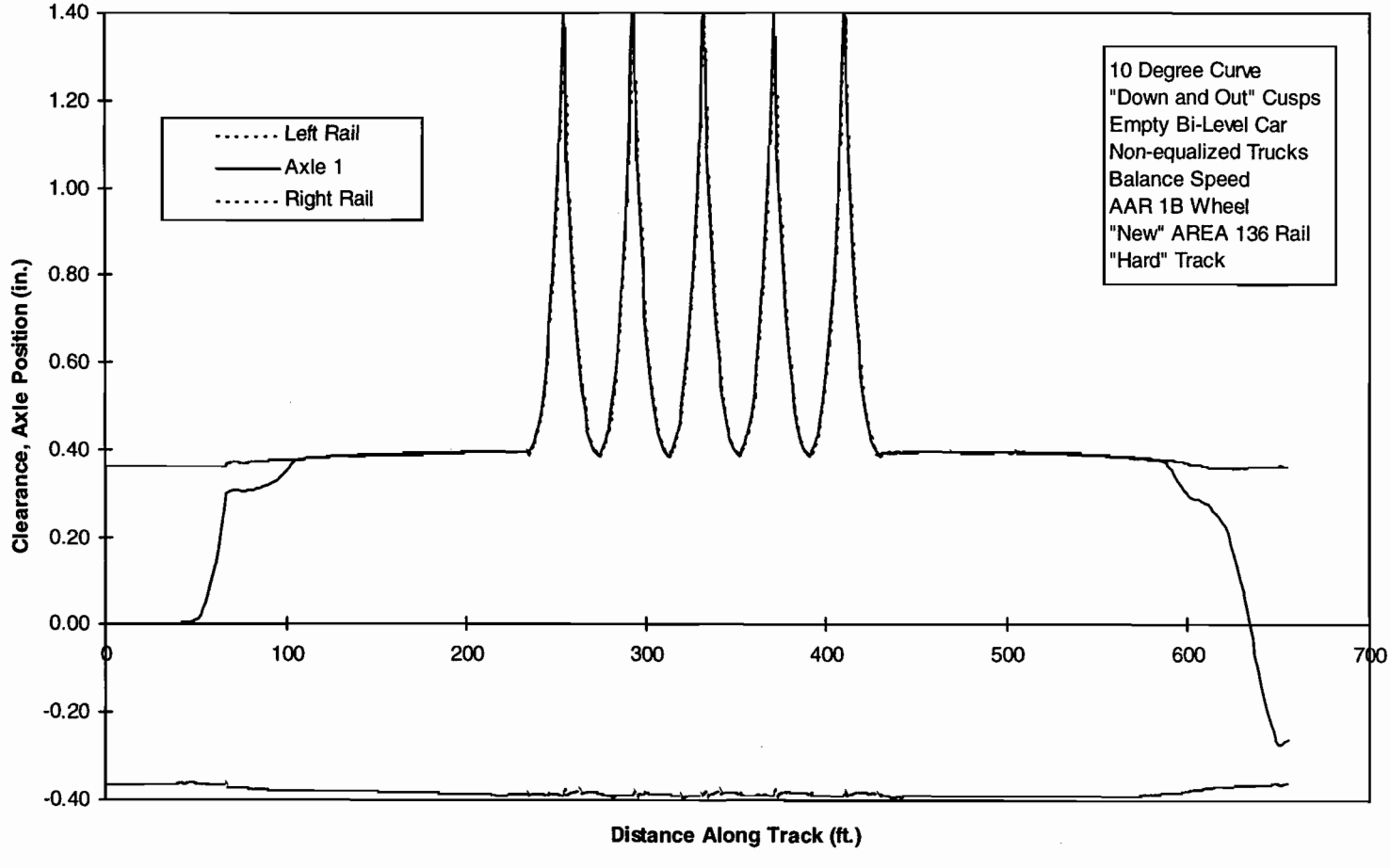

Figure 6-7. Lateral motion of lead axle in the flangeway clearance

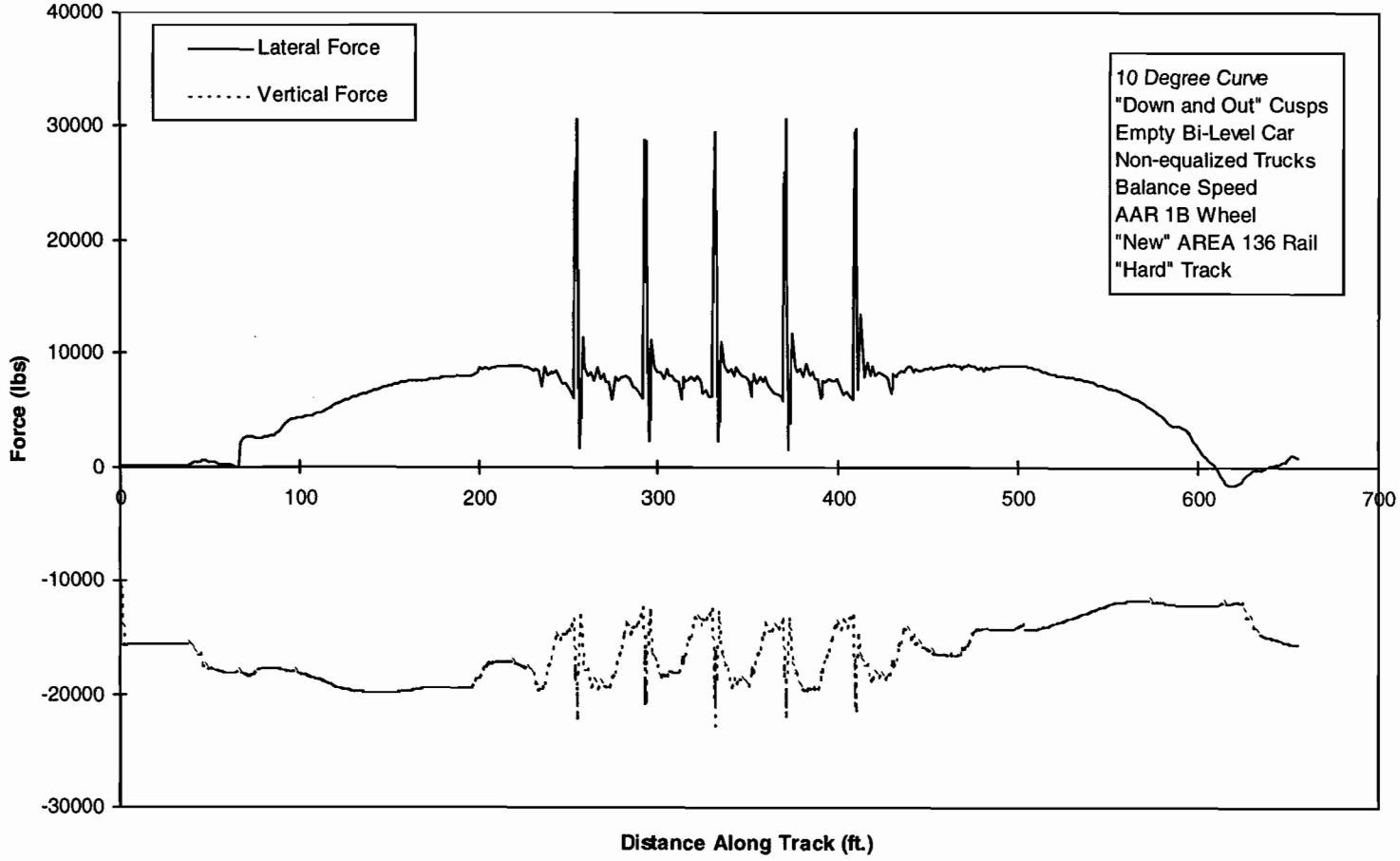

Figure 6-8. Lateral and vertical forces on lead outer wheel

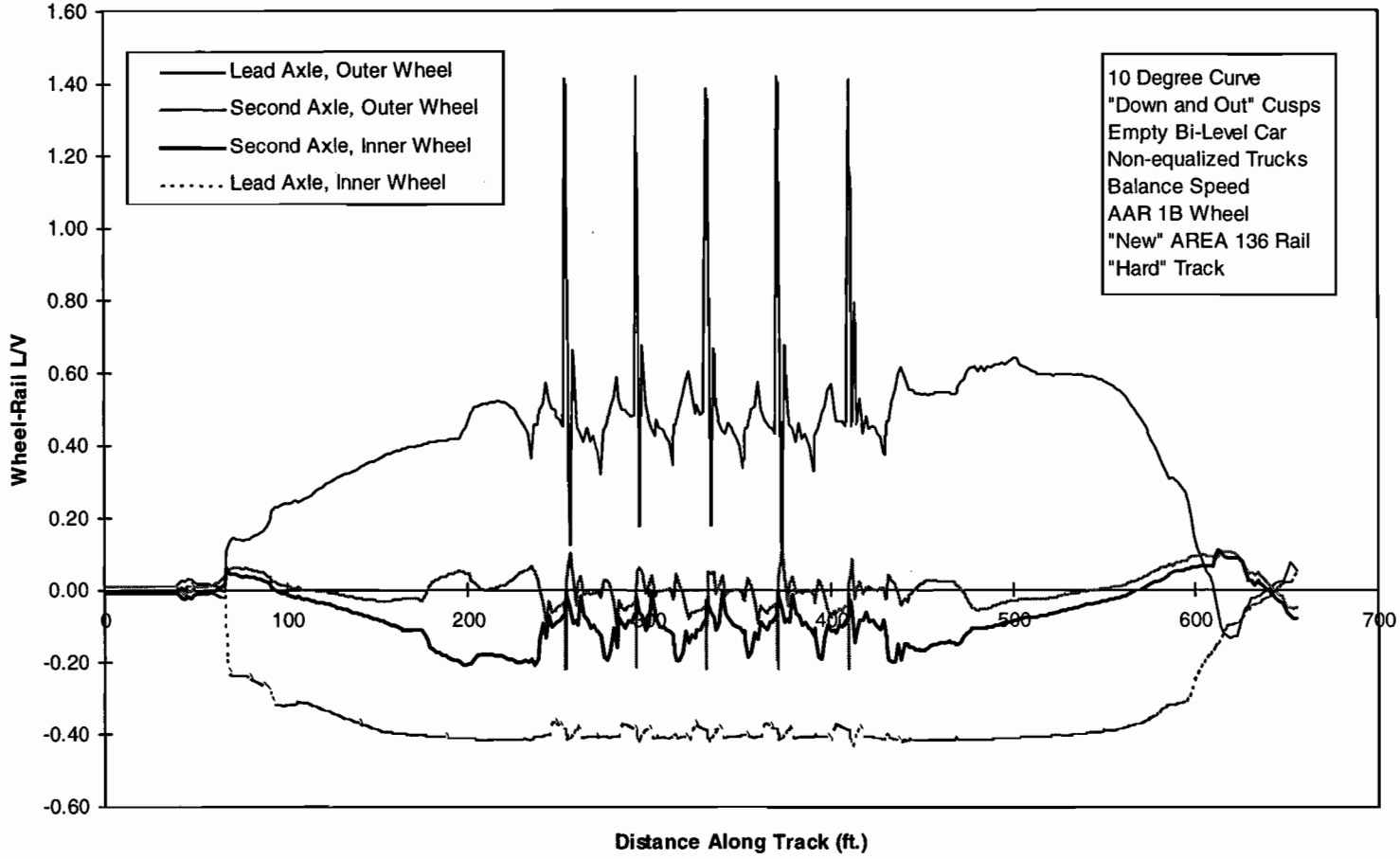

Figure 6-9. L/V ratios on leading wheels

The appearance of these results leads immediately to the conclusion that the behavior at each cusp is similar during any run, implying that body dynamics have little effect on the axle behavior in the cars examined.

The transient vertical response of the wheel on the rail when passing a discontinuity, such as the second joint cusp under investigation, has been discussed in the literature and is generally separated into two parts. The first resulting peak force, labeled P_1, has a wavelength around 2 in. and the second, P_2, a wavelength of the order of a foot. It has been noted that the P_1 force is due to the wheel on the contact stiffness and P_2 to the wheel and rail on the vertical rail flexibility. There is a noticeable correspondence between these wavelengths and those associated with some short and long rail corrugations. Closer examination of the simulation output over the second rail cusp show some correspondence to this behavior for the short wavelengths. Figure 6-10 shows the lateral and vertical forces at the second cusp for the car with equalized trucks. The initial vertical "spike" in response at wheel passage over the discontinuity is followed by a response of longer duration as suggested. The results show that very large forces can occur and that small differences in the contact and support stiffness can make for significant changes in the output forces.

The effect of the initial response "spike" is examined in detail in the discussion of the results presented. Two methods of avoiding this sharp response are examined and compared, filtering the forces at the output and filtering the input rail shape. Both are possible in OMNISIM. The former does not modify the performance or change a derailment if predicted. The apparent derailment may, however, be due to errors in the prediction of P_1 forces. Figure 6-11 shows the filtered result for the base case given previously unfiltered in Figure 6-10. The output low pass filter is set to 60 Hz. Figure 6-12 presents the result for the same system only with filtered input at the rails eliminating the discontinuity at the joint. The wavelength of the low pass filter in this case was 15.75 in., the lowest possible for this run with the present version of OMNISIM. At the balance speed of 30 mph, this wavelength is equivalent to a frequency of 33.5 Hz. Figures 6-11 and 6-12 show some similarity in the forces for this case, with the initial spike eliminated by filtering as discussed.

6.1 The Effect of Static Wheel Load

The effect of the variation in load and body type to the vehicle response to staggered joints is investigated using the three different approaches outlined in Figures 6-10 to 6-12 for the empty single and bi-level cars and the loaded bi-level cars. OMNISIM runs are made for all three systems using all three methods at balance speed. Only the single-level car predicted a derailment at this cusp. Its lead axle's wheel climb motion is shown in Figure 6-13 for the car with equalized trucks and Figure 6-14 for that with non-equalized trucks. While there is a slight difference between the truck types in the apparent speed of the derailment following wheel climb, they both derail at the cusp when fitted to the empty single-level carbody but significantly do not under the other body types and loads simulated. This difference therefore provides a good opportunity to investigate the variables generally used to define the derailment and its potential.

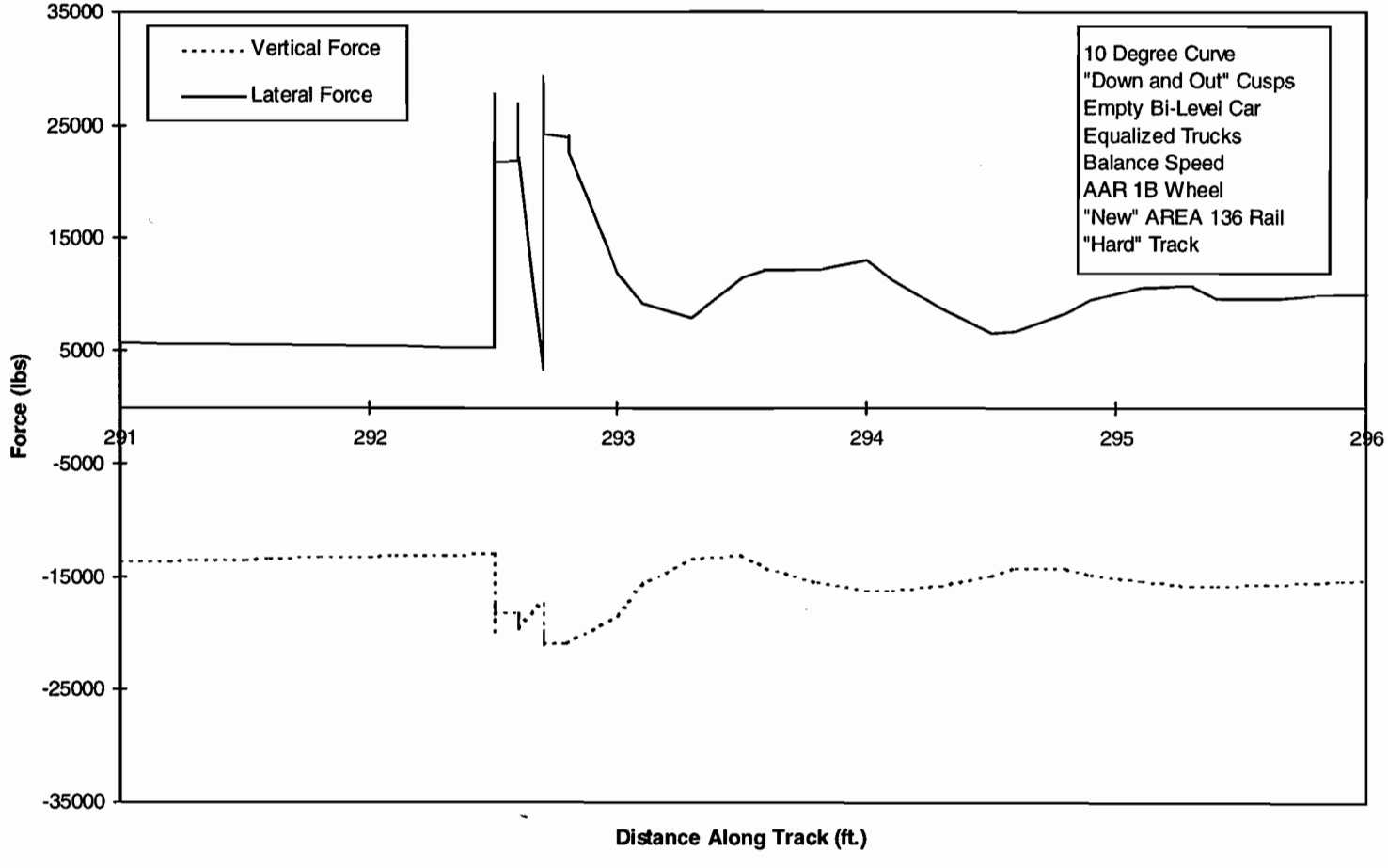

Figure 6-10. Lateral and vertical forces on lead outer wheel - unfiltered

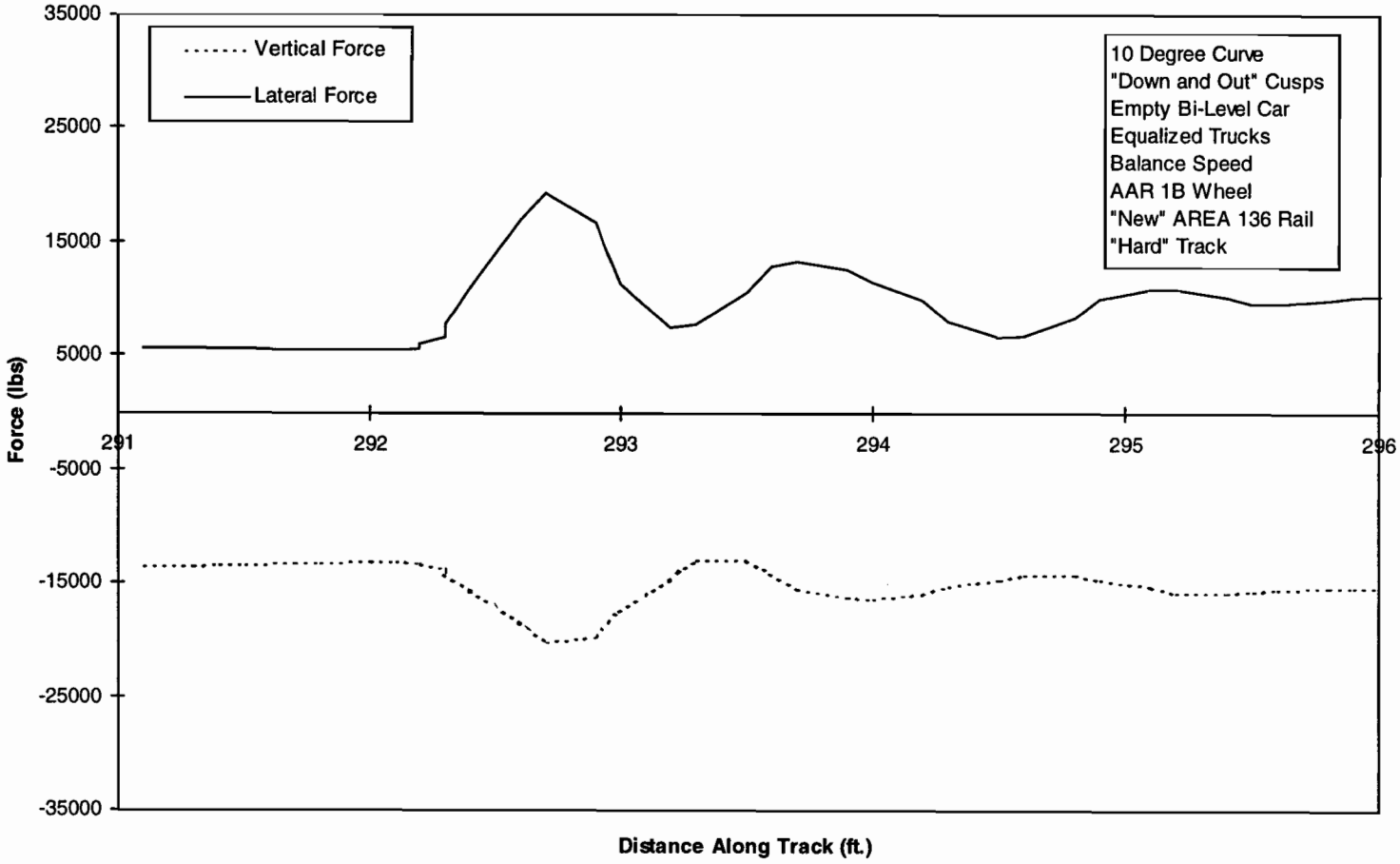

Figure 6-11. Lateral and vertical forces on lead outer wheel - post-filtered at 60 Hz

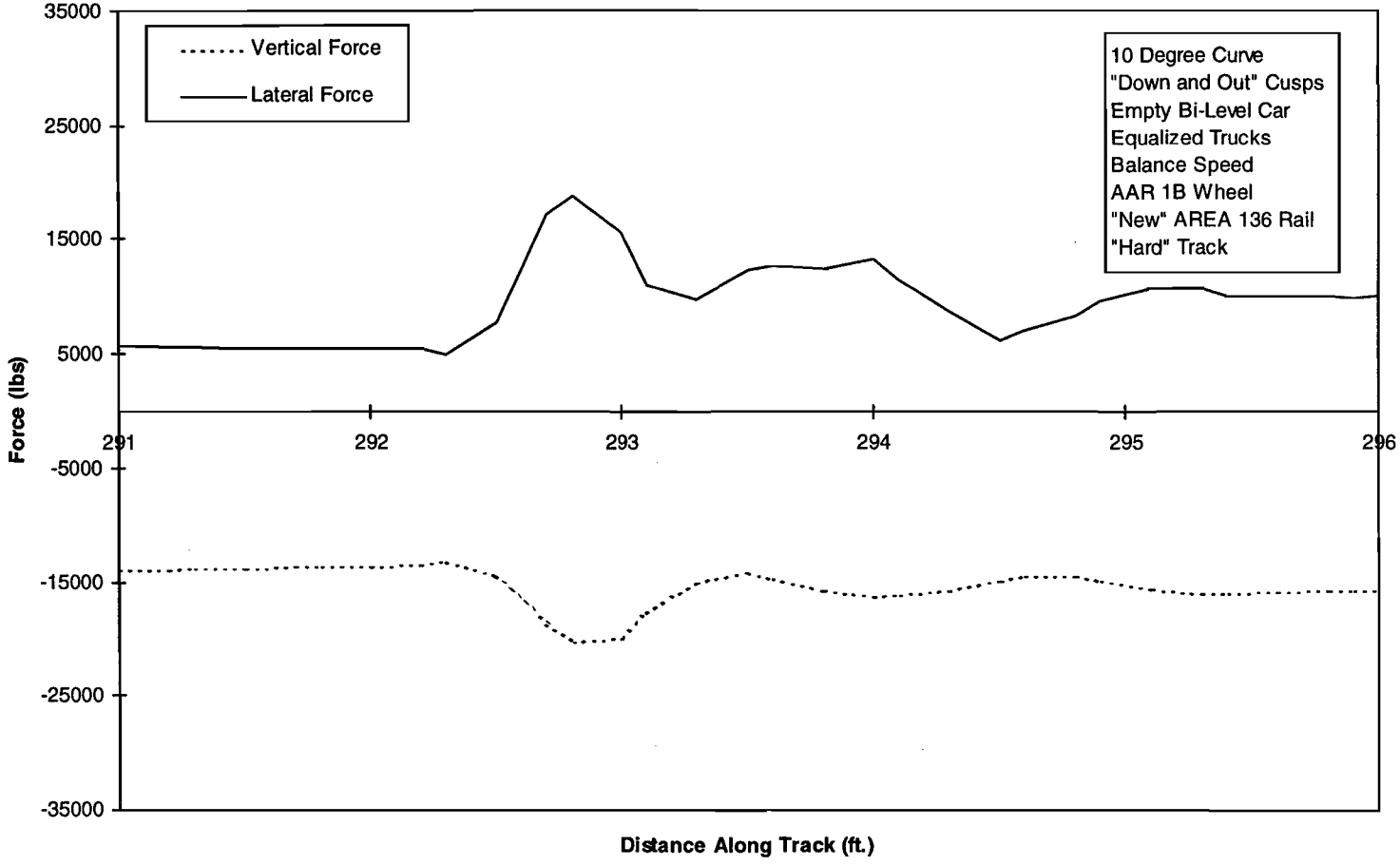

Figure 6-12. Lateral and vertical forces on lead outer wheel - rails pre-filtered at 15.75 in.

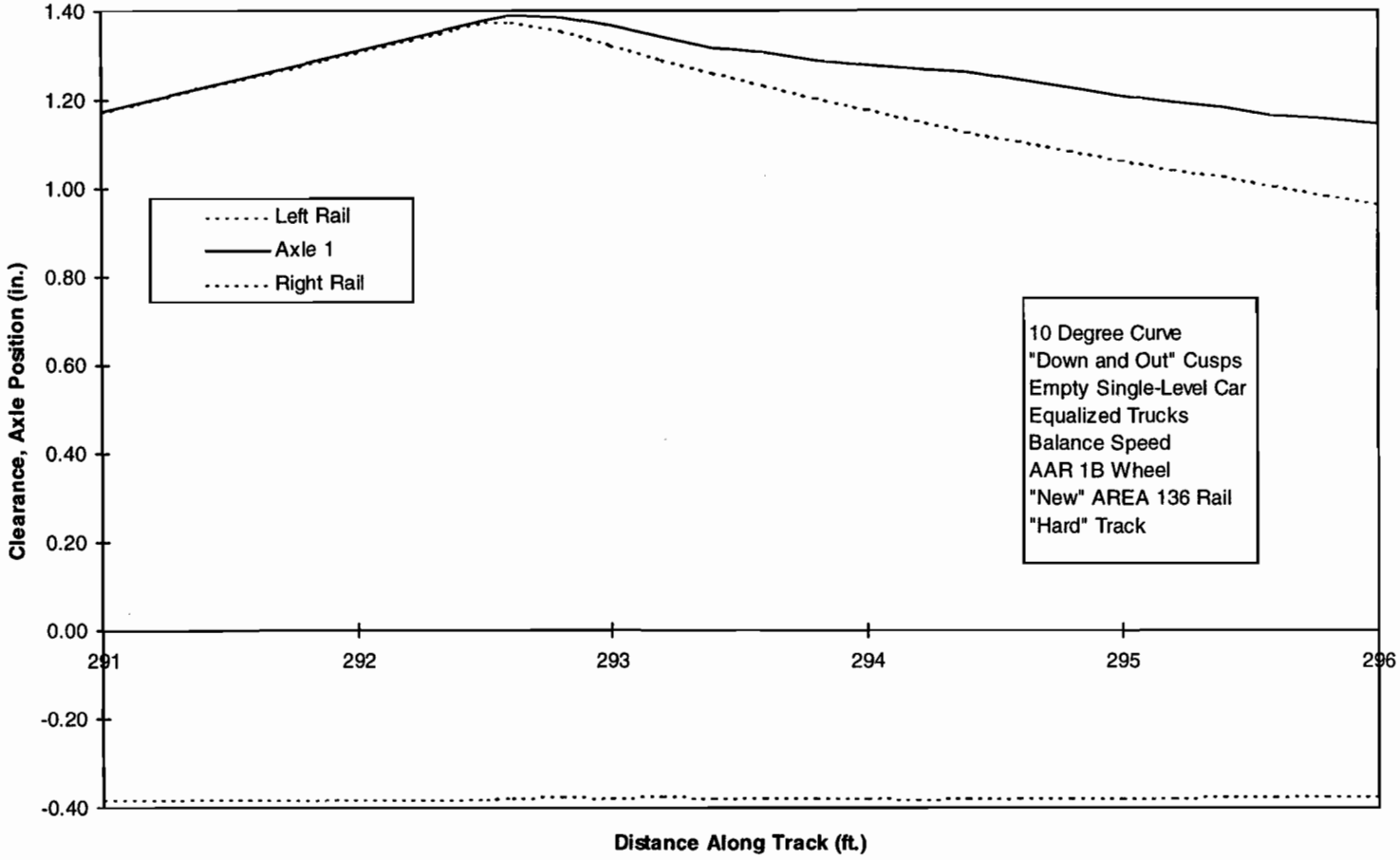

Figure 6-13. Wheel climb derailment of lead axle at the second cusp

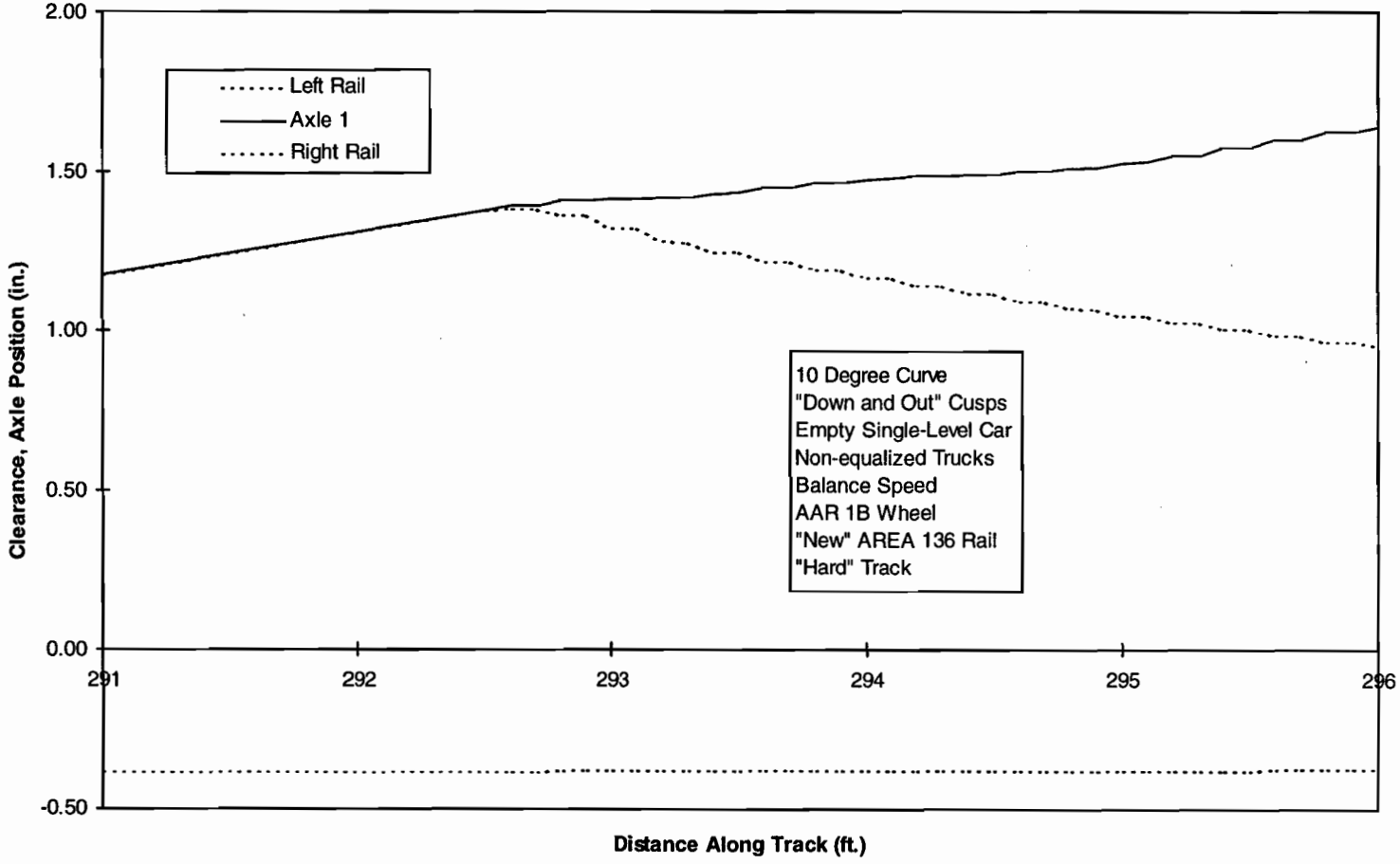

Figure 6-14. Wheel climb derailment of lead axle at the second cusp

The results for the peak wheel L/V and their positions on the derailment plot are summarized in Figures 6-15 and 6-16. They are not what was initially expected.

Figure 6-15 shows a comparison of the peak values for the lead axle L/V of the car systems with equalized trucks predicted at or near the cusp for the three analytic methods described. The single-level result for which OMNISIM predicts derailment is the first of the three results in each case. The first case, representing the unfiltered peak values, shows virtually no difference between the single wheel L/Vs determined with accuracy at the cusp. The same graph for the cars with non-equalized trucks is given in Figure 6-16. The preliminary conclusion is that the L/V value alone does not provide an adequate determination of a derailment, although there is clear evidence of a large value when derailment occurs. There is also a probability that the initial "spike," while representing the real phenomena of the wheel bouncing on its contact stiffness, is not presently modeled to sufficient accuracy in OMNISIM. The result which identifies the car most likely to derail using the highest L/V as a criterion is that obtained from the study by pre-filtering the rail shape inputs.

The results for the same run, but with output values filtered at 60 Hz, much higher than the 15 Hz that frequently used in freight car assessment, show a complete reversal of the normally assumed trend. The peak L/V is lowest in the derailing cars, leading to the conclusion that the direct method of filtering the results to eliminate the "spikes" can lead to significant errors in the conclusions. However, in the final method, where the abruptness of the discontinuity is reduced by smoothing the rail input to eliminate wavelengths at the cusp of less than 15.75 in., the trend is that expected and the derailing single-level has a markedly higher peak L/V value than the other cars, although none derail. This method may provide useful additional information of the vehicle behavior. It may also give some credence to setting L/V limits with a requirement for a dwell time or distance.

6.2 The Effect of Unbalance and Speed in Curves

Figure 6-17 shows the lack of variation with either speed or unbalance for the base cars between 21 mph (-3 in. unbalance) and 42 mph (+6 in. unbalance) investigated with and without the rails smoothed through pre-filtering as discussed previously. It is noticeable that the unfiltered results are greater than the Nadal value for the wheel and rail profiles used. This confirms that Nadal is conservative and also suggests that the lead axle is close to wheel climb throughout.

Figure 6-18 shows a comparison of the unfiltered initial peak L/V values for a range of unbalance conditions in the 5 and 10 deg curves with identical perturbations. The largest L/V values are in the 5 deg curve. On closer inspection this is due to the fact that the lead left wheel is not in flange contact at the cusp but its flange hits the gage face of the rail just past the cusp at a relatively low angle of attack. Thus it can sustain high L/V values without a wheel climb derailment. A full table of values is given in Table 6-1 below for the bi-level cars.

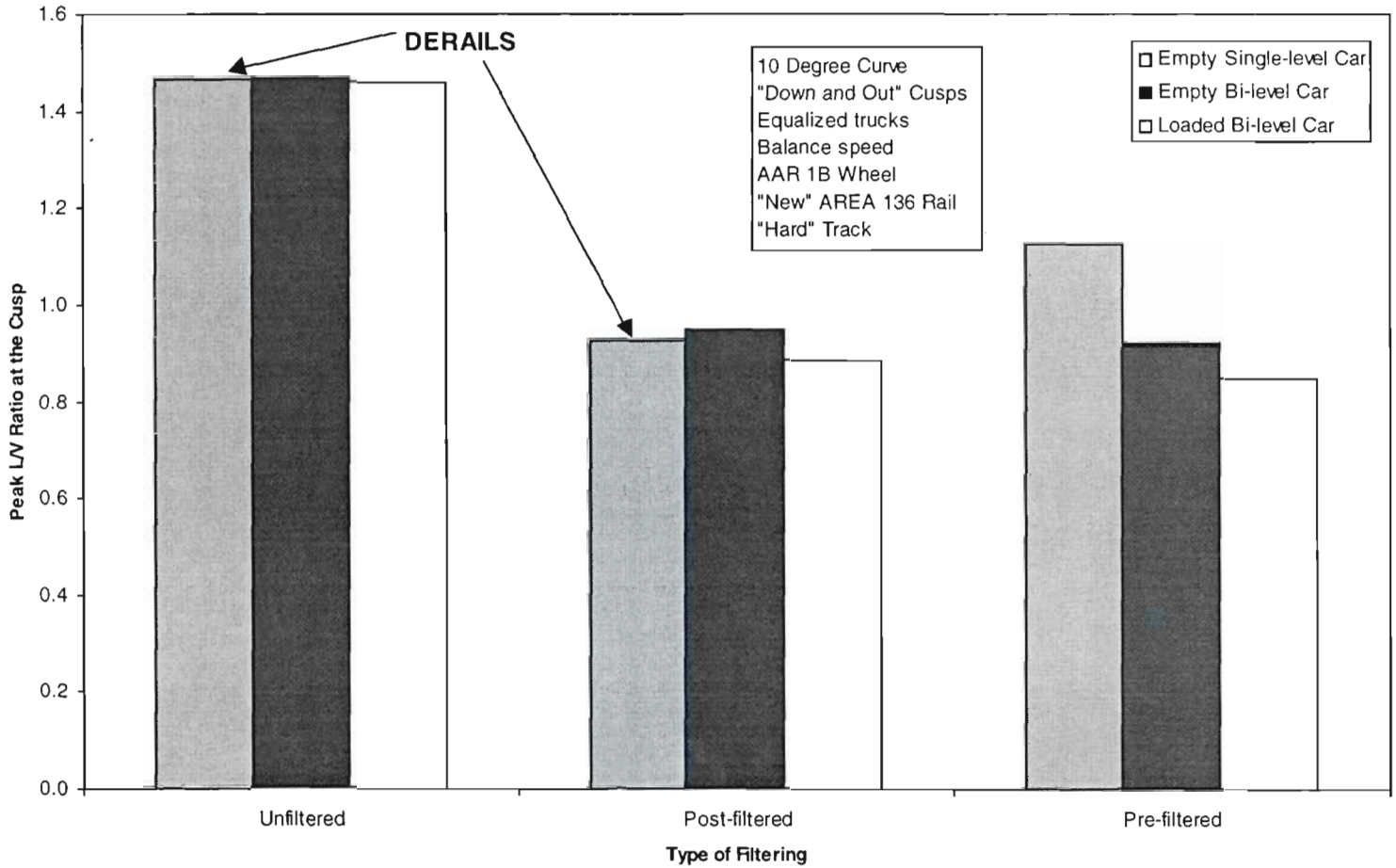

Figure 6-15. Peak L/V ratios on leading wheels at the second cusp (equalized trucks)

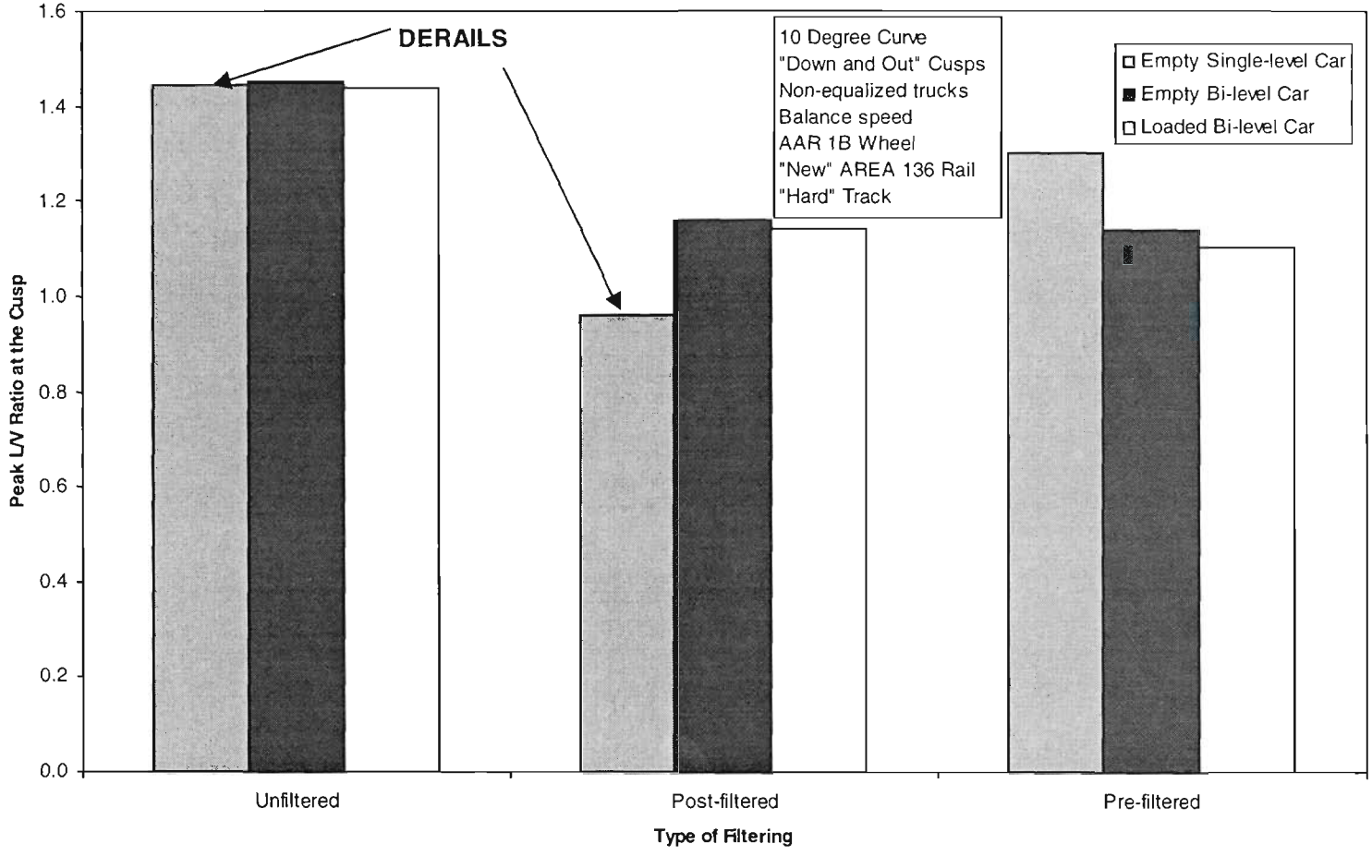

Figure 6-16. Peak L/V ratios on leading wheels at the second cusp (non-equalized trucks)

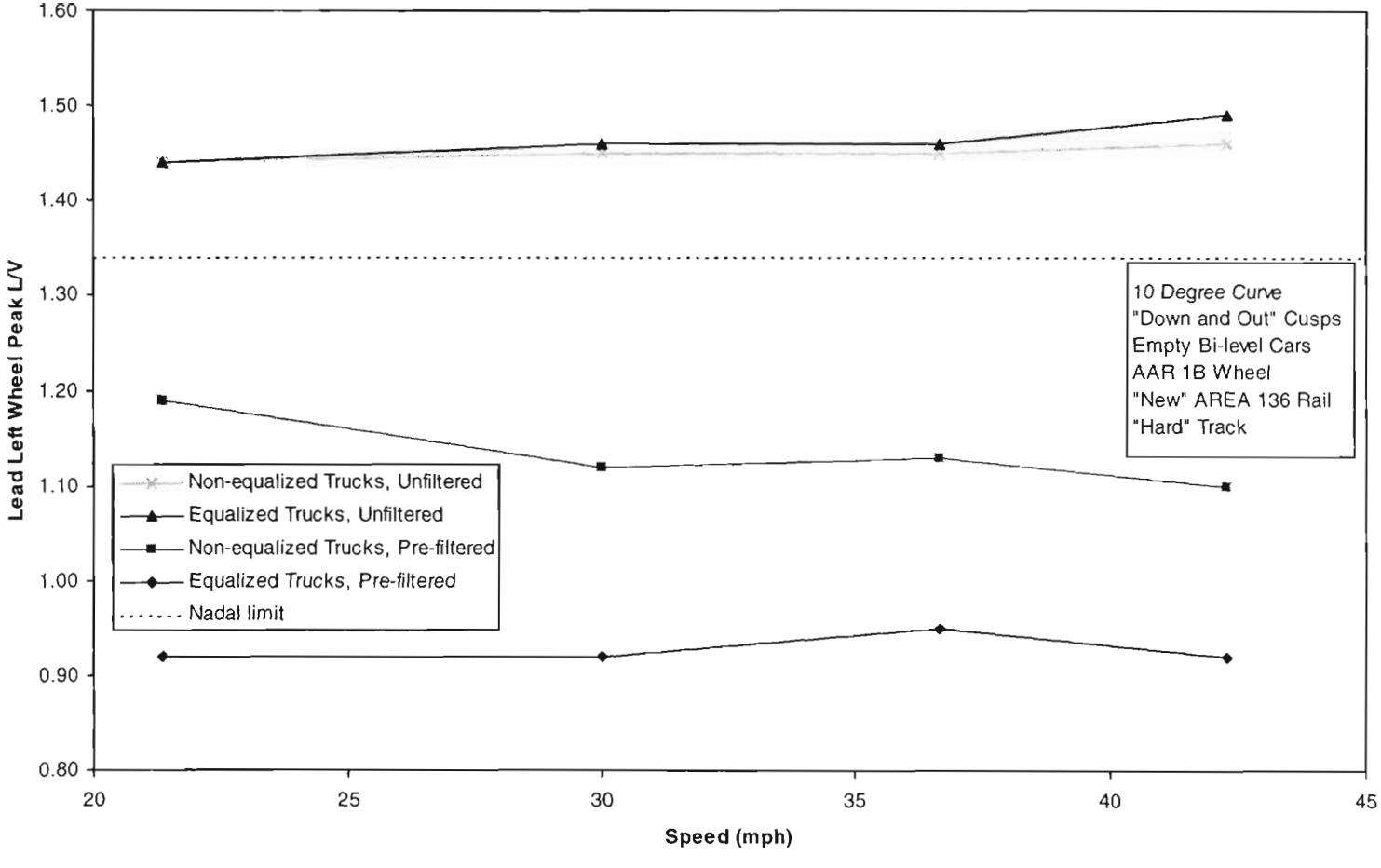

Figure 6-17. Largest unfiltered and pre-filtered L/Vs on the lead outer wheel at various speeds

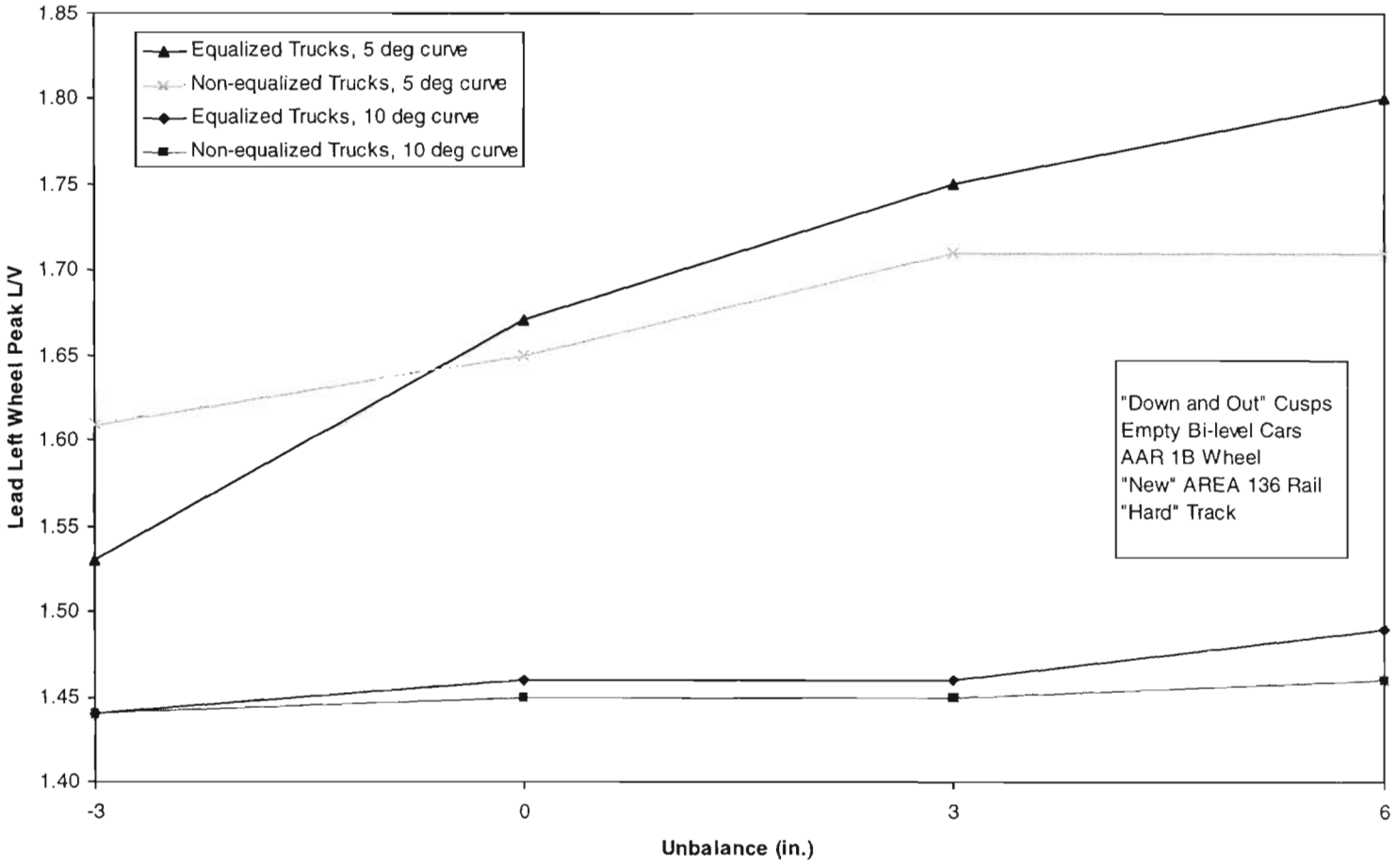

Figure 6-18. Largest unfiltered L/Vs on the lead outer wheel at various unbalances

Table 6-1. Peak L/V values on lead outer wheel in perturbed curves (empty bi-level cars)

Balance	Equalized Trucks				Non-equalized Trucks			
(in.)	Trk A	Trk B	Trk C	Trk D	Trk A	Trk B	Trk C	Trk D
-3	0.92	1.44	1.53	1.53	1.19	1.44	1.61	1.60
0	0.92	1.46	1.67	1.65	1.12	1.45	1.65	1.69
+3	0.95	1.46	1.75	1.72	1.13	1.45	1.71	1.70
+6	0.92	1.49	1.80	1.80	1.10	1.46	1.71	1.72

Note: Track A is the unsmoothed 10 deg curve, track B is the smoothed 10 deg curve, track C is the unsmoothed 5 deg curve and track D is the smoothed 5 deg curve. The smoothing, as described earlier, is provided by a filtering with a corner frequency equivalent to a shortest wavelength of 15.75 in. providing continuity at the cusp.

6.3 The Effect of "Soft Track"

Finally, in this section, the effect of "soft" track was investigated. The peak L/Vs in the initial dynamic response from runs on the "soft" track showed only a small difference from those previously predicted for "hard" track, and only then with smoothed or pre-filtered track as shown in Table 6-2.

In the 10 deg curve at balance speed the difference in track has little effect on the dynamic response of the wheel on the rail at the cusp.

Table 6-2. Comparison of peak L/V values on "hard" and "soft" track in the 10 deg perturbed curve (empty bi-level cars)

Truck Type	Equalized		Non-equalized	
Track Type	"Hard"	"Soft"	"Hard"	"Soft"
Unfiltered	1.46	1.46	1.45	1.45
Pre-filtered	0.92	0.85	1.12	1.10

7. MOVEMENT THROUGH SWITCHES

Large motions of the body can occur at sudden changes in the direction of the guiding rails such as at switches. These can cause large lateral forces between the wheel and rail. OMNISIM was used to simulate the behavior of the vehicles running through an American Railway Engineering and Maintenance-of-Way Association (AREMA) No. 8 crossover at speeds from 5 to 25 mph. The potential for derailment may appear as a wheel climb, or static and dynamic gage widening leading to wheel drop. Wheel climb potential is examined from direct measurement of the movement of the wheel up and on to the rail head and through the examination of the proximity of the value of L/V to that precomputed to be limiting for the effective angle of attack of the wheel to the rail from the simulation. The lateral shift of the rails is also monitored for increase in gage beyond safe limits.

Figure 7-1 shows the curvatures in the number eight crossover. There is a sudden change in yaw angle at the entry to the switch at 50 ft which is indicated by a large curvature over a short distance. This is followed by a straight switching rail up to 67.1 ft. The yaw angle is then increased progressively along a curved rail with curvature equivalent to just over 11 deg, followed by the entry to the frog which is straight. The gage is slightly tightened at the switch entry to represent the width of the point of the switched rail. The second part of the crossover is a reverse mirror image of the first. In later runs a 3 in. low joint is added at the entrance to the frog. The location and vertical profile for this is given in Figure 7-2. The deflected lateral positions of the rails with clearance are given in Figure 7-3, showing the step in gage at the switch rail point and the variation under load.

Simulation runs are made through the crossover at speeds of 15 and 25 mph. The results were inspected for high frequency transient responses as seen previously in Section 6. They were not a difficulty and the results as presented are not filtered, nor is the track smoothed. The results for the base vehicles, the empty bi-level car with equalized and non-equalized trucks, are rather similar through the crossover with no perturbations other than those necessary for the design. They are shown graphically in pairs, the even figure number being the axle path in the flangeway clearance and the odd number showing the L/V values for the lead axle in the lead truck. Figures 7-4 to 7-7 are for the bi-level car with equalized trucks. Figures 7-4 and 7-5 are at 15 mph and Figures 7-6 and 7-7 are at 25 mph. Similar results for the bi-level car with non-equalized trucks are shown in Figures 7-8 to 7-11. Neither the speed nor the truck design difference seems to change the L/V values significantly over the unsuperelevated crossover. The tracking shows the lateral movement at the yaw angle and gage change at the point, movement to flange contact in the curved rails after the switch, movement away from the flange through the straight frog, flanging on the other side in the curved rails and away again through the straight switch rail and a small response at the angle and small gage change. Significant but safe L/V

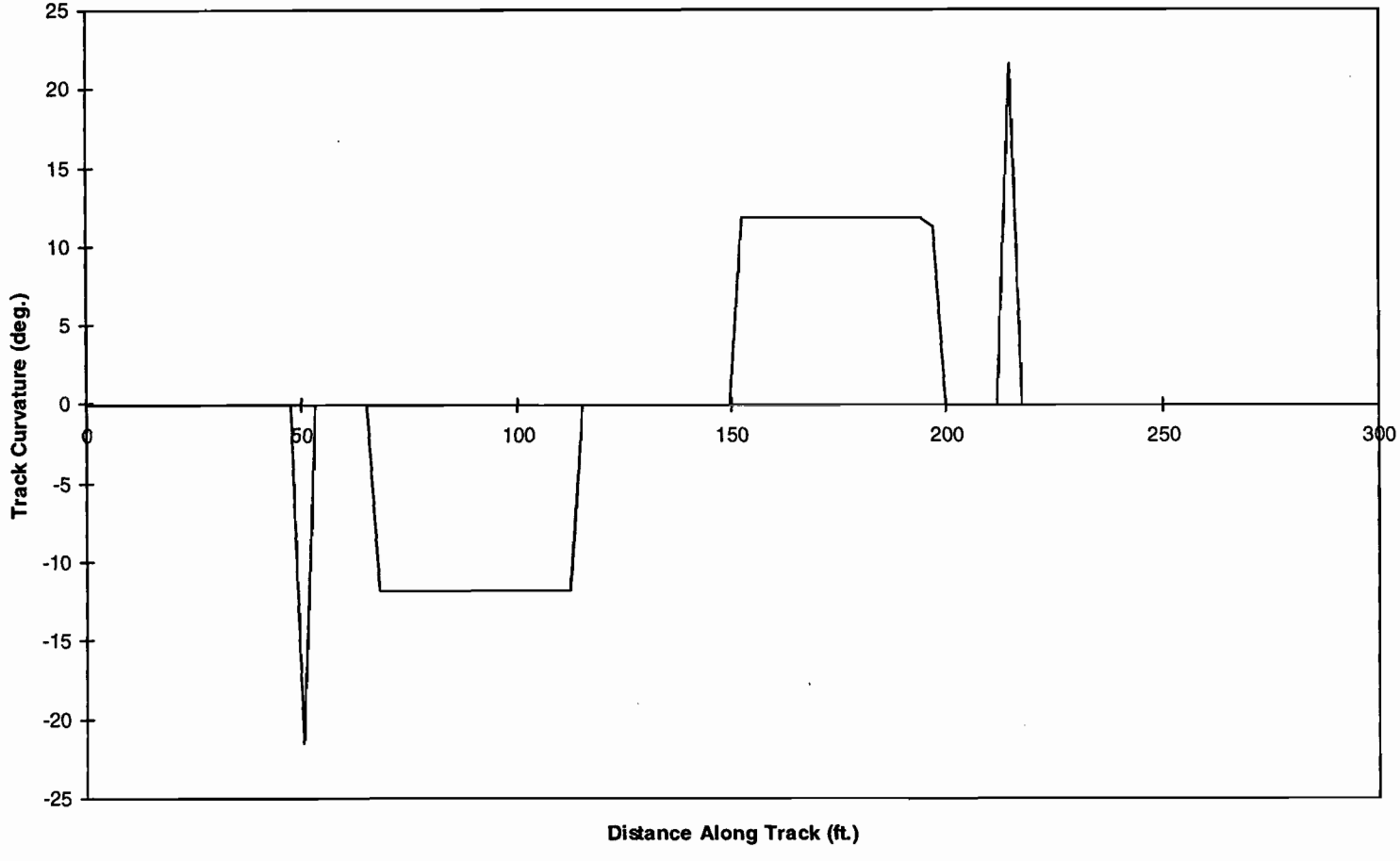

Figure 7-1. Track curvature through the No. 8 crossover

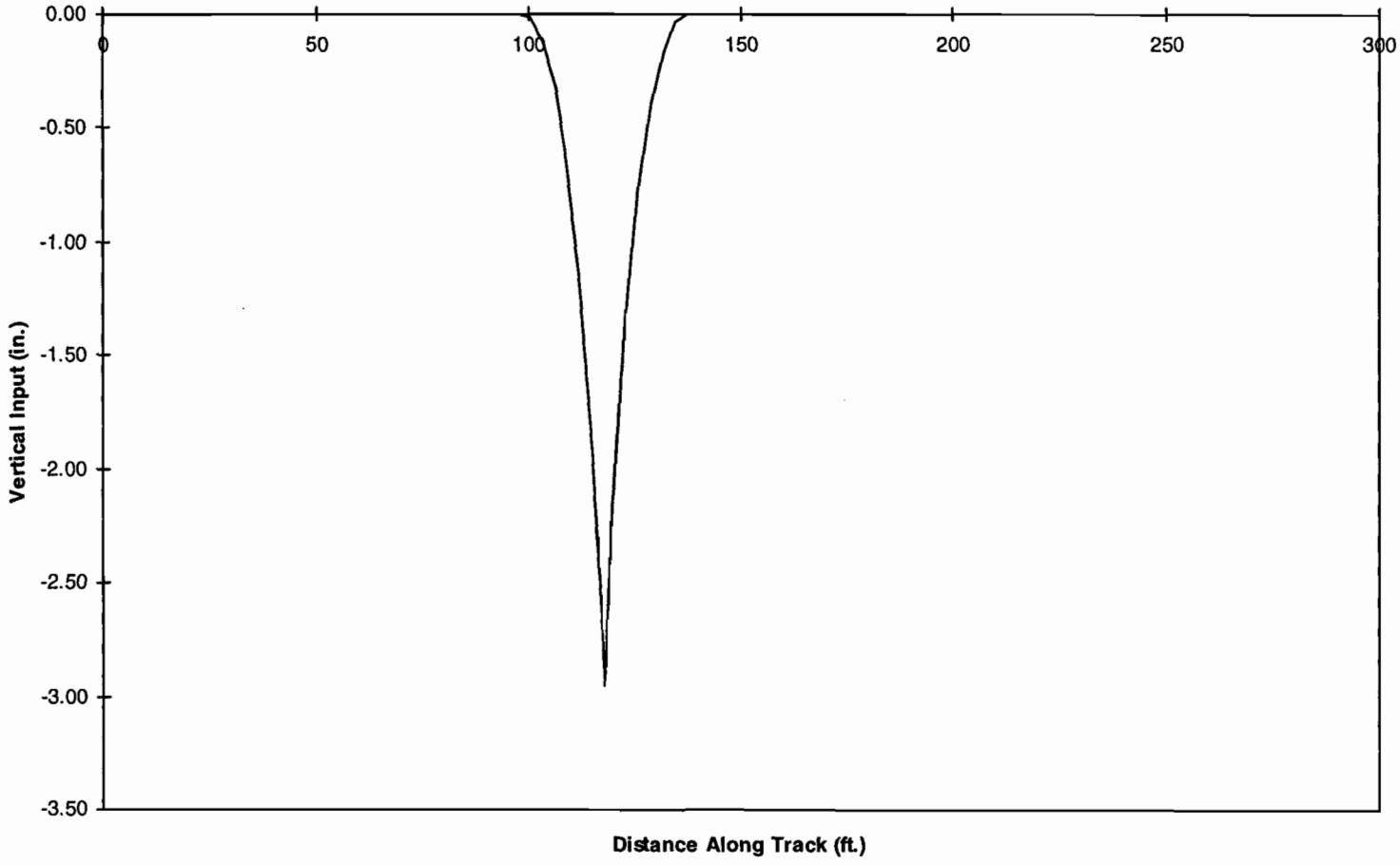

Figure 7-2. Vertical rail profile through the No. 8 crossover showing the imperfection

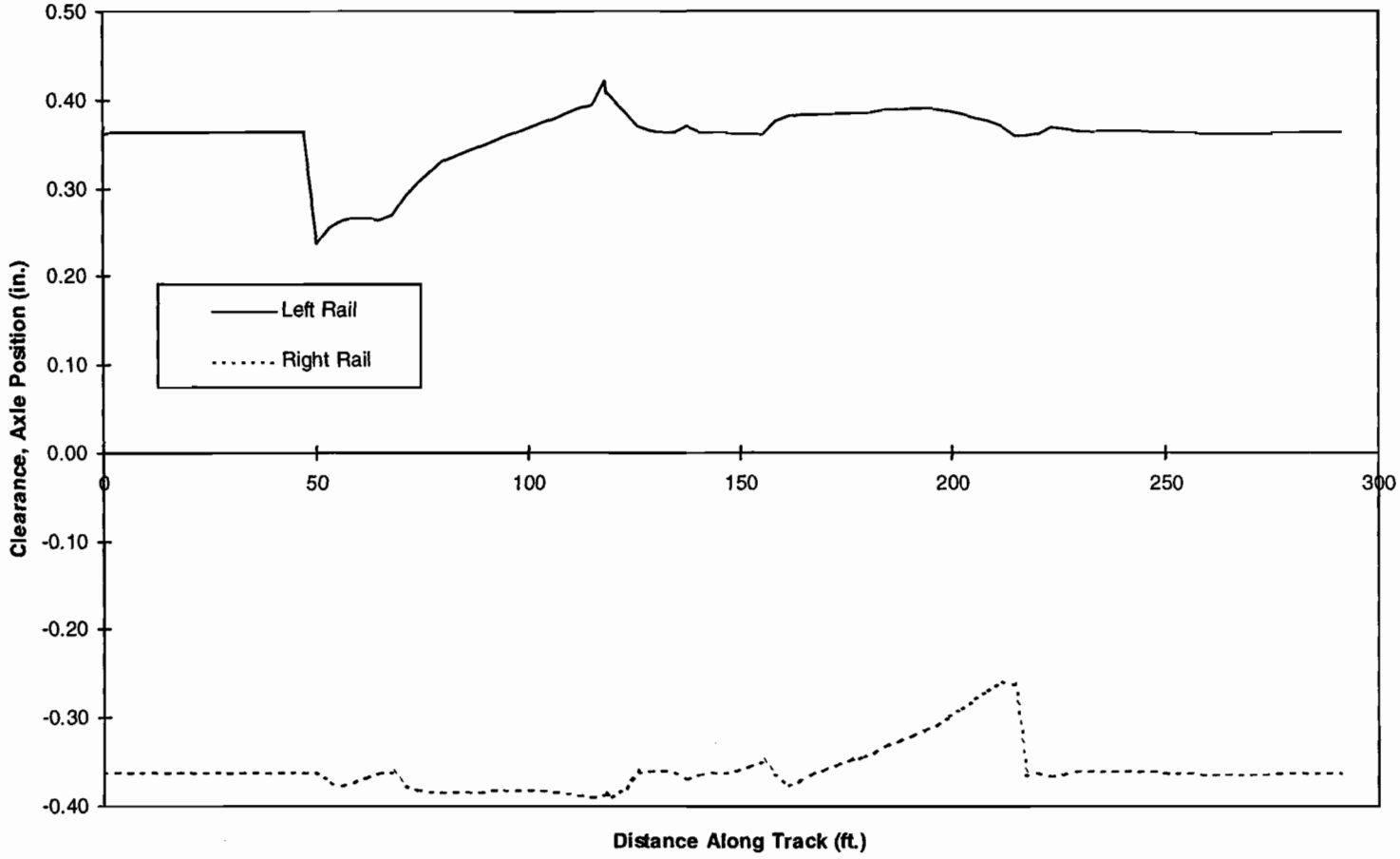

Figure 7-3. Lateral rail deflected position with flangeway guidance clearance through the No. 8 crossover

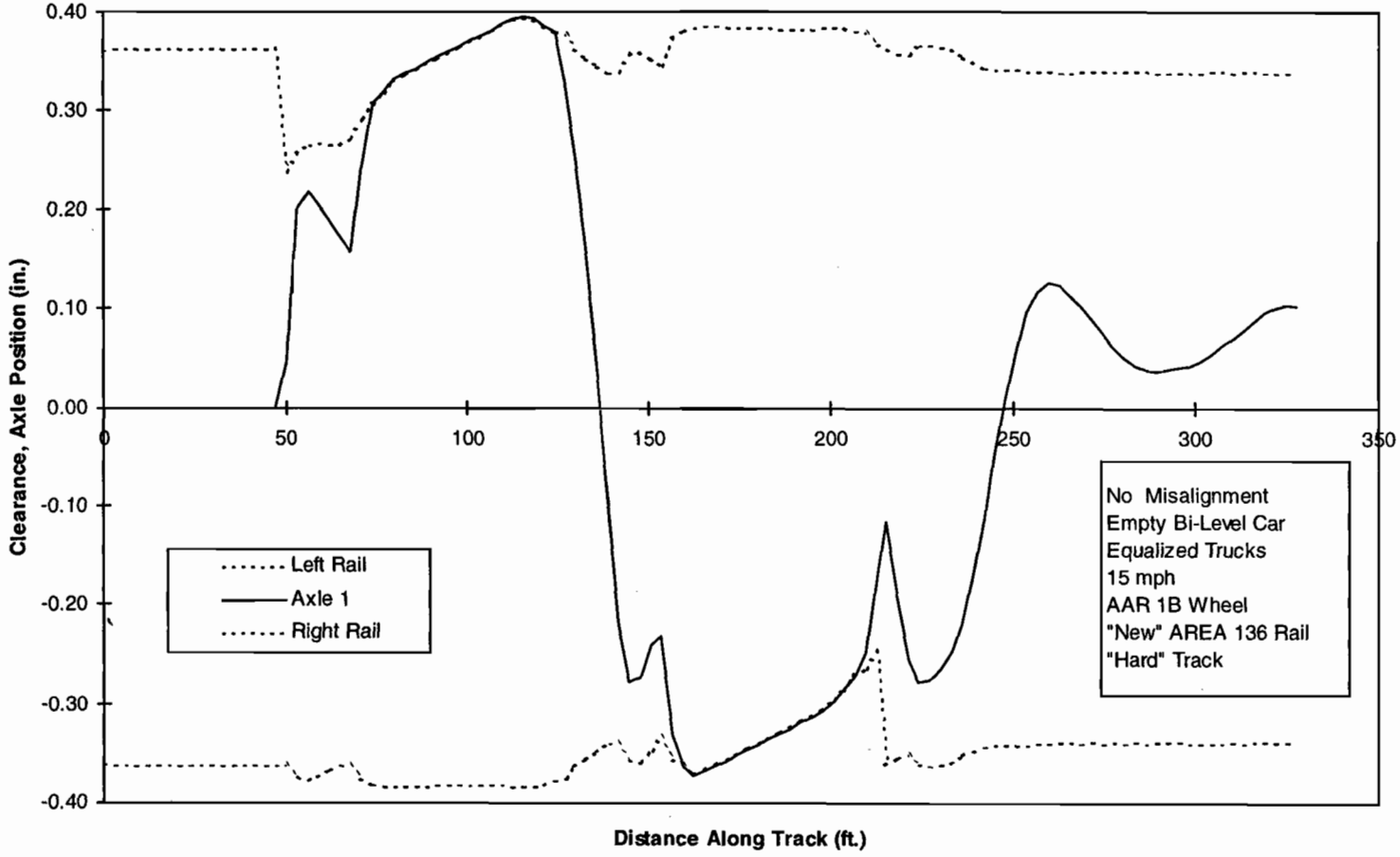

Figure 7-4. Lateral motion of lead axle in the flangeway clearance through the No. 8 crossover

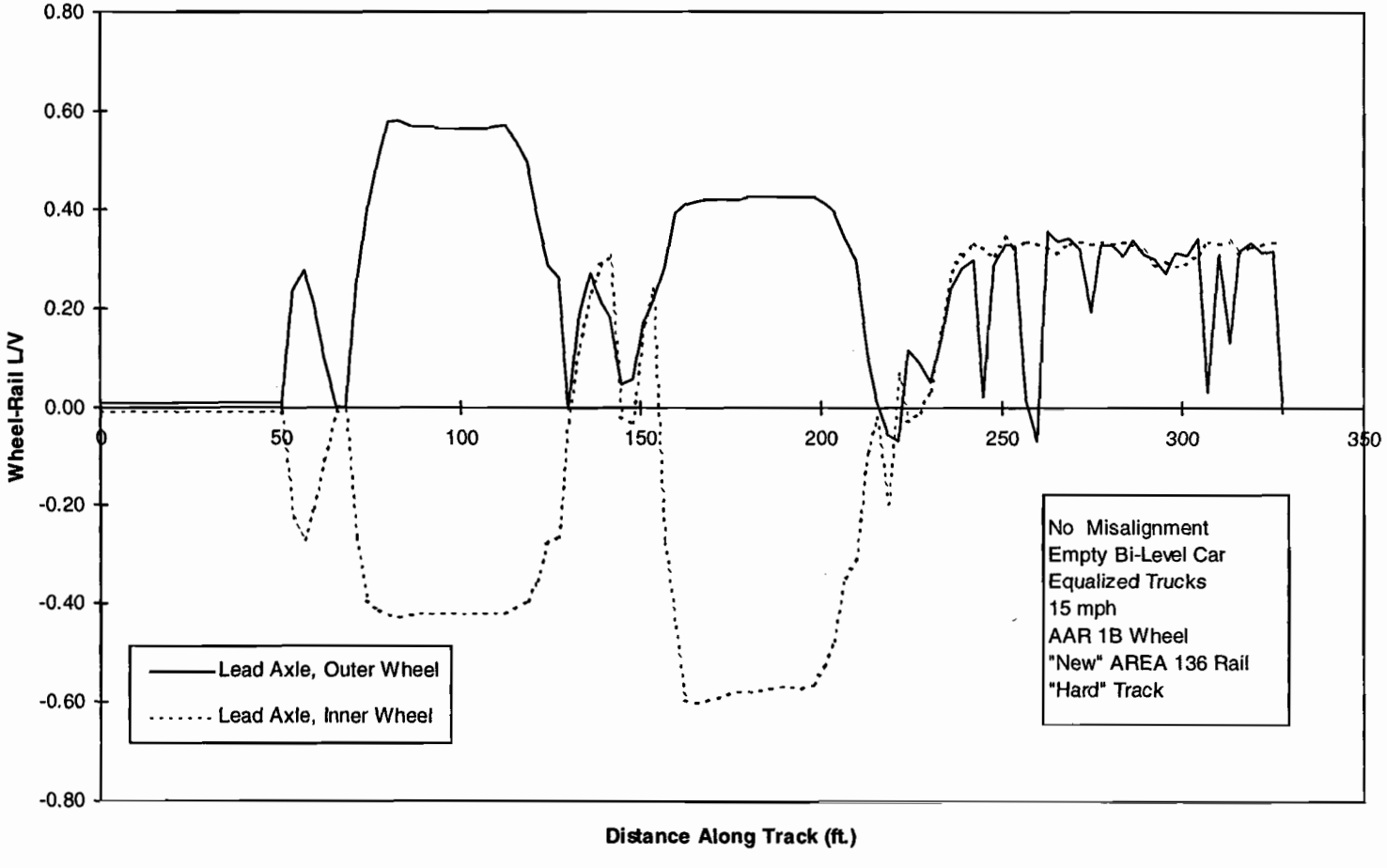

Figure 7-5. L/V ratios on leading wheels through the No. 8 crossover

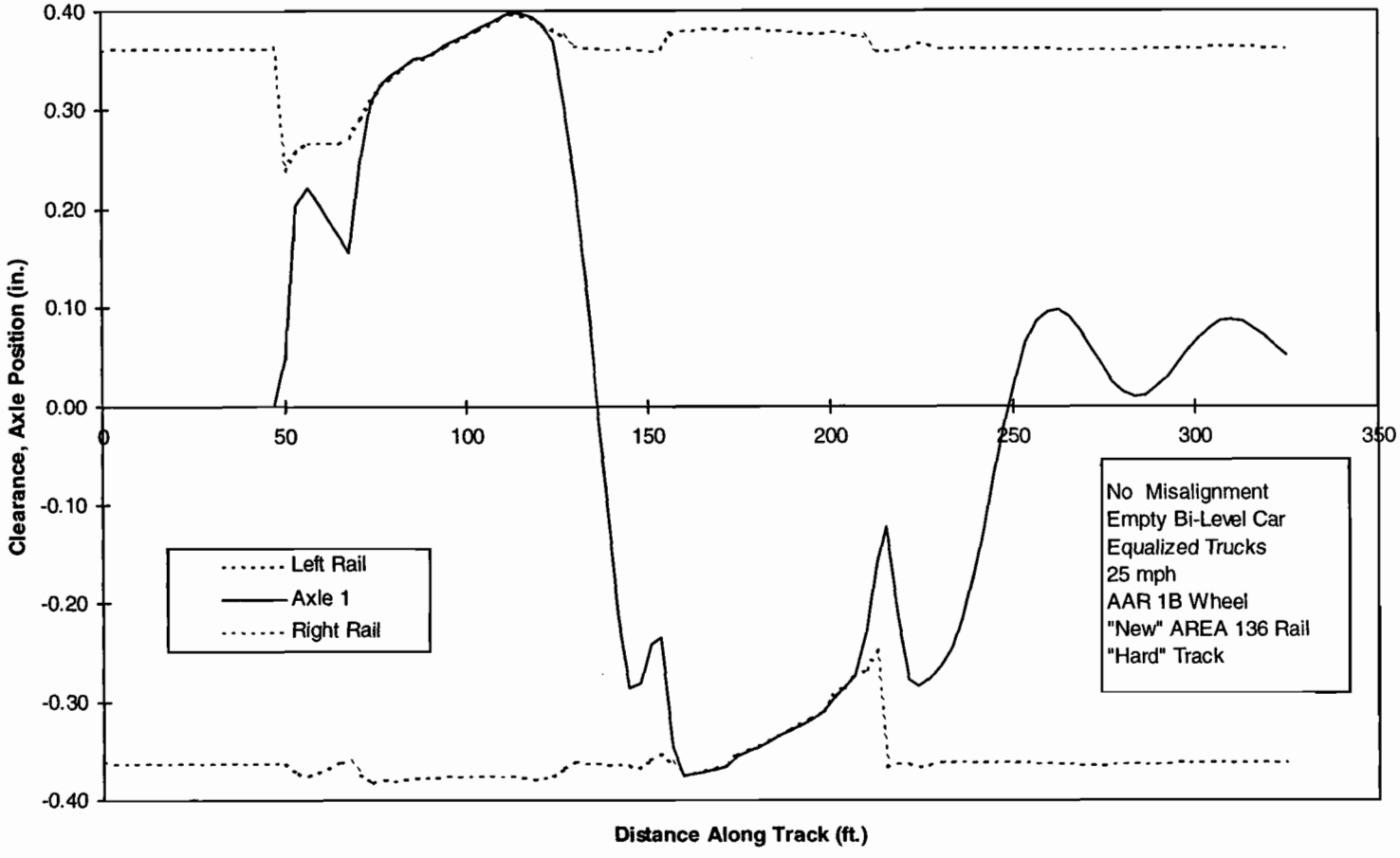

Figure 7-6. Lateral motion of lead axle in the flangeway clearance through the No. 8 crossover

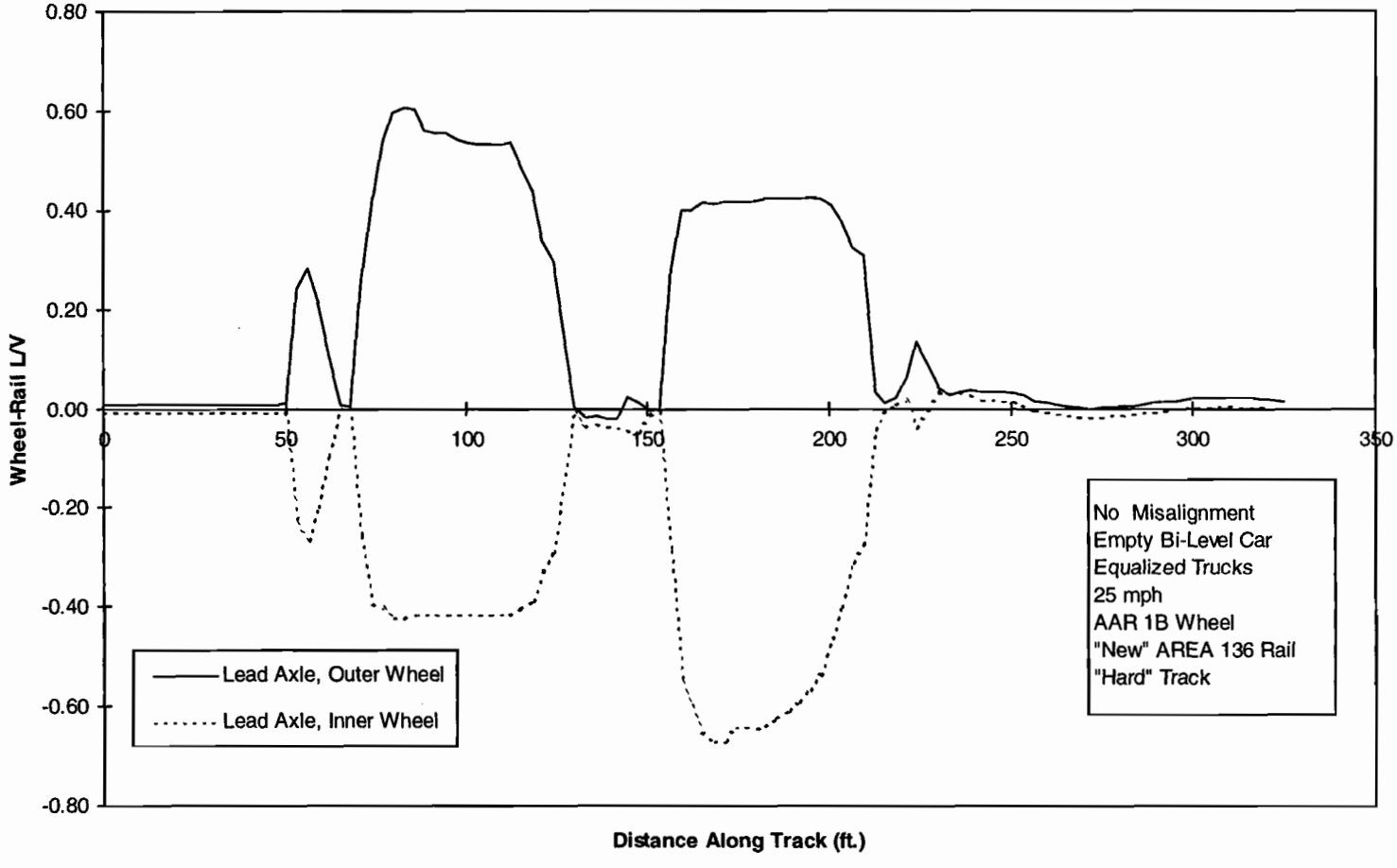

Figure 7-7. L/V ratios on leading wheels through the No. 8 crossover

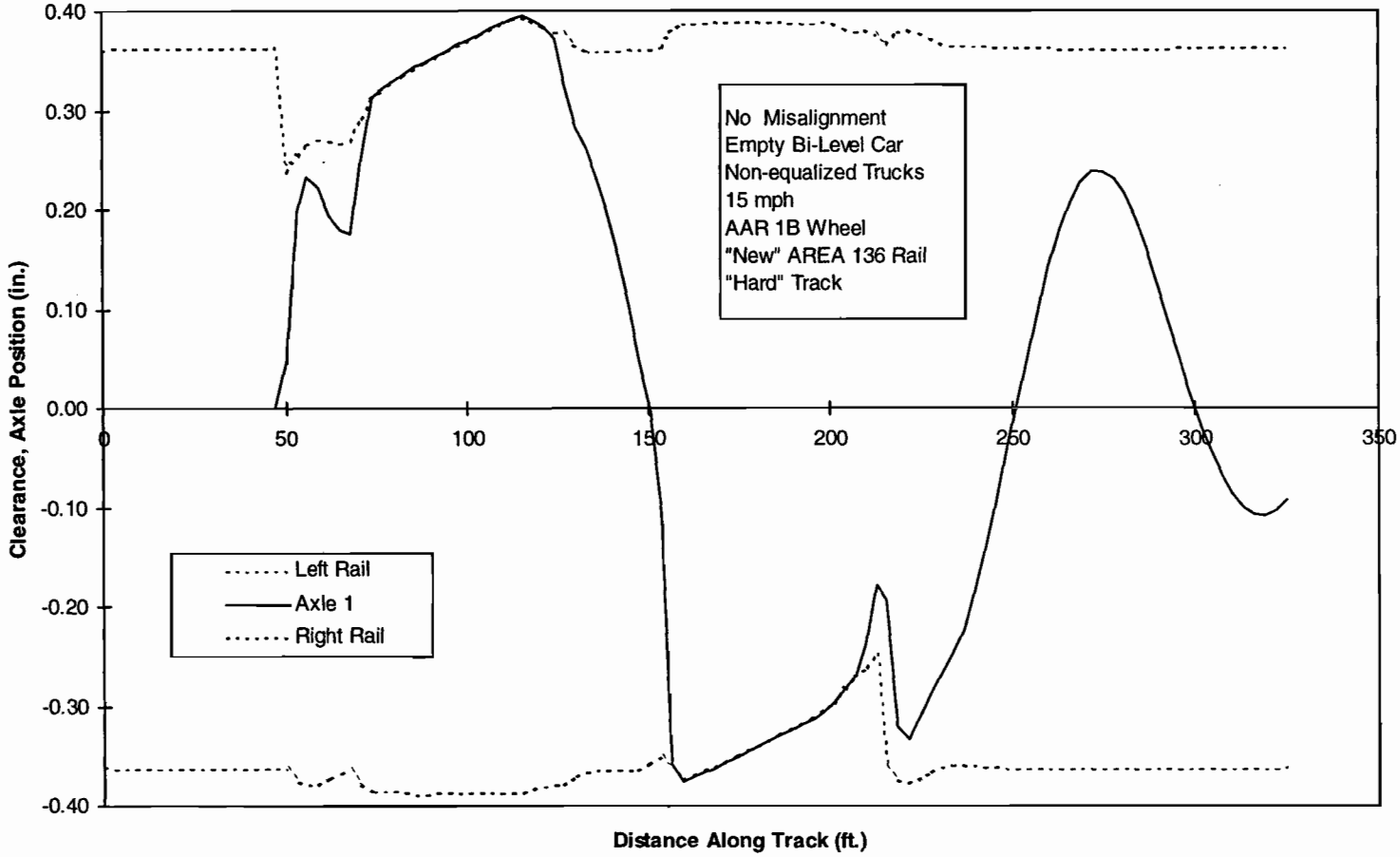

Figure 7-8. Lateral motion of lead axle in the flangeway clearance through the No. 8 crossover

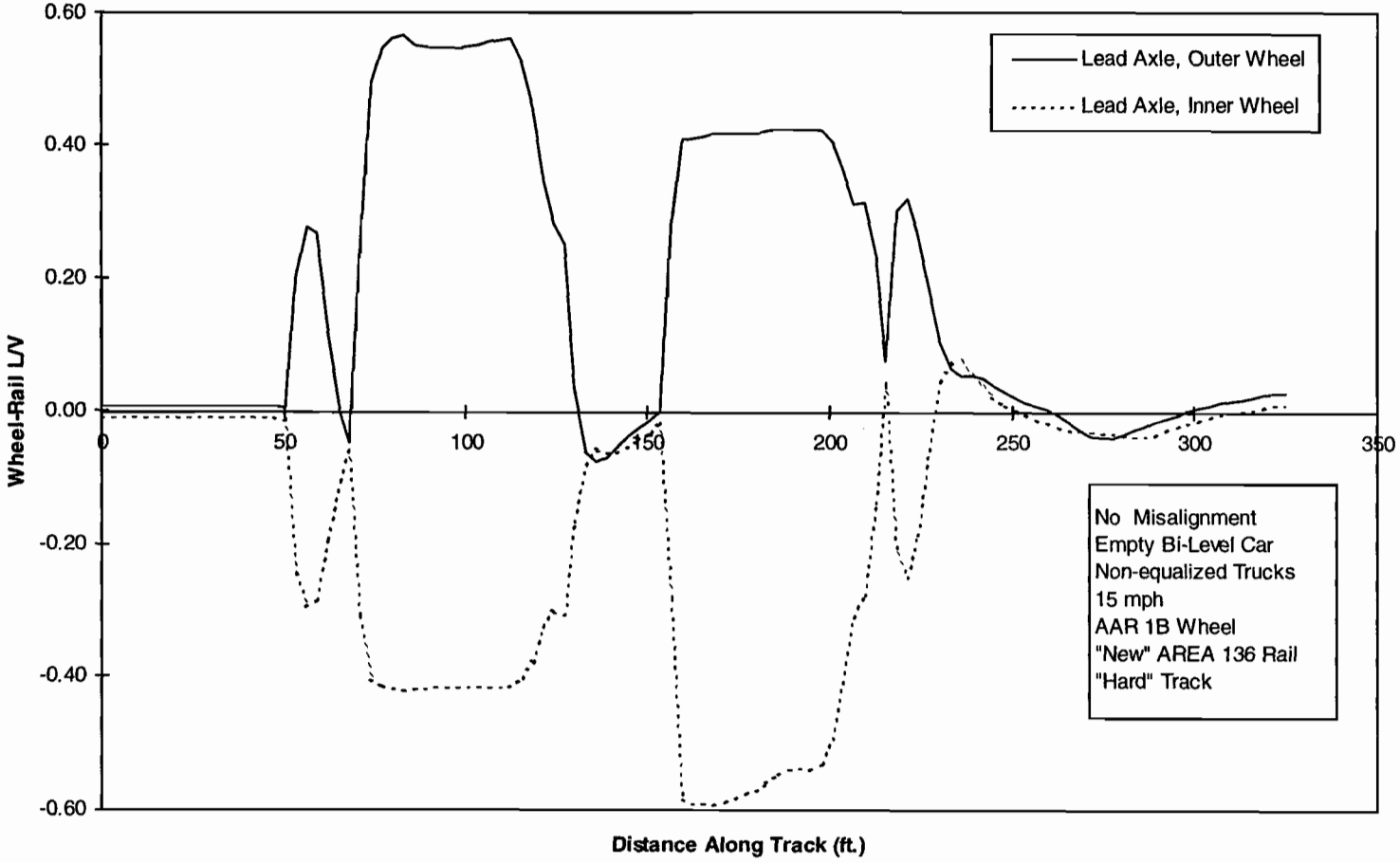

Figure 7-9. L/V ratios on leading wheels through the No. 8 crossover

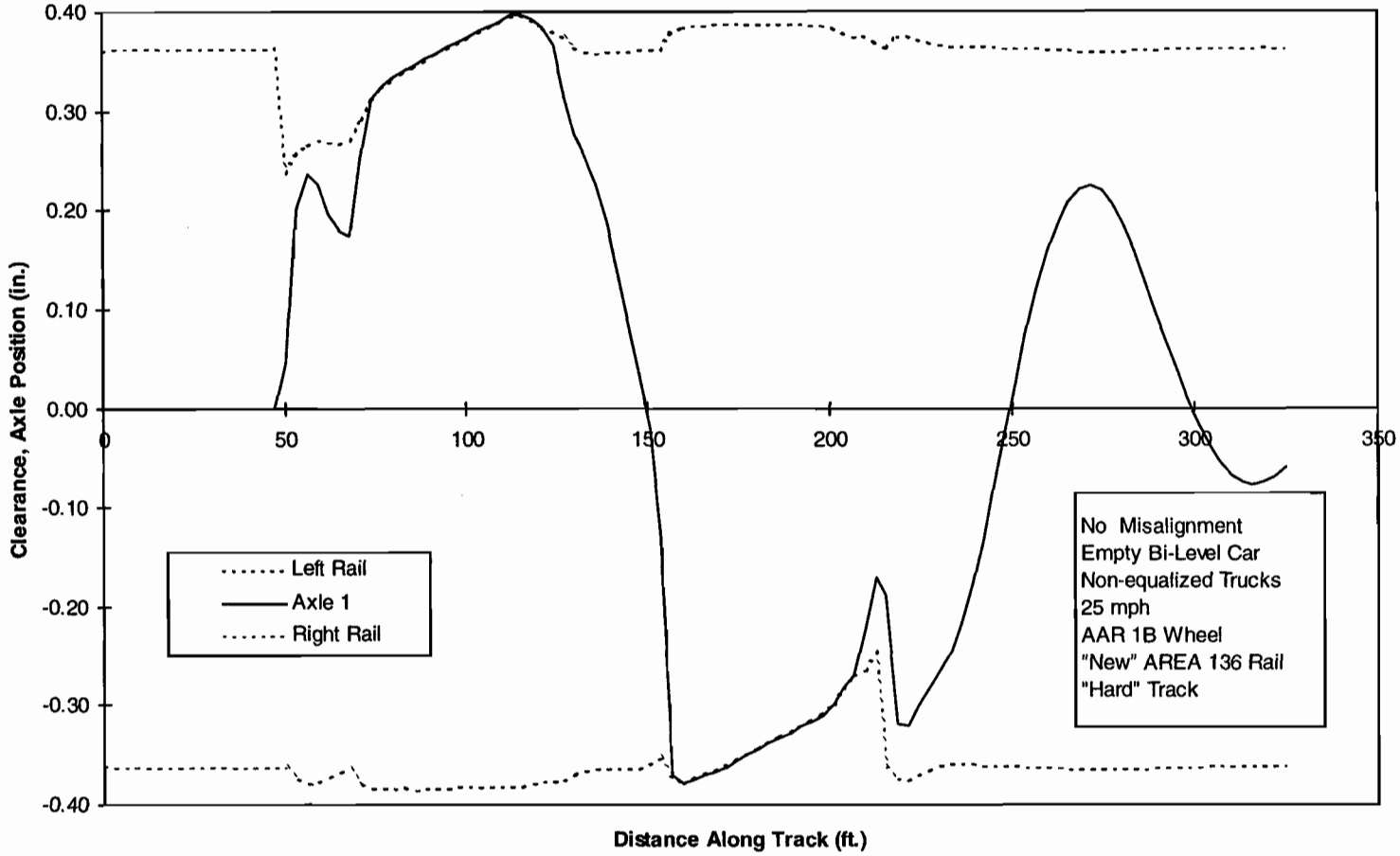

Figure 7-10. Lateral motion of lead axle in the flangeway clearance through the No. 8 crossover

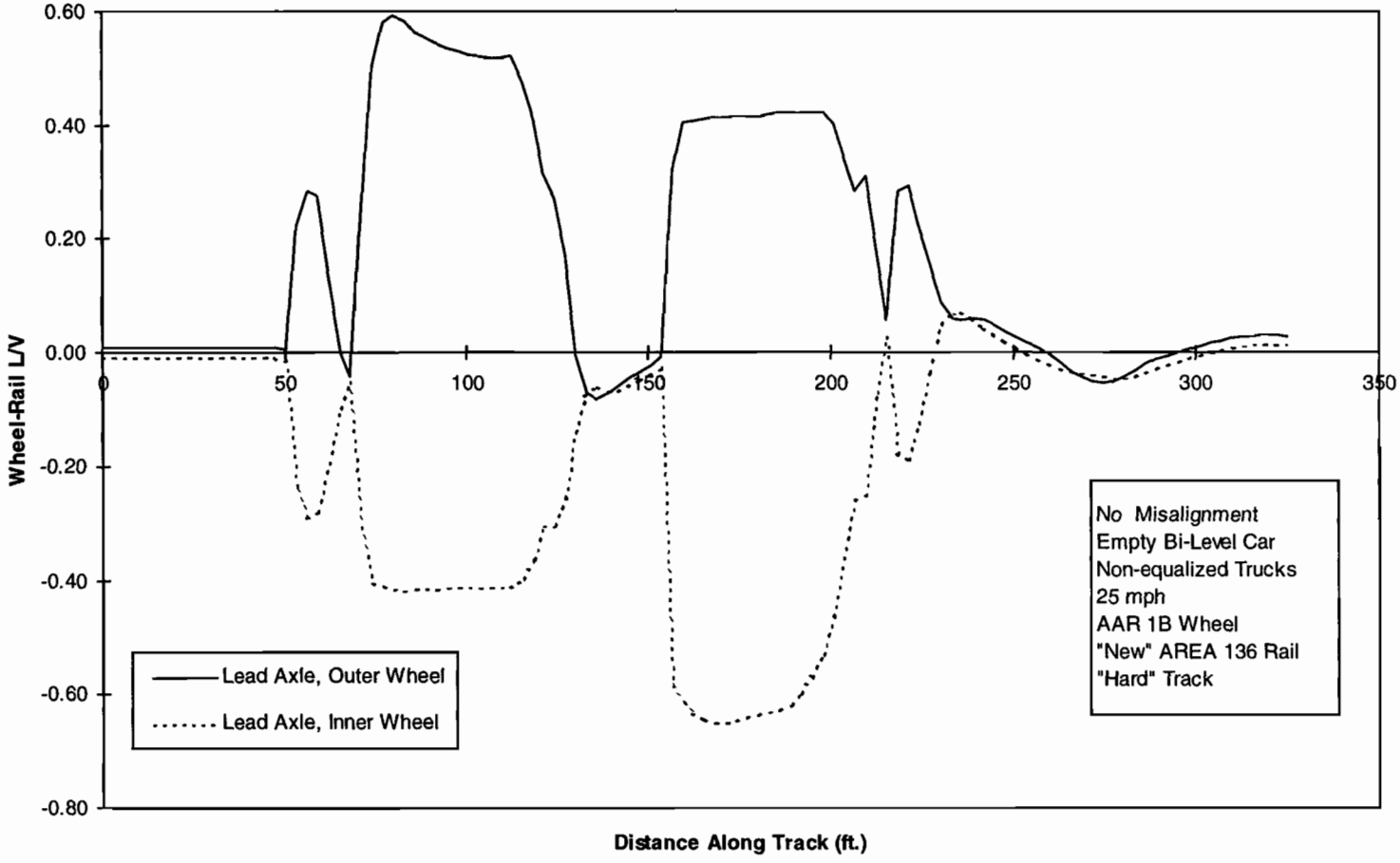

Figure 7-11. L/V ratios on leading wheels through the No. 8 crossover

values occur at initial flange contact and through the curved sections as shown. The non-equalized truck shows marginally better steering in the curves.

Figures 7-12 to 7-19 cover the two base cars at 15 and 25 mph as before but with a 3 in. downward cusp at the end of the outer curved rail of the crossover. Figures 7-12 to 7-15 for the car with equalized trucks show that the equalization results in only modest increases in the L/V ratio at the cusp to a maximum of 1.2, not close to Nadal's limit. However the car with non-equalized trucks derails at both speeds. The wheel climb at 25 mph is temporary for the lead axle but permanent for the third axle not shown. The L/V at the climb exceeds 1.5, greater than the Nadal value of 1.34 for the profiles used and the coefficient of friction of 0.4 used throughout these simulations. The derailment is similar to those investigated in Section 4. The number 20 crossover was not simulated. It was felt that the No. 8 experience was adequate to identify the techniques and validation would require additional simulation of the switch or crossover used in the test.

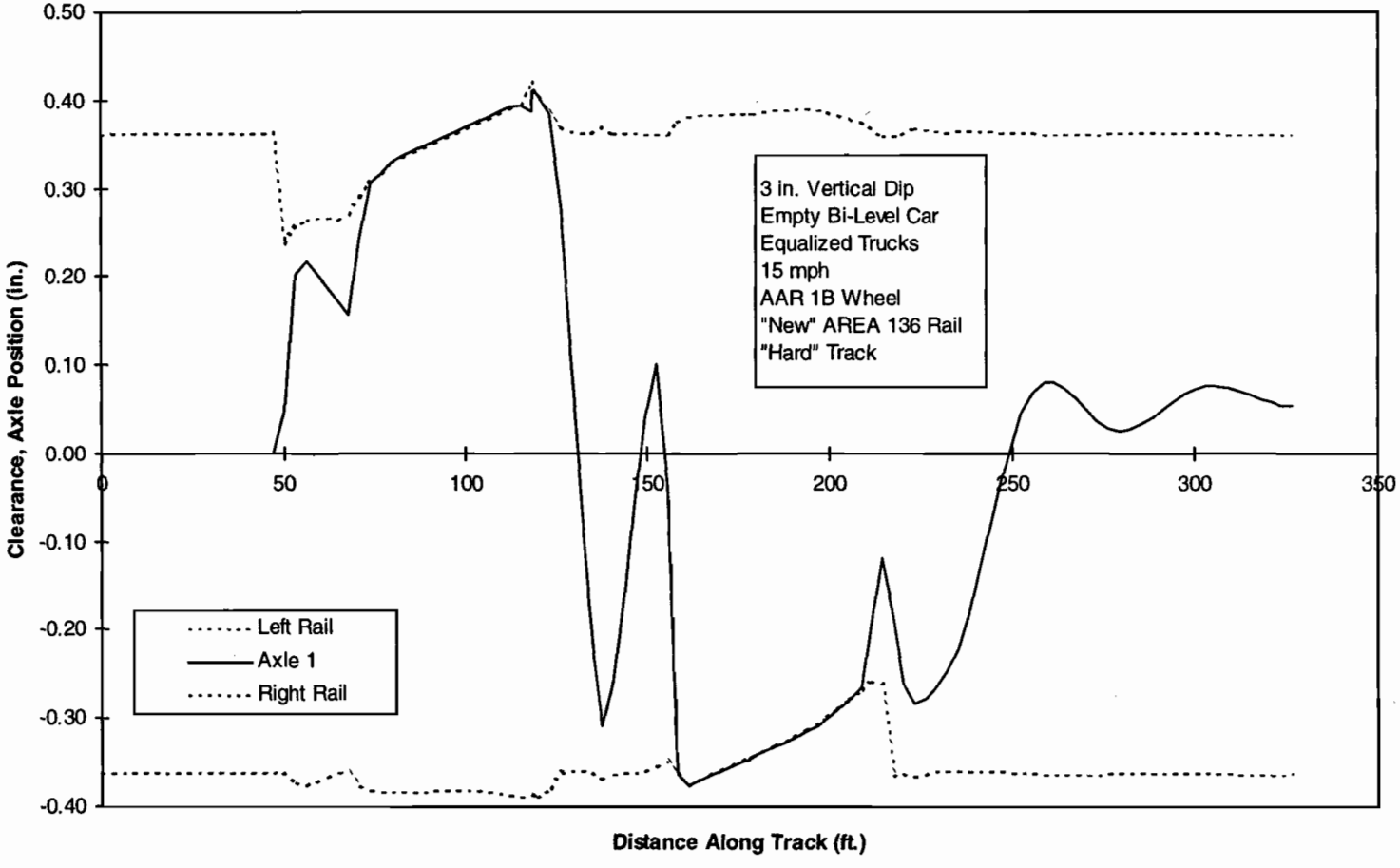

Figure 7-12. Lateral motion of lead axle in the flangeway clearance through the No. 8 crossover

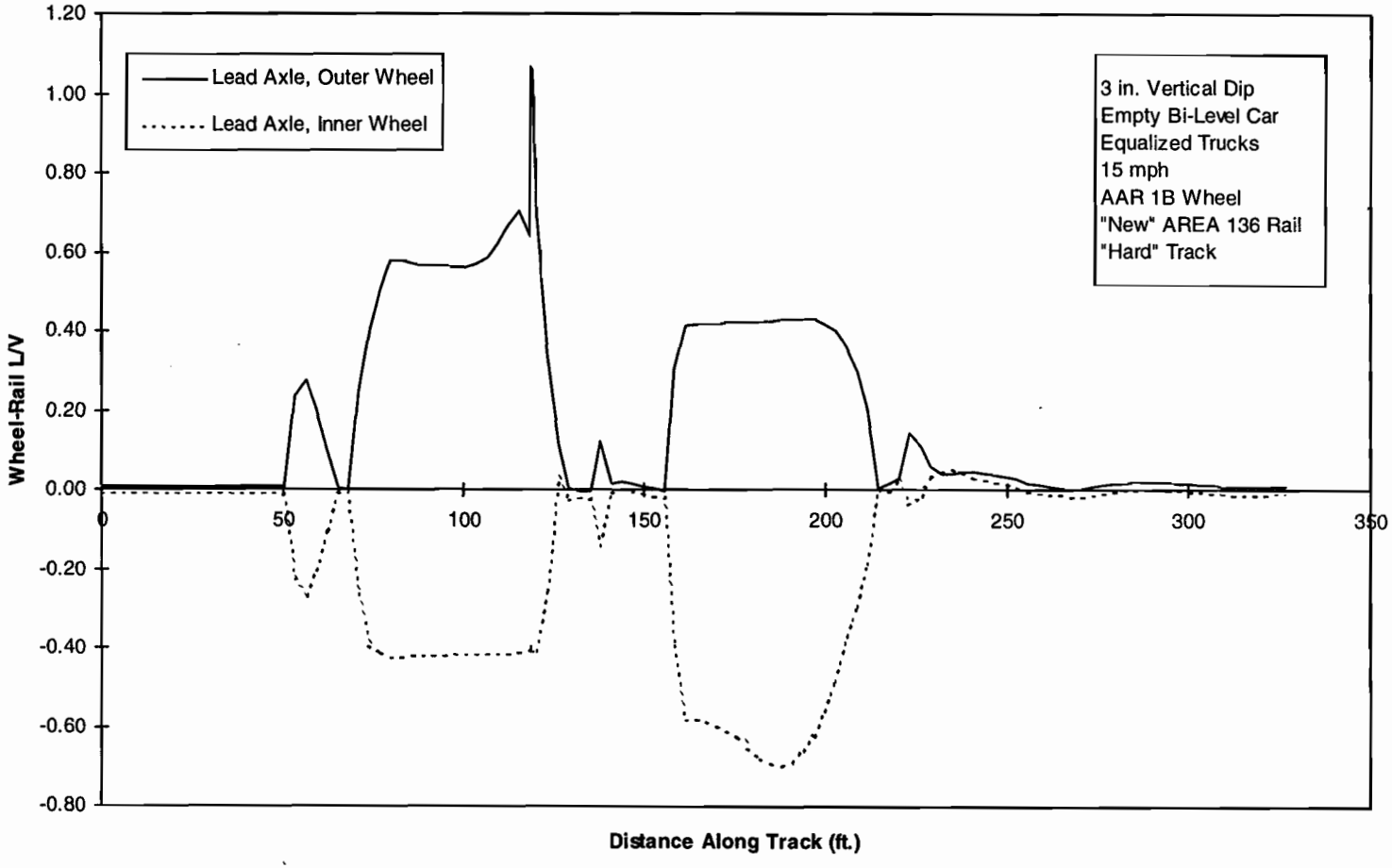

Figure 7-13. L/V ratios on leading wheels through the No. 8 crossover

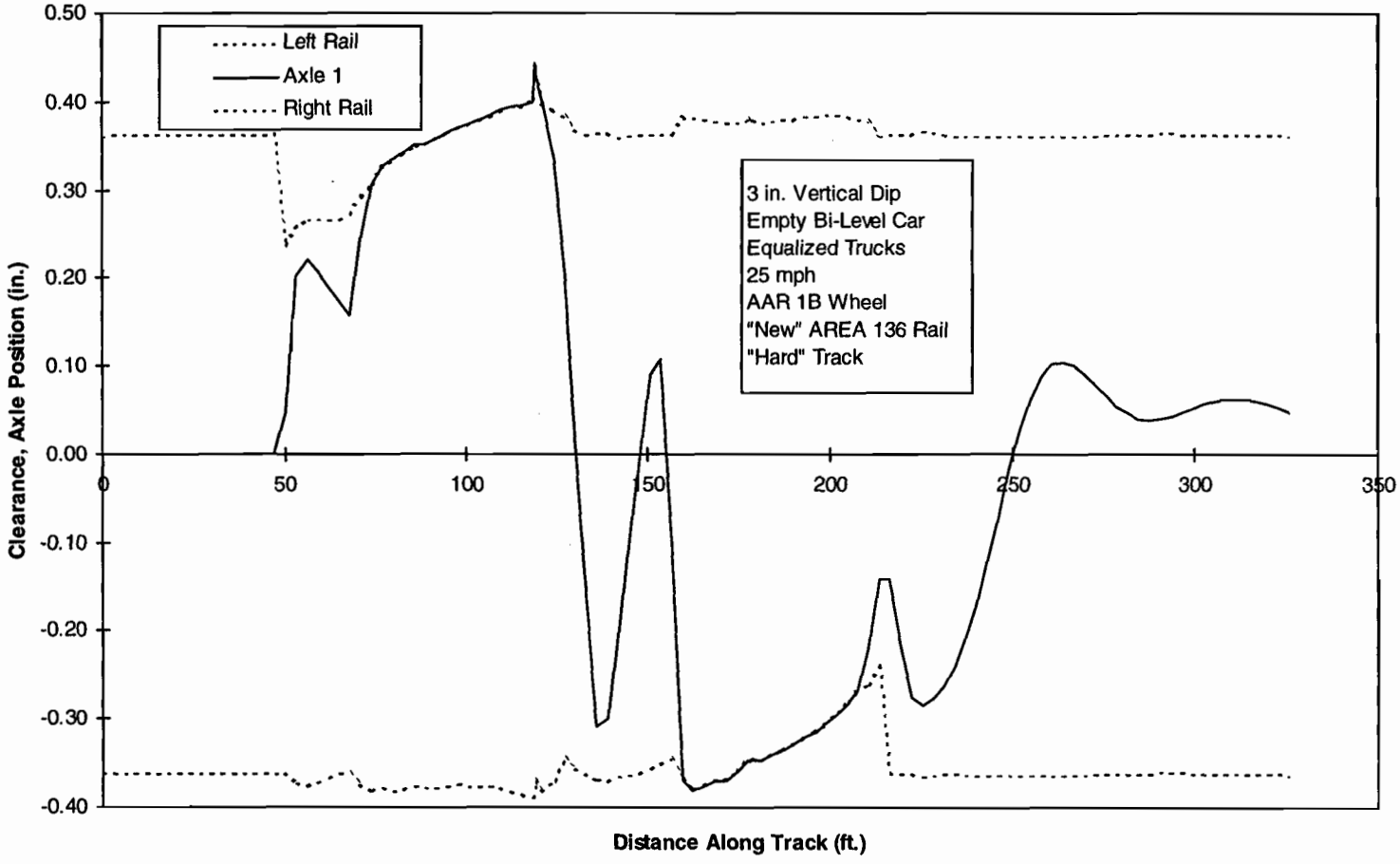

Figure 7-14. Lateral motion of lead axle in the flangeway clearance through the No. 8 crossover

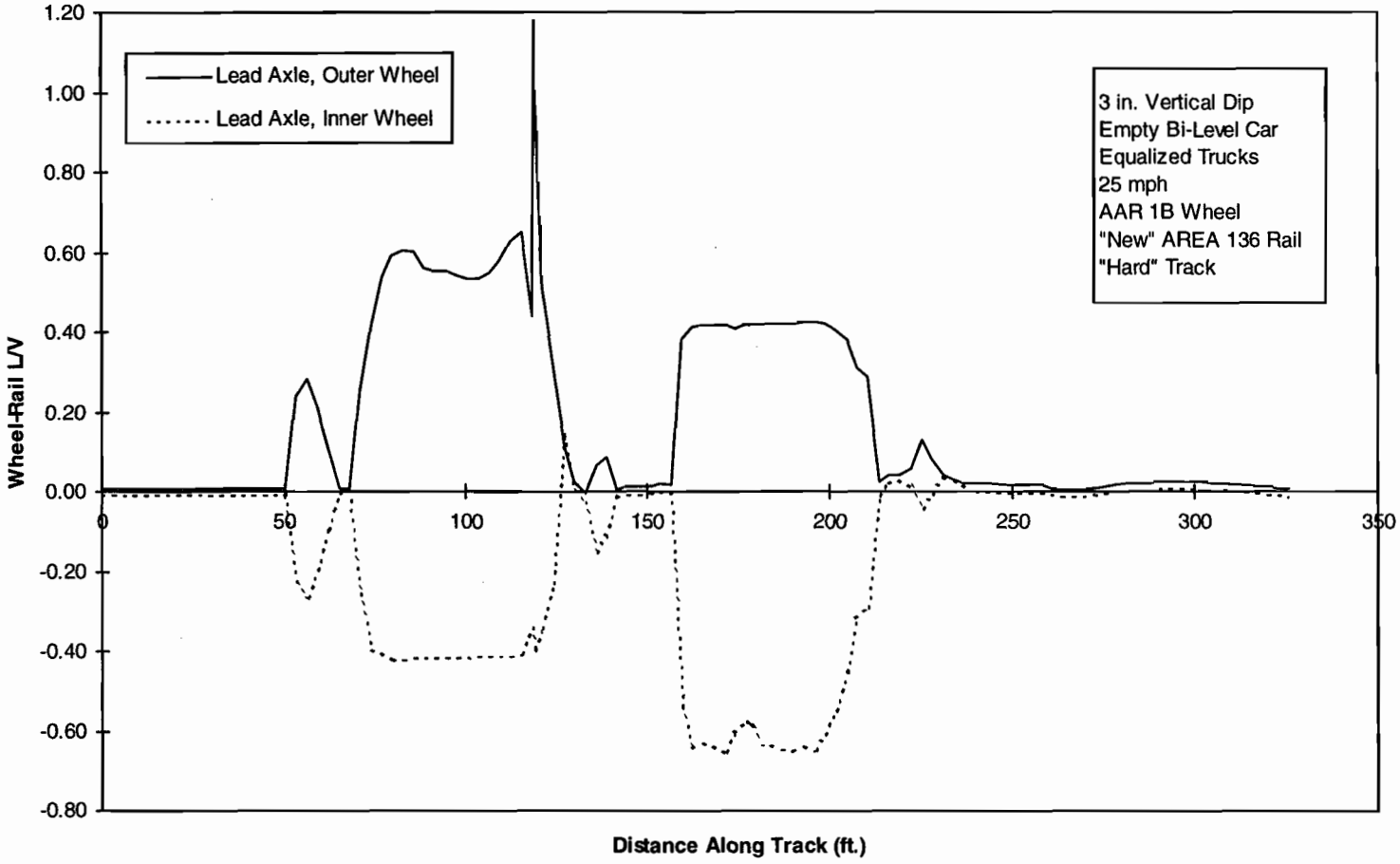

Figure 7-15. L/V ratios on leading wheels through the No. 8 crossover

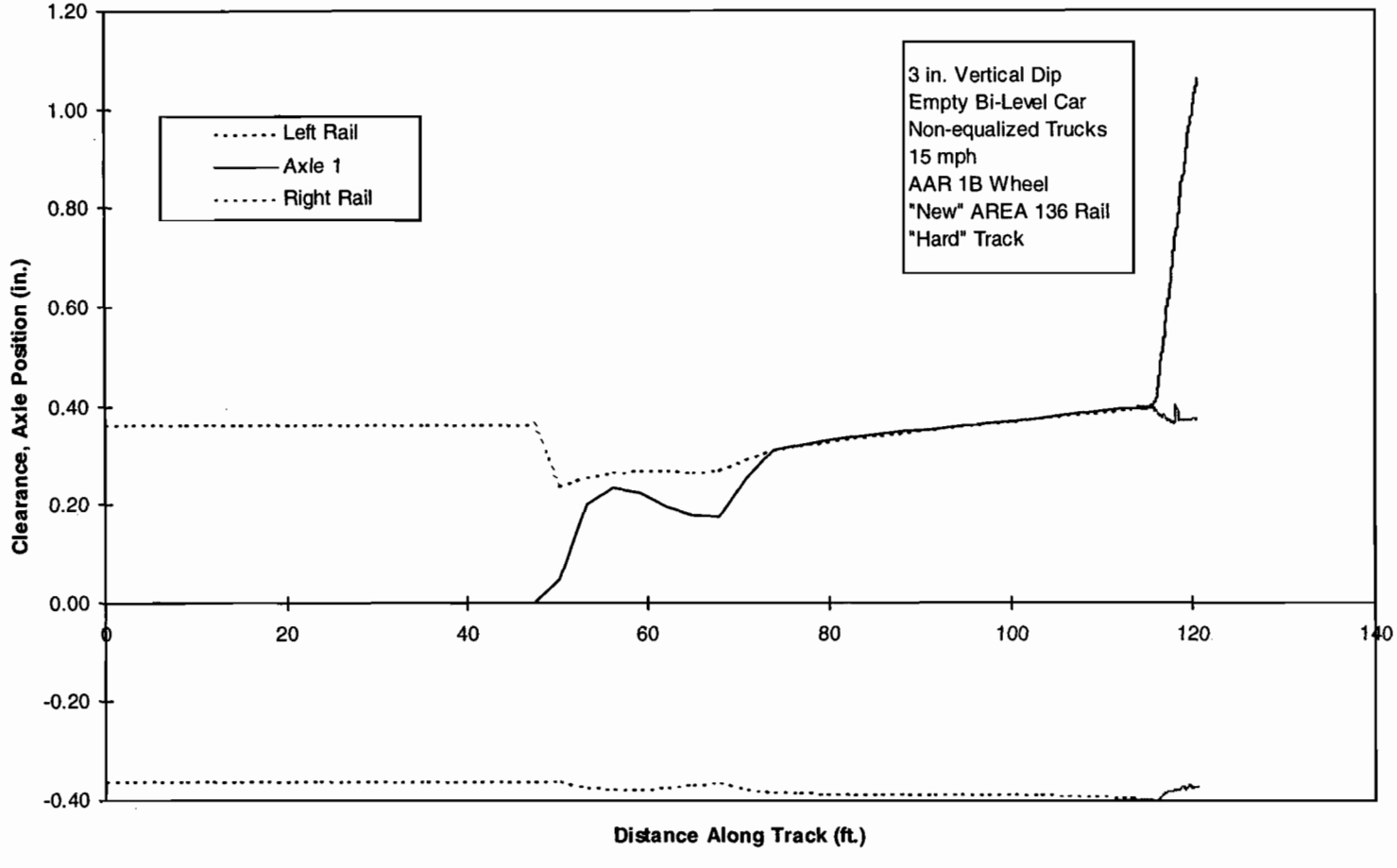

Figure 7-16. Lateral motion of lead axle in the flangeway clearance through the No. 8 crossover

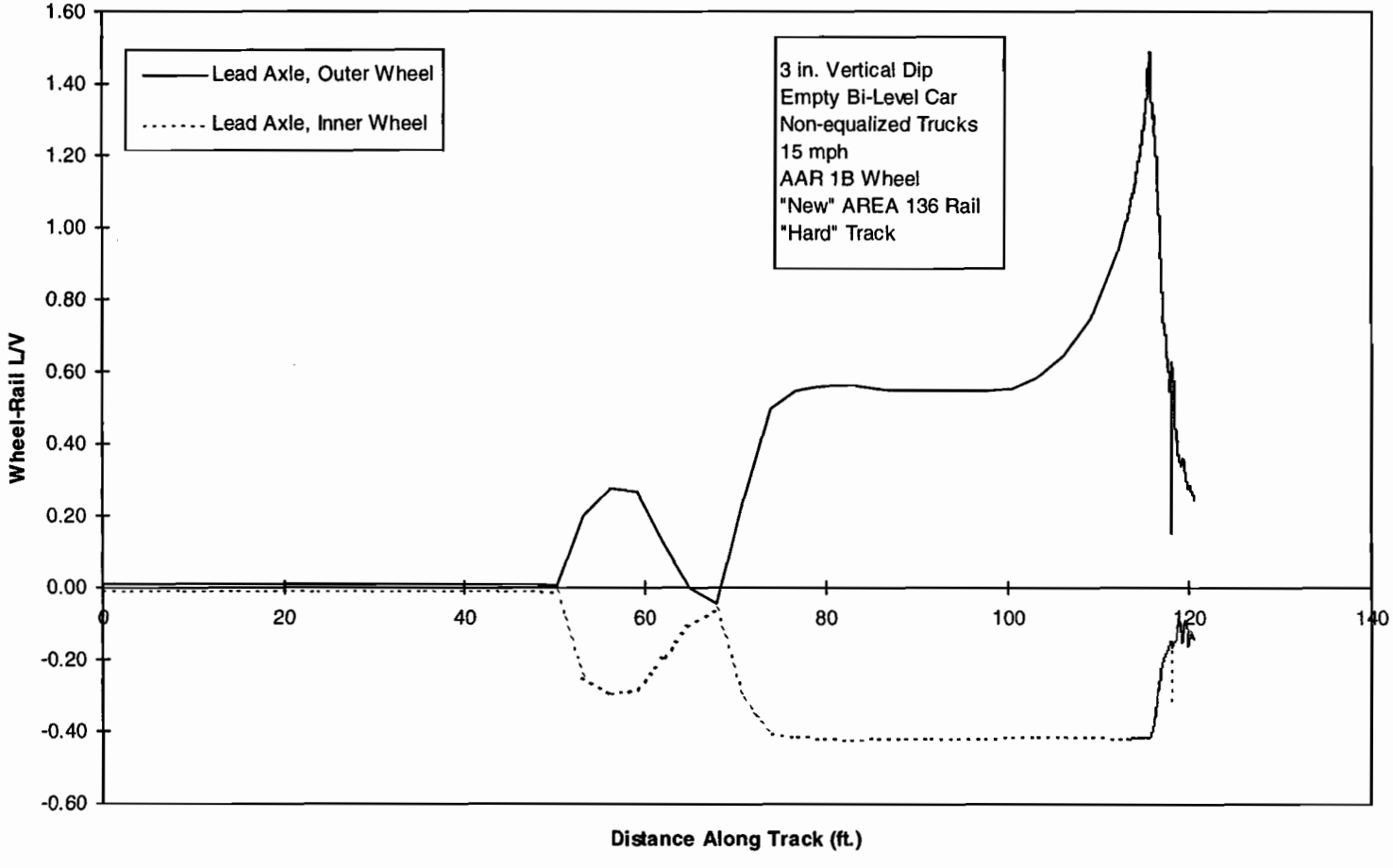

Figure 7-17. L/V ratios on leading wheels through the No. 8 crossover

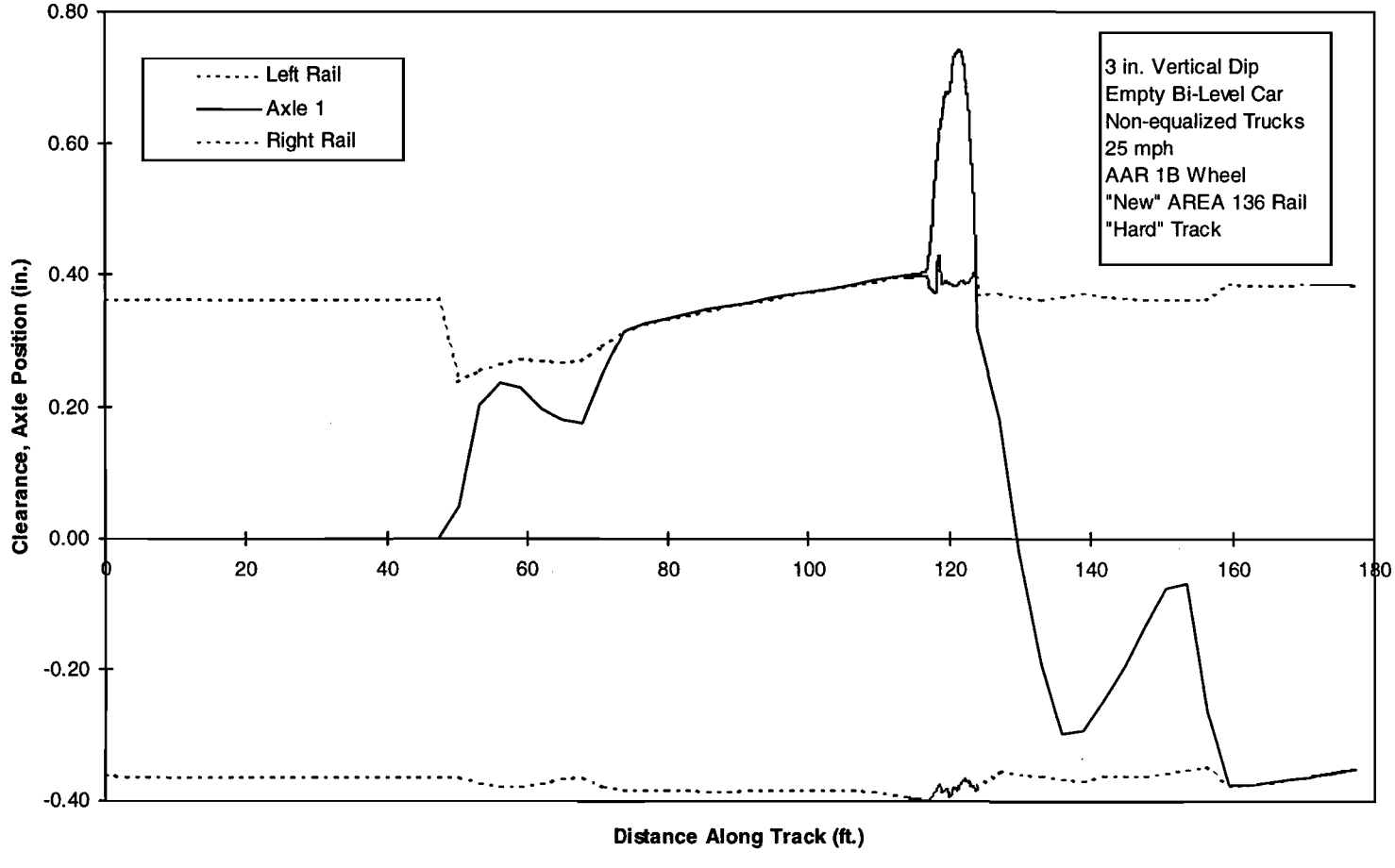

Figure 7-18. Lateral motion of lead axle in the flangeway clearance through the No. 8 crossover

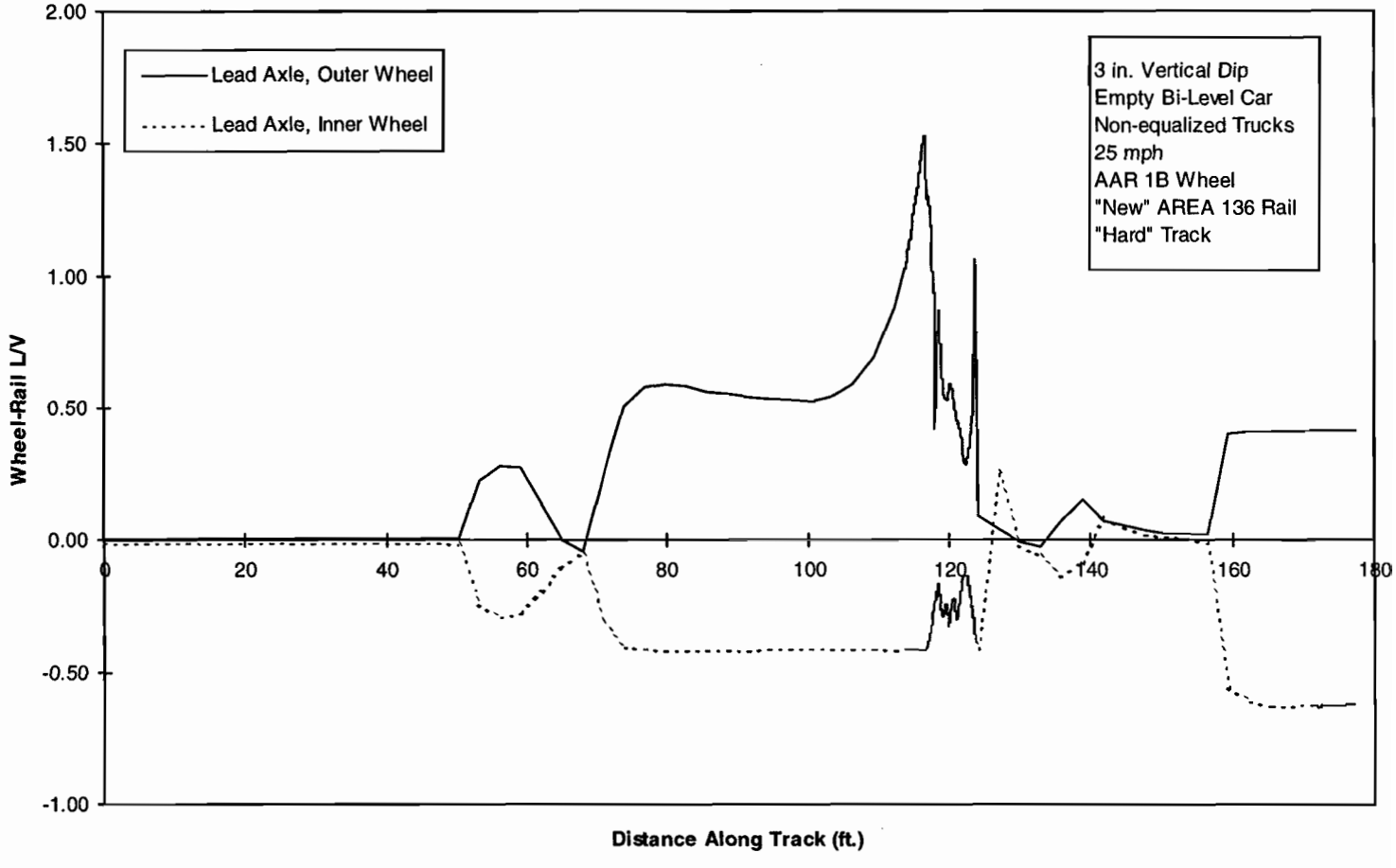

Figure 7-19. L/V ratios on leading wheels through the No. 8 crossover

8. CONCLUSIONS

The work described leads towards the following recommendations. A set of safe performance limits are formalized for the two types of trucks (equalized and non-equalized) and have been presented in the companion report, Volume I.

8.1 Safety Methodology

A safety assessment methodology for conventional passenger vehicles has been presented. The methodology identifies required vehicle parameters, critical vehicle operational scenarios and required analysis tools for quantification of vehicle dynamic response and potential for vehicle derailment.

- The commuter vehicle types can be conveniently grouped as those of single/bi-level car bodies and equalized/non-equalized truck types, which are representative of the variations in the current vehicle dynamic behavior, and their safety performance. The vehicle parameters required for predicting dynamic behavior can be broadly classified as 1) mass and inertias, 2) primary suspension stiffness, 3) secondary suspension stiffness and damping, 4) geometry and c.g. location and 5) wheel profiles.

- The vehicle operational scenarios studied include 1) truck hunting on tangent track, 2) steady curving, 3) dynamic curving on tracks with single cusp imperfections, 4) dynamic curving on tracks with multiple "down and out" cusp imperfections, 5) negotiation of gage narrowing variations and 6) negotiation of switches with imperfections.

- The safe performance limits for the operational scenarios can be expressed in terms of appropriate parameters such as critical speeds for hunting, safe cusp amplitudes for dynamic curving, safe speeds at gage narrowing, safe maximum vertical irregularities at switches, and also in terms of safe maximum wheel L/V ratios. The safe performance limits are included in the companion report, Volume I.

8.2 Analysis Issues

1. Deficiencies in known linear models can be significant and caution must be exercised in their use for the assessment of safety. The linear models are useful in defining optimal regions for the suspension parameters for design comparisons.

2. Steady curving forces are traditionally determined using static analysis. In general, the results do not agree with those from OMNISIM. However, during flange contact, certain limiting values of forces can be reasonably predicted using the static analysis.

3. Cusps in curves are studied using a traditional static method and OMNISIM (fully dynamic). The results do not agree with one another. The static method is considered to be deficient due to the lack of truck shear.

8.3 Safety Limits

1. For the assumed vehicle parameters, OMNISIM simulation results show that truck hunting is not likely to occur for the vehicles considered here within their normal operational range. The lowest speed at which cyclic full-flange contact can occur is about 160 mph for the single car with non-equalized trucks on worn wheels and "hard" (stiff) track conditions. The "soft" track tended to give higher critical speeds for the cars with equalized trucks, however, the opposite was true for cars with non-equalized trucks.

2. For the assumed vehicle parameters, the simulation results do not show any specific derailment potential for the vehicles under steady curving on tracks up to 20 deg curvatures at balance speeds. No problems are anticipated on cant deficient curves, permissible according to the existing FRA specifications (3 in. cant deficiency) for vehicles with similar parameters to those considered.

3. In the negotiation of a single cusp over a long wavelength, the vehicle with non-equalized trucks did not perform as well as that with equalized trucks. The single-level car with an equalized truck can negotiate a 2 in. cusp over a 39 ft wavelength on tracks up to 15 deg curvatures, whereas with non-equalized trucks, it can negotiate no more than 1.5 in. cusp amplitudes on tracks with up to 5 deg curvature. The example bi-level car with a non-equalized trucks can negotiate safely up to 2 in. cusp amplitudes (over a 39 ft wavelength). An example of the same car with an equalized truck has a wider safe range of 3 in. amplitude on tracks with a 10 deg curvature limit.

4. The conclusion on safe performance comparisons of vehicles on "down and out" cusps is qualitatively similar to the foregoing conclusion for the single cusp. As an example, the single-level car with an equalized truck can negotiate "down and out" cusps with 1.4 in. vertical and 0.7 in. lateral amplitudes safely on tracks with up to 10 deg curvatures, whereas the same car with a non-equalized truck is restricted to curvatures under 5 deg for safe negotiation of similar cusps. Again, bi-level cars fare better than the single-level cars in these scenarios.

5. A valuable key parameter is the "Gage Reduction Ratio" for the assessment of safety on gage narrowing scenarios. A scenario simpler than the traditional sinusoidal gage narrowing is identified and simulated, which is represented by a straight rail angled to represent a constant rate of gage reduction. The Gage Reduction Ratio is defined as

the inverse of this constant. The maximum safe vehicle speed can be expressed as a function of the Gage Reduction ratio parameter (in field conditions, this is an equivalent of the maximum rate of gage variations, which can be easily measured). Typical safe maximum speeds are presented for the assumed vehicle parameters. The vehicle with equalized trucks has a higher safe speed than the one with non-equalized trucks for the same level of gage narrowing condition.

6. Negotiation of the AREMA No. 8 crossover has been simulated in this study. An added cusp at the entrance to the frog causes a response similar to that investigated for the single cusp in a curve and showed the importance of retaining vertical wheel load during curving. Only the non-equalized trucks derailed and then only at the 3 in. amplitude cusp.

REFERENCES

1. Bing, A.J., Berry, S.R., and Henderson, H.B., *Engineering Data on Selected North American Railroad Passenger Car Trucks*, DOT Report No. DOT/FRA/ORD-96/01, July 1996.
2. Greif, R. and H. Weinstock, *Limiting Forces on Transit Trucks in Steady-State Curving*, DOT Report No. UMTA-MA-06-0025-82-1, May 1982.
3. Blader, F.B., and Kurtz, Jr., E.F., *Dynamic Stability of Cars in Long Freight Trains*, ASME Journal of Engineering for Industry, pp. 1159 - 1167, November 1974.
4. Kalker, J. J., *The Computation of Three Dimensional Rolling Contact with Dry Friction*, International Journal for Numerical Methods in Engineering, Vol.14, pp.1293-1307, 1979.
5. Samavedam, G., et al., *Analyses of Track Shift Under High-Speed Vehicle-Track Interaction – Safety of High-Speed Ground Transportation*, DOT Report No. DOT/FRA/ORD-97/02, June 1997.
6. Blader, F.B., *Analytic Studies of the Relationship between Track Geometry Variations and Derailment Potential at Low Speeds*, DOT Report No. FRA/ORD-83/16, September 1983.
7. Blader, F. B., et al., *Development and Validation of a General Railroad Vehicle Dynamics Simulation (NUCARS)*, Proceedings of the 1989 IEEE-ASME Joint Railroad Conference, April 25-27, 1989, Philadelphia, Pennsylvania, pp.39-46.
8. Cooperrider, N. K., and Heller, R., *User's Manual for the Asymmetric Wheel/Rail Contact Characterization Program*, Federal Railroad Administration Report FRA/ORD-78/05, December 1977.

APPENDIX A

ANALYTIC AND SIMULATION TOOLS

As stated in Section 1 of this report, there are several safety issues to be studied, as the vehicle negotiates different track scenarios. Table A-1 gives a list of safety issues arising from vehicle dynamic responses which are activated under different track scenarios. The analytic and simulation tools considered appropriate for the safety evaluation under these responses are included in the table. NEWHUNT is a simplified analysis program for determining hunting speeds. Static Analysis represents a simpler approach compared to the full blown dynamic analysis for steady curving and crosslevel in curves. On the other hand, several general purpose simulation programs are also available to address any track scenario. A review of the general purpose vehicle-track interaction codes has been carried out and will be published in a forthcoming document. The general purpose code used in this work is OMNISIM, developed by Foster-Miller for the Volpe Center.

A brief description of the analytic tools used in this report is presented here.

Table A-1. Relationship between vehicle dynamic responses, safety issues, and analysis tools

Wheel Dynamic Responses	Safety Issues	Tools
Lateral Instability (Hunting)	Track Shift, Human Fatigue, Wheel Climb	OMNISIM, NEWHUNT
Steady Curving	Wheel Climb, Wheel Lift, Gage Spreading, Track Shift	OMNISIM, Pseudo-Static Analysis
Twist with Curve Variation	Wheel Climb, Wheel Lift, Gage Spreading, Track Shift, Personal Injury	OMNISIM, Static Analysis
Twist and Roll	Wheel Lift, Human Fatigue	OMNISIM
Pitch and Bounce	Wheel Lift, Human Fatigue	OMNISIM
Yaw and Sway	Wheel Climb, Gage Spreading, Track Shift, Personal Injury, Human Fatigue	OMNISIM
Dynamic Curving and Switches	Wheel Climb, Wheel Lift, Gage Spreading, Track Shift, Personal Injury, Human Fatigue	OMNISIM
Transient Lateral and Vertical Motions	Wheel Climb, Wheel Lift, Gage Spreading, Rail Damage, Personal Injury	OMNISIM

A.1 Static and Psuedo Static Analyses in Crosslevel and Curves

Three simplified analyses used in the work are described in this section.

A.1.1 Simplified Twist Analysis - Method A

Equilibrium equations are written for the two vehicles with equalized and non-equalized trucks. These equations are developed from free body diagrams. For each of the two vehicles, a linear system of 21 equations is developed. This method is used in the simplified twist analysis and is found in Appendix B.

A.1.2 Simplified Twist Analysis - Method B

This method is used for comparisons with dynamic unloading and the inclusion of the effect of truck shear stiffness. In this method the change in load between wheel and rail is computed directly for a wheel lift or drop. The arrangement for a four axle car with two flexibly framed trucks and a flexible body is shown in the Figure A-1. Not shown on the figure are equalizers which may be added and will be assumed to have a ratio, r (<1). The ratio, r, is defined as the ratio of longitudinal primary spring spacing to the longitudinal axle spacing.

Since vertical movement of an axle does not affect the load at the wheels, only a roll rotation of the lead axle is considered in the model shown in Figure A-1. The general arrangement for the torsional and roll stiffnesses of the primary and secondary suspensions and the truck frame and body torsion are shown in the block diagrams of Figures A-2 and A-3, initially for a rigid framed truck with primary suspensions at the axle bearings.

Where

$K_1 = 2d_p^2\ K_p$ the roll stiffness of the primary suspension

$K_2 = 2d_s^2\ K_s$ the roll stiffness of the secondary suspension

$K_3 = Kbody$ the car body torsional stiffness between trucks

$K_4 = K_{frame}$ the truck frame torsional stiffness between axles

$K_g = \frac{-W_{body}h}{2}$ the negative roll stiffness due to pendulum forces

h is the height of the body cg above the roll center

ϕ_1 is the roll angle of axle 1, and

ϕ_2 is the roll angle of axle 2.

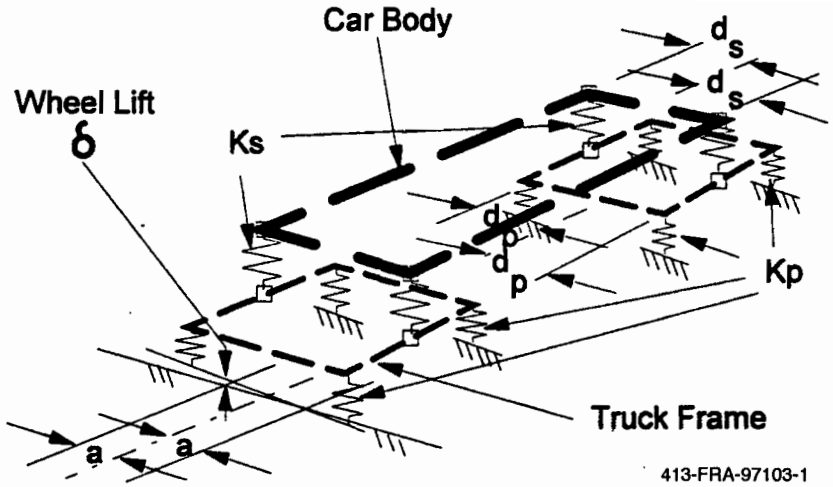

Figure A-1. Basic roll motions in a four axle passenger car subject to a single wheel lift

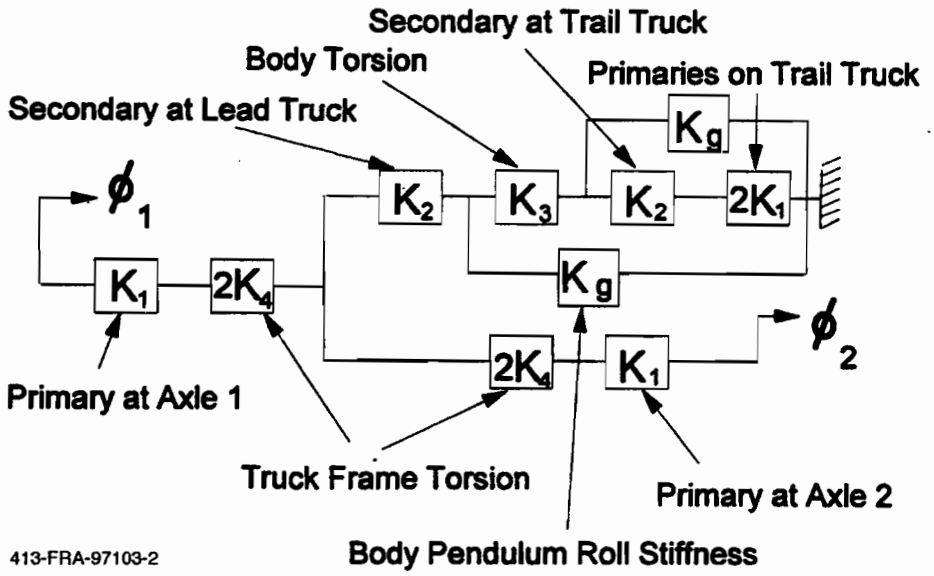

Figure A-2. Vehicle torsional stiffnesses as a block diagram

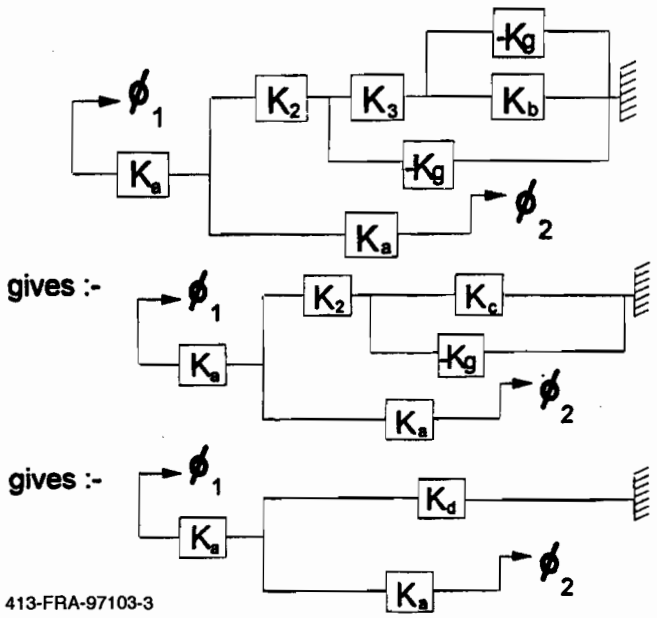

Figure A-3. Reduction of torsional stiffnesses through manipulation of the block diagram

The arrangement in Figure A-2 can be reduced to the arrangement in Figure A-3.

Thus

$$K_a = \frac{2K_1K_4}{K_1 + 2K_4}$$

$$K_b = \frac{2K_1K_4}{2K_1 + K_2}$$

$$K_c = \frac{K_3(K_b - K_g)}{K_b - K_g + K_3}$$

$$K_d = \frac{K_2(K_c - K_g)}{K_c - K_g + K_2}$$

The apparent stiffness at the lifted wheel, K_{wheel} may be found as follows if ϕ_n is the angle at the lead truck frame center. From the above block diagrams it can be seen that

$T_1 = K_a (\phi_1 - \phi_n)$, $T_2 = K_a (\phi_2 - \phi_n)$ and $T_1 + T_2 = K_d \phi_n$.

Noting for the general truck, now including equalizer beams, ϕ_{i1} is the roll angle of the lead axle, and ϕ_{i2} is the roll angle of axle 2, at the lead primary

$$\phi_1 = \frac{(1+r)}{2}\phi_{i1} + \frac{(1-r)}{2}\phi_{i2}$$

and at the 2nd primary

$$\phi_2 = \frac{(1-r)}{2}\phi_{i1} + \frac{(1+r)}{2}\phi_{i2}$$

for lead axle roll only, the frame roll becomes

$$\phi_n = \frac{K_a}{K_d + 2K_a}\phi_{i1}$$

Recognizing the moment relationship for the lead axle in terms of those at the primaries,

$$T_{i1} = \frac{(1+r)}{2}T_1 + \frac{(1-r)}{2}T_2$$

the effective stiffness at one wheel of the lead axle when raised becomes,

$$K_{wheel} = \frac{K_a}{8a^2}\left\{r^2 + \frac{K_d}{K_d + 2K_a}\right\}$$

where K_a and K_d are as given previously.

Further values were computed for the percentage unloading due to the relative roll between axles in the lead truck and the same across between truck frames at A and B ends. This expression was modified during the research as described in the results to include the effect of the shear stiffness,

$$\%staticF_v = \frac{100}{2aF_v}\left\{\left(K_e + \frac{r^2K_a}{2}\right)(\phi_{i1} - \phi_{i2}) + \left(\frac{K_d}{2}\right)\phi_n\right\}$$

where

$$K_e = R_0^2\left[\frac{1}{K_{py}} + \left(\frac{L}{B}\right)^2 \frac{1}{K_{px}}\right]^{-1}$$

and R_0 is the wheel rolling radius, B is the lateral distance between primaries, L is the lateral distance between wheel/rail contacts.

This method was used for comparisons with dynamic unloading and the inclusion of the effect of truck shear stiffness.

A.1.3 Simplified Curving Analysis of Asymptotic Behavior

Analytic expressions for simplified curving exist. An example of these expressions are developed in the paper entitled "Limiting Forces on Transit Trucks in Steady-State Curving" (2). The equations are developed for tight curves and gross wheel sliding. When these values are compared to the values obtained by the simulation code, it is to be expected that the tighter curve cases will be in closer agreement.

The results using the simulation code were compared to the results using the closed-form equations found in (2). A case with an empty bi-level car was used to compare the two methods. The closed-form equation method yielded an L/V = 0.54. The L/V from the simulation code was 0.53 and 0.57 for 10 deg and 15 deg curves, respectively. This shows good correlation between the two methods for tight curves. For the same case on a 2.5 deg curve, the simulation code predicts an L/V = 0.23, which is about half of the result using the closed-form equations.

A.2 NEWHUNT - Linear Hunting Analysis

Based on an existing CARHNT program developed by Battelle Columbus Laboratories and furnished by VNTSC, Blader developed an enhanced software package for linear hunting analysis. It includes a corrected representation of the equalized truck mechanics and an automatic analysis of the linearized rolling contact forces. The new program has been renamed NEWHUNT for use here.

NEWHUNT relies on analytical methods in the frequency domain which only work with linear descriptions of the system to be analyzed. Because of this, the results are only exact for small lateral motions of the axles on the rails. The speed beyond which these motions begin to increase rapidly is called the critical speed and this value when in the running range for the vehicle is frequently used to identify unsatisfactory behavior of the vehicle or train. In addition, since vertical degrees of freedom are not included in the model, the linearized wheel-on-rail forces assume that the static vertical load remains constant in the contact force model. This linear methodology is well suited to general investigations of the effects of parameter variations and design changes on the rail vehicle lateral dynamic stability. The results obtained from them

can also be used to establish direction and priorities for more detailed numerical simulations such as the program OMNISIM used here.

The "hard-wired" mathematical model in NEWHUNT assumes that the rail vehicle consists of a carbody with two dual-axle trucks. The body and the major truck components are represented by rigid masses that are interconnected by linear elastic springs and linear viscous dampers. These discrete elements represent not only any physical springs and dampers, but also the effects of distributed elasticity and energy dissipation. Equivalent viscous damping is used to represent the inherently nonlinear Coulomb friction and a suitable equivalent value was precomputed for entry, based on the energy dissipated per cycle.

The complete model has seventeen degrees of freedom. The car body is modeled as having three degrees-of-freedom: lateral translation, yaw, and roll. The center-of-mass of the car body moves down the track at a constant velocity, which is the independent variable in the linear hunting analysis. The truck is modeled as having seven degrees-of-freedom: lateral translation and yaw for each wheelset, lateral translation of the truck frame, roll of the truck frame, and yaw of the truck frame.

The change in potential energy associated with axle motions gives rise to forces and moments related to motion of the wheelset over the rails often called the "gravitational stiffness" terms. In these, the increase in height at the wheelset center is related to the wheelset displacement through the geometry of the wheel-to-rail profiles. While vertical motions of the vehicle are not considered as active degrees-of-freedom in the analysis, these gravitational effects are important and are included in the analysis. Certain terms become important only where the wheels are sufficiently worn to present a concave profile in contact with the rail head radius. During initial tread contact, the effect of gravitational terms in wheelset yaw are generally negligible.

Other terms of importance due to the lateral shift of the wheelset result from the difference in the rolling radius at each wheel. This gives rise to another profile geometric parameter called the effective conicity of the wheel, which is used to determine the relative longitudinal velocity and forces of the wheel over the rail. The gravitational terms and those forces due to effective conicity are fundamentally interconnected through the profile shapes and although it has been suggested that describing functions might be used to define them optimally for a linearized model, the correct analysis is complex involving two coupled describing functions in the axle degrees of freedom.

A simpler method is used in NEWHUNT which involves reducing the wheel and rail profiles to constant circular arcs of radius close to the points of contact with the axle centered on the track. The wheel profile radius is used as a variable in the resulting expressions and its value is determined from the required effective conicity, using a value chosen for the rail head radius. Linearized geometric relationships assuming the circular arcs are used to compute the gravitational terms and, with the effective conicity, are inserted into the equations of motion for determining the roots. The coupling between them is correctly represented using this method. A full description of the relationships required may be found in (3). The relationships are:

For the gravitational stiffness

$$k_g = \frac{W}{R_w - R_r}\left\{\frac{L + R_w\Delta}{L - R_0\Delta}\right\}^2$$

and for the effective conicity

$$\lambda = \frac{R_w\Delta}{R_w - R_r}\left\{\frac{L + R_r\Delta}{L - R_0\Delta}\right\}^2$$

where

- W is the axle load
- R_w is the wheel profile radius
- R_r is the rail head profile radius
- R_0 is the wheel rolling radius
- Δ is the contact angle with the wheelset centered
- L is the semi-distance between contact points

The wheelset equations of motion have terms for the rolling contact forces as follows, neglecting the uncoupled spin terms which are very small,

Lateral force

$$\left\{k_g - \frac{2f_3}{R_0(R_w - R_r)}\right\}y + 2f_2\frac{y}{V} - 2f_2\psi$$

Yaw moment

$$\frac{2Lf_1\lambda}{R_0}y + \{2f_3 - WL\Delta\}\psi + 2f_1L^2\frac{\psi}{V}$$

The Kalker (4) values for the creep coefficients are computed within the new code NEWHUNT.

An additional modification was made to the initial code to permit an optimal representation of the truck with equalizer beams. Thus the effective primary lateral stiffness, K_2, is adjusted at the lead position to have the value $(1+r^2)K_2$, and coupling terms are added between the axles of $(1-r^2)K_2$, between the lead and trail axles. Additional terms are also required between the axles and truck frame in yaw. Since primary dampers were not included at the equalizer springs, the damping terms were assumed to act at the axle and the equations left unaltered. These would

need modification if primary dampers were to be needed at the spring locations. The equations of motion for the wheelsets are asymmetric, owing to the non-conservative forces at the wheel/ rail interface described above.

An exponential solution is assumed for the degree-of-freedom vector having real and imaginary parts to the exponent, i.e., $e^{\{\alpha + i\beta\}t}$. The imaginary part, where non-zero, provides sinusoidal oscillations of known frequency, one for each pair of complex conjugate terms in the non-zero solution. The real part defines the history of the amplitude in time. If it is positive, the amplitude grows and is generally descriptive of the onset of hunting. The model is increasingly approximate as the amplitudes become large relative to the flangeway clearance but the speed at which the solution becomes unbounded is the critical speed and is generally quite accurate. A formal method known as the QR algorithm is used, as supplied with CARHNT, to solve the equations for their roots, and the least damped modal amplitude, (that with the most positive real part), is tracked against speed to find the critical speed at which the oscillation becomes unbounded. In reality, this oscillation may be bounded by the nonlinearities into a limit cycle or oscillation of fixed amplitude, beyond which further dynamic instability may occur.

A.3 OMNISIM (5)

For more detailed simulation with full representation of the system nonlinearities, sophisticated computer programs are now in general use which employ numerical schemes for predicting new values for the degrees of freedom by stepping the nonlinear differential equations-of-motion in time. In order to simulate the dynamics of a range of passenger rail vehicle types and configurations accurately, the software must possess certain important features:

1. The ability to model arbitrary system geometries with any number of bodies and connecting elements including nonlinear characteristics.

2. An accurate means of representing measured or analytic wheel/rail profile contact geometry.

3. Accurate nonlinear creepage relations for steel wheels on rail.

4. The input of track geometry and perturbations including analytically represented and measured track.

5. The capability to add arbitrary forcing functions, such as wind loads.

Under a previous contract with the Volpe National Transportation Systems Center (Volpe Center), Blader developed, for Foster-Miller, a new vehicle dynamics simulation program package called OMNISIM, based on his earlier work reported in references (6,7). OMNISIM is an advanced general system simulation code using a formal lumped-parameter multi-body system methodology to model both rail vehicles and track systems. It was initially used for the study of track lateral shift caused by high speed train operations. A full model of the track can be included which permits calculation of track motions during all types of derailment processes,

including wheel climb, gage spreading, track shift, and vehicle rollover. It is the only program presently available that combines this capability with an accurate model of rolling contact and was selected for use in this work. A full description of the program is given in (5).

OMNISIM can work with English or metric units, and with measured or analytically constructed inputs or a combination of both. It presents a unified approach to predicting rail vehicle response to a variety of inputs, such as those from the track, an actuator or wind forces. Vehicle ride quality may also be assessed. The flexible structure of the input allows the user to model any new or existing vehicle design. In addition to the main run processor, pre- and post-processing programs have also been created. Each system is defined in a text file called the definition file, using an appropriate word processor. This file is then preprocessed to the required format and units by the preprocessing program DEFINE. This program rearranges the data and the system units and permits the user to see the system in diagrammatic form, displaying its geometry and characteristics. DEFINE will also display previously pre-processed files.

Means are provided in the definition file to identify the degrees of freedom for each body required in the model. The potential choices include all translational and rotational rigid body motions and the first beamlike free-free flexible modes in twist and in vertical and lateral bending. The interaction of rigid or flexible bodies is defined through hard or soft connections (e.g., metal to metal or suspension elements). The program requires the user to define a vehicle and track system model with inertial and geometric properties, connection characteristics, wheel/rail geometry data, and displacement or force inputs.

There are a number of different types of track and vehicle interbody connections available. Their characteristics range from simple spring and damper pairs in parallel or in series to more complex friction elements. The characteristic of each spring and damper is defined using piecewise linear functions of displacement and velocity, respectively. Hysteresis requires two piecewise linear functions that represent the asymptotic loading and unloading curves. Additional information, such as that which controls the speed of closure to the asymptote in hysteresis, may also be specified.

The present wheel/rail connection assumes no roll rotation of the rail, with the vehicle and track system in the same moving coordinates. This is equivalent to a track model that generates the same behavior at the wheel as the vehicle moves down the track. Although useful in identifying rail motions, further improvements are contemplated. These will allow the rails to be modeled as a stationary continuum with a potential reduction in the number of degrees of freedom, and will release the rail support model from moving with the vehicle.

Each individual wheel/rail connection uses a look-up table representing the required variables at the point of contact between the wheel and rail so that the rolling contact forces may be calculated for the steel wheels on steel rails. The profile data tables are precomputed using a more flexible version of Law and Cooperrider's program WHRAILA (8), named PROFIT, for PROfile FIT. A four-dimensional look-up table of creep force coefficients, according to Kalker (4) and as adapted by British Rail, is used in determining the forces and moments on each wheel.

The rotational speed of the wheel or axle, which may be a solid or have independently rotating wheels, is regarded as a special variable and is required to obtain the wheel/rail forces. The method assumes that the dominant changes in the wheel/rail contact geometry are those due to local relative displacement between each wheel and the rail to which it is connected.

The inputs to the system under study may be measured or analytically constructed in segments using several optional functions. Those representative of laboratory simulation, generally as a function of time, can be formed in the input text file that is read directly by the stepping processor at commencement. A swept frequency sine wave allows vibration testing of a stationary vehicle. However, at the option of the user, the input file may request some or all of the data from a file of either measured or analytically defined histories, formed using the preprocessor called INFORM. This may be filtered and is formatted as digital information in steps along a chosen path or track. If measured data is to be used, it is called into INFORM, from a measured track geometry file. INFORM uses a text setup file to identify the source and preprocess the path and input data that may be of mixed measured and analytic origins.

The short wavelength inputs are regarded as local perturbations, and are introduced as variations in lateral or vertical position of the rails or guideway. For the analytically defined inputs, a repeated shape and amplitude for a segment of the rail may be chosen from a combination of cusps, bends, or sine waves. The long wavelength variations define the overall path and are linearly interpolated from positions along the track at which curvature and superelevation are either chosen analytically or taken from the measured data set. These are transformed into components of the connection strokes, so that the degrees of freedom for each body remain those relative to its local inertial coordinate system. Provision is made to allow both external displacement and forcing inputs to the model. Rail perturbations are an example of displacement inputs, whereas a coupler loads due to train action are an example of a forcing input.

For post-processing, PLOTS produces graphs of the output for monitor display or for hardcopy output. TEXTS produces numerical information for viewing or passing to other post-processors, such as a spreadsheet, for further manipulation. Much of the work in this report was postprocessed using a spreadsheet program.

APPENDIX B

SIMPLIFIED TWIST ANALYSIS RESULTS

Track spirals have the potential for derailment due to superelevation gradients that statically induce twist in the carbody. For lightly loaded cars that are long and torsionally rigid, this twist may cause an unbalanced sharing of the vertical load between wheels on the same axle. Reduction in vertical wheel load will be used to identify the potential loss of guidance, and thereby assess the safety of spiral negotiation.

This task has three parts. The first part involves determining the wheel/rail forces generated by the commuter passenger rail vehicles during steady curving. The second is to investigate the static equalization (i.e., redistribution) of wheel load resulting from jacking/lowering a single wheel as well as both wheels on one side of a truck (truckside). The third part involves combining this load redistribution study with the results of the steady curving analysis to investigate the potential for derailment as a function of track curvature.

B.1 Steady Curving

The objective of this task was to determine the wheel/rail forces generated by the generic commuter passenger rail vehicles during steady curving. Steady curving, as investigated neglects the transient dynamic response which occurs when a rail vehicle traverses the entrance and exit spirals found in all real-word curve track geometry. However, the assumption of steady curving is a useful tool for engineering studies and design tradeoffs.

Closed-form solutions are available which allow design studies and performance comparisons to be performed for a range of vehicle and track variables such as curvature, speed and crosslevel. However, in general models with accurate component representations, convergence difficulties resulting from the coupled nonlinearities frequently occur. Consequently, it was determined at the start of this project that steady curving solutions would be obtained via numerical simulation using OMNISIM. However, certain limiting case solutions were employed as checks on the numerical results.

OMNISIM was used to obtain steady curving solutions under balance speed conditions. Curves of 2.5, 5, and 7.5 deg were traversed at 35 mph. Curves of 10, 15, and 20 deg were traversed at 20 mph. Both single-level and bi-level vehicles in the empty and loaded conditions were considered. Each vehicle type was evaluated with equalized and non-equalized trucks.

For each combination of vehicle and track configuration/parameters, the lead-outer wheel lateral force and the wheel L/V ratio were plotted as functions of track curvature. Figures B-1 and B-2 present these results for single-level cars. The Nadal limit of 1.34 for a wheel/rail coefficient of friction of 0.4, is also indicated on Figure B-2. Figures B-3 and B-4 present similar results for bi-level cars. Figures B-3 and B-4 include results for a "degraded suspension." The vehicle model with the degraded suspension has a pedestal clearance (longitudinal and lateral) that is twice that of the baseline vehicle model.

In all of the cases that were investigated, OMNISIM did not indicate the occurrence of a wheel climb derailment. No derailments were indicated by the Nadal limit.

B.2 Static Load Equalization

The first part of this task was concerned with investigating the static equalization (redistribution) of vertical wheel load resulting from the prescribed vertical motion of either a single wheel or one side of an entire truck. The motion of a single wheel reflects a crosslevel gradient between the axles of a single truck, while the truckside motion reflects a crosslevel gradient between the trucks at either end of a vehicle. An accurate static equalization model of the forces in the suspension and carbody was developed, and is described in Appendix A. This model includes suspension stiffnesses for the vertical translation and roll axis degrees-of-freedom, as well as a representation of the car body torsional stiffness. The model was implemented in a PC spreadsheet program, which enabled it to be rapidly evaluated.

For single wheel and truckside raising/lowering in the range ±3 in., vertical wheel loads were plotted as functions of vertical displacement. Figure B-5 shows the numbering system that was employed in the model to identify and label the vertical wheel reactions. It is important to note that other than the wheel(s) that is being raised/lowered, all of the wheels are constrained to have zero vertical displacement. Hence, a calculated negative vertical reaction at one of these "fixed" wheels indicates that lift-off has occurred.

Figures B-6 and B-7 show the vertical wheel reactions for a single wheel lift on a bi-level car with equalized trucks for Truck A (lead) and Truck B (trailing). Figures B-8 and B-9 show the vertical wheel reactions for a truckside lift on a bi-level car with equalized trucks for the lead and trailing trucks. Other combinations of trucks (equalized and non-equalized) and cars (single-level and bi-level) were also analyzed.

B.3 Twist Analysis

Spiral negotiation involves a combination of superelevation gradient and curving. The potential for a derailment was evaluated by combining the results of the static load redistribution study of subsection B.2 with the steady curving results of subsection B.1. More specifically, the objective was to determine the difference in crosslevel between truck axles and the difference in crosslevel between truck centers, both as functions of track curvature that could potentially cause derailment. This was accomplished by combining the change in vertical load due to single wheel or truckside raising/lowering with the steady curving vertical wheel loads calculated by

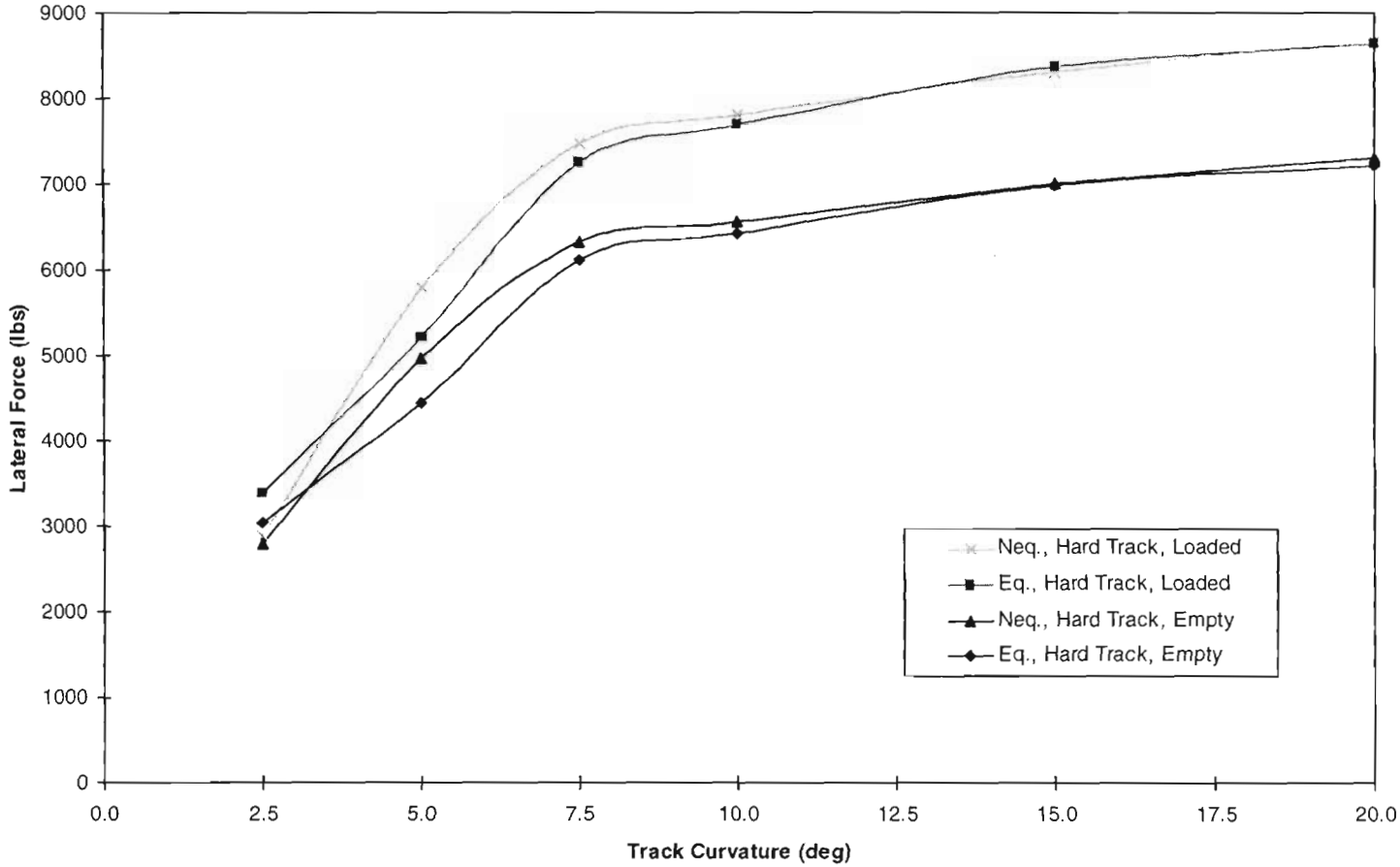

Figure B-1. Lead outer wheel lateral force versus track curvature (single-level car)

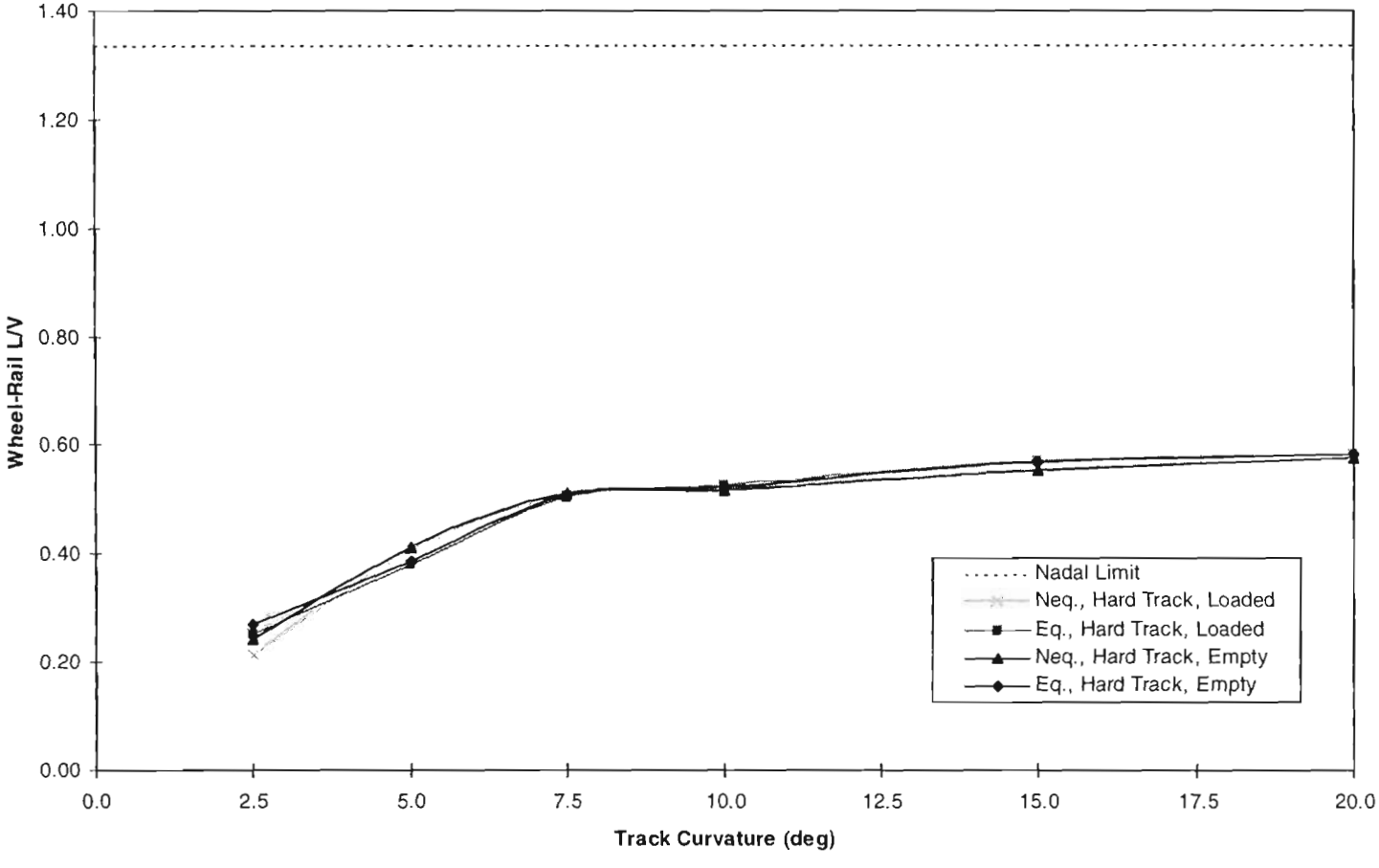

Figure B-2. Lead outer wheel L/V versus track curvature (single-level car)

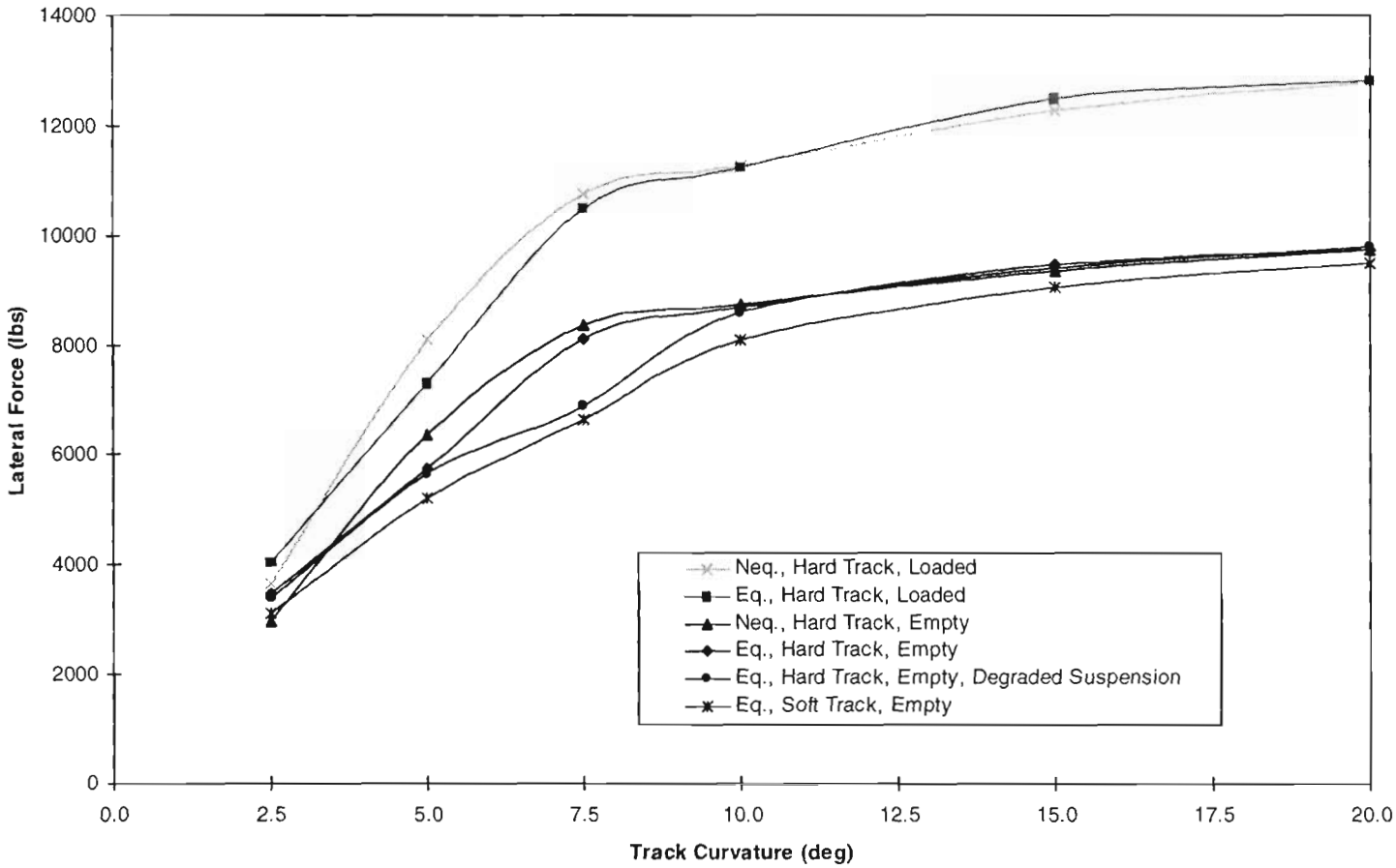

Figure B-3. Lead outer wheel lateral force versus track curvature (bi-level car)

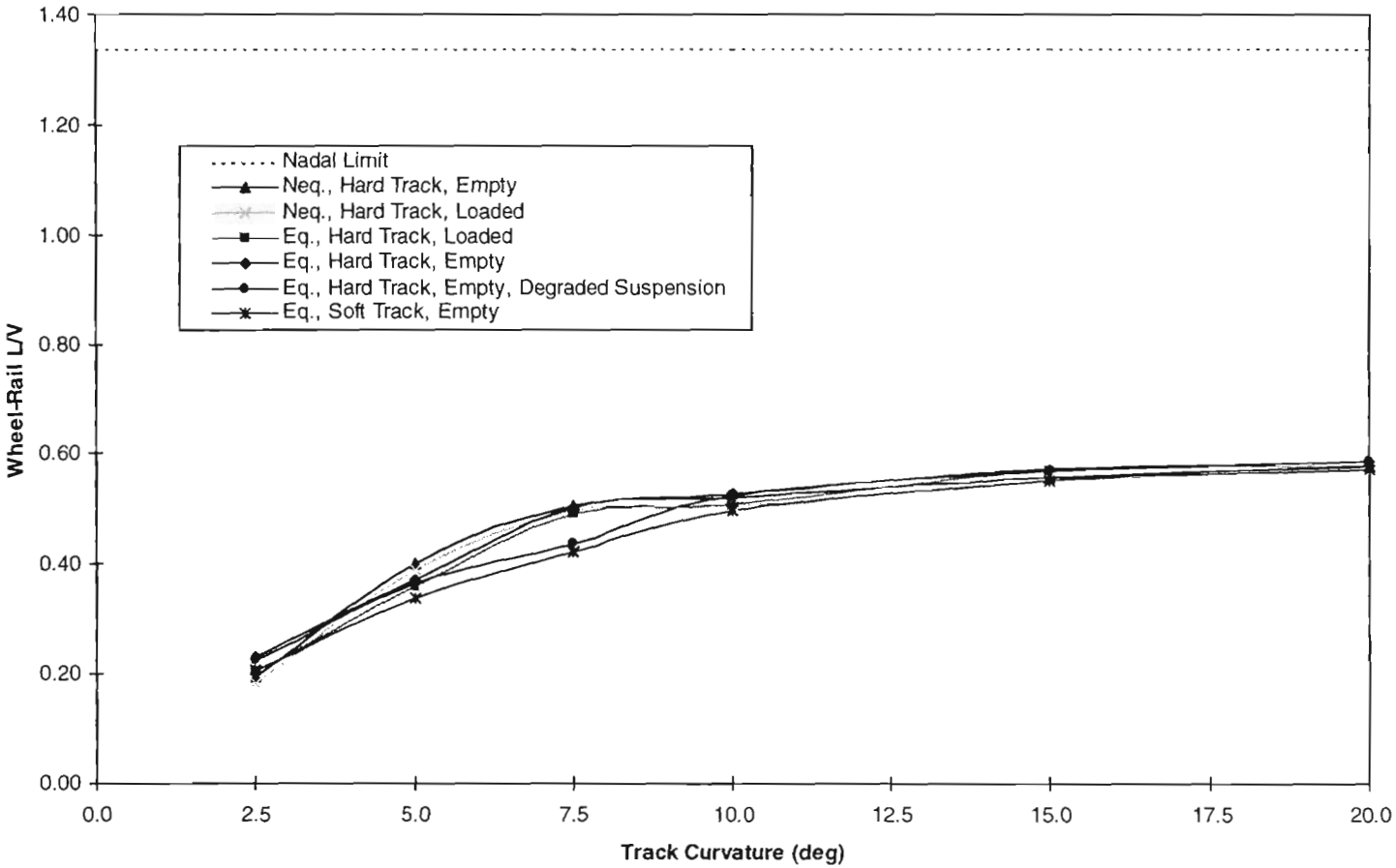

Figure B-4. Lead outer wheel L/V versus track curvature (bi-level car)

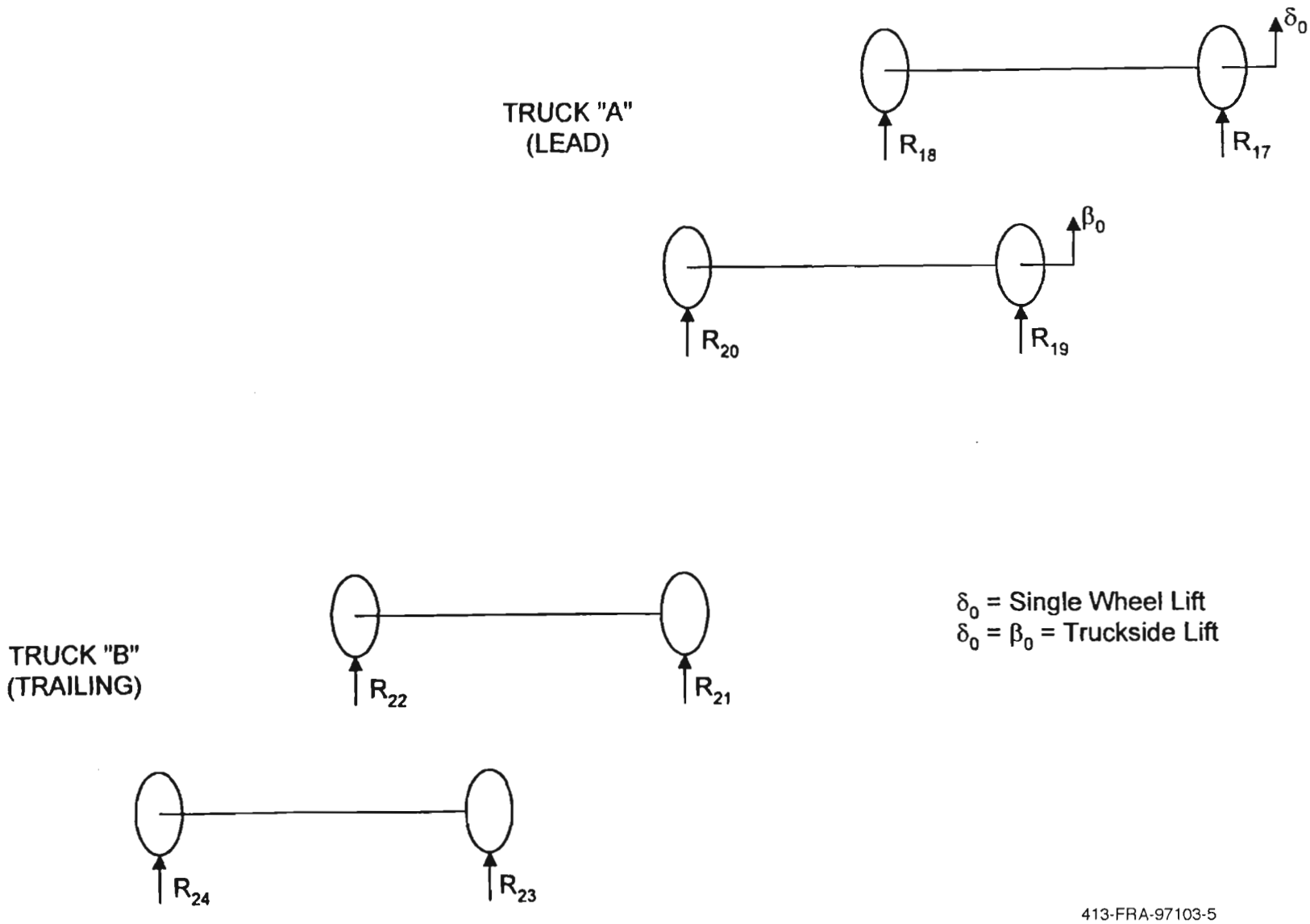

Figure B-5. Static equalization model wheel reactions

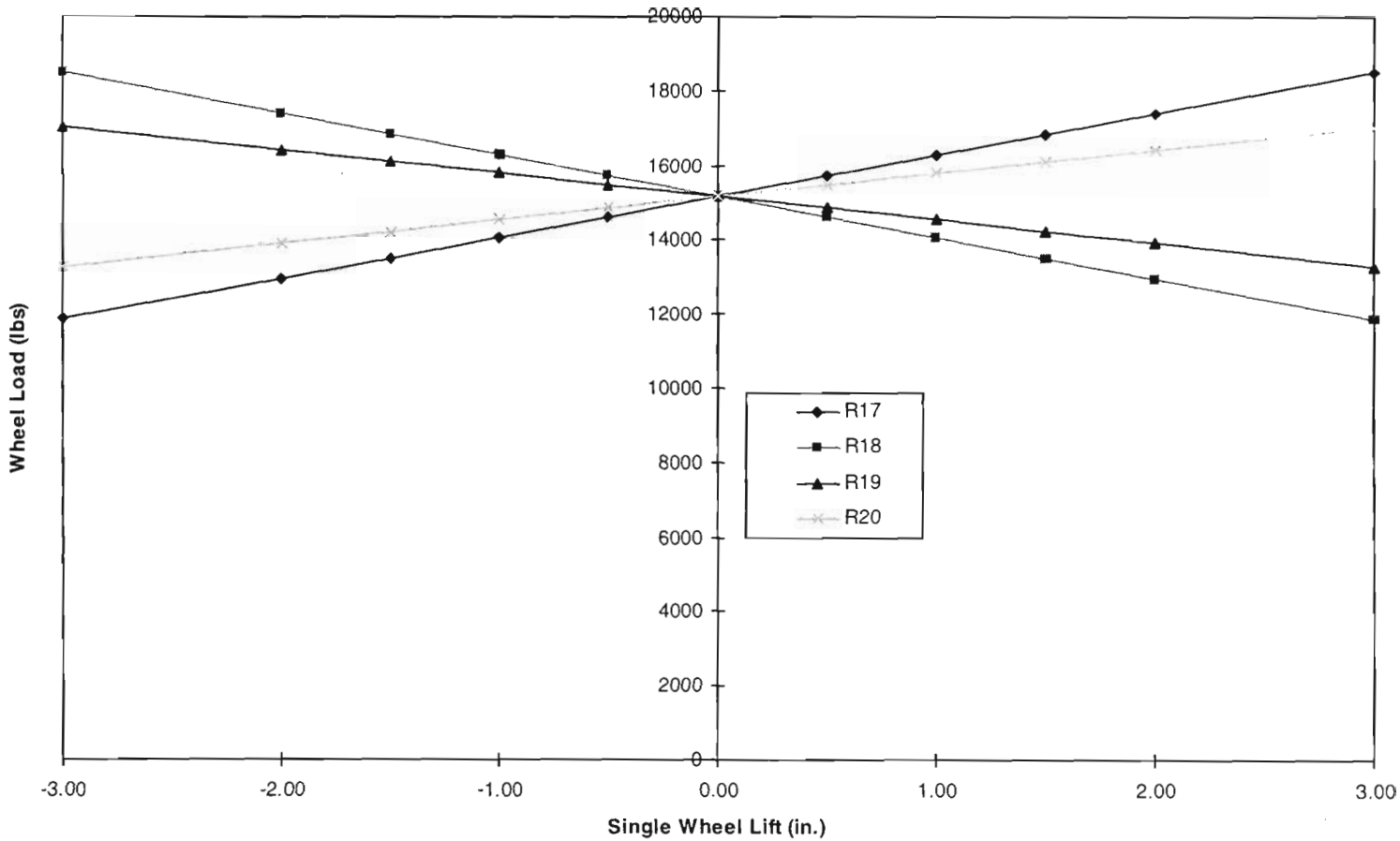

Figure B-6. Wheel load versus single wheel lift (truck A, bi-level car, equalized trucks)

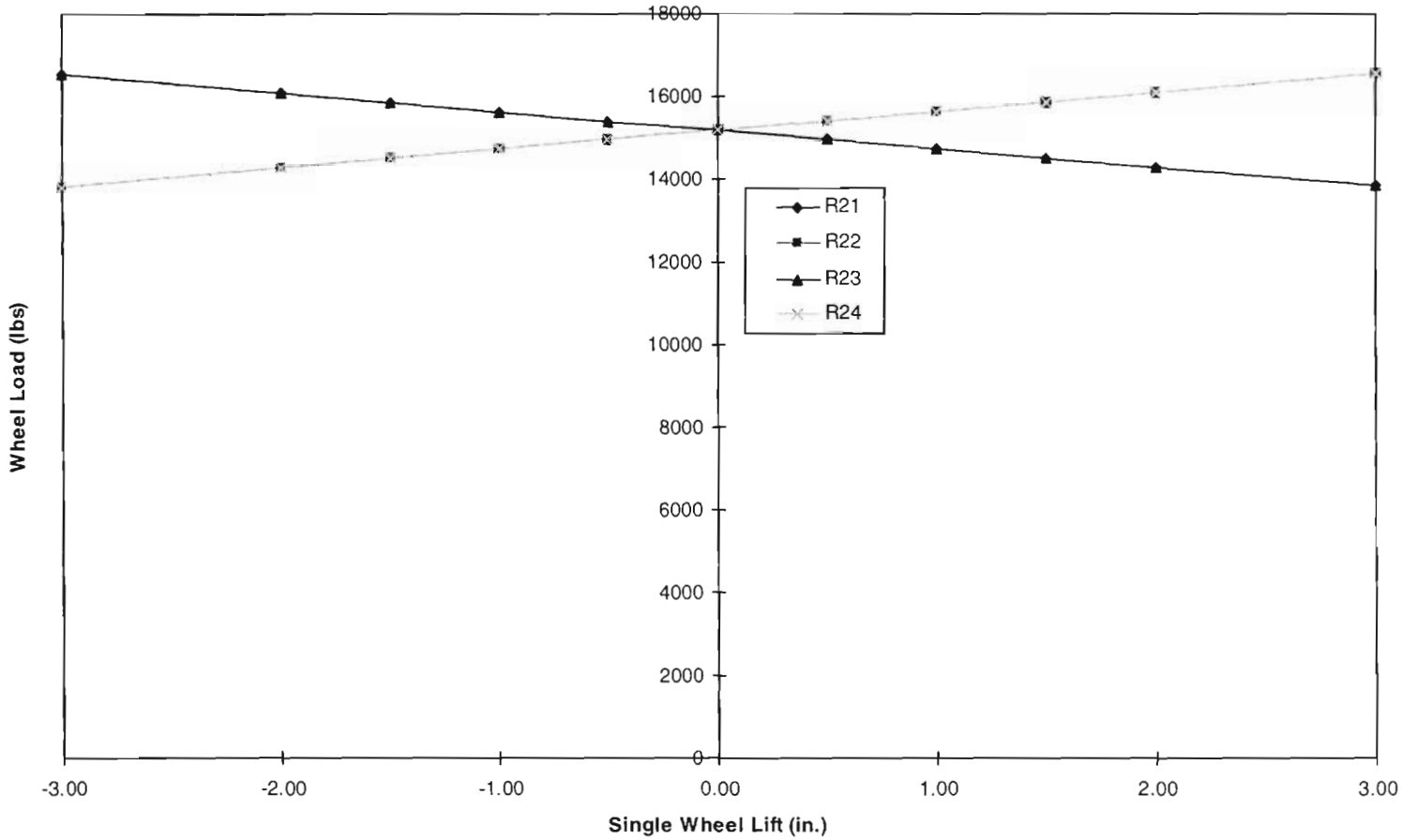

Figure B-7. Wheel load versus single wheel lift (truck B, bi-level car, equalized trucks)

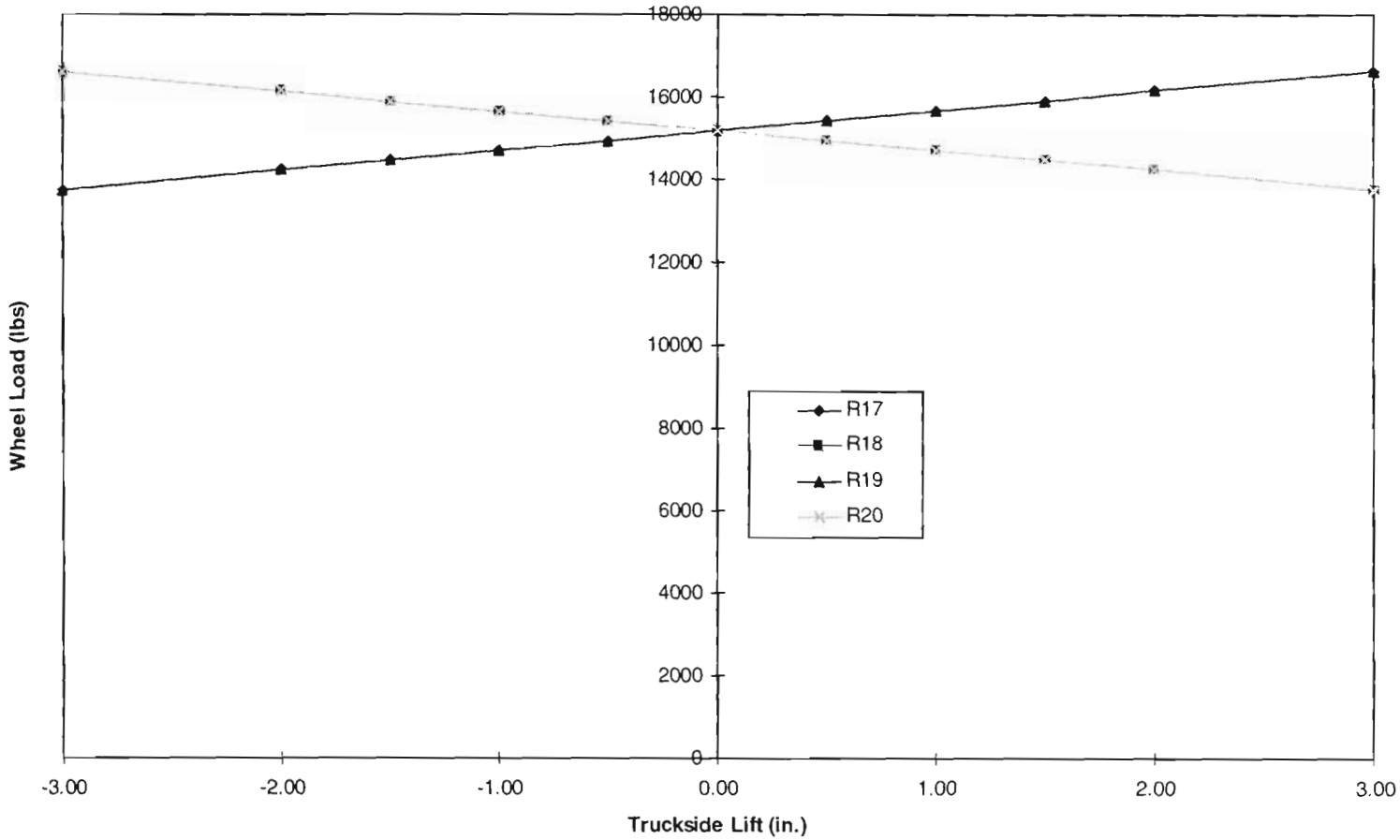

Figure B-8. Wheel load versus truckside lift (truck A, bi-level car, equalized trucks)

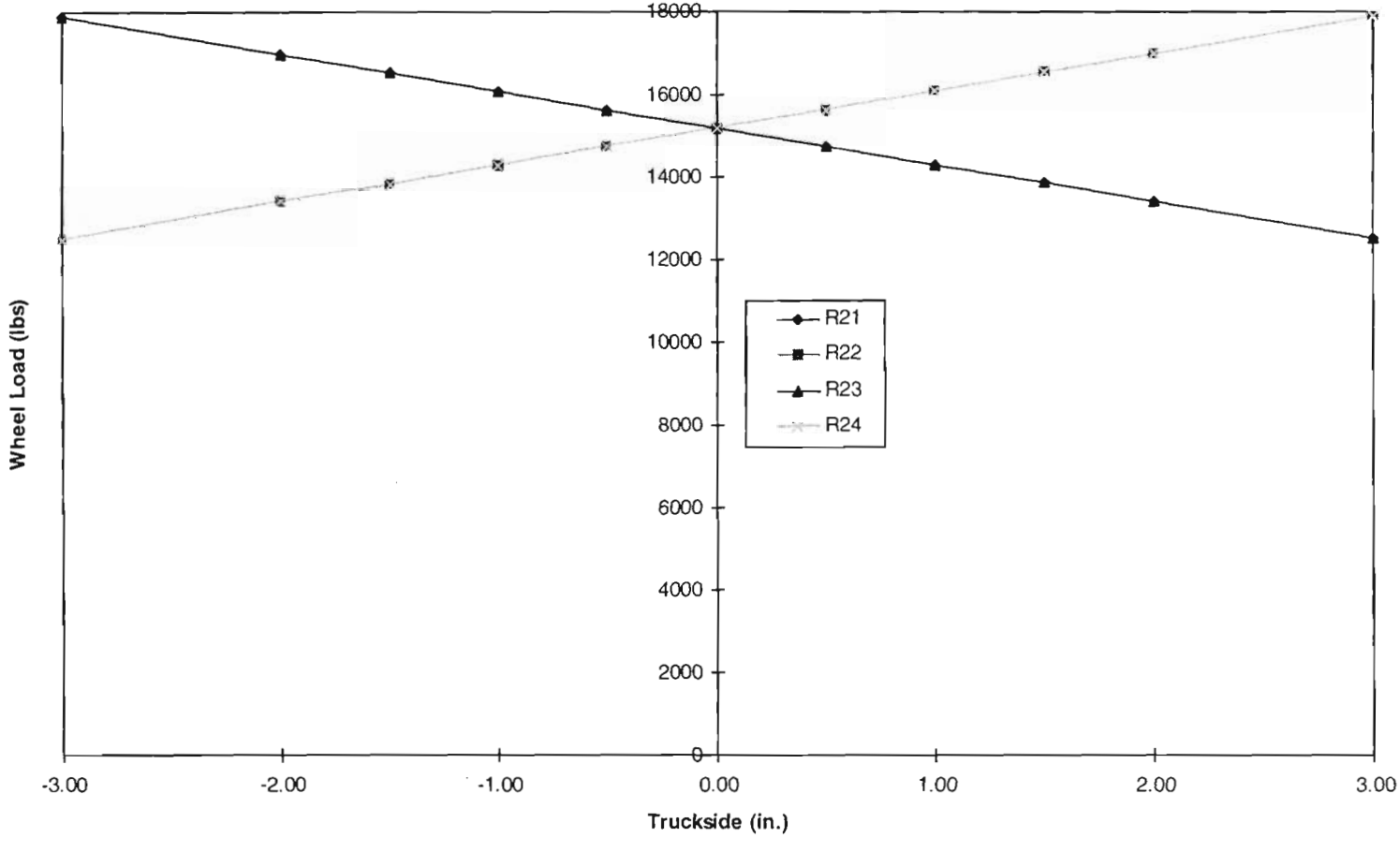

Figure B-9. Wheel load versus truckside lift (truck B, bi-level car, equalized trucks)

OMNISIM. This modified vertical load was then combined with the steady curving lateral wheel force (also calculated by OMNISIM) to obtain new L/V ratios for the outer leading wheel.

Figures B-10 and B-11 show the lead outer wheel L/V ratio as a function of wheel and truckside lift, respectively, for a single-level car with non-equalized trucks. Each figure includes a range of track curvature. The Nadal limit of 1.34 for a wheel/rail coefficient of friction of 0.4 is also indicated.

Figures B-12 and B-13 show the lead outer wheel L/V ratio as a function of wheel and truckside lift, respectively, for a bi-level car with non-equalized trucks.

Figures B-14 and B-15 show the lead outer wheel L/V ratio as a function of wheel and truckside lift, respectively, for a single-level car with equalized trucks.

Figures B-16 and B-17 show the lead outer wheel L/V ratio as a function of wheel and truckside lift, respectively, for a bi-level car with equalized trucks.

Figure B-18 summarizes the results for permissible crosslevel difference between adjacent axles. The permissible crosslevel difference is obtained when the Nadal limit of 1.34 is exceeded. It shows the maximum amount of crosslevel that can be safely negotiated as a function of track curvature. Greater amounts of crosslevel difference will sufficiently unload the lead outer wheel so that the Nadal limit of 1.34 is exceeded. Figure B-19 is a similar plot as Figure B-18, but for the equalized trucks. The maximum crosslevel difference is found when the L/V ratio exceeds the Nadal limit.

Figure B-18 shows that both the single-level and bi-level vehicles with non-equalized trucks can safely sustain more than ±3 in. of crosslevel variation (between truck centers) for all of the curves that were investigated. However, the figure also shows that neither the single-level or bi-level vehicles with non-equalized trucks can safely sustain more than ±3 in. of crosslevel variation (between adjacent axles) for all of the curves that were investigated. This is also shown in Figure B-20 that is similar to Figure B-18, but only shows the crosslevel variation (between adjacent axles) for the vehicles with non-equalized trucks.

From Figure B-19 it is clear that both the single-level and bi-level vehicles with equalized trucks can safely sustain more than ±3 in. of crosslevel variation (between adjacent axles and between truck centers) for all of the curves that were investigated.

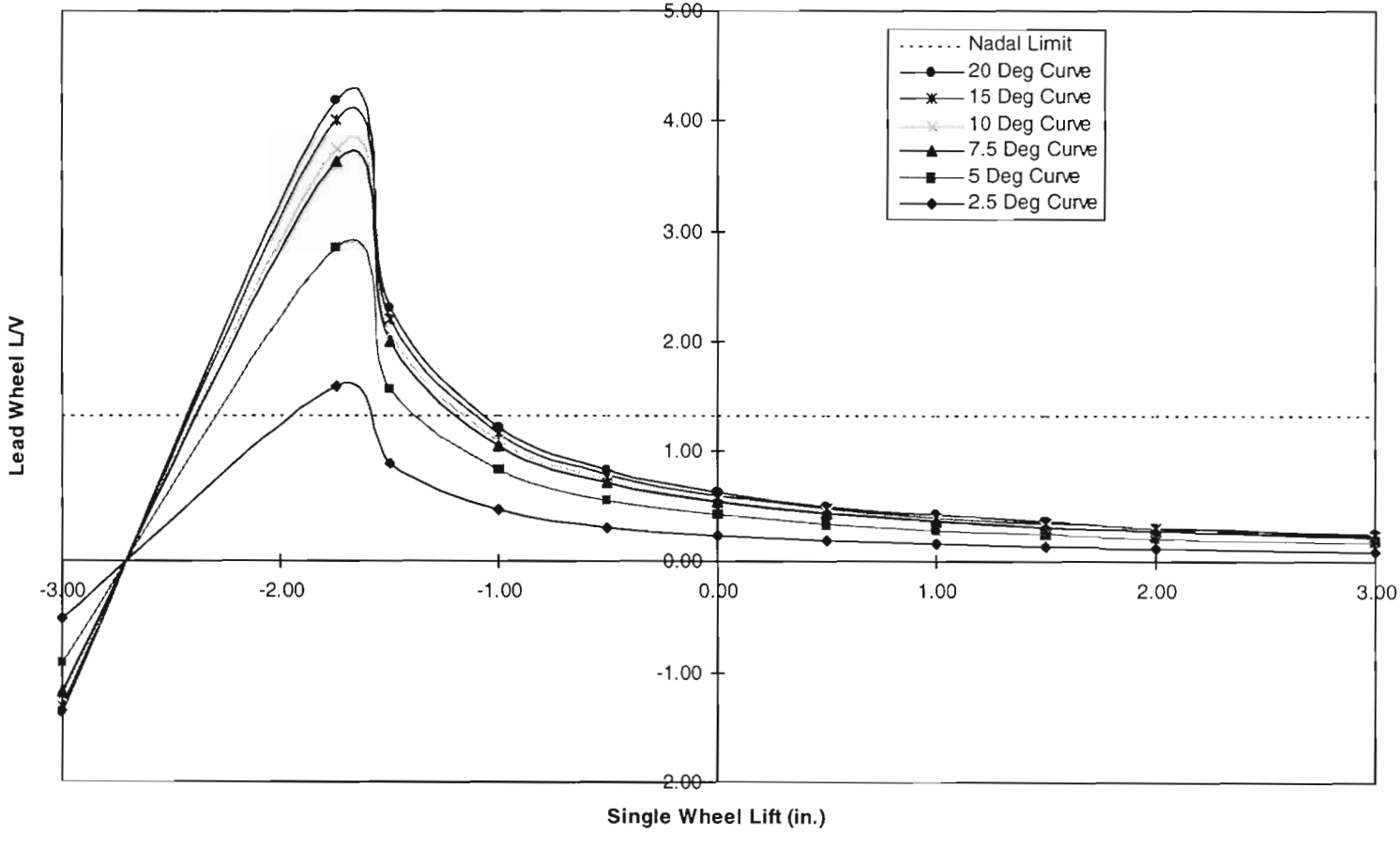

Figure B-10. Combined wheel L/V versus single wheel lift (single-level car, non-equalized trucks)

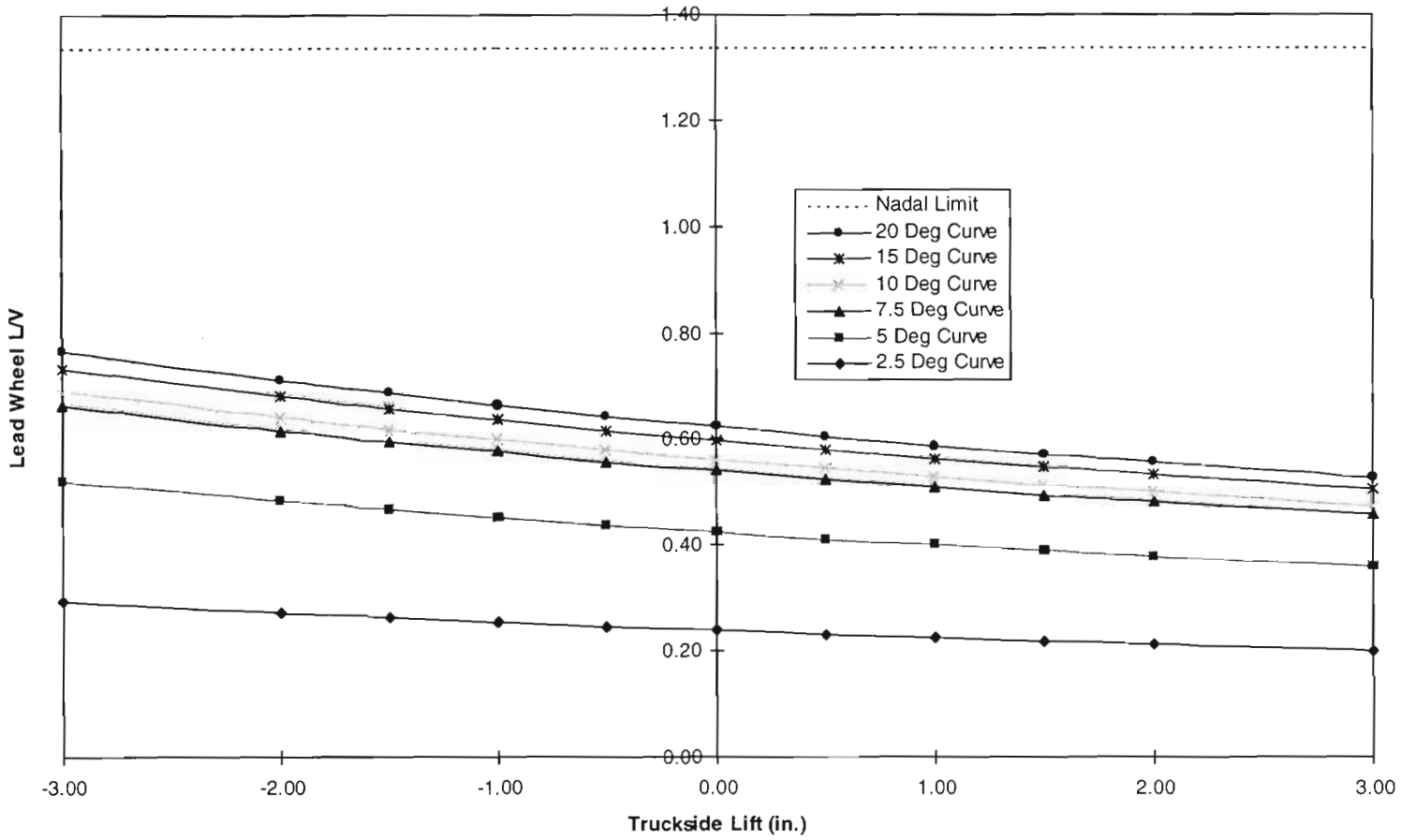

Figure B-11. Combined wheel L/V versus truckside lift (single-level car, non-equalized trucks)

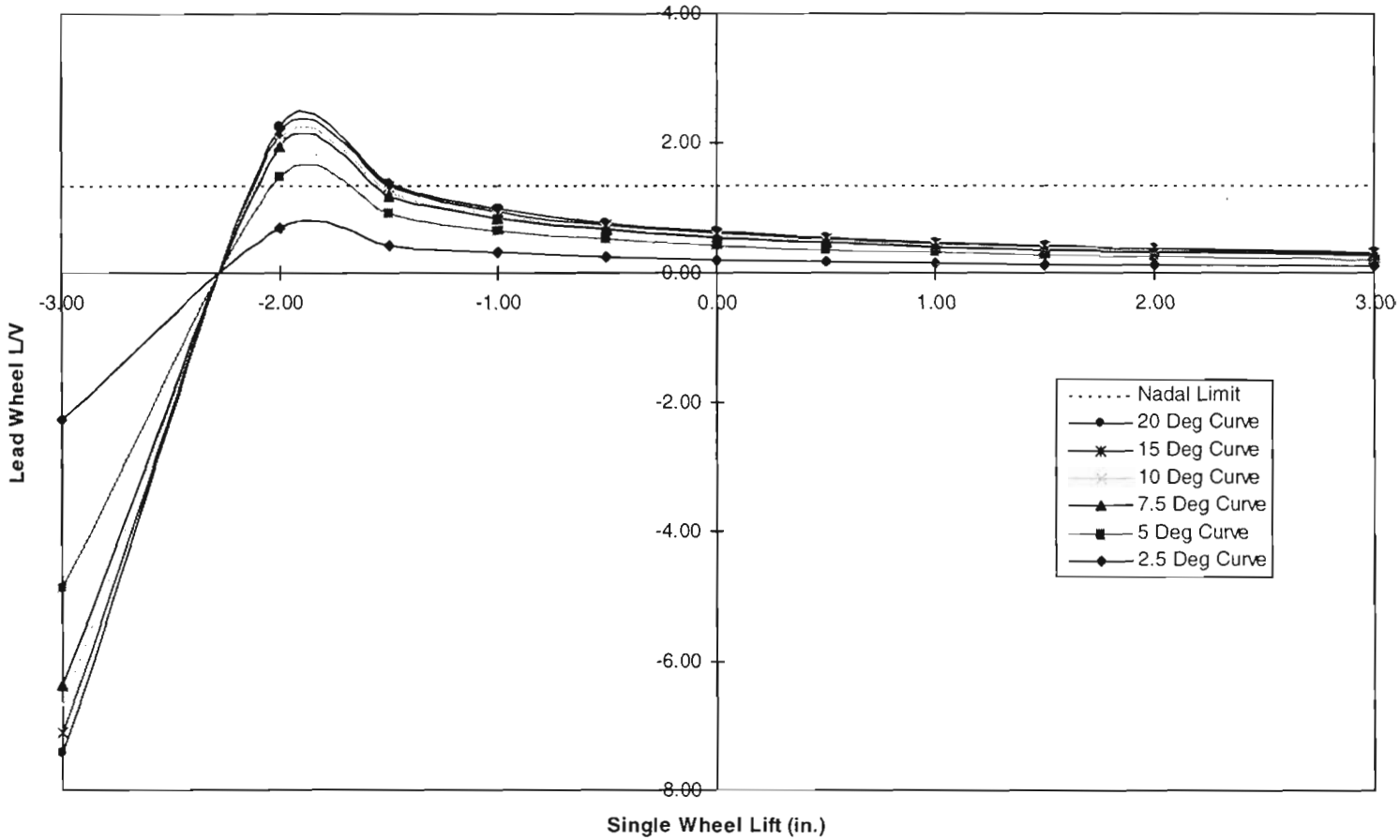

Figure B-12. Combined wheel L/V versus single wheel lift (bi-level car, non-equalized trucks)

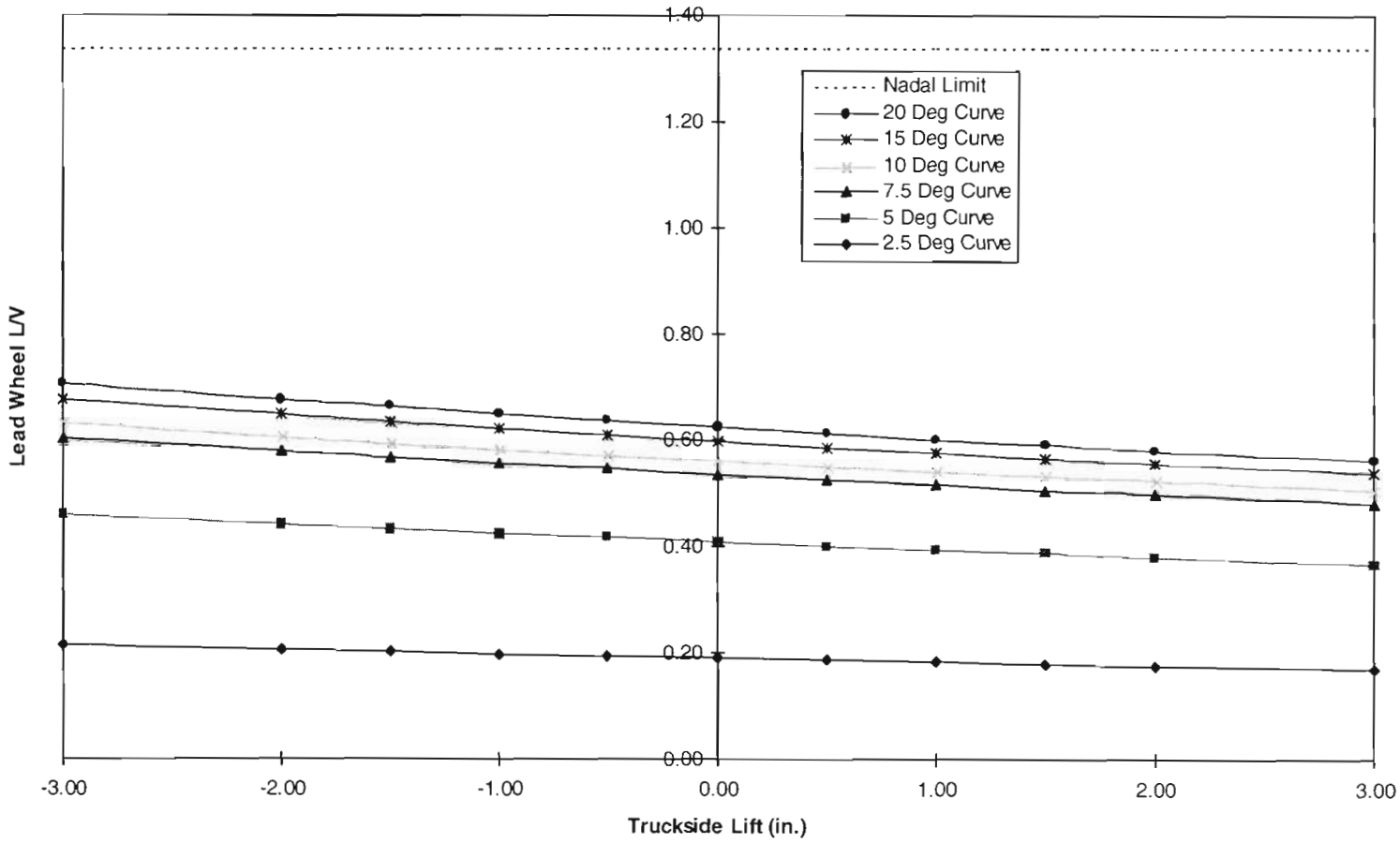

Figure B-13. Combined wheel L/V versus truckside lift (bi-level car, non-equalized trucks)

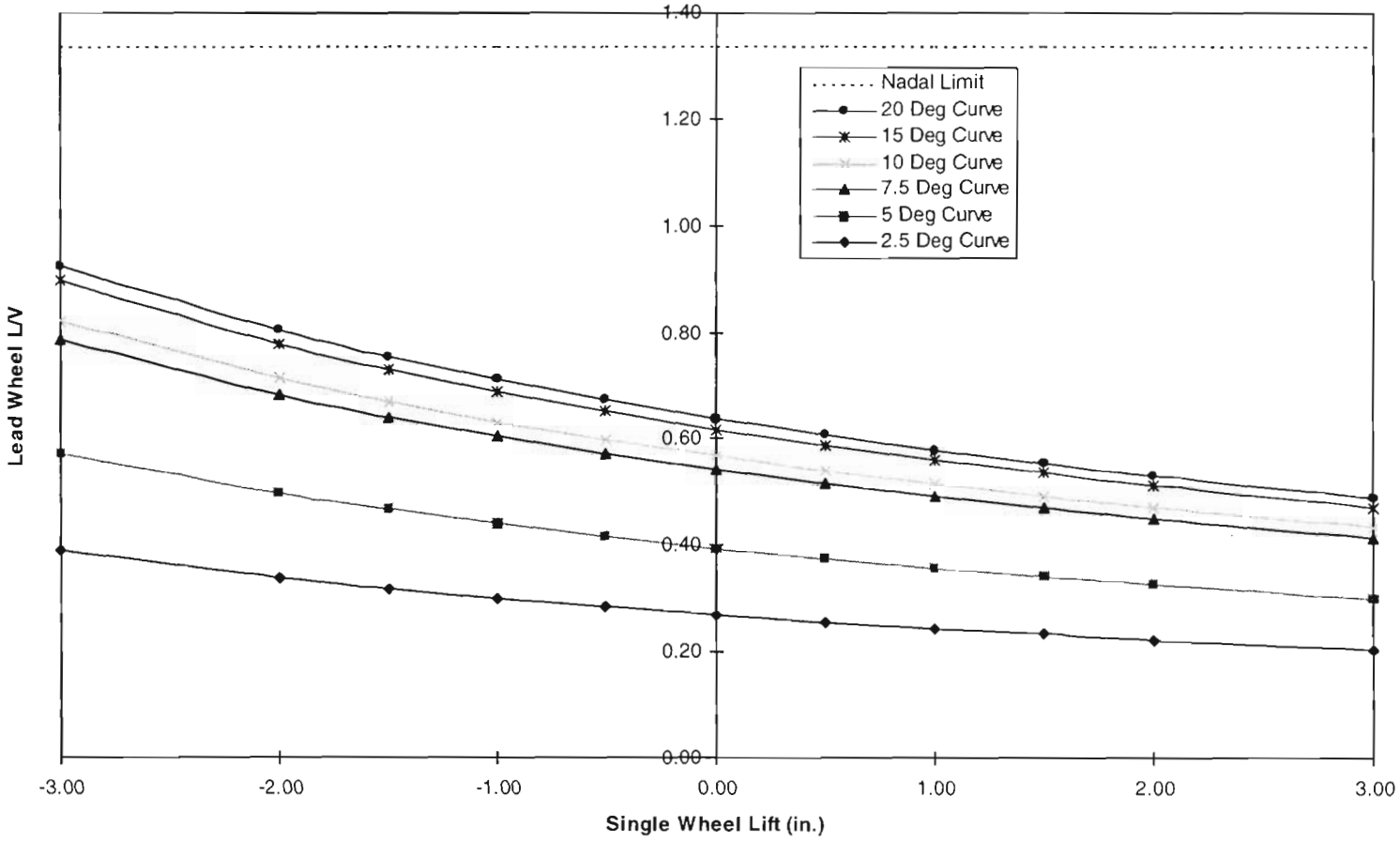

Figure B-14. Combined wheel L/V versus single wheel lift (single-level car, equalized trucks)

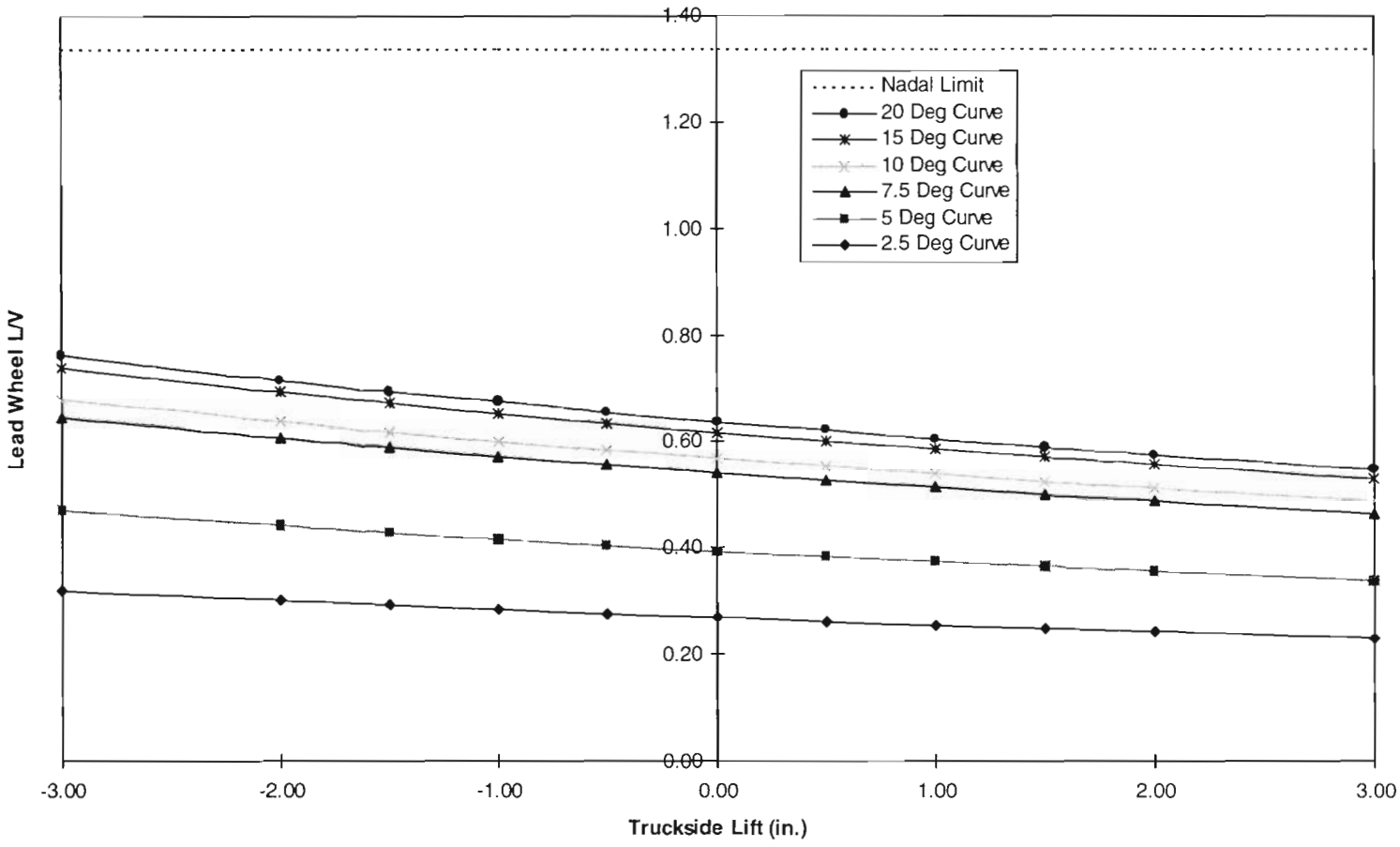

Figure B-15. Combined wheel L/V versus truckside lift (single-level car, equalized trucks)

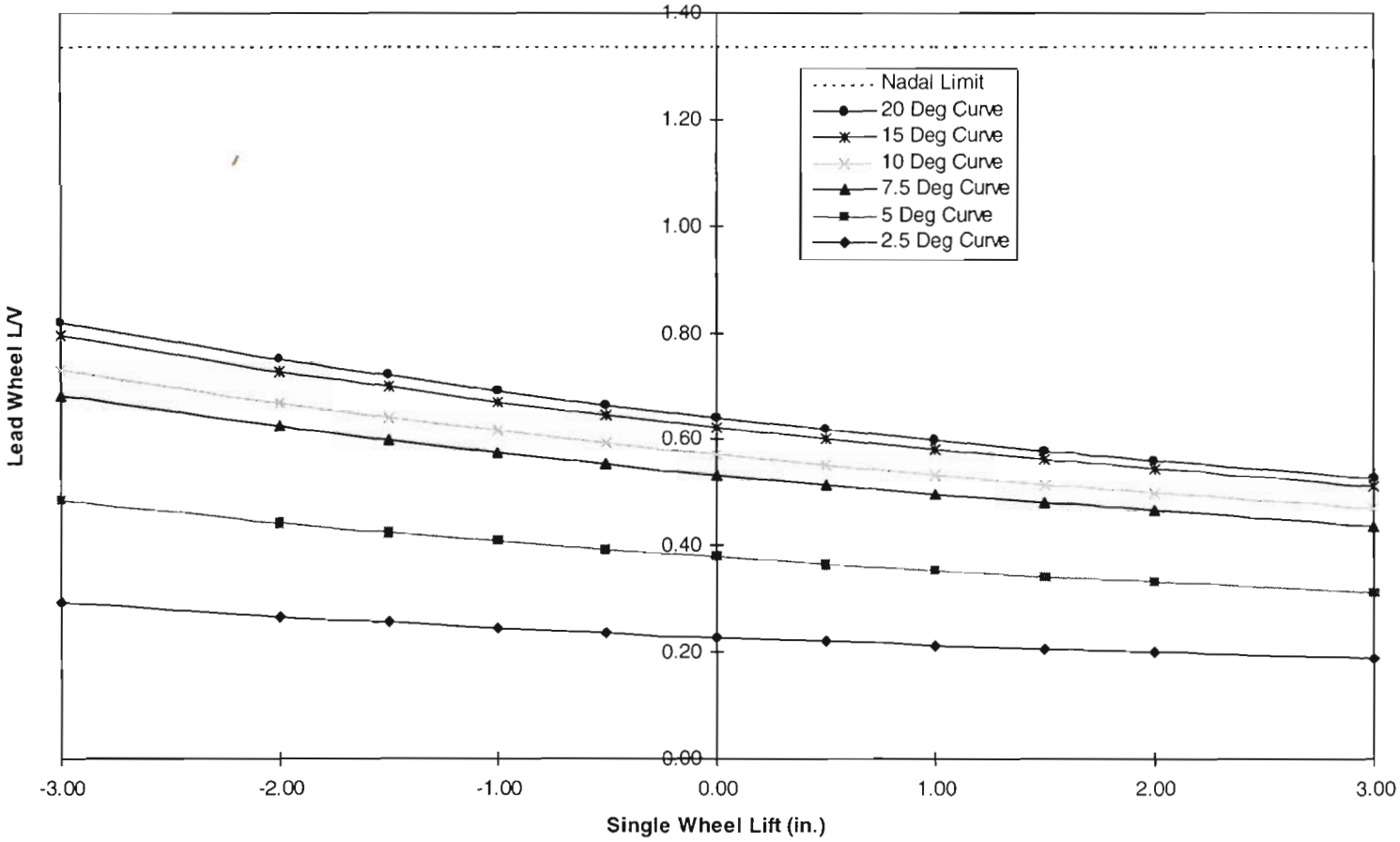

Figure B-16. Combined wheel L/V versus single wheel lift (bi-level car, equalized trucks)

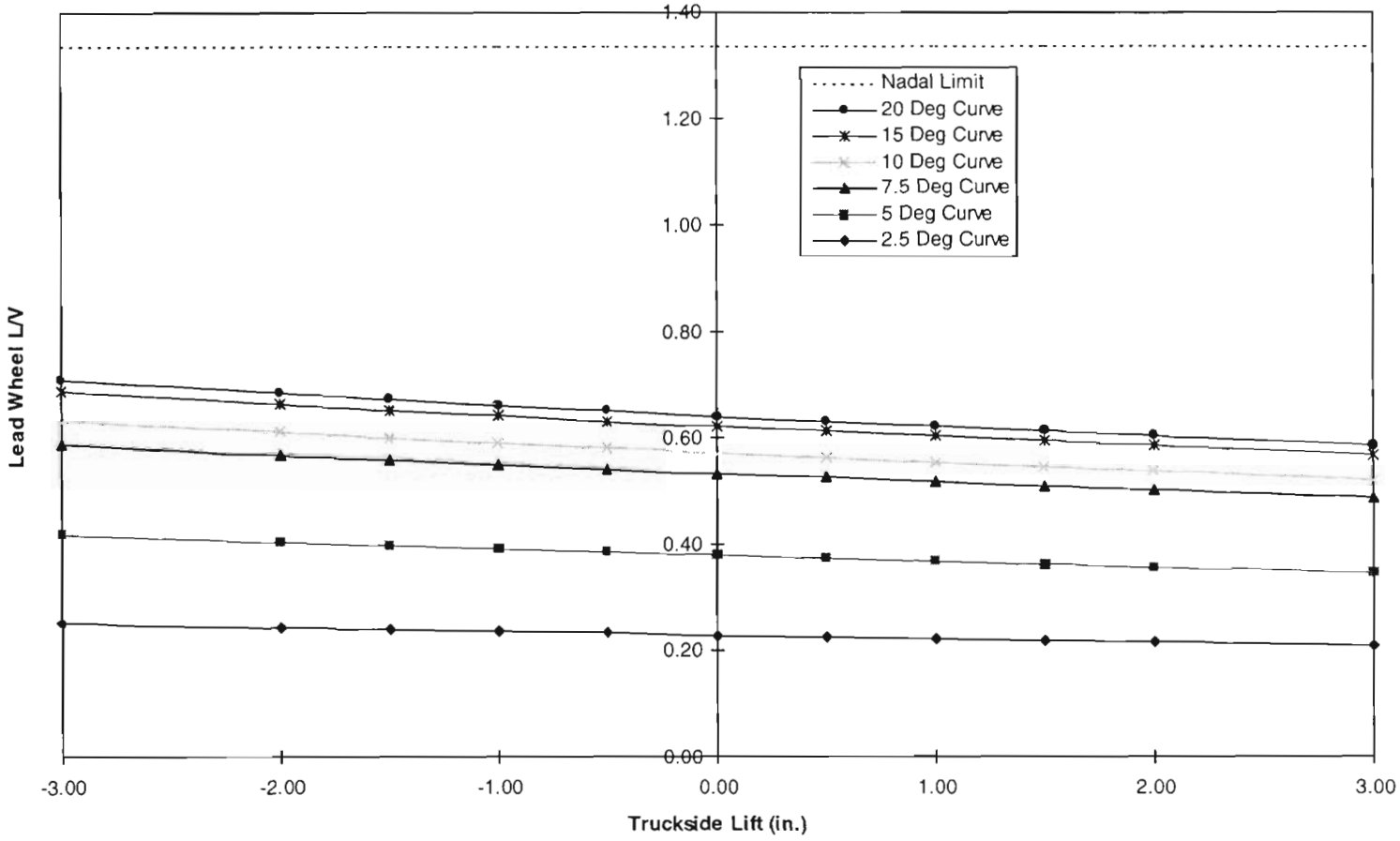

Figure B-17. Combined wheel L/V versus truckside lift (bi-level car, equalized trucks)

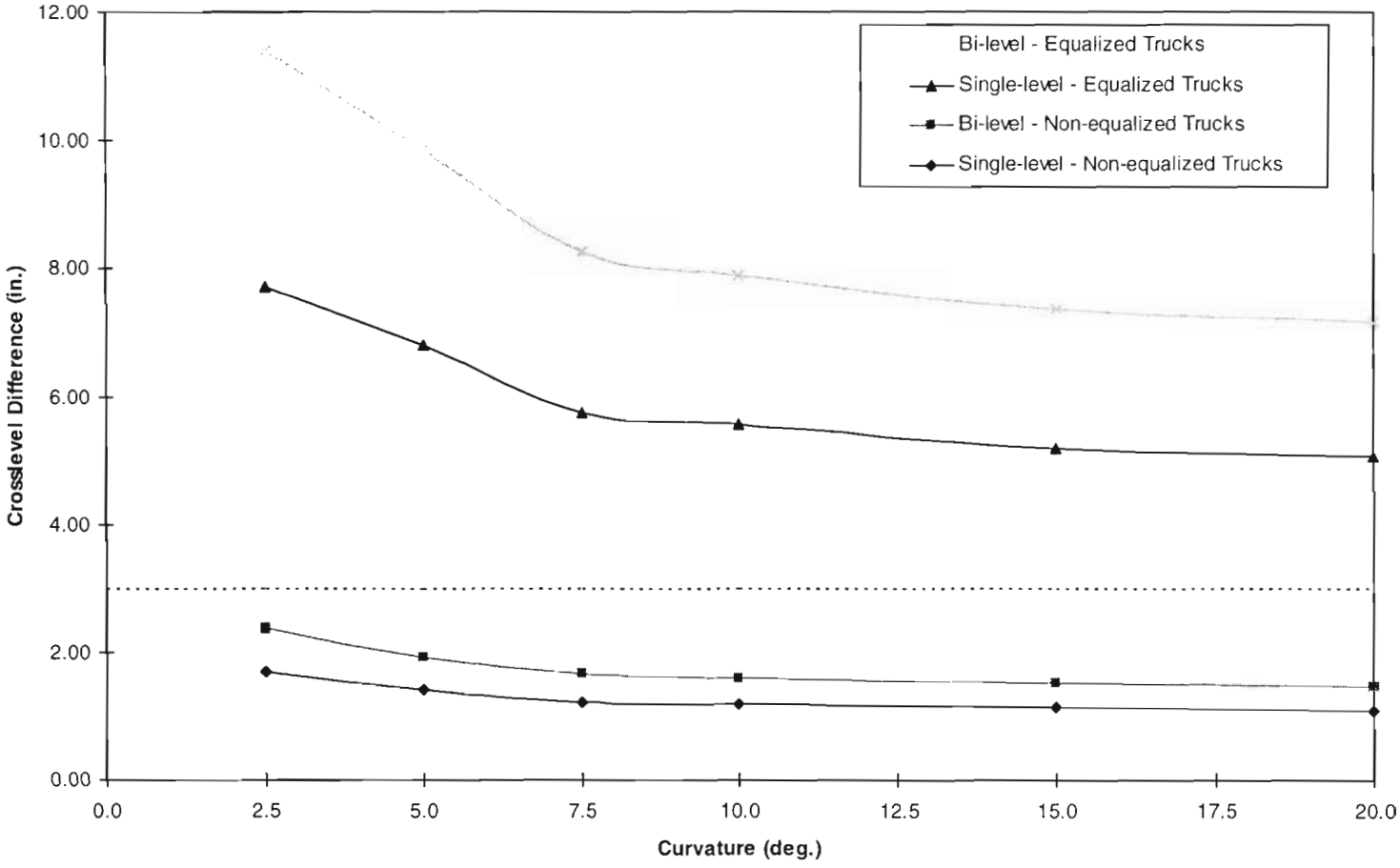

Figure B-18. Maximum permissible crosslevel difference between adjacent axles

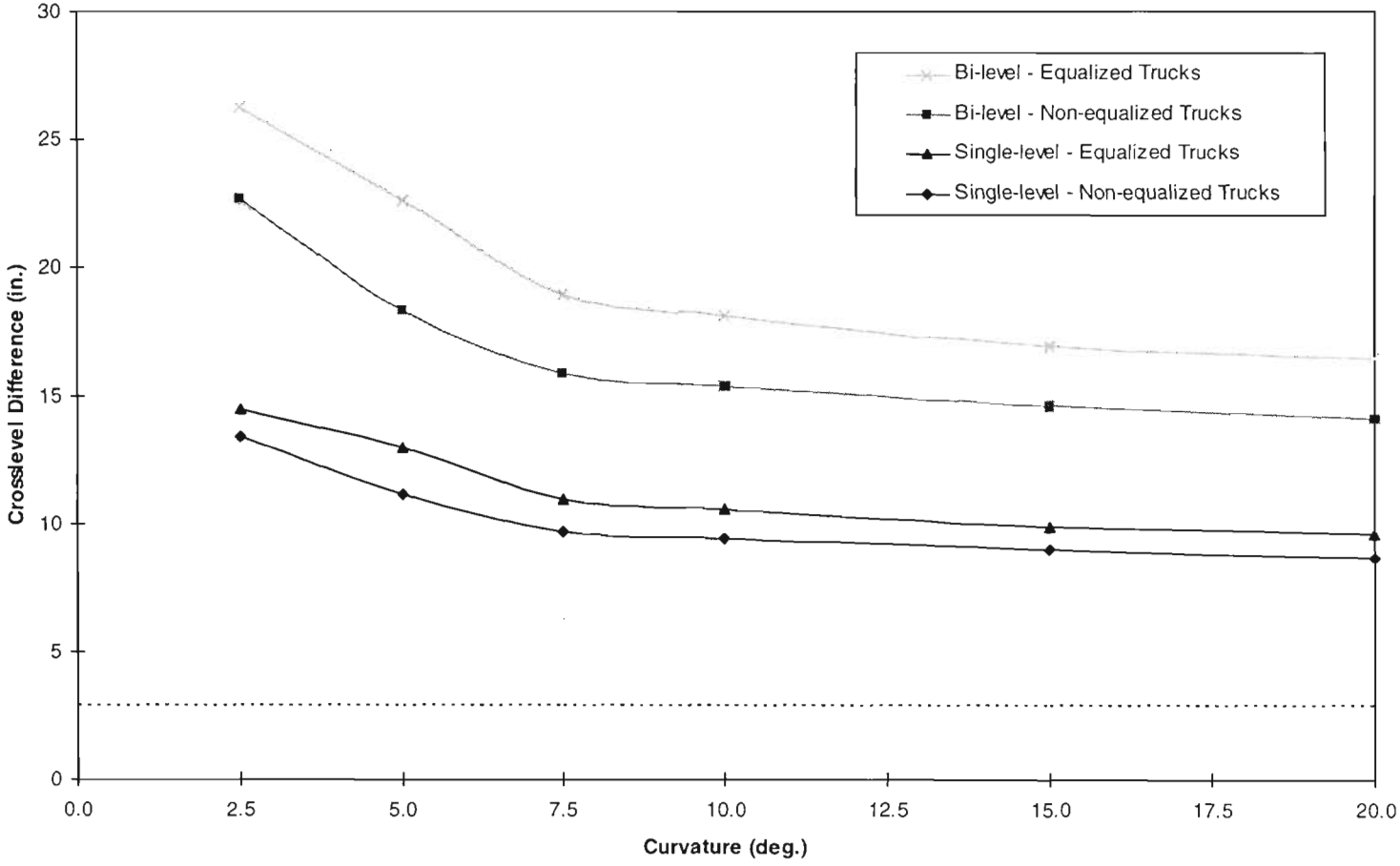

Figure B-19. Maximum permissible crosslevel difference between truck centers

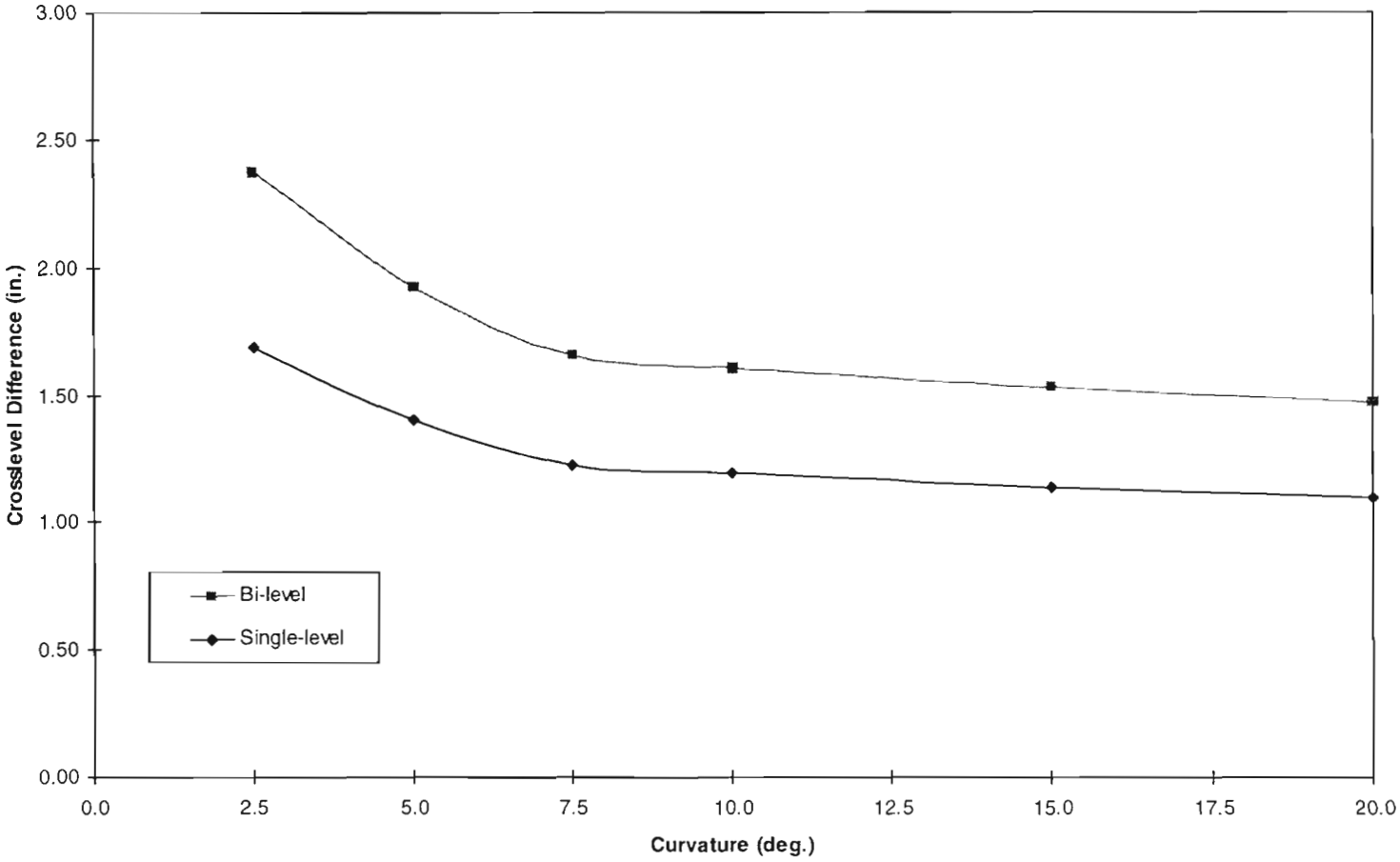

Figure B-20. Maximum permissible crosslevel difference between adjacent axles (non-equalized trucks)